[redacted] GEOCHEMISTRY AND PETROGENESIS OF THE UPPER [redacted] PILLOW LAVAS, TROODOS COMPLEX, CYPRUS

GEORGE STANLEY LANGDON

THE PETROLOGY, GEOCHEMISTRY and PETROGENESIS of the UPPER PILLOW LAVAS, TROODOS OPHIOLITE COMPLEX, CYPRUS

© George Stanley Langdon, B.Sc.

A thesis submitted in partial fulfillment of the requirements for the degree of Master of Science

Department of Earth Sciences
Memorial University of Newfoundland

April 1982

ABSTRACT

The Upper Pillow Lavas of the Troodos Ophiolite Complex, Cyprus, were formed in a back-arc basin environment by a second-stage partial melting event, which produced magmas depleted in large ion lithophile elements and enriched in magnesium. Renewed, second-stage melting to produce these magmas was facilitated by dehydration of subducted oceanic lithosphere as the spreading axis along which they were extruded moved away from a subduction zone. These parental magmas migrated upward to accumulate in shallow magma chambers and ultimately were extruded off-axis as the Upper Pillow Lava Series.

The Upper Pillow Lavas exhibit genetic ties with the underlying Lower Pillow Lavas of the Troodos Ophiolite Complex insofar as the latter represent the 'normal' first-stage partial melting (21-23%) of 'fertile' upper mantle, erupted at a back-arc basin spreading centre above a subduction zone. The Upper Pillow Lavas, however, are considered distinct in character from the Lower Pillow Lavas, based on compositional and metamorphic criteria. The petrographic and field classification of Smewing (1975) has been slightly modified, and the Upper Pillow Lavas are divided into four types: ultrabasic rocks, basaltic komatiites, olivine basalts and aphyric basalts. Major element extraction calculations and trace element modelling have shown that the magma parental to the Upper Pillow Lavas series could have been produced by ~5% partial melting of a depleted source peridotite, and that the less primitive rocks of the Upper Pillow lavas (olivine and aphyric basalts) could have been derived by the fractional crystallization of 24-32% olivine from this parental magma; the ultramafic lavas represent accumulation of this olivine. This

concept of olivine extraction was tested by comparing the calculated composition of olivines which would crystallize from the parental liquid, and the actual composition of the cumulus olivines.

Projections into the basalt tetrahedron and C-M-A-S systems confirm that early-crystallizing olivine was followed down-temperature by orthopyroxene and clinopyroxene in the komatiites, and that quenching of the groundmass glass occurred before plagioclase became a liquidus phase.

TABLE OF CONTENTS

LIST OF FIGURES IN TEXT

LIST OF TABLES IN TEXT

I. INTRODUCTION

I.1. General Statement

Cyprus is an island of some 9300 km^2 in the extreme eastern part of the Mediterranean Sea. It is situated 75 km south of Turkey and 105 km west of the coast of Syria, and is readily accessible by major air or sea routes.

This project was conceived in 1977 as a study of the geochemistry and petrogenesis of the Upper Pillow Lavas of the Troodos Ophiolite Complex. The author went to Cyprus in the early summer of 1978 and travelled around the island extensively, collecting samples representative of the diversity of the Upper Pillow Lavas.

I.2 Topography and Climate

The topography of the island is dominated by two east-west-trending mountain ranges separated by a central plain, the Mesaoria. The Kyrenia Range of the north comprises folded Mesozoic sedimentary rocks which form a gentle arc along the northern coast and are considered the southernmost portion of the Tauro-Dinaric Alps. Towards the south the Troodos Mountains reach an imposing 6400 feet above sea level and dominate the southwest corner of the island. Here there is a general coincidence of geology and topography, for the resistant mafic and ultramafic rocks of the Troodos Ophiolite Complex form the core of a dome, manifest as the Troodos Mountain Range. Outward from this core less resistant rock types crop out, i.e. gabbros, diabase and pillow lavas/sediments, with a corresponding decrease in topographic relief. Hence the Upper

Pillow Lavas at the periphery of the Complex occur on the edge of the mountain range as well, and are cut by numerous mountain-born streams which provide the most accessible sections.

The island of Cyprus has long been known for its healthy and agreeable climate. The mean daily temperature in the Mesoaria Plain ranges from about 10°C in winter to about 32°C in summer. In the mountains the mean temperature is usually about 11° lower, with a further substantial drop in temperature at night. Alleviation from the sometimes stifling heat of the interior plain can be found along the coast, where sea breezes blow along shore. During summer, evening on the central plain is regularly heralded by a cool breeze from the west, blowing landward from Morphou Bay. The very low relative humidity of the atmosphere, however, generally makes life fairly comfortable at all times of the year.

I.3 Location and Access; Method of Investigation

The author's field work dealt primarily with the collection of geological specimens from the Upper and Lower Pillow Lavas, although work was concentrated upon the former unit. Where a distinction in the field between the two units was difficult to make, collection was made with the aim in mind of subsequently allocating the rocks on the basis of petrographical and/or chemical analyses. Maps generously supplied by the Geological Survey Department and the Hellenic Mining company, Nicosia, were used in the field and are reproduced as sample location maps in Plates 1 - 3.

A small car enabled the author to make use of the many secondary roads which wander through the peripheral foothills of Cyprus; these, along with abundant dried stream beds render most areas of exposure of the lavas readily accessible.

Most of the Upper Pillow Lava outcrop area has been extensively mapped on a scale of 1:31680 and 1:10000. This work was carried out in the late 1950's and 1960's by members of the Geological Survey Department, and no attempt was made in the present work to remap the units. Work was concentrated on the northeastern and southeastern portions of the Upper Pillow Lavas; the more highly weathered aspect of the rocks in the western part of the Troodos Complex as well as more limited exposure made the collection of good samples from these areas difficult. Certain areas of the Upper Pillow Lava outcrop, such as the isolated patch north of Larnaca, and the northwestern exposure from Kokkina Point to the vicinity of Skouriotissa, were politically inaccessible, as the United Nations-patrolled unofficial boundary between the southern and Turkish-occupied northern part of Cyprus runs through these areas.

I.4 Acknowledgements

A number of people provided invaluable assistance during the course of this study. I would like to thank my supervisor, Dr. J. Malpas, who initially conceived this project, and who provided continued financial and critical support. The author hereby acknowledges the support of a Memorial University of Newfoundland and Newfoundland Provincial Government Graduate Fellowship during his period of enrolment as a graduate student, as well as the Hugh Lilly Award for 1977-1978.

The technical and analytical staff of the Department of Geology, Memorial University of Newfoundland were most helpful at all times during my sojourn; I am especially indebted to D. Press, G. Andrews, H. Longerich, P. Davis, L. Warford, G. Ford, F. Thornhill and J. Vahtra for their assistance. A. Doherty and R. Hildebrand gave me analytical assistance and R. Talkington and Dr. D. Strong provided invaluable feedback upon numerous occasions.

Dr. J. Pearce of the Open University, England, kindly undertook the analyses of rare earth elements by neutron activation.

My sincere thanks are also extended to Drs. A. Panayiotou and Th. Pantazis of the Geological Survey Department, Nicosia, Cyprus, who provided indispensible advice and logistical support during the summer of 1978. N. Adamides of the Hellenic Mining Company supplied much helpful discourse on the geology of the Troodos Complex near Kalavasos. This Company also provided the author with accommodations during his two-week stay in Kalavasos.

I am grateful to Carmen Schmidt for an expert typing job and to Hudson's Bay Oil and Gas Company Limited, Calgary, for the use of word processing facilities. I am indebted to my sister Lorna for preparation of tables.

A special vote of appreciation is reserved for the Honourable Donald Jamieson, who, in his capacity as Secretary of State for External Affairs in late 1978, arranged the shipment of some 200 kg of rock specimens from the United Nations base at Nicosia to the Canadian Forces base at Trenton, Ontario. Without this favour the continuation of this study would have been difficult, if not impossible.

Dean F. Aldrich and Dr. D. Skevington deserve credit for their advice and patience during my career as a graduate student. Furthermore as this work effectively represents a culmination of my formal training at Memorial University it would be appropriate to thank the Faculty and Staff of the entire University for an unforgetable but ultimately rewarding seven years.

Finally, my family helped me along with a hot meal on many a late night; their logistical was only outdone by their moral support.

II. REGIONAL GEOLOGY OF CYPRUS

II.1 Previous Work

The mineral resources of Cyprus have been know since the days of the ancients. Aristotle knew of its copper, and various doctors and geographers of the time of the Roman Empire made reference to the general shape of the island and the form of its mountains.

The French geologist M. Albert Gaudry carried out the first systematic geological study in 1853 and 1854, which resulted in the publication of a report and sketch map in 1862. He observed a series of fine-grained basaltic rocks which were intruded by serpentinites and "granitones". In 1865 F. Unger and Th. Kotschy published a paper on the geology of Cyprus which included some revision of the work of Gaudry. In 1892 A. Bergeat published a more comprehensive study of the igneous rocks, concentrating on the mafic and ultramafic rocks of the Troodos Mountains. L. Finkh in 1898 compared the serpentinite of the Troodos Massif to similar rock types in North Syria.

In 1905 C.V. Bellamy produced a map of scale 5 1/2 inches to a mile, which later in the same year included a memoir conjointly published by Bellamy and A.J. Jukes-Browne. These authors supported the earlier view of Gaudry that the Troodos igneous rocks were intruded into Idalian sediments during late Miocene times and that the high positive relief of the Troodos Massif resulted from powerful igneous activity.

A petrological study of the Troodos area was published in 1910 by A. Zdarsky, who noted the presence of olivine gabbro and gabbro-pegma-

tites, and paid particular/attention to chrysotile asbestos deposits within bastite-serpentine. In 1915 Kober suggested that the Troodos igneous rocks were Cretaceous to Eocene in age, based on a comparison with serpentine intrusions of the Kurdish Mountains of Turkey, Iraq, and Iran.

In 1921 C. Gilbert Cullis and A. Broughton were commissioned by the British Colonial Office to report on the cupriferous deposits of Cyprus. As their work was primarily concerned with the finer grained rocks which hosted the copper deposits, they were apparently the first to recognize the significance of the pillowed structures and their submarine affinity. They concluded that the lavas were extruded during Miocene time and were followed by the deposition of the Idalian sediments, which were subsequently transformed from basal marls to umber by manganiferous solutions emanating from the underlying lavas. A vertical compressive movement then injected Troodos plutonic rocks into the diabase (Cullis and Edge, 1922).

The earliest geophysical study was published in 1939 by C. Mace and made an important contribution to the understanding of the subsurface geology of Troodos. From 1946 to 1949 F.R.S. Henson, R.V. Browne and J. McGinty produced a map and report, in which, based on detailed paleontological studies, they delineated two formations within the Idalian sediments of Bellamy, the older of which Henson found to be of Upper Cretaceous to Eocene age. This discovery suggested that the volcanic rocks were older than Miocene, which was the age previously assigned to them. By analogy with similar volcanics of northwest Syria, these workers proposed that the pillow lavas were erupted during Middle or Upper Cretaceous times.

D.W. Bishopp in 1952 published a paper in which he referred to the diabase as a series of intensely folded lava flows of pre-Triassic age, thus noting their planar structure. He also suggested that there was a possible correlation between red shales in the Troodos pillow lavas and dated red beds within the Mamonia Complex of southwest Cyprus, and consequently that the pillow lavas might be Triassic in age.

The above studies provided the basis for a number of extensive geological projects on the immediate Troodos area and vicinity by members of the Geological Survey Department of Cyprus; their work was pulished between 1959 and 1967 as a series of memoirs and maps at a scale of 2 inches to a mile (Carr and Bear, 1960; Bear, 1960; Gass, 1960; Bagnall, 1960; Moore, 1960; Pantazis, 1967).

It is not difficult to detect in the above account the preponderance of investigation of the Troodos Complex as regards the geology of Cyprus as a whole. This has become even more the case in the last dozen or so years since the theory of plate tectonics has been more or less universally accepted. The Complex is now familar to academic and economic geologists alike; not only has it been hailed as the world's best preserved ophiolite complex, but it has also provided economic geologists with one of the best examples of sulphide mineralization at accreting plate boundaries (i.e. "Cyprus-type massive sulphides"). Within the last several years the reinterpretation of the Troodos Ophiolite Complex as a preserved portion of oceanic crust has resulted in a flurry of research concerned primarily with various petrologic and petrogenetic aspects of the unit (e.g., Juteau, 1970: Moores and Vine, 1971; Peterman et al., 1971; Smith, 1971; Greenbaum, 1972; Lapierre and Parrot, 1972; Gass and Smewing, 1973; Mesorian et al., 1973; Miyashiro, 1973a; Margaritz and

Taylor, 1974; Menzies and Allen, 1974; Spooner et al., 1974). Further reference will be made to much of this research in later portions of the present work.

II.2 General Geology

Bear (1963) divided the island of Cyprus into six topographic and geologic belts:

(1) a northern coastal belt, averaging two miles in width, which consists primarily of rocks of the Athalassa and Kythrea Formations (limestones and sandstone flysch deposits, respectively); both are sporadically capped with fanglomerates and secondary limestones (unnamed).

(2) the Kyrenia Range, underlain by the Hilarion Limestone, which is flanked bilaterally by chalks and shales of the Lapithos Formation, and intercalated with contemporaneous lava flows and sills. Almost all contacts between the core rocks of the Kyrenia Range and the Lapithos Formation are faulted, suggesting this zone as a major thrust front. To the south the Kythrea Formation represents flysch shed from the tectonically uplifted rocks of the Kyrenia Range.

(3) the Mesaoria or Central Plain, comprising undeformed, horizontally-disposed rocks of the Mesaoria Group, which overlies the Kythrea flysch with marked unconformity. To the south the Mesaoria Group overlies with less distinct unconformity the rocks of the Dhali and Lapithos Groups, mostly calcareous sediments, which flank the Troodos Complex.

(4) the northern foothills of the Troodos Mountains, represented geologically by the Upper and Lower Pillow Lavas Series, which weather to produce a hummocky topography.

(5) the Troodos Mountains, comprising intrusive rocks of the Troodos Ophiolite Complex. The complex is exposed as a large domal structure, with the ultramafic and mafic rocks at the core passing outward (and stratigraphically upward) into the Sheeted Intrusive Complex and Basal Group.

(6) the southern foothills of Troodos, comprising sediments of the Dhali and Lapithos Groups which overlie the pillow lava units and contain large inliers of volcanic, sedimentary and metamorphic rocks of the Trypa Group and Mamonia Igneous Complex.

According to Lapierre and Rocci (1975) the Mamonia nappe system, which represents an important volcanic event of late Triassic age, was emplaced during the late Maestrichtian. The volcanism can be divided stratigraphically into three episodes; a) pyroclastic rocks with associated sandstones representing explosive eruption in graben, b) basic-intermediate submarine flows interbedded with sandstones, limestones and cherts, and c) columnar trachyte flows. Geochemically the lavas belong to an alkaline basaltic suite which has many similarities to the Afar volcanics and is likewise interpreted as belonging to an intraplate volcanism in a rift system. Swarbrick (1980) however, considered the Mamonia Complex to be mainly sedimentary, and to represent a piece of late Jurassic-early Cretaceous (continental) marginal crust.

II.3 The Troodos Ophiolite Complex (Figure II.1)

II.3.1 Geological Description

The following account is based upon Coleman's (1977) description of the Troodos Complex.

FIGURE II.1 The Geology of the Troodos Complex, after Bear (1963b).

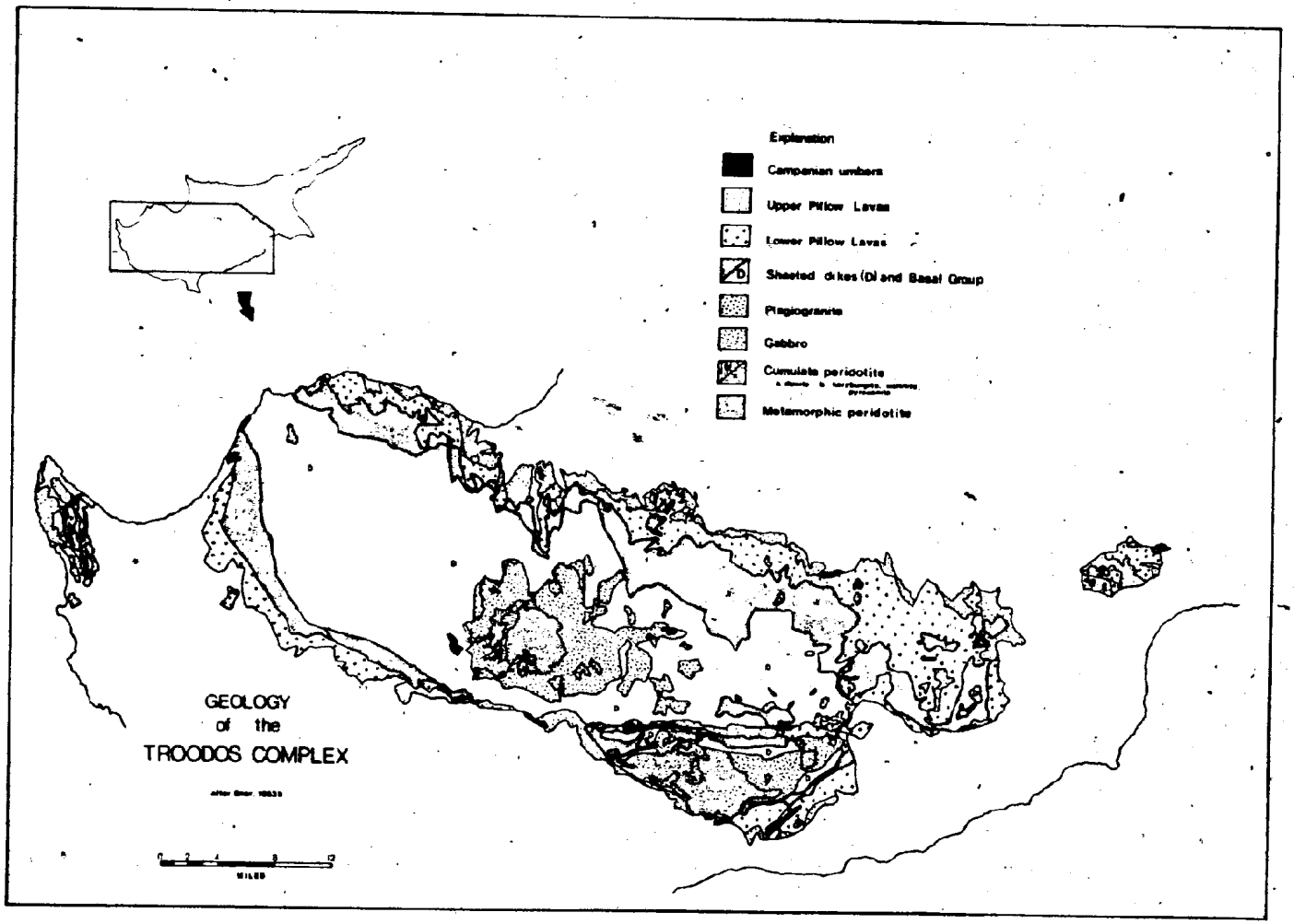
Explanation
Campanian umbers
Upper Pillow Lavas
Lower Pillow Lavas
Sheeted dikes (D) and Basal Group
Plagiogranite
Gabbro
Cumulate peridotite
Metamorphic peridotite
GEOLOGY
of the
TROODOS COMPLEX

The Troodos Ophiolite Complex can be divided into four parts for descriptive purposes. These are, from lower to upper units: (1) peridotites or mantle tectonites; (2) gabbros and granophyres, including the cumulus ultramafic rocks of the transition zone; (3) Sheeted Diabase Complex and Basal Group (Wilson, 1959); (4) Upper and Lower Pillow Lava Series.

The metamorphic peridotites were originally described as intrusive igneous rocks into older gabbros (Wilson, 1959; Bear, 1960). Contact relations between the two rock types, however, do not corroborate this theory; the peridotite/gabbro contacts for the most part are exposed as faults delineated by sheared serpentine, with a complete lack of chilling features, although peridotites are occasionally seen to cut gabbros. Gass and Masson-Smsith (1963) described a large negative gravity anomaly centred below Mount Olympus which they interpreted as a large mass of mobilized serpentinite derived from the peridotite during its emplacement; indeed serpentinization approaches 80 - 100% within much of the peridotite mass of Mount Olympus. Such a light body of rock would tend to adjust gravitationally and move upward relative to the heavier gabbros and unserpentinized ultramafic rocks overlying it. To this is attributed the dome structure of the Complex.

The peridotite itself is composed of harzburgite and minor dunite in probable fault contact. North-south oriented ultramafic bands, containing varying amounts of olivine and clinopyroxene cut across harzburgite/dunite boundaries. Menzies and Allen (1974) considered that this banding was produced during sub-solidus recrystallization and partial melting. Harzburgites contain 80% modal Fo_{90-92}, 20% modal En_{90-92},

(with exsolved diopside) and accessory aluminous Cr-spinel; dunites contain mainly olivine (Fo_{92}) and chromite. Both rock types exhibit a xenomorphic granular texture and are classified as [redacted]tle tectonites. Plagioclase lherzolite (mode: 65% olivine, 15% othopyroxene, 8% plagioclase, 2% spinel) is present as small outcrops within the harzburgite near its western contact with the dunite.

The serpentinite assemblage consists mainly of lizardite, chrysotile, brucite and magnetite with minor antigorite. Extremely high $\delta^{18}O$ values (+12.6 to +14.1) indicate very low temperature and near surface formation of serpentinite from meteoric rather than heated oceanic waters (Margaritz and Taylor, 1974) which lends further support to the contention that the serpentinite was formed during and after the emplacement of the peridotite as part of the main orogenic event.

Tectonism and serpentinization have all but obfuscated relationships in the field between the peridotites and overlying cumulate ultramafic rocks and gabbros (Wilson, 1959; Moores and Vine, 1971). The ultramafic cumulates are best exposed on the western and southern flanks of Mount Olympus. They grade downward from the gabbros and contain successively more mafic components; Greenbaum (1972) envisaged the following cumulus sequence developed from bottom to top by magmatic differentiation: chromite, olivine + chromite, olivine + clinopyroxene, olivine + clinopyroxene + orthopyroxene + plagioclase, clinopyroxene + orthopyroxene + plagioclase.

The basal dunites, pyroxenites, wehrlites, troctolites and gabbro-norites grade upward into cumulus gabbros and gabbro-norites where clinopyroxene progressively becomes more uralitized as the plagiogranite

or granophyre zone is approached (Wilson, 1959). This zone is defined by the gradual increase in modal quartz accompanied by a concomitant decrease of modal pyroxene. These quartz-sodic plagioclase rocks are found in the very irregular roof or screen zone between the underlying gabbros and overlying diabase. No sharp contacts are seen, but leucogabbros and granophyres interdigitate and contain inclusions of each other. The plagiogranites which are now thought to represent the end product of magmatic differentiation are affected by greenschist metamorphism which is pervasive downward into the uralite gabbros. This metamorphic imprint is attributed to a static hydrothermal event associated with the circulation of hot sea water at a spreading ridge (Spooner et al., 1974).

The Sheeted Diabase Complex is some 1.2 to 1.4 kilometres thick and overlies the plagiogranites. Most of the individual dykes are chilled against the underlying rocks and are probably derived from the uralite gabbros, as they do not penetrate deeper than the latter rocks. Upward the unit comprises 100% subvertical dykes which are 0.3 to 4.5 metres wide, subparallel, strike north-south and have fine-grained diabasic textures with asymmetric chilled margins. The primary mineral assemblage of Ca-clinopyroxene, plagioclase (An_{30-60}) and iron oxides has been almost completely transformed by low grade hydrothermal alteration to one of albite, actinolite, chlorite, epidote and quartz. The dykes are interpreted as representative of extension and development of new oceanic crust by sea-floor spreading at a midocean ridge (Moores and Vine, 1971; Kidd and Cann, 1974).

The Basal Group, lying between the Sheeted Diabase Complex and the Upper and Lower Pillow Lava Series, constitutes a transitional zone

between the two; it is similar to the Sheeted Diabase Complex in character with the exception that occasional small pillow lava screens occur with the sheeted dykes.

Two discrete pillow lava units separated by an unconformity overly the dykes and have been described as follows by Gass and Smewing (1973): "Upper Pillow Lavas. Generally undersaturated, often olivine-bearing basalts with more ultramafic varieties (limburgites and picrites) occurring at the top of the sequence. Dykes form less than 10% by volume, absence of silica and celadonite, calcite and analcime common. Lower Pillow Lavas: Mainly oversaturated basalts, often intensely silicified, celadonite common. Dykes, sills and massive flows forming between 30 - 60% of the outcrop."

These units also show the effects of hydrothermal metamorphism; assemblages within the Upper Pillow Lavas indicate zeolite facies conditions, while the Lower Pillow Lavas have higher temperature metamorphic assemblages indicative of conditions within the zeolite and lower greenschist facies. Various petrologic and metamorphic features led Gass and Smewing (1973) to propose a genetic distinction between the two units.

As the Upper Pillow Lavas are the present study topic a more detailed description of their petrologic character will be presented hereafter. The Lower Pillow Lavas will also receive some further discussion by virtue of their close association with the Upper Pillow Lavas.

II.3.2 Petrogenetic and Tectonic Implications

The complete sequence of the Troodos Complex is thought to represent a polygenetic association; there is considerable evidence

against the basal peridotites and all overlying rocks being part of one genetic unit. The basal harzburgites show subsolidus deformation and appear to represent material residual from an early partial melting event (Greenbaum, 1972; Menzies and Allen, 1974); the abundant veins and dykes of pyroxenitic and dunitic material within the harzburgite may represent partial melts, and these channels could have fed the overlying cumulates. There appears, however, to be a significant difference in age between the depleted harzburgite and the cumulates; this has been corroborated in other ophiolites where strontium isotope data indicate an extreme difference in age between the two units (Faure and Powell, 1972), i.e., the basal harzburgites may be the residuum of a much older mantle melting event and may not be genetically related per se to the overlying cumulates, although no evidence of this earlier melting event is present. Again, field observations fail to provide any firm resolution to the problem. A complex situation is envisaged where basal cumulates may locally be included in the harzburgite zone (e.g., Wilson, 1959).

The overlying rocks, however, including the cumulates, dykes and Lower Pillow Lavas are interpreted as a comagmatic suite formed by differentiation within a magma chamber below the axial zone of a slow-spreading ridge. Most workers concur with this interpretation but Miyashiro (1973a) reviewed the chemistry of the Lower Pillow Lavas and dyke complex and concluded that their apparent calc-alkaline trend indicates an origin within an island arc developed on thin oceanic crust. With the ensuing flurry of protestations, however, (Gass et al., 1975 ; Hynes, 1975; Moores, 1975), Miyashiro's argument appears to be less than convincing (Smith, 1975). Miyashiro's work was based on major elements,

which were considered by most of these authors to be relatively mobile during alteration processes and therefore unreliable. Perhaps the strongest evidence to counter Miyashiro's arguments is the lack of coarse-grained clastic and volcanoclastic sequences normally associated with island arc evolution, as well as the presence of the ubiquitous sheeted dyke swarms indicative of spreading centres. Ewart and Bryan (1973), however, suggested that island arc volcanic rocks may rest on fragments of oceanic crust or be tectonically imbricated one with the other. A back-arc or marginal basin may be suitable scenario for the juxtaposition of such processes.

Further evidence for a spreading ridge is provided by the metamorphic assemblages, which vary with depth and indicate high heat flow and circulation of sea water in a ridge environment. The massive sulphide deposits are also associated with this low grade hydrothermal metamorphism, and Spooner et al. (1974), on the basis of isotope geochemistry, have concluded that there must be widespread metamorphism in the upper portions of the oceanic crust near spreading centres.

The bulk of the evidence seems to indicate that the Troodos Ophiolite Complex was formed at an axial spreading centre or within a marginal basin at the periphery of the Tethys Ocean. Its obduction onto the African plate as a small fragment of oceanic crust is interpreted as being part of a relative north-south movement between Africa and Eurasia during late Cretaceous times. Geophysical surveys have supported this concept; positive Bouguer gravity anomalies (100-250 mgals) situated beneath the Troodos Ophiolite Complex (Gass and Masson-Smith, 1963) suggest that it is a rootless slab of oceanic crust resting on African continental crust (Gass, 1968; Vine et al., 1973).

Lapierre and Rocci (1975) in their study of the Mamonia Complex had much to say regarding its tectonic significance. Volcanic suites of similar age and affinity to the Mamonia Complex are widespread in the east Mediterranean Alpine orogenic domain, i.e., in the Antalya Nappes of Turkey, the Baer-Bassit of Syria, the Othrys-Pindos region of Greece, and in southern Italy. Lapierre and Rocci thus recognized the Mamonia volcano-sedimentary complex as part of an extensive late Triassic magmatic event which is widespread in the Mediterranean-Alpine region and which is always found in tectonic association with ophiolites. They proposed the existence of a rift system associated with an alkaline basalt suite along the northern edge of the African plate during the late Triassic, which by Jurassic - Cretaceous times had developed into a mid-ocean ridge. They further suggested that the southeasternmost ophiolitic sequences, namely Troodos, Hatay (southeastern Turkey), Zagros and Oman came from a marginal sea which existed along a mid-tethyian ridge north of the African plate, separated from the Tethys and the main ophiolite zone to the north by a carbonate shelf. During the orogenic event this small marginal sea was obducted southward onto the African plate.

III. THE UPPER PILLOW LAVAS

III.1 Field Aspects

Extensive descriptions of the field characteristics of the Upper Pillow Lavas in their various areas of outcrop have been given by several authors, e.g., Wilson, 1959; Gass, 1960; Bagnall, 1960; Carr and Bear, 1960; Bear, 1960; and Pantazis, 1967. Smewing (1975) described the general nature of the unit as seen in the field. It is proposed here to briefly review the field aspects of the Upper Pillow Lavas based on both the authoritative work of the aforementioned authors and the field observations of the present writer.

III.1.1 Exposure

The Upper Pillow Lavas are considered the peripheral unit of the Troodos complex and are bounded above and below by Upper Cretaceous - Lower Tertiary sediments, and the Axis Sequence, respectively. They outcrop around nearly 60% of the perimeter of the massif, being most continuously found on its northern and southeastern edges and absent in most of its western parts (Figure II.1).

The lavas are well exposed throughout as vegetation is generally very sparse. Although pillowed forms are discernible in most cases, fresh samples are difficult to procure as the rocks are highly decomposed and generally disintegrate to rubble when struck with the hammer. Considerably fresher samples, however, were often found in dry stream beds where running water has removed much of the rubbly material. The Upper

Pillow Lavas have in most places attained a characteristic light blue-grey colour which is attributed to the production of clays within them as an effect of low grade hydrothermal metamorphism (Smewing, 1975).

III.1.2 Morphological Types

The lavas range up to 200 metres but average about 100 metres in thickness (Gass and Masson-Smith, 1963). They occur as a variety of intrusive and extrusive types, including pillows, dykes, flows, sills, breccias and hyaloclastites. Pillow lavas are by far the most voluminous morphology, composing about 80% of the exposure, with the other types listed above in order of decreasing abundance (Plates 4-7).

The pillows generally take the shape of ellipsoids (Plates 4 and 5). The long axes average 1 to 1 1/2 metres in length; long/short axis ratios are of the order 3:2. The pillows contain numerous vesicles and veins, these being generally lined by montmorillonite and infilled with calcite and zeolites. Carbonates, zeolites and umberiferous sediments occur between individual pillows.

Dykes within the unit are considered feeders to the lavas and commonly group together to form discrete eruption zones (Gass, 1960). They are of 1/2 to 1 metre width, and being more resistant to erosion, generally protrude outward from ambient lavas, often forming small elongate hills. At Asgata Potamos (river), just north of the village Asgata, dyke-flow relations are well exposed. Protruding dykes cut across the stream transversely at intervals of 50 - 100 feet, while less resistant pillow lavas form the stream bed. The dykes show good chilled margins against the lavas (Locality KL-36, Plate 7).

Plate 4: Flow structures in aphyric basalt just west of Asproyia.

Plate 5: Pillowed basalt from roadside, one mile west of Akapnou.

Plate 6: Pillow with 'ropy' surface pattern.

Plate 7: Dykes cutting Upper Pillow Lavas at Asgata Potamos.

Massive flows are often vesicular and commonly contain interbedded units of different petrologic nature (e.g., near Kalavasos, Locality Kl-17).

III.1.3 Compositional Types

Smewing (1975) divided the Upper Pillow Lavas into four types based on macroscopic phenocryst assemblages: (1) picrite basalt and ultrabasic rocks, (2) olivine basalts, (3) aphyric basalts, (4) fine-grained basal lavas. Here these types will be described according to Smewing's field distinction. However, based on his own petrographical and geochemical data, the present author will be subsequently rearranging this breakdown, more for the purposes of facility in his own discussion than as a proposal of a new nomenclature for the rocks. The classification of Smewing and that of the present author are summarized in Table III.2.

The picrite basalt and ultrabasic rocks (here referred to together as ultrabasic rocks) have been previously described by Gass (1958, 1960a), and Searle and Vokes (1969). They are generally considered to be shallow intrusive or hypabyssal bodies, i.e., dykes, sills or bosses, but occasionally are found as pillow lavas (Gass, 1958). In the field they tend to form low resistant ridges, or as is the case near Margi (Localities DL-38,40) they may occur as narrow sills found concordantly between the flow bodies of aphyric basalt, as is the case near Kalavasos (Locality KL-17). The position of these rocks near the top of the pillow lava sequence suggests that they were extruded at a later stage in the tapping of a magma chamber.

Table II.1 Modal Analyses of Specimens From the Upper Pillow Lavas

	DL-36	DL-45	KL-33	DL-23	DL-31	KL-69	PL-19	PL-10
Phenocrysts								
Olivine	66.28	54.80	5.67	1.76	3.73	-	-	-
Opx	-	-	10.04	-	-	-	-	-
Microphenocrysts								
Cpx	1.73	3.58	-	-	-	-	-	-
Opx	0.11	6.93	-	-	-	-	-	-
Chr	0.92	0.78	-	-	-	-	-	-
Groundmass								
Cpx	-	-	-	-	13.49	-	14.12	-
Cpx (zoned, quenched)	-	-	28.85	-	-	-	-	-
Cpx (plumose)	-	-	-	58.94	-	-	-	-
Plag	-	-	-	-	29.29	19.05	20.79	26.40
Magnetite	-	-	-	-	0.93	-	1.01	0.98
Glass	-	-	53.23	38.82	-	-	-	-
Fine gd. basaltic mat./devit. glass	16.65	32.09	-	-	-	69.26	-	33.50
Vesicles	-	-	-	-	-	5.59	-	-
Amygdales								
Zeol/Carb	-	-	1.39	-	18.93	-	-	-
Alteration Minerals								
Antigorite	0.50	1.8	-	-	-	-	-	-
Celadonite	-	-	-	-	-	-	12.20	-
Carbonate	13.81	-	0.79	0.47	-	-	2.37	-
Other*	-	-	-	-	33.62	0.89	49.48	24.70
Total Counts	869	894	1005	850	1178	1233	885	1012

Rock Types Represented

DL-36: ultrabasic rock, vitrophyric
DL-45: ultrabasic rock, holocrystalline
KL-33: komatiite, hyaloplitic
DL-23: komatiite, variolitic
DL-31: olivine basalt
KL-69: aphyric basalt
PL-19: aphyric basalt

* includes smectite, other clay minerals, zeolites, hematite

TABLE III.2 Petrographical classification of Smewing (1975), A; and the present work, B.

Pillow edge to centre →

Field Groups	Phenocrysts and (microphenocrysts)	Groundmass mineralogy	Groundmass textural types: Vitrophyric (fresh/altered)	Hyalopilitic (fresh)	Variolitic (altered)	Intersertal (altered)
			glass/ devitrified glass	cpx + glass ± plag	plag + sm ± tm ± cpx ± ze ± ca	cpx + plag + sm + tm ± ze ± ca
Picrite basalt and ultrabasic rocks	ol (chr)			●		
Olivine basalt	ol cpx opx (plag) (chr)	With hyalopilitic rim	●	●	●	●
		Without hyalopilitic rim			●	●
Aphyric basalt	cpx plag				●	●
Fine gd. basal lava	(cpx) (plag) ol				●	●

Field Groups	Phenocrysts and (microphenocrysts)	Groundmass mineralogy	Groundmass textural types: Vitrophyric (fresh/altered)	Hyalopilitic (fresh)	Variolitic (altered)	Intersertal (altered)	Holocrystalline (fresh/altered)
			glass/devit. glass ± ca ± ze	glass cpx microlites	glass ± cpx + sm ± tm ± ze ± ca	cpx + plag + sm + tm ± ze ± ca ± he ± cel	cpx + plag ± tm ± ant ± sm ± ca ± ze
Ultrabasic rock	ol (cpx, opx chr)		●				●
Komatiite	ol, opx		○	●	●	○	
Olivine basalt	ol (cpx)				●	●	
Aphyric basalt (inc. fine-grained basal lava)	(cpx, plag)				○	●	

Abbreviations

ol - olivine
cpx - clinopyroxene
opx - orthopyroxene
plag - plagioclase
chr - chromite
sm - smectite
tm - titanomagnetite
ze - zeolite
ca - carbonate
ant - antigorite
he - hematite

Symbols

● common
○ rare

Olivine basalts are found generally at or near the top of the Upper Pillow Lava succession and are identifiable in the field by their brownish pseudomorphed olivine phenocrysts, now completely replaced by iron oxide and carbonate. This field distinction is also borne out in thin section. These rocks are most commonly found as highly weathered pillows which are pervaded by carbonate- and zeolite-filled vesicles and veins.

In some of the pillows a fresh black glassy margin is preserved which varies in width from 1 - 15 centimetres and is found under the microscope to have hyalopilitic texture. Smewing (1975) distinguished between two types of olivine basalts, based primarily on the presence or absence of this fresh black glassy margin which surrounds the altered cores of the pillows. The present author proposes to separate these two types further on the basis of petrographical and geochemical data. Gass (1960a) and Bear (1960) have referred to the olivine basalts containing this margin as Limburgites. These lavas are readily identified in the field; their black glassy edges stand out from the crumbly remains of the normal olivine basalts. As these rocks are distinguishable mainly on petrographical criteria their nomenclature and character will be fully discussed in the section on petrography.

The aphyric basalts are by far the most abundant type of rock within the Lavas, forming wide areas of outcrop where the sequence is thickest; their main occurrence is as pillow lavas, with flows and sills occasionally being found. These lavas are perhaps best characterized in the field by their consistantly altered state. Generally whole pillows

can be broken down by a few hammer blows, owing to a pervasive network of cracks and joints.

The fine-grained basal lavas are discontinuously exposed at the base of the section along the northern edge of the massif. They are characteristically black or brown in colour and are most commonly aphyric; occasionally they contain small microphenocrystic pseudomorphs after olivine. These lavas closely resemble the underlying Lower Pillow Lavas but are considered to be part of the Upper Pillow Lavas because of their similar metamorphic assemblage (Smewing, 1975).

III.2 Petrography

III.2.1 General

Smewing (1975), in his description of the petrography of the Upper Pillow Lavas, recognized four distinct groundmass mineralogies and textures which generally are found as a gradation from core to margin in individual pillows. These are, from the core of a pillow to its edge, intersertal, variolitic, hyalopilitic and vitrophyric (see Table III.2). Smewing considered that the succession owed its heterogeneity to the varied development of phenocryst assemblages and pillow zones; furthermore, the different textural types show differences in their susceptibility to alteration. Basalts which have developed only the intersertal or variolitic textures are invariably found in a highly altered condition, with the primary mineralogy of the groundmass [illegible]ut completely replaced by smectites, zeolties and calcite. Hyalopilitic and vitrophyric types, however, are much more pristine and clearly show original textures with a minimum of replacement by secondary minerals.

In the following discussion the rocks of the Lavas are classified and described on the basis of their petrography.

III.2.2 Ultrabasic Rocks

These rocks are found in the field as both extrusive and intrusive types, this dichotomy leading to the development of two textures: vitrophyric and holocrystalline, respectively. The vitrophyric type has a dominance of olivine phenocrysts which are set in a glassy groundmass, and which compose up to 66.28% by volume of the rock (see modal analysis, Table III.1). These unzoned olivine phenocrysts ($\sim Fo_{92}$) range up to 2.2 by 0.5 centimetres in size; they normally show euhedral but slightly corroded boundaries (Plates 8-13). The grains are often fresh but more commonly show alteration to antigorite along fracture planes. In some grains this alteration is accompanied by rounded patches of magnetite, which tend to occupy the corroded interiors.

Fresh clinopyroxene occurs also as a phenocryst phase but is much less abundant than olivine and forms much smaller grains (average 0.5 mm). These are commonly euhedral and occasionally show well developed twinning along 100. Euhedral crystals of chromite exist in small amounts and reach 0.6 mm in diameter. They are often present as inclusions within large olivine grains, where they appear to serve as loci for fracture and serpentinization.

Partially devitrified glass of basaltic composition makes up the groundmass (determined by microprobe). Microlites of clinopyroxene are disposed parallel to phenocryst boundaries. Carbonates and zeolites

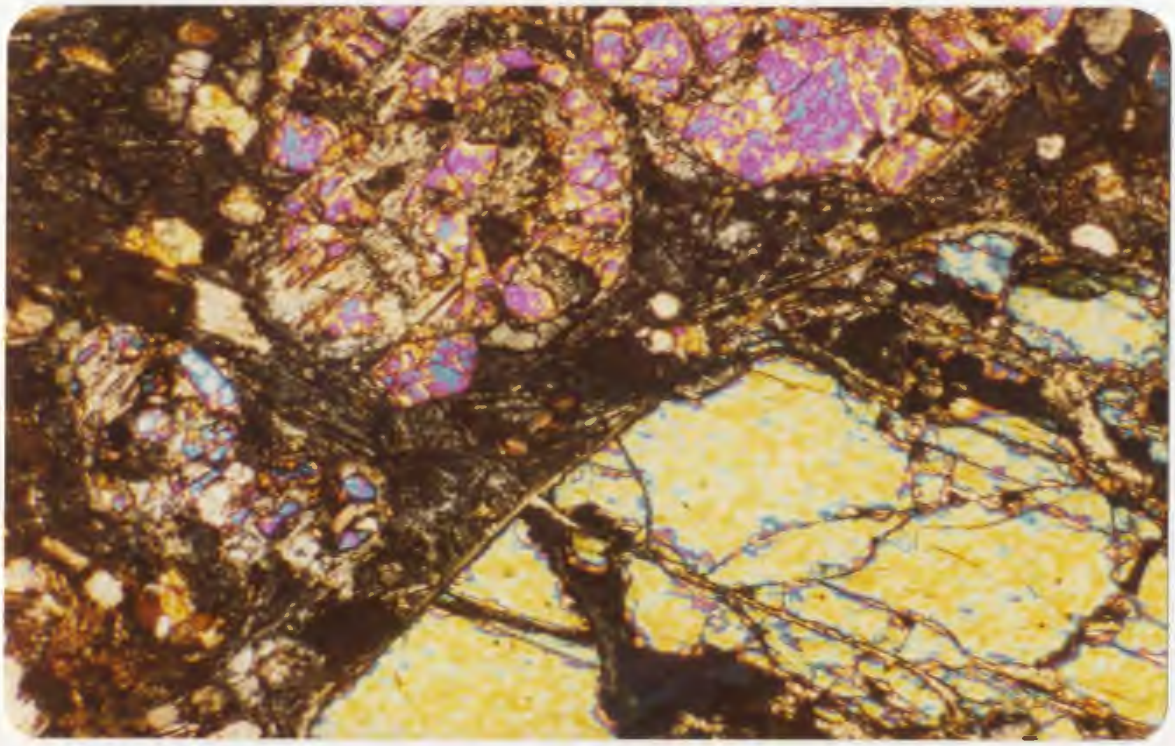

Plate 8: Ultrabasic rock. Vitrophyric texture; fairly fresh olivine; small clinopyroxene grains; partially devitrified matrix. DL-36. XN. 31X.

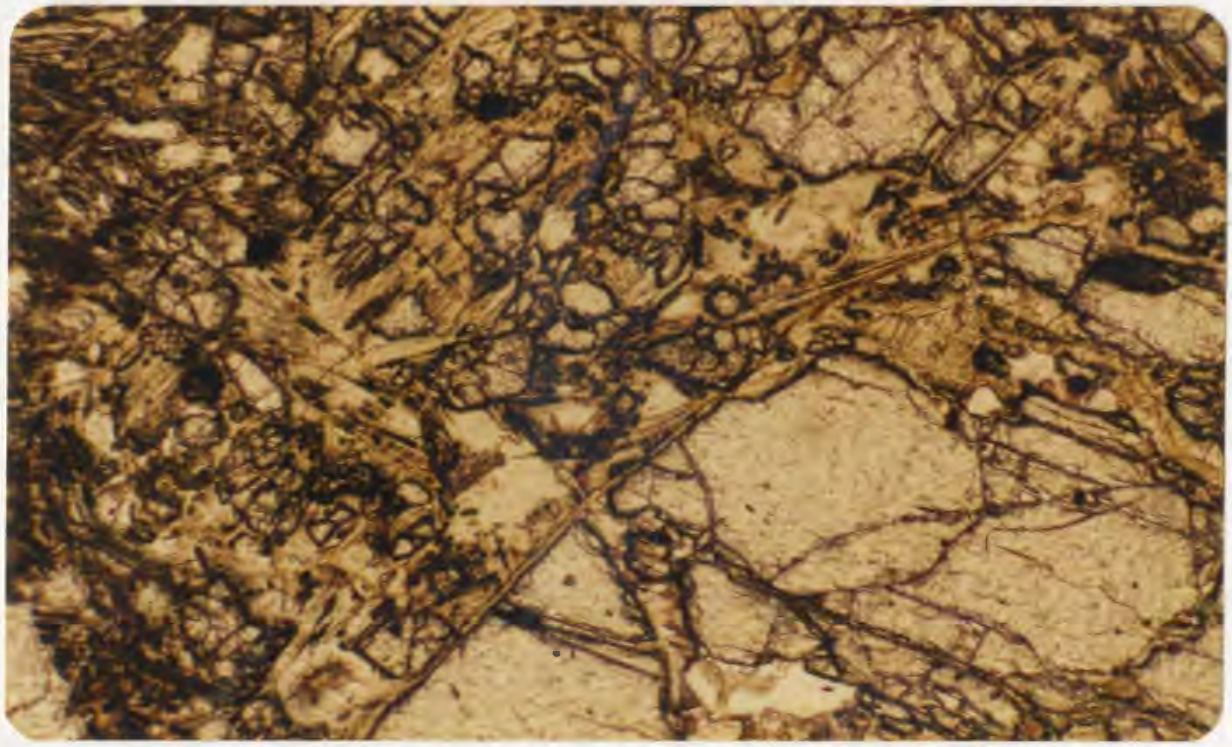

Plate 9: As above, plane-polarized light (PPL).

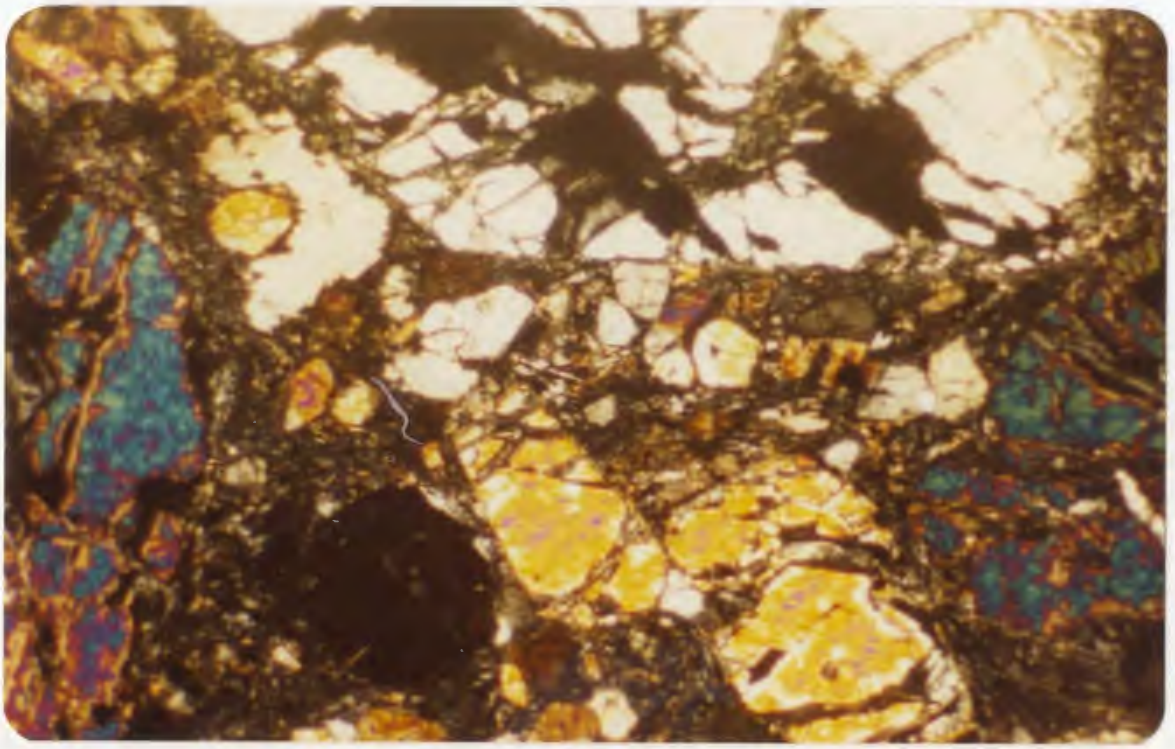

Plate 10: Ultrabasic rock. Vitrophyric texture; large olivine phenocrysts; small clinopyroxene grains. Partially devitrified groundmass. DL-36. XN. 31X.

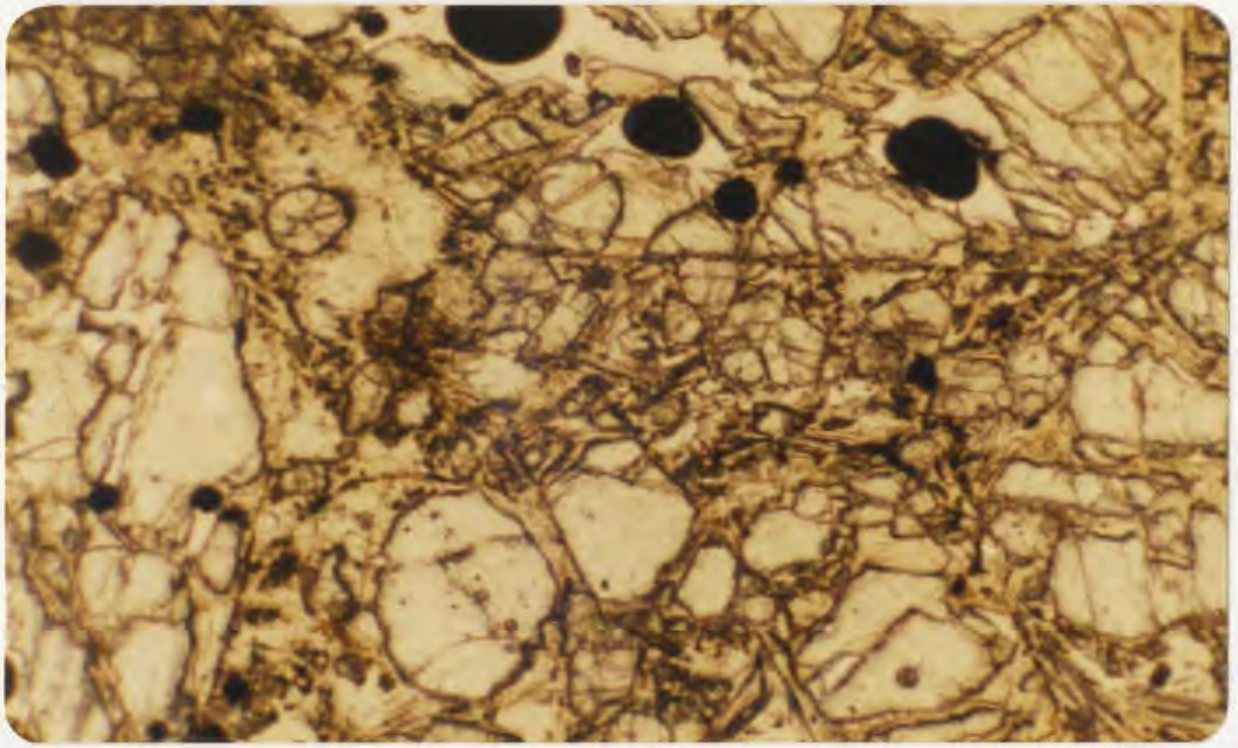

Plate 11: As above, PPL. Round 'pools' of magnetite within voids in olivine.

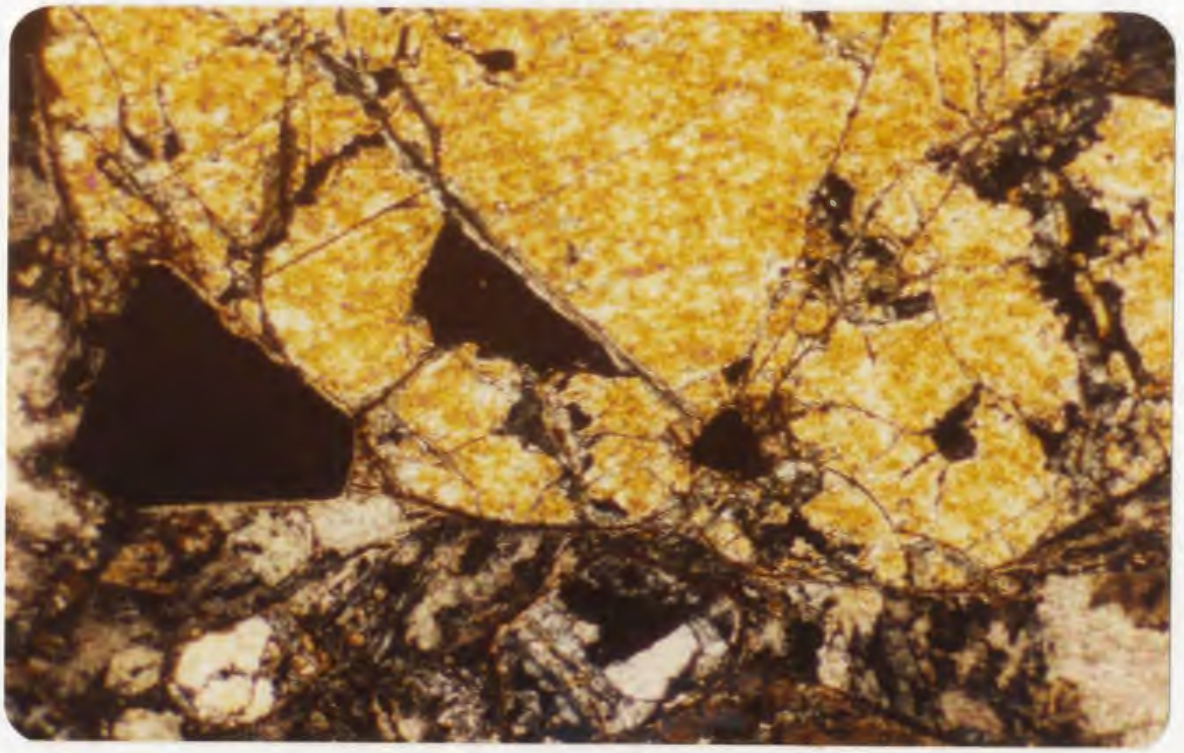

Plate 12: Ultrabasis rock. Vitrophyric texture. Euhedral chromite grain partially enclosed by olivine. Carbonatized groundmass. DL-37. XN. 31X.

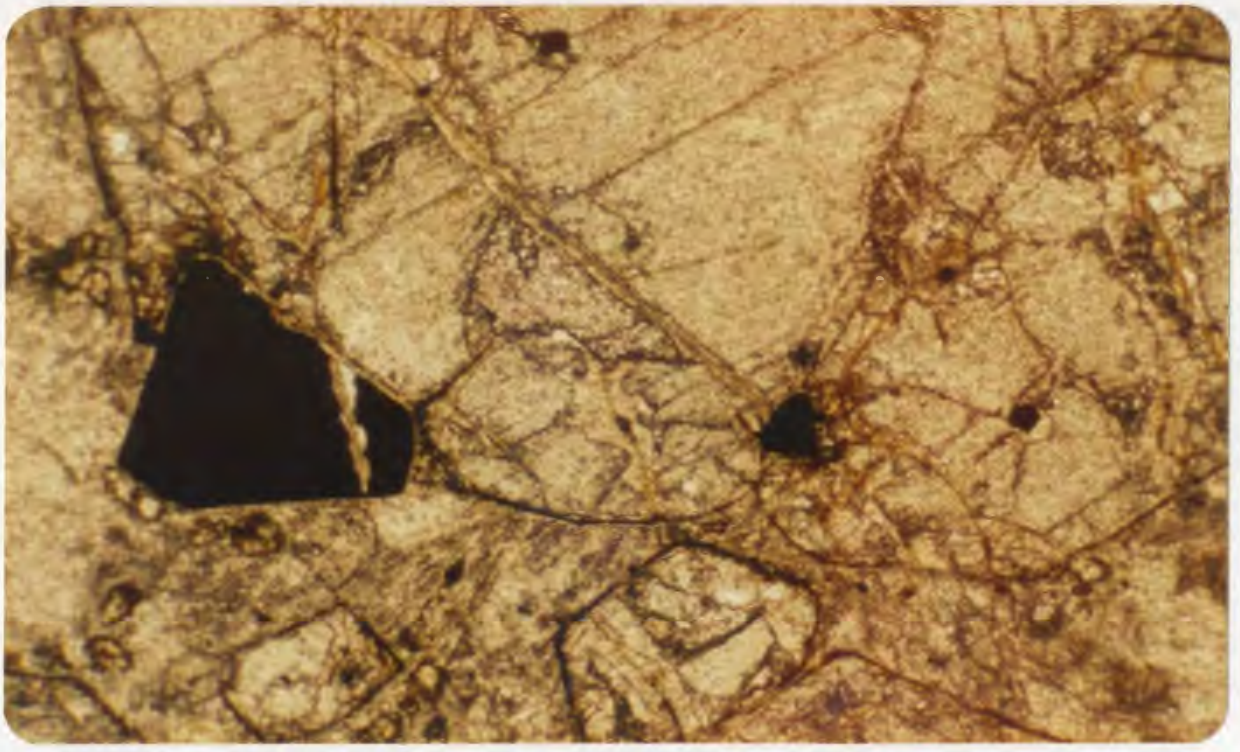

Plate 13: As above, PPL.

occur both in amygdules and throughout the groundmass as deuteric patches.

Ultrabasic rocks with a holocrystalline texture show much higher degrees of alteration, a groundmass which is entirely crystalline and a reduction in the size of olivine phenocrysts (average 2 mm) as compared to the vitrophyric type (Plates 14-16). The average olivine composition is $Fo_{90.8}$ as determined by electron microprobe (see Appendix B.2). Small (0.8 - 1 mm) well-preserved euhedral magnesian augite grains ($Wo_{41.26}En_{50.96}Fs_{7.77}$) occur as a phenocryst phase. Olivine euhedra are pervasively altered to fibrous antigorite, especially near the grain boundary and along fractures within the crystal. Chromite is present as intergranular euhedra and as inclusions within the olivine. Small magnetite inclusions within olivine appear to have developed as a by-product of antigoritization.

Small grains of orthopyroxene ($En_{84.2}$) are sparse. Plagioclase is a fairly important constituent of the groundmass, being intergrown with augite in an intersertal texture. Much of the original holocrystalline aspect of the groundmass, however, has been lost during deuteric alteration. Primary pyroxenes and plagioclase have been extensively replaced by antigorite, magnetite, smectite and zeolites.

III.2.3 Magnesium-rich Lavas

III.2.3.1 General

This group of rocks has been referred to collectively as olivine basalts of Smewing (1975) who further subdivided them into two types on the basis of the presence or absence of hyalopilitic zone in the outer

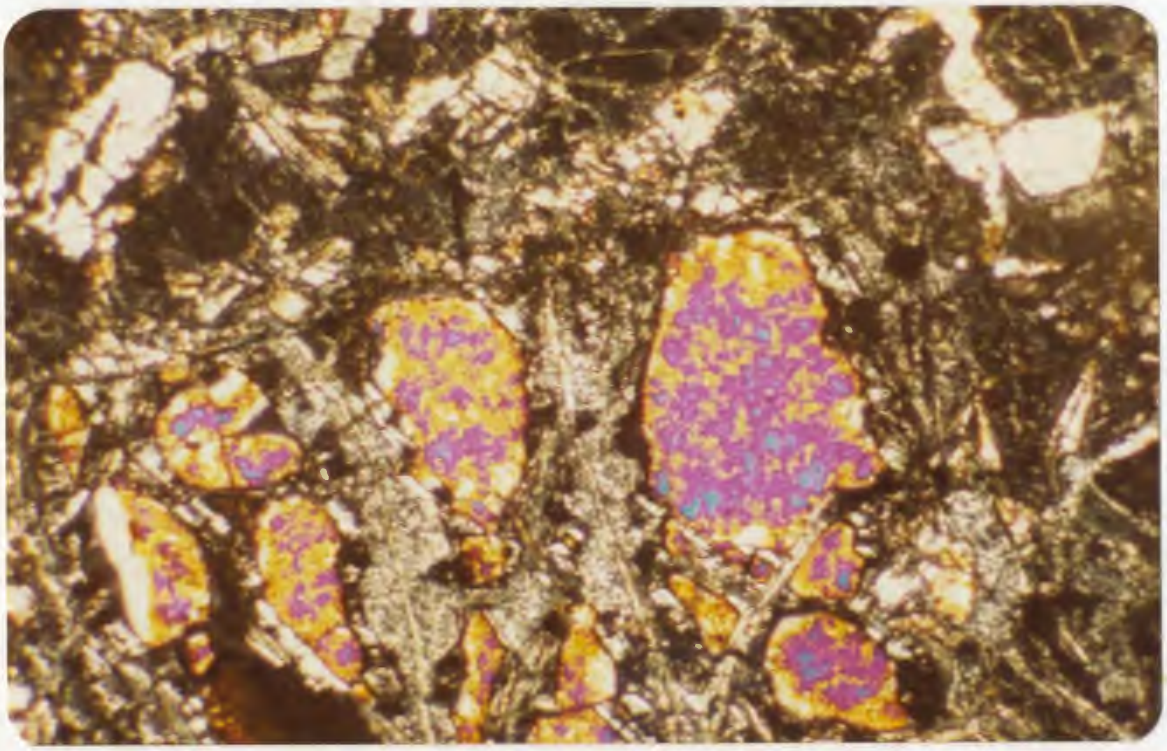

Plate 14: Ultrabasic rock. Holocrystalline texture. Skeletal serpentinized olivine; poikilitic clinopyroxene partially enclosing small grain of olivine at upper right. Serpentinized groundmass. DL-45. XN. 31X.

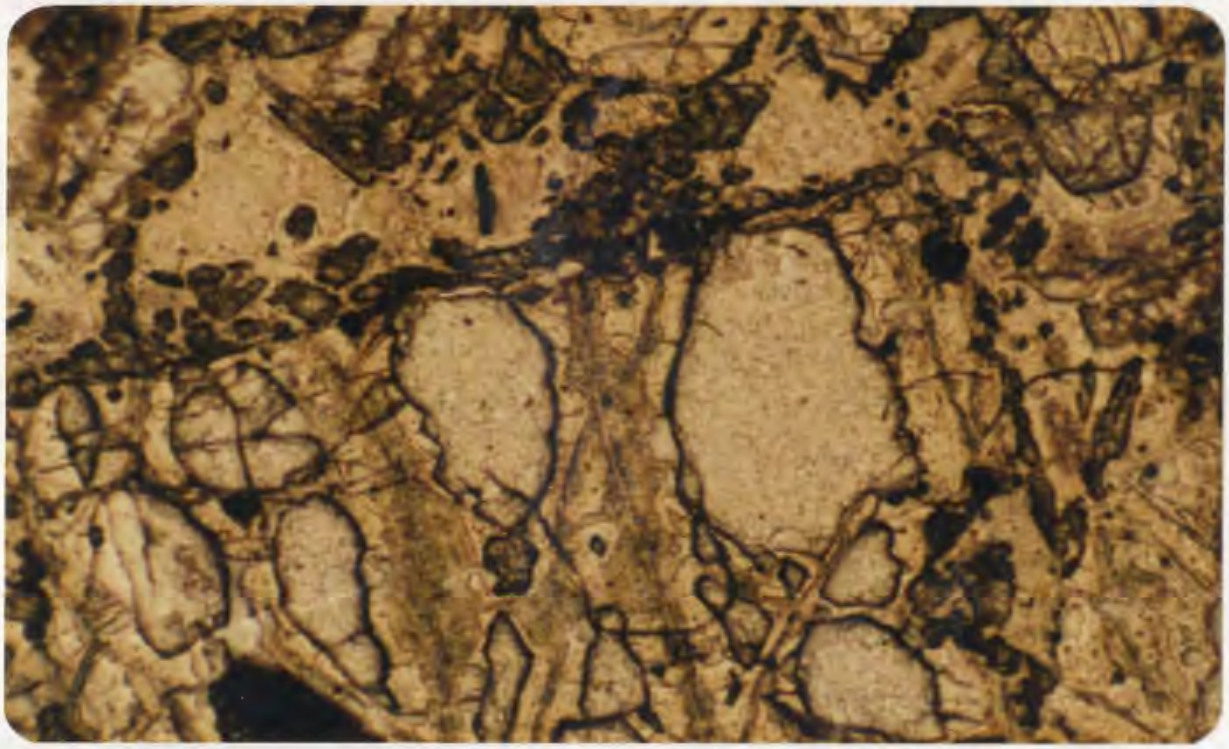

Plate 15: As above, PPL.

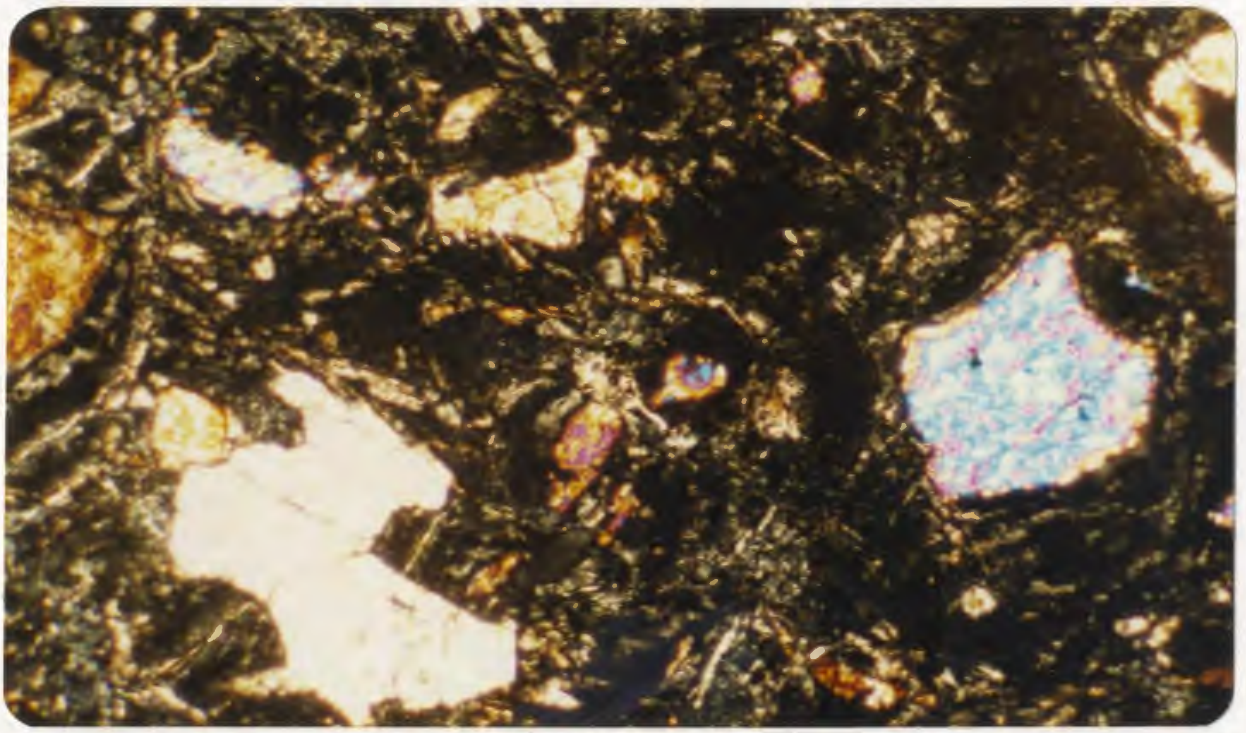

Plate 16: Ultrabasic rock. Holocrystalline texture. Large serpentinized olivine grain; clinopyroxene partially encloses small olivine grain; plagioclase in groundmass. DL-45. XN. 31X.

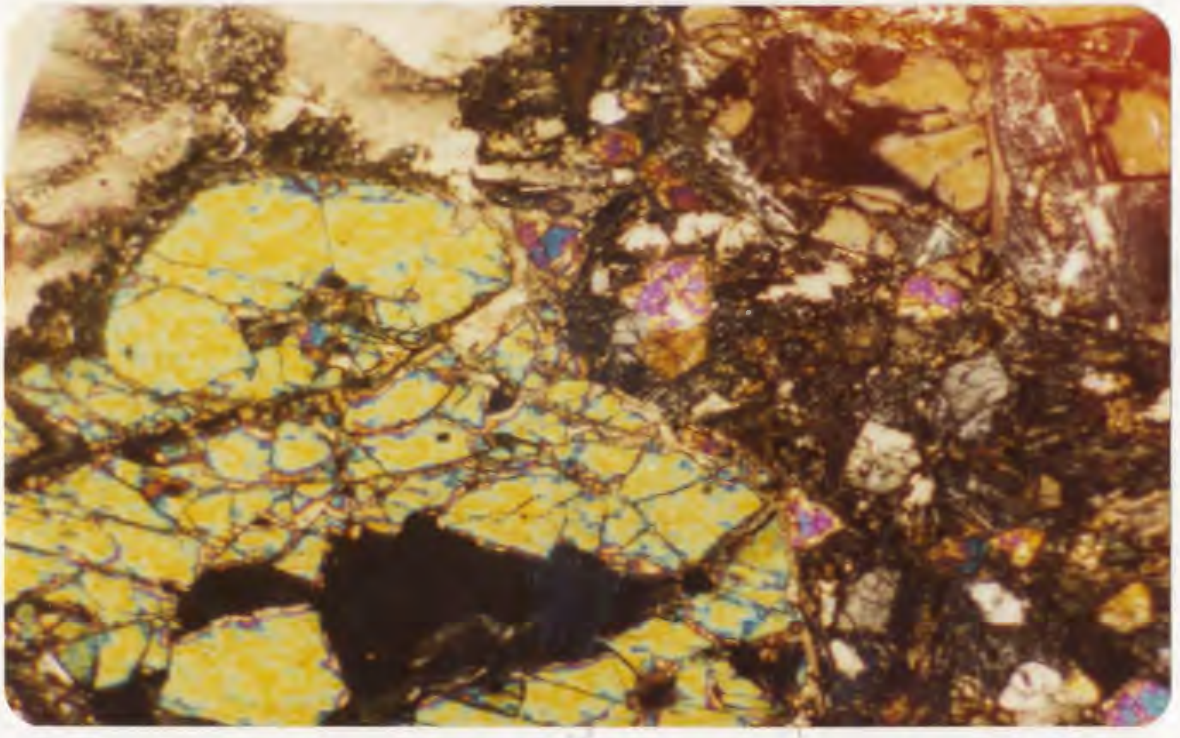

Plate 17: Ultrabasic rock. Vitrophyric texture. Fresh olivine with corroded core; note orthopyroxene and clinopyroxene microphenocrysts and carbonate in matrix. DL-36. XN. 31X.

parts of individual pillows. In the present study this hyalopilitic zone is considered fundamental, and rocks with a glassy groundmass are deemed to form a genetically distinct group. They are also found to be considerably richer in magnesium than rocks with non-quenched, intersertal textures, and thus represent products of a rapidly cooled Mg-rich magma. Quench textures often pervade to the cores of pillows and are highly reminiscent of those described from basaltic komatiitic lavas of Precambrian and Paleozoic age (e.g., Arndt et al., 1977). Rocks in this study which fit this description will subsequently be referred to as komatiitic lavas, or simply komatiites, which includes all the olivine basalts which display a glassy character both in the field and in thin section. This group so defined, then, is roughly equivalent to the rocks defined by Smewing as having a hyalopilitic rim. Where Smewing categorizes them as including all four textural types (Table III.2), the present author considers that the majority of specimens assigned to this group have vitrophyric, hyalopilitic or variolitic texture. Specimens collected from the centres of pillows rarely showed intersertal texture; variolitic texture characterized by the presence of interstitial glass is most common. Vitrophyric samples can occasionally be recovered from the outermost selvedge of pillowed structures.

The more conventional olivine basalts stand in marked contrast to the types described above. The principal difference that immediately catches the eye is the intensity of alteration of both phenocrysts and groundmass within these rocks. Their principal textural type is intersertal, and variolitic textures contain no intersertal wedges of glass.

A separate section will be devoted to the comparison of the present quenched rocks to documented komatiites, and to the geochemical corroboration of the distinction made here between the two Mg-rich lava types. The present purpose is to describe the petrography of the rocks.

III.2.3.2 Komatiitic Lavas

The komatiitic lavas are characterized by their very fresh condition and the well-preserved nature of both phenocryst and matrix phases. The rocks display hyalopilitic, variolitic, and rarely, intersertal and vitrophyric textures. Hyalopilitic types contain phenocrysts of olivine ($Fo_{88.9-89.6}$) and orthopyroxene ($En_{87.9}$) and microlites of subcalcic augite and pigeonite set in a glassy groundmass (Plates 18-24). Olivine forms euhedral phenocrysts which reach 2.4 mm and average 0.4 mm at their long dimension. They are occasionally completely fresh but more often occur as euhedral skeletal forms in which alteration has attacked the interior of the grains along fracture planes. Antigorite is the common alteration product although some iron oxide is present along fractures.

The character of the pyroxenes is significantly different from that of olivine in that grains have developed forms and shapes indicative of rapid quenching. Orthopyroxene is the earliest pyroxene to nucleate as it forms stubby uniform grains averaging about 0.5 mm in length. Occasionally it attains an attenuate or acicular habit, more akin to that of the clinopyroxenes. Some grains have developed a mantle of clinopyroxene which presumably represents a lower temperature reaction of Mg - Fe pyroxene with a liquid enriched in calcium.

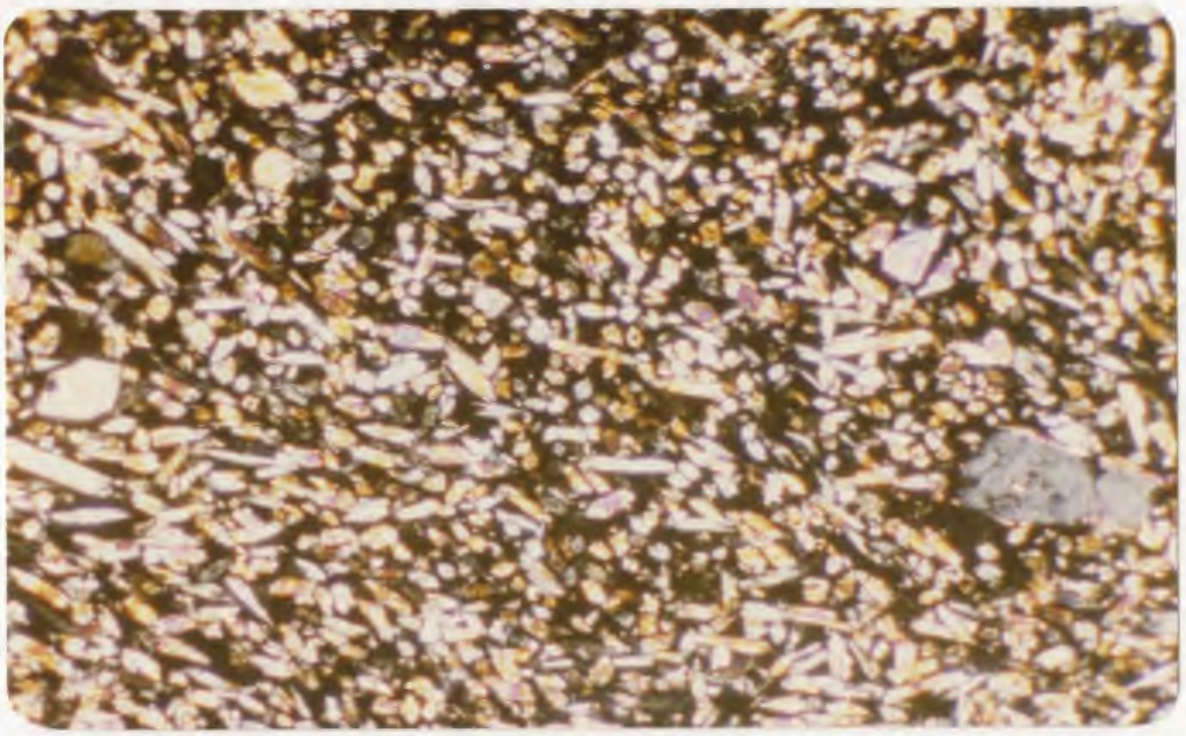

Plate 18: Komatiite. Hyalopilitic texture. Euhedral olivine, quenched clinopyroxene forms; large stubby orthopyroxene grains mantled by clinopyroxene. Glass matrix. KL-18. XN. 31X.

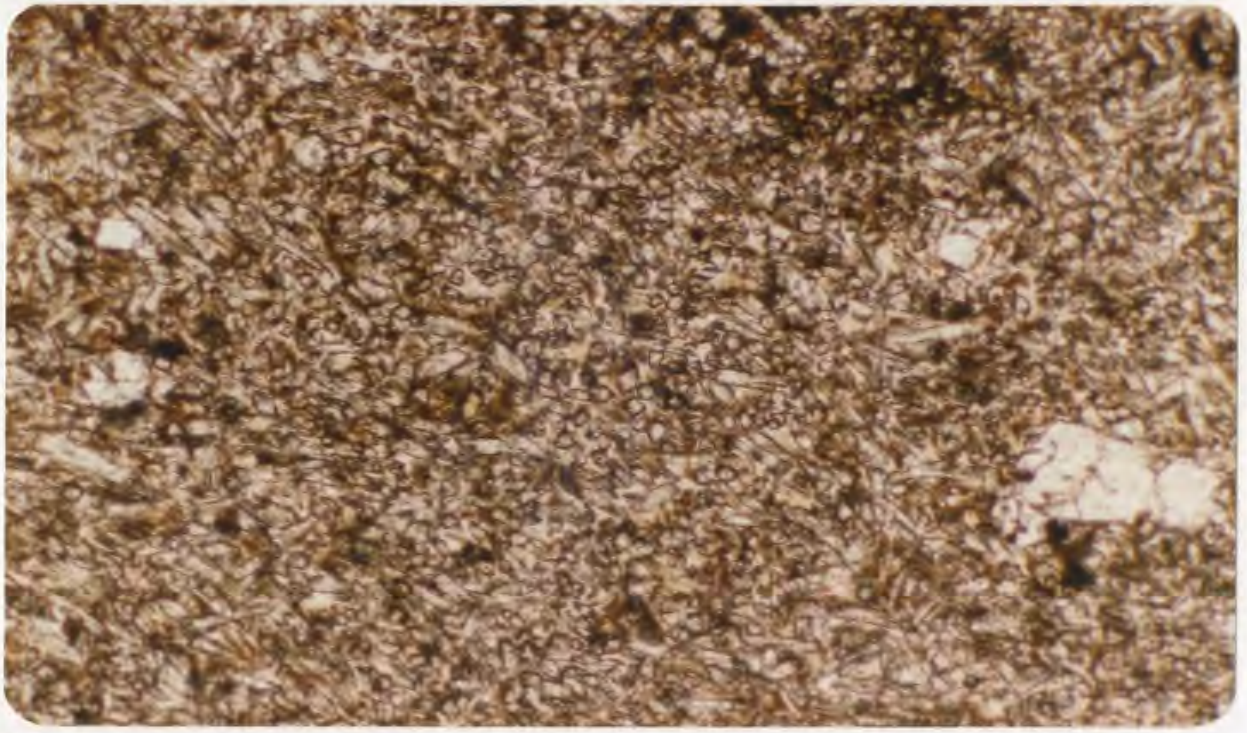

Plate 19: As above, PPL.

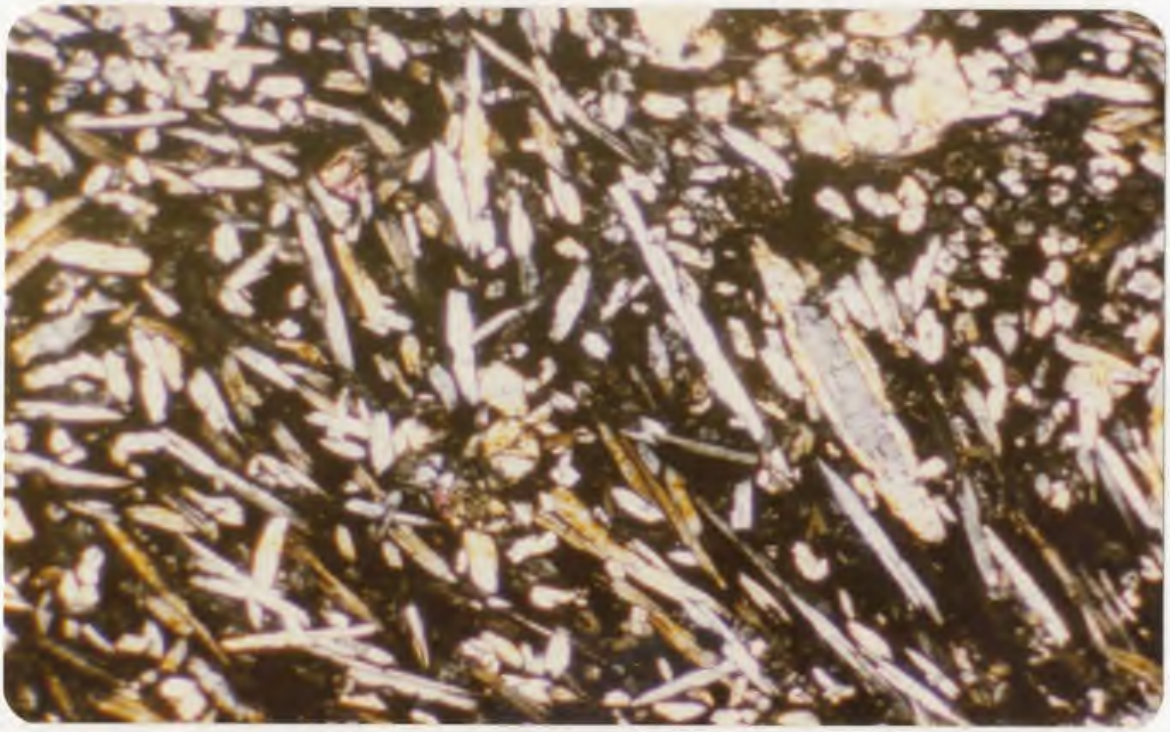

Plate 20: Komatiite. Hyalopilitic texture. Acicular clinopyroxene with sub-parallel disposition; stubbier orthopyroxene mantled by clinopyroxene; corroded olivine grains. KL-34. XN. 31X.

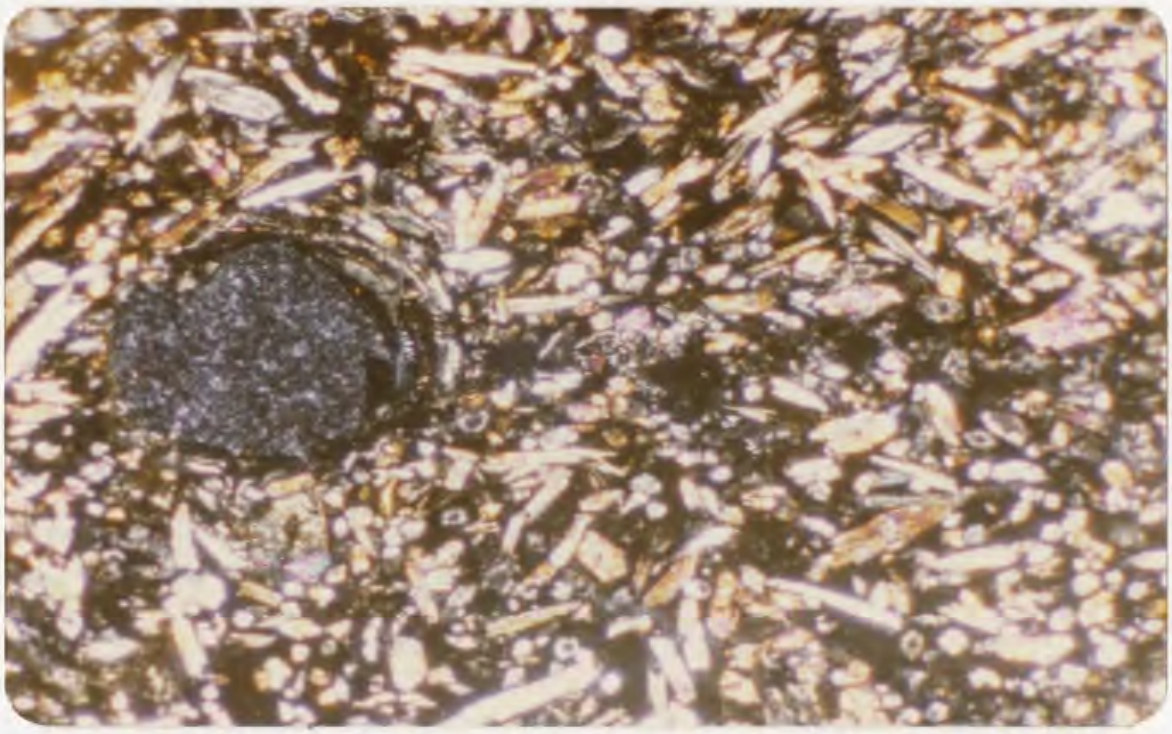

Plate 21: Komatiite. Hyalopilitic texture. Fluxioning of pyroxene grains around amygdale. KL-33. XN. 31X.

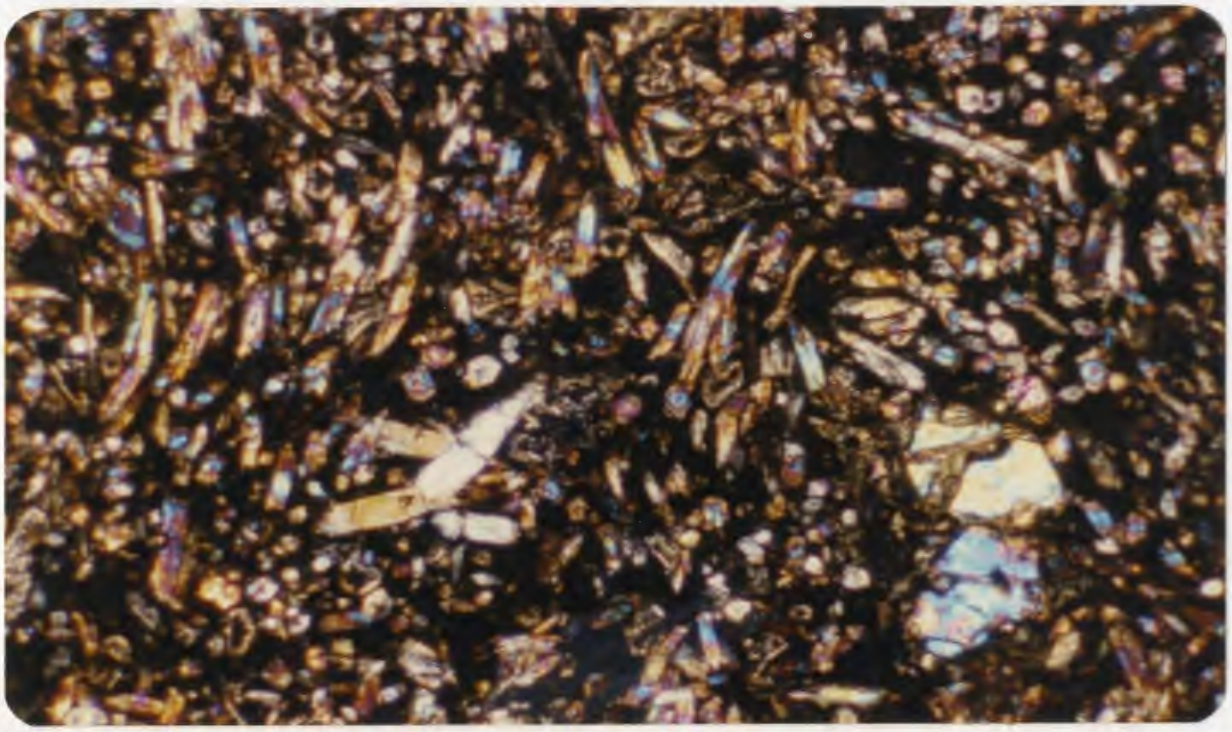

Plate 22: Komatiite. Hyalopilitic texture. Zoned subcalcic augites/pigeonites. Olivine and orthopyroxene also present. KL-33. XN. 31X.

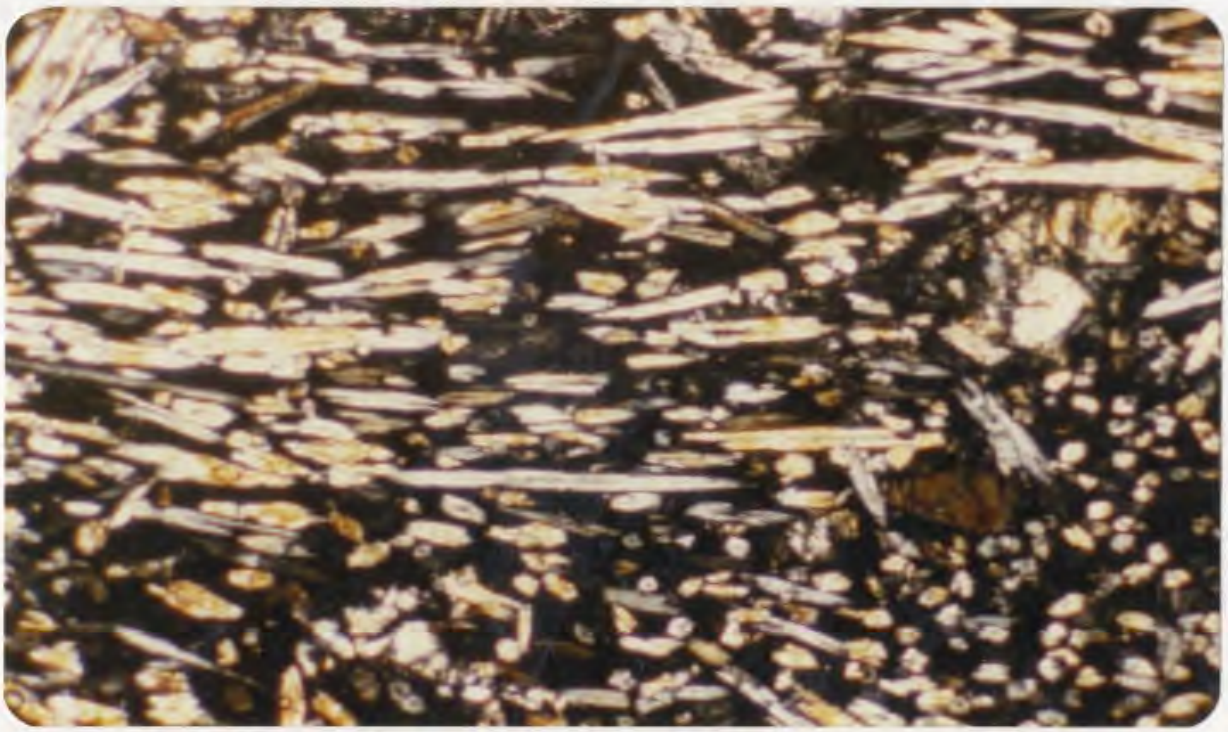

Plate 23: Komatiite. Hyalopilitic texture. Acicular and swallow-forms of clinopyroxene; marked fluxioning seen both parallel and perpendicular to long axes of grains. KL-34. XN. 31X.

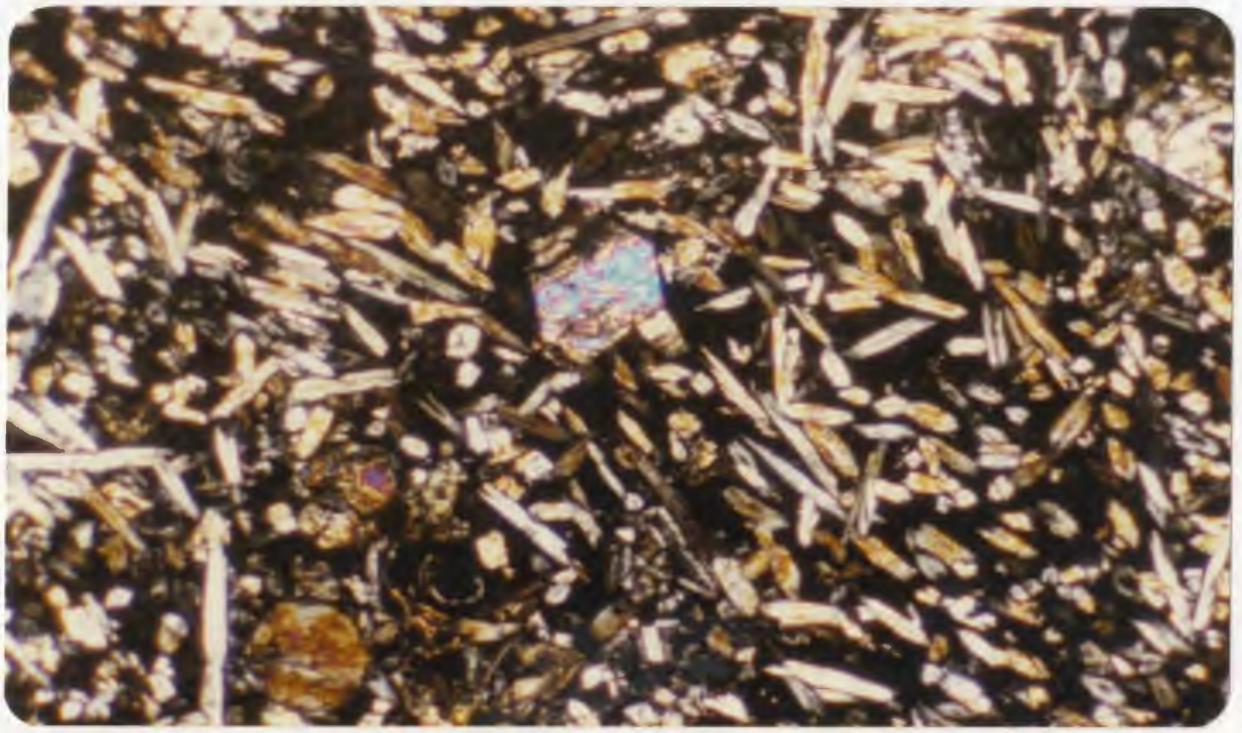

Plate 24. Komatiite. Hyalopilitic texture. Euhedral olivine phenocrysts. KL-34. XN. 31X.

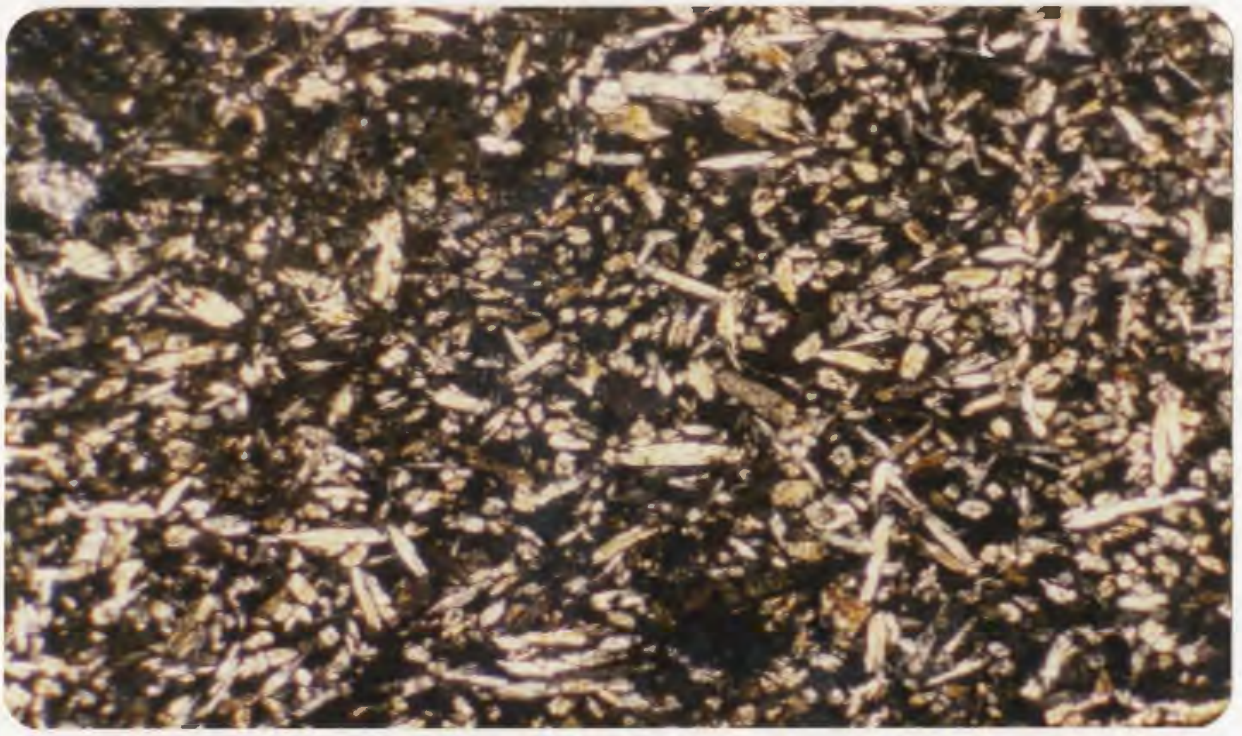

Plate 25. Komatiite. Transitional between hyalopilitic and variolitic zones of pillow. KL-53. XN. 31X.

Augite ($Ca_{26.6-42.6}$) is the most common monoclinic pyroxene in the rock. Subcalcic augite ($Ca_{20.8-21.3}$) and the high temperature form pigeonite ($Ca_{3.4-12.7}$) are present in subsidiary amounts, and are difficult to separate under the microscope. The absence of exsolved augite lamellae in orthopyroxene, diagnostic of inverted pigeonite, suggests a rapid cooling history for these rocks.

The calcic pyroxenes are collectively characterized by their relatively fine-grained (0.2 - 0.4 mm) and quenched aspect, i.e., 'swallowtail', and occasionally, hourglass structure. Irregular compositional zoning is discernible under crossed nicols and has been verified by microprobe analyses (see Chapter V).

The great variety of shapes of monoclinic pyroxenes in thin section is attributed to their random orientations which theoretically produces a infinite variety of cross sections. These pyroxenes in the hyalopilitic texture can therefore take the form of equant hexagonal or diamond-shaped basal grains with corroded cores, lenticular-acicular grains with irregular terminations and narrow central corrosion/resorption zones, or any variation in between (see Plate 22). Corroded cores of grains are always connected to the groundmass by minute cracks disposed along cleavage planes; these cracks may have acted as miniature conduits along which lower temperature liquids could react with cores formed at higher temperatures.

In the well-developed hyalopilitic specimens grains of like disposition tend to aggregate and form iso-oriented clusters (Plate 23). Where these grains are oriented parallel to the section they define a fluxion texture which clearly bends around phenocrysts and amygdules.

The compositions of ortho- and clinopyroxenes of the groundmass have been studied extensively under the microprobe. This mineral chemistry will be discussed in a later chapter; the microprobe work has been referenced here to support and facilitate the petrographic description of the rocks.

Pyroxenes of the variolitic textured-basalts differ markedly from those of the hyalopilitic basalts; they characteristically form highly skeletal or acicular grains which may congregate in radial growths (Plates 25-32). Average lengths are of the order of 1 - 1.2 mm but occasionally lengths up to 2 mm are attained. In most sections studied dendritic, plumose or sheaflike varieties are present, and in the better-developed specimens (e.g., DL-24, Plate 31) these grains form 'vertebrae' structures. The difference between this and the hyalopilitic texture is best seen by comparing Plates 18 and 26.

Olivine and orthopyroxene are considerably less abundant within rocks with this texture; olivine tends to form skeletal grains altered to antigorite and iron oxide. Glass also forms a smaller proportion of the rock, mainly due to the interlocking mesh of pyroxene forms. A higher susceptibility to alteration is characteristic of this texture.

Opaques are very sparse in all the olivine-phyric rocks. Minute (0.1 -0.2 mm) grains of chromite occur in clusters or as inclusions within larger pyroxene grains, and constitute a very small proportion of the groundmass.

Near the edge of pillows hyalopilitic texture grades outward into vitrophyric texture with a decrease in crystalline pyroxene as a constituent of the groundmass. Near the centres of larger pillows vario-

Plate 26: Komatiite. Variolitic texture. Plumose and fine-grained 'vertebrae' forms of clinopyroxene; large olivine phenocryst. KL-12. XN. 31X.

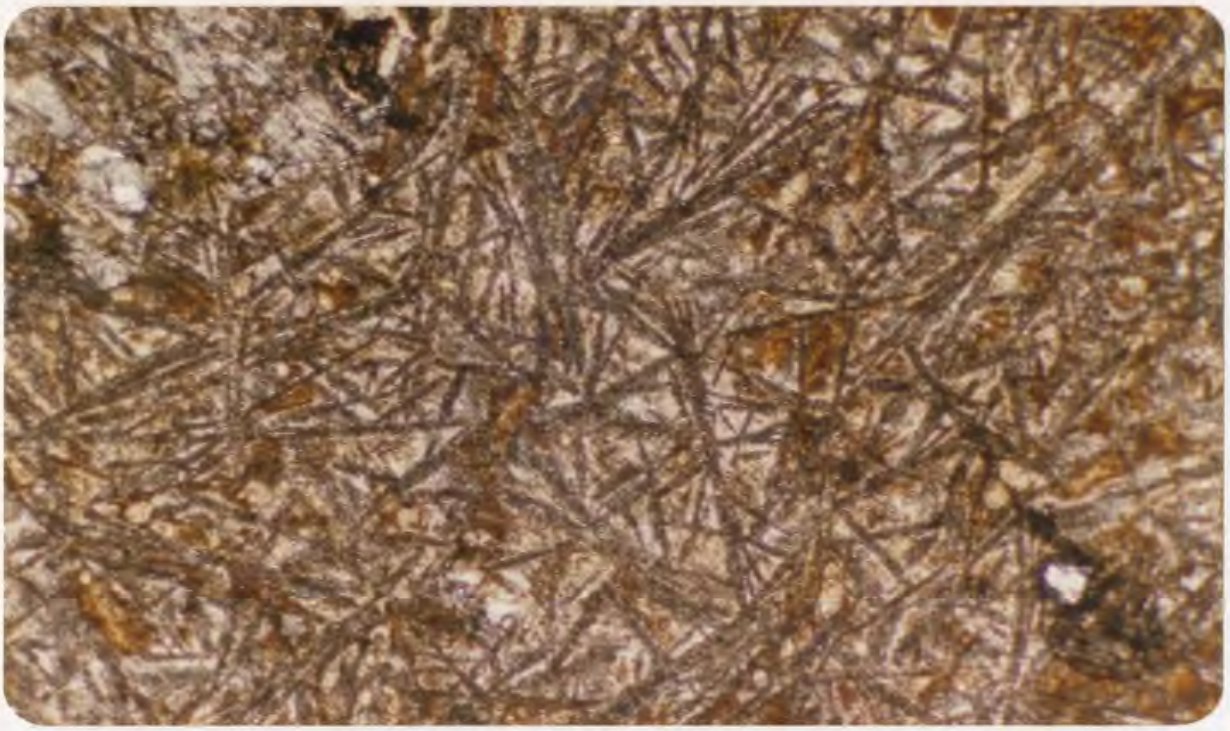

Plate 27: As above, PPL.

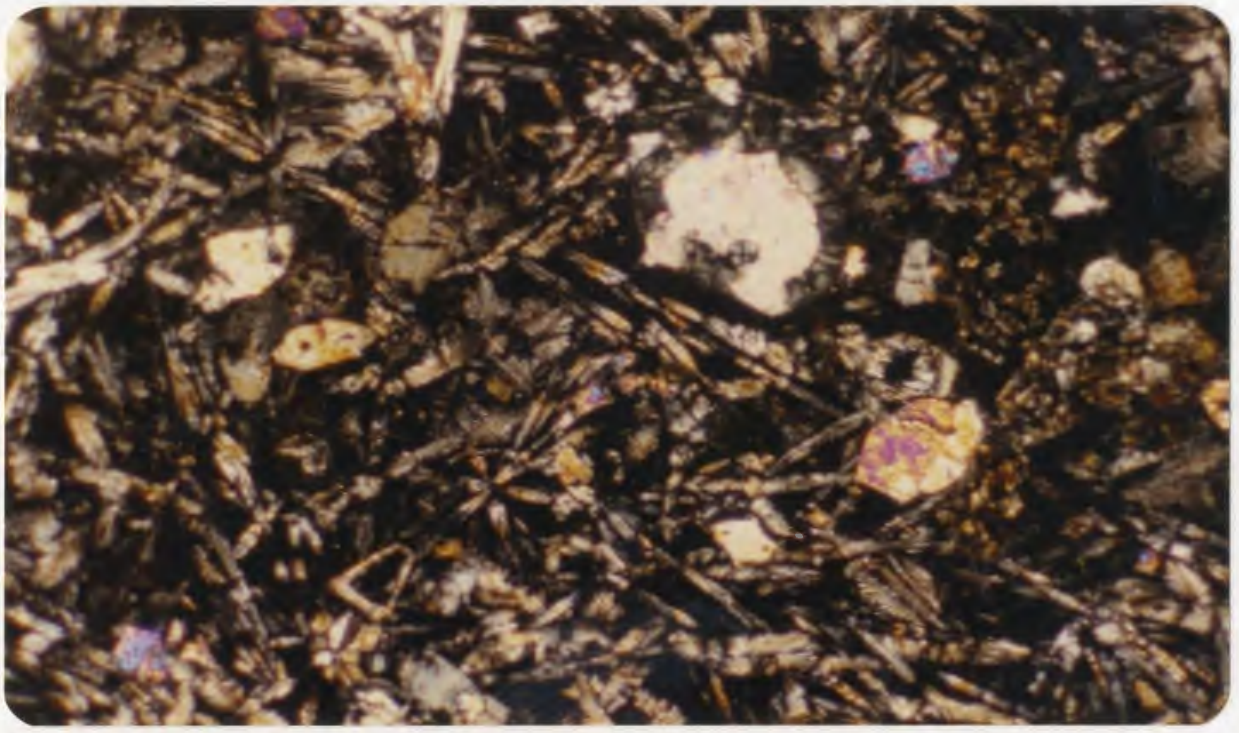

Plate 28: Komatiite. Texture intermediate between hyalopilitic and variolitic textures; note radial development of clinopyroxene grains. KL-77. XN. 31X.

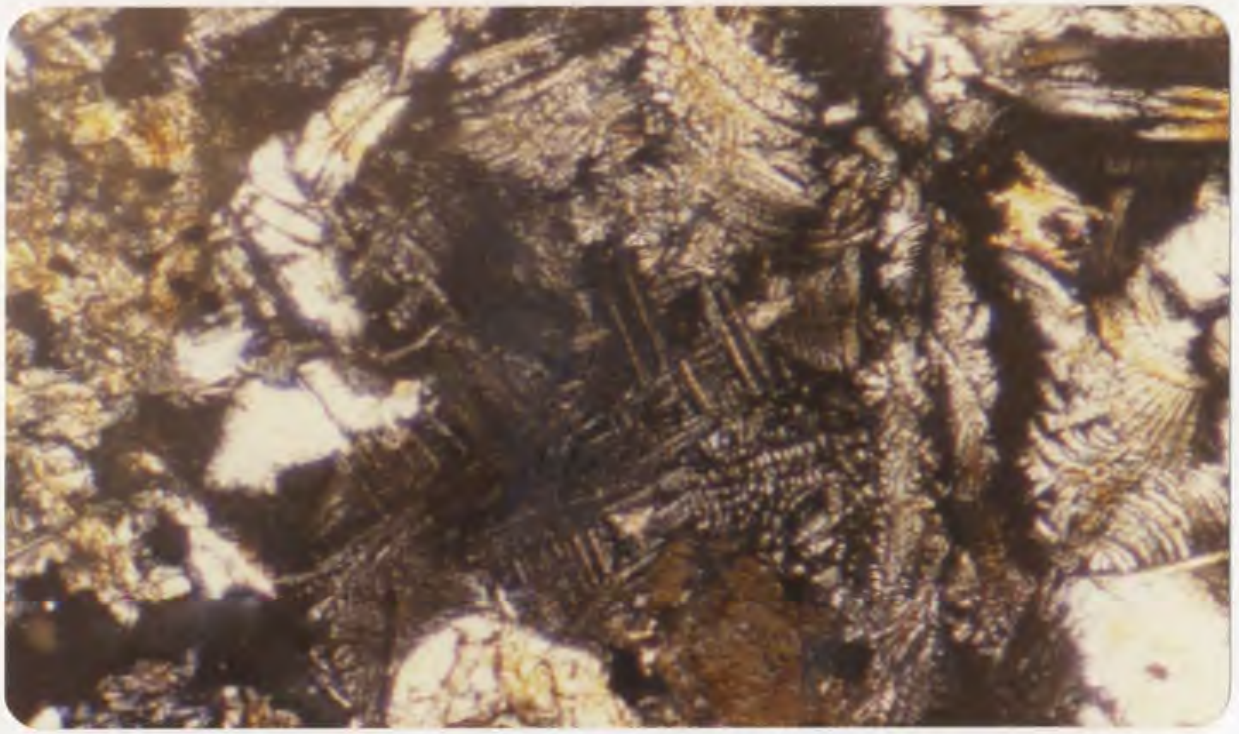

Plate 29: Komatiite. Same section as above at 125X. Shows incipient crystallization of groundmass clinopyroxene and possibly plagioclase. KL-77. XN.

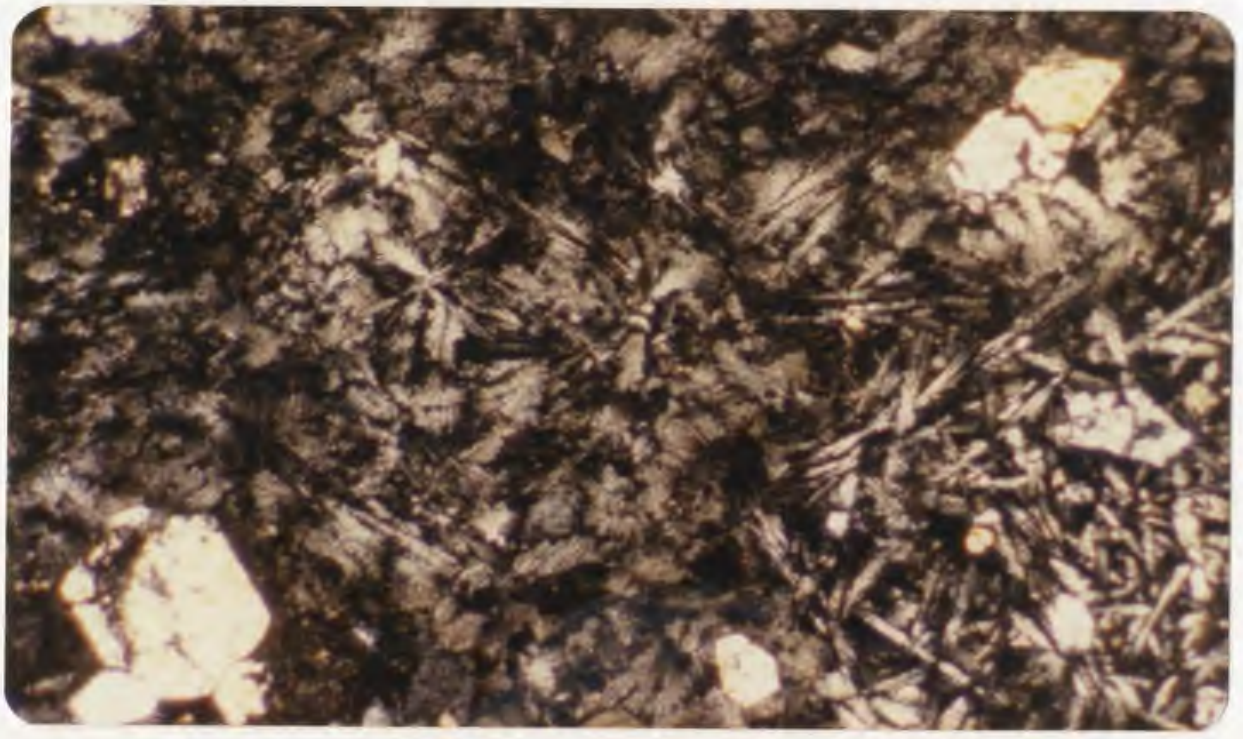

Plate 30: Komatiite. Intermediate hyalopilitic-variolitic texture. Note incipient crystallization of glass. KL-70. XN. 31X.

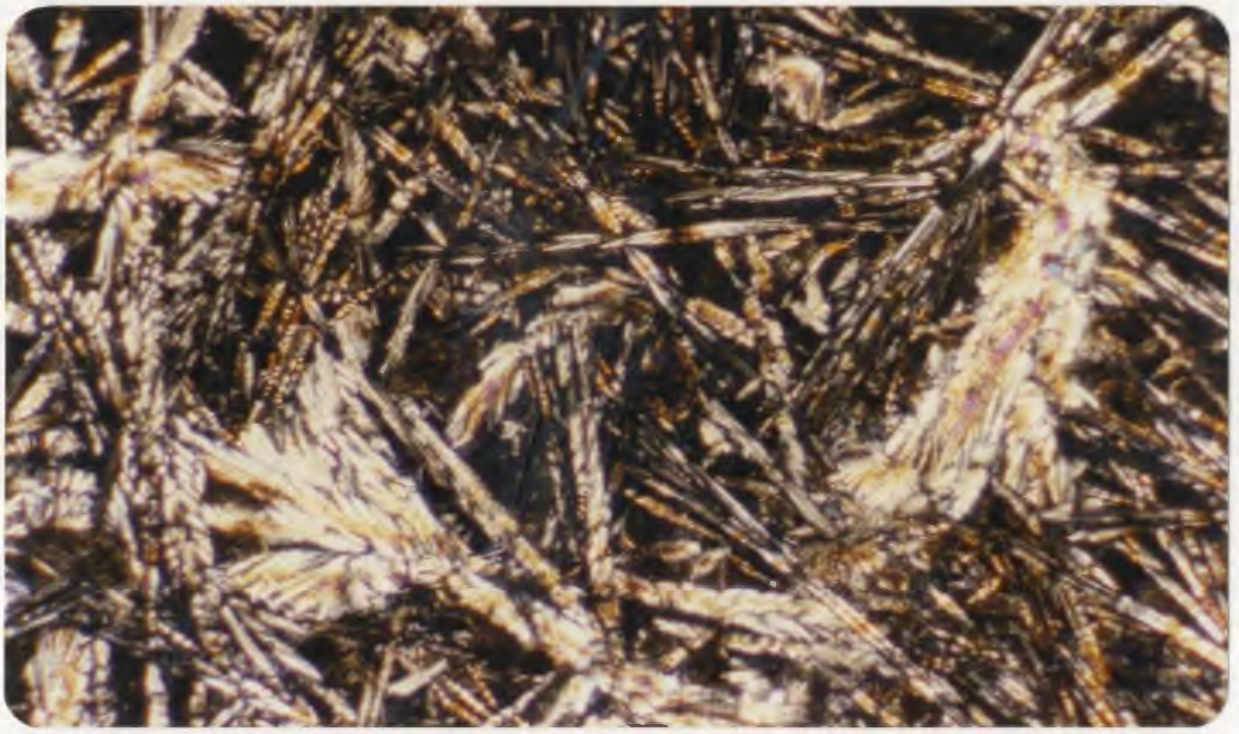

Plate 31: Komatiite. Variolitic texture; plumose and acicular pyroxene forms. DL-24. XN. 31X.

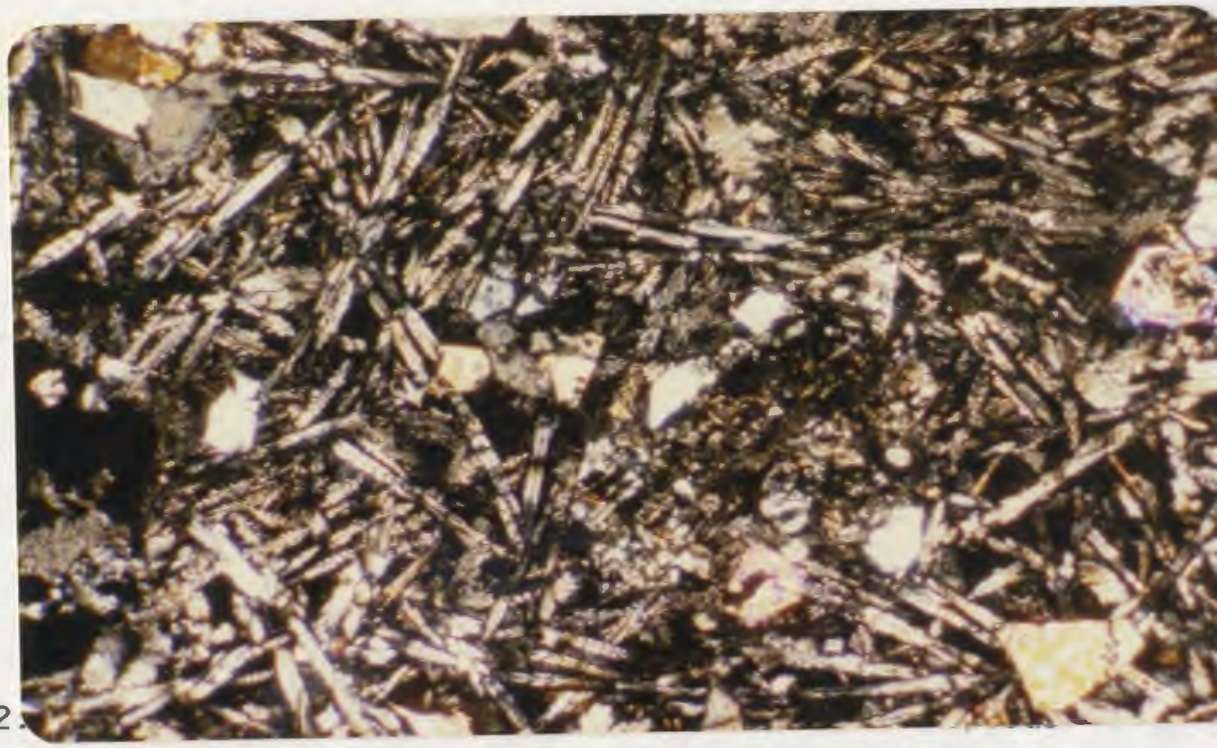

Plate 32. olivine and orthopyroxene phenocrysts. Skeletal, acicular clinopyroxene forms. KL-77. XN. 31X.

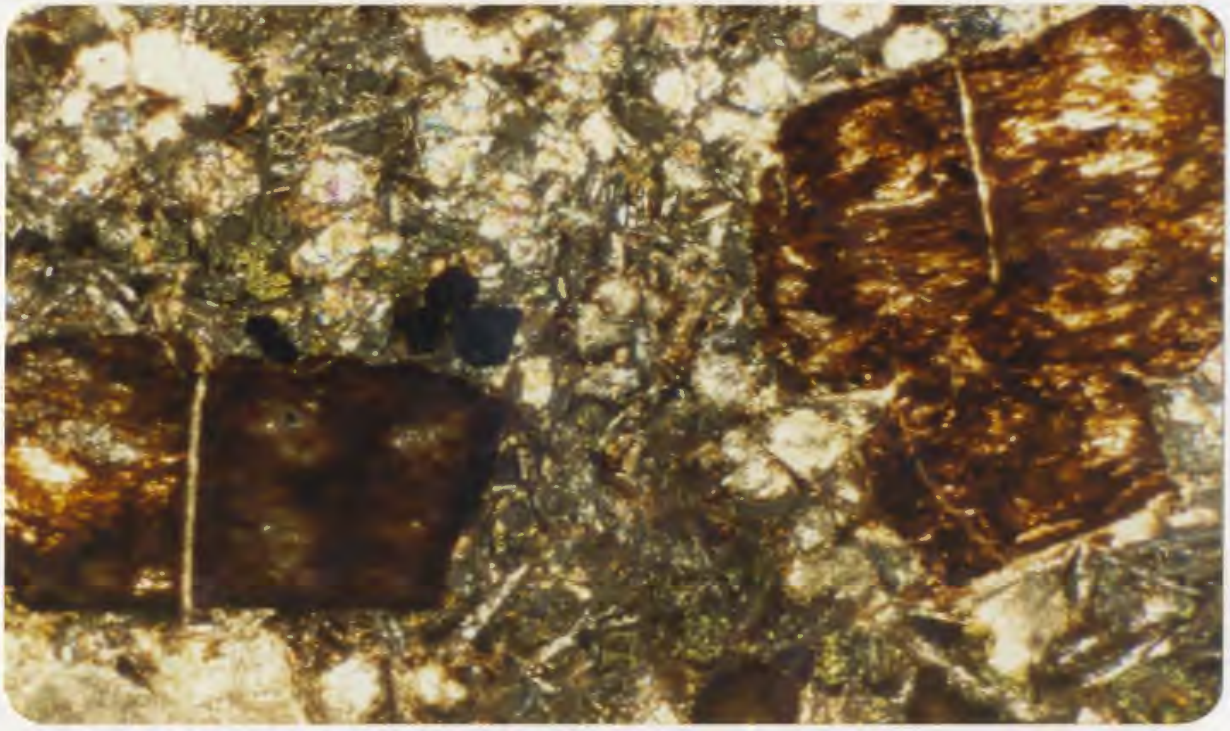

Plate 33. Olivine basalt. Large olivine phenocrysts pseudomorphed by iron oxide. Abundant clinopyroxene microphenocrysts. Groundmass intensely altered to smectite. KL-104. XN. 31X.

litic texture tends to grade inward towards intersertal, although this was not found to be anywhere well-developed.

The exclusive occurrence of olivine as a phenocryst phase, and clinopyroxene as a groundmass phase has genetic implications which will be briefly discussed here. Olivine is always in an unquenched state and can be allocated to the pre-eruptive or intratelluric stage of the magma, i.e., olivine had begun to crystallize, presumably in a magma chamber, prior to extrusion and experienced little or no post-extrusive growth. There is clearly a continuum from obviously accumulative rocks to true liquids, and the degree to which the porphyritic rocks are accumulative is in some cases, difficult to ascertain, and has consequences for the interpretation of major element geochemistry. Growth of clinopyroxene, however, is restricted to the extrusion stage, where rapid cooling produced an uninverted pigeonite/sub-calcic augite assemblage. Orthopyroxene may occupy an intermediate genetic position; nucleation and growth had been initiated in the intratelluric stage as some large grains display the typical chunky form of orthopyroxene. Others, however, show the quenched form noted for the monoclinic pyroxenes, and could only have formed after lava extrusion.

III.2.3.3 Olivine basalts

Almost without exception these rocks in thin section are more intensely altered than the quenched lavas. The great majority of specimens reveal a groundmass completely and penetratively altered to an assemblage of hematite, fibrous zeolites, and patches of carbonate. A few fresh specimens enable description of the primary texture of the rock, but even in the freshest specimens olivine phenocrysts are totally pseudomorphed by hematite or calcite.

Representative photographs of olivine basalts are contained in Plates 33-37. The most notable digression from the komatiitic types is

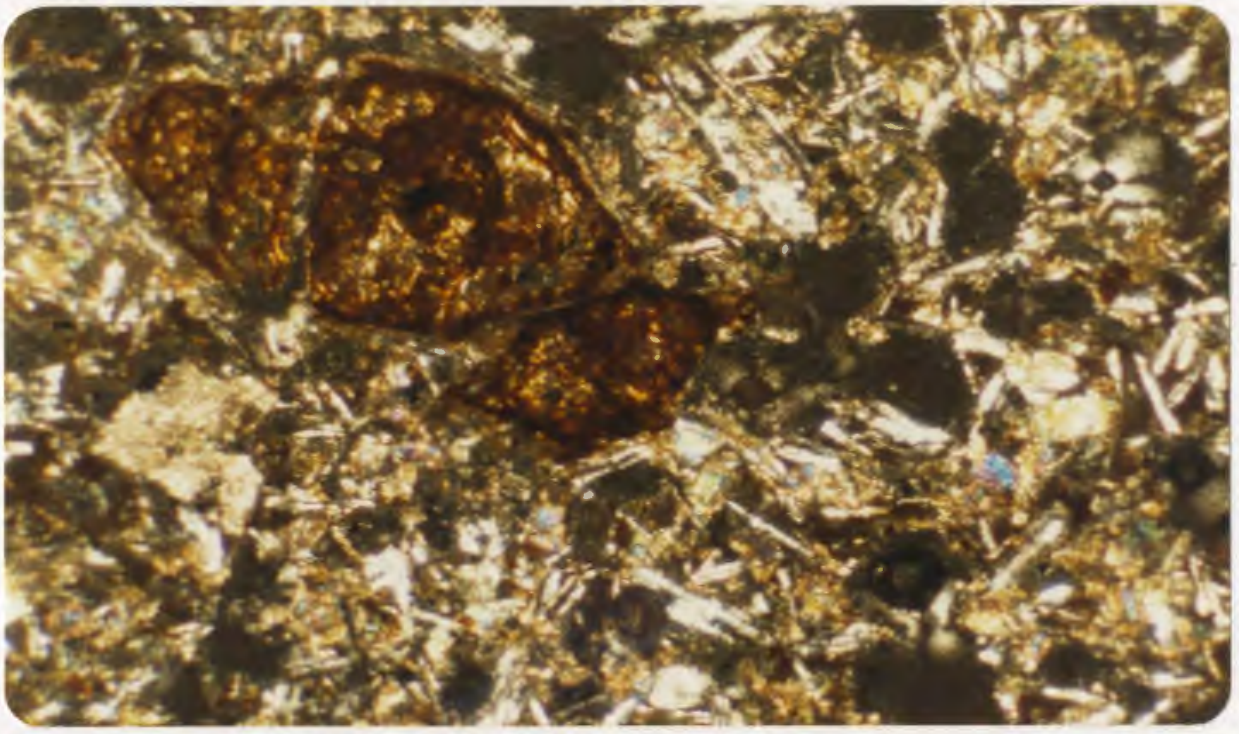

Plate 34: Olivine basalt. Intersertal texture; vesicular.
DL-31. XN. 31X.

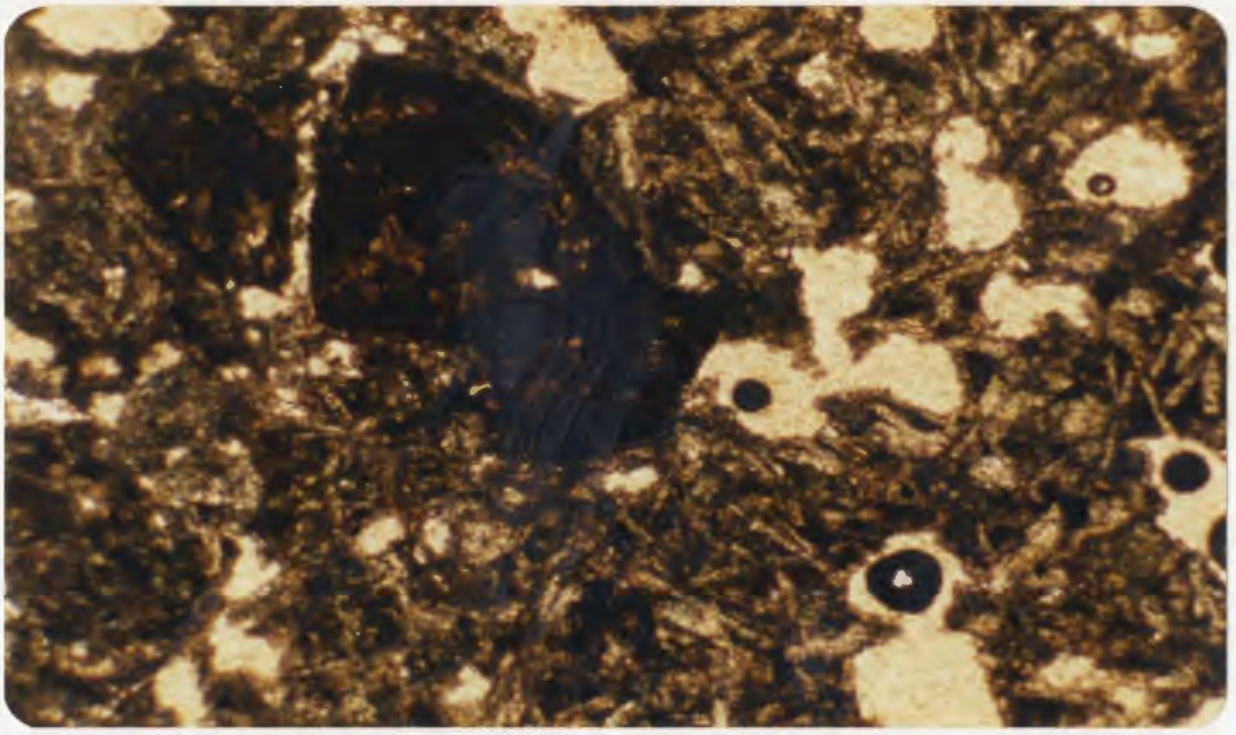

Plate 35: As above, PPL.

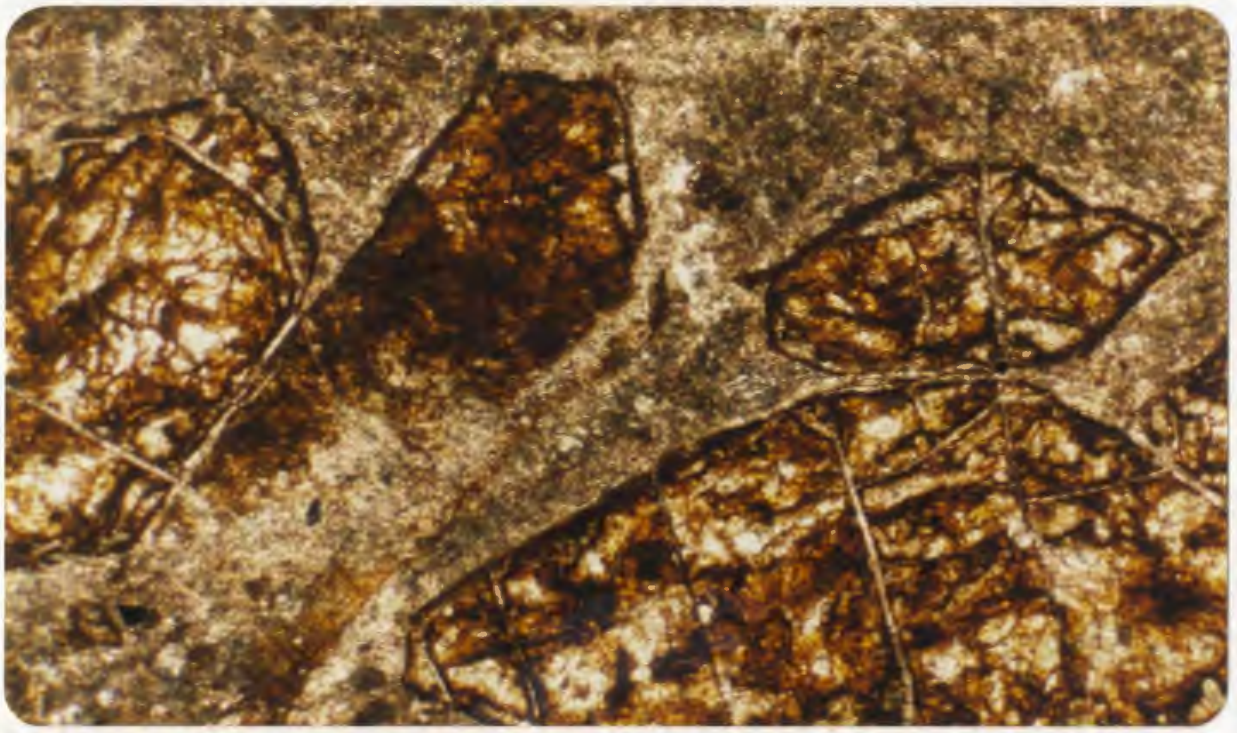

Plate 36: Olivine basalt. Porphyritic texture; highly decomposed but good preservation of olivine forms. DL-58. PPL. 31X.

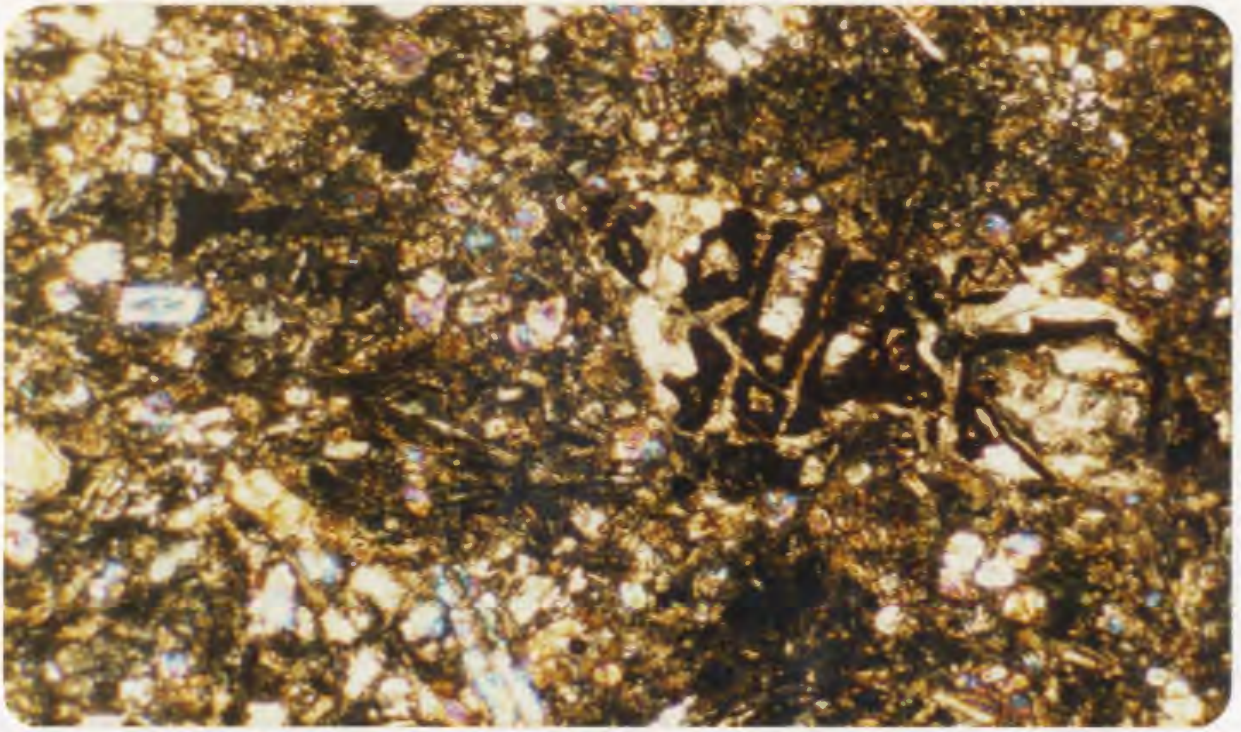

Plate 37: Olivine basalt. Pseudomorphed olivine grains; copious fresh cpx grains. Highly altered groundmass. PL-34. XN. 31X.

the absence of quench textures and the consequent appearance of plagioclase as a crystalline phase in the groundmass. Equigranular clinopyroxene and plagioclase average 0.2 mm in size. The occurrence of deuteric material and opaques in the interstices defines an intersertal texture. Clinopyroxene ranges from groundmass size up to microphenocrysts of 1.6 mm diameter. Such grains are always fresh, even in the more altered rocks, and tend to form glomeroporphyritic clusters.

Pseudomorphs after olivine form 0.4 - 2.6 mm grains. In some of the fresher specimens orthopyroxene is recognizable as small grains which occasionally are mantled by clinopyroxene.

In the outer parts of olivine basalt pillows variolitic texture is suggested by the radial arrangement of pyroxenes. A gradual decrease in grain size is encountered from core to margin of pillows.

III.2.4 Aphyric Lavas

This type of basalt forms both pillows and massive flows throughout the area. The rocks are thoroughly crystalline and display intersertal or intergranular texture. Small patches of variolitic texture can occasionally be found near vesicles, where faster cooling could occur. These rocks differ from the more mafic lavas in the absence both of olivine phenocrysts and a glassy mesostasis. Microphenocrysts of clinopyroxene are very common and range from groundmass size (0.1 mm) up to 1.5 mm. Plagioclase normally forms laths in the groundmass ($\sim$0.4 mm) but occasionally occurs as microphenocrysts which reach 1.6 mm in length. Minute euhedra of magnetite generally constitute less than 5% of the rock

and average 0.02 mm in diameter. A complete modal analysis is included in Table III.1. Plates 38-46 contain photomicrographs of these rocks.

A ubiquitous feature of this group of rocks is their intense and pervasive alteration. Celadonite is a common deuteric mineral, occurring as bright green patches replacing pyroxene or in amygdules. In many sections hematite has almost completely obfuscated the primary textures. Fine-grained pyroxene and magnetite are the phases most commonly affected by hematization. Many thin sections examined consisted only of secondary carbonates, zeolites and clay minerals. In some of the rare fresh specimens the primary intergranular/intersertal texture can be observed. Occasionally clinopyroxene microphenocrysts are absent and fluxioned plagioclase laths of uniform size define a pilotaxitic texture.

Fine and coarser-grained types occur within the succession. At the base of the Upper Pillow Lavas a fine-grained unit (fine-grained basal lavas of Smewing, 1975) sporadically outcrops, which contains 0.1 - 0.2 mm grains of clinopyroxene and plagioclase with interstitial smectite. 1.2 - 1.3 mm clinopyroxene microphenocrysts are common. The succession also contains some coarser grained bodies which presumably were intruded at shallow depths into warm pillow lavas. These rocks may be aptly termed microgabbro and consist of 0.5 mm plagioclase and 0.4 mm pyroxene grains intergrown in an intergranular texture. Titanomagnetite is more common than within the fine-grained rocks. While pyroxene is similar in habit and abundance to its occurrence in fine-grained bodies, the increase in abundance and grain size of plagioclase is the most definitive aspect of this rock. Alteration is less intense than but

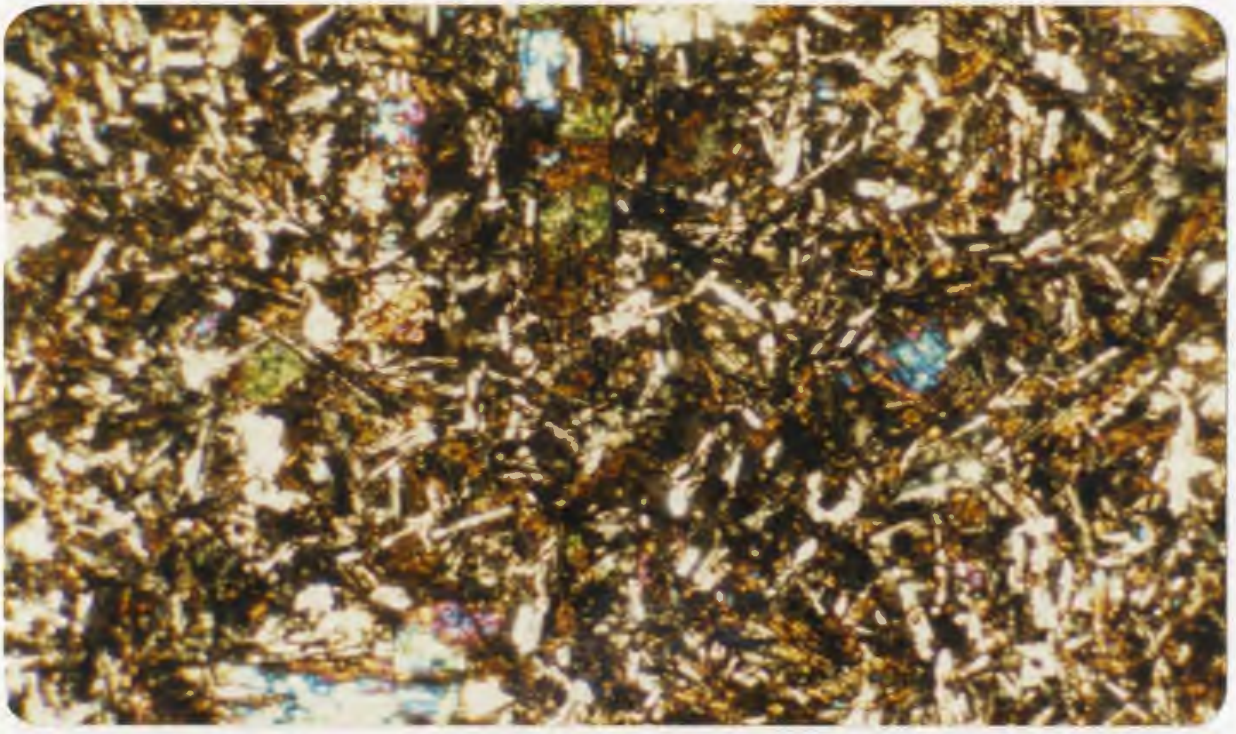

Plate 38: Aphyric basalt. Fresh clinopyroxene microphenocrysts partially replaced by green celadonite. KL-23. XN. 31X.

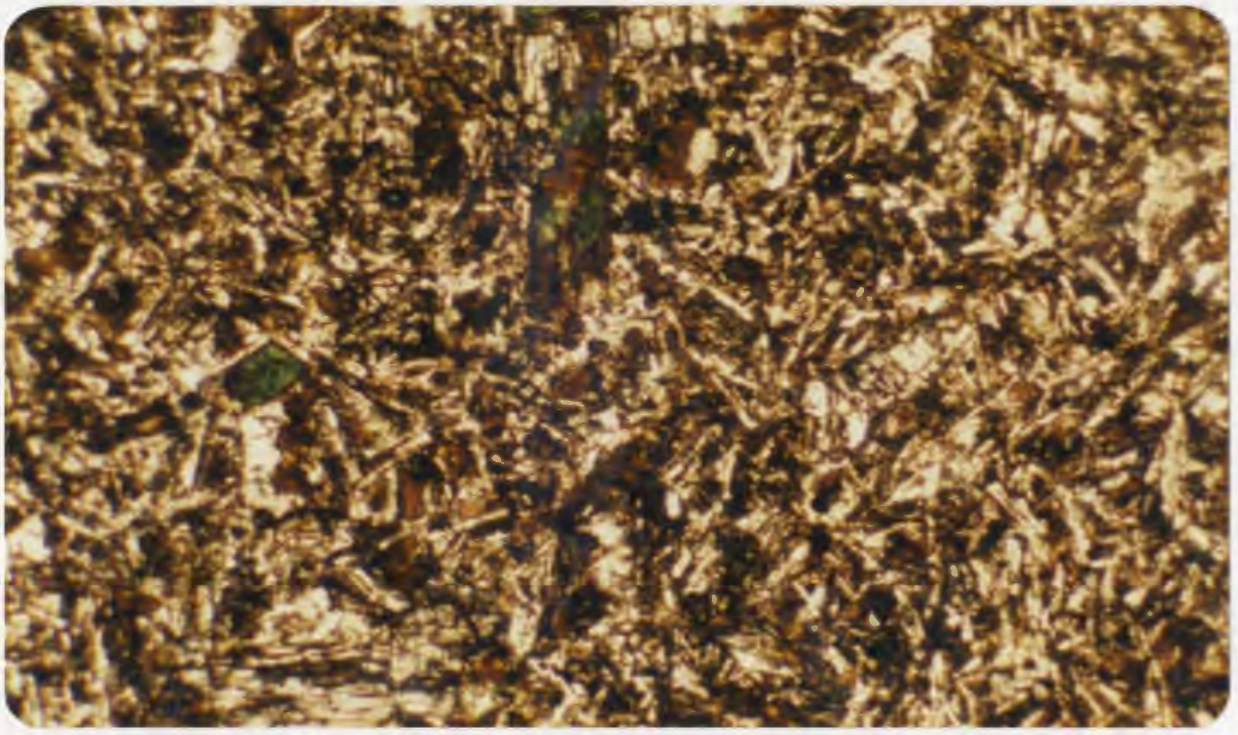

Plate 39: As above, PPL.

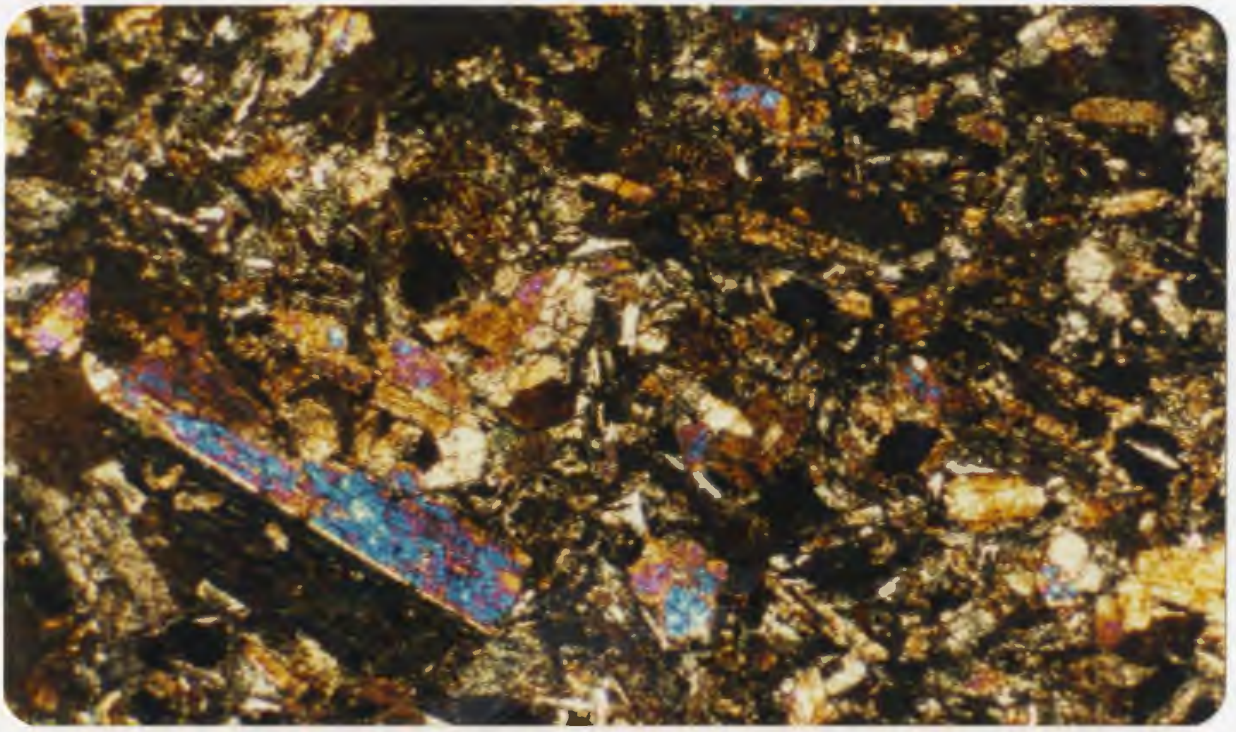

Plate 40: Aphyric basalt. Clinopyroxene microphenocrysts, some of which are twinned. Zeolitized groundmass. KL-51. XN. 31X.

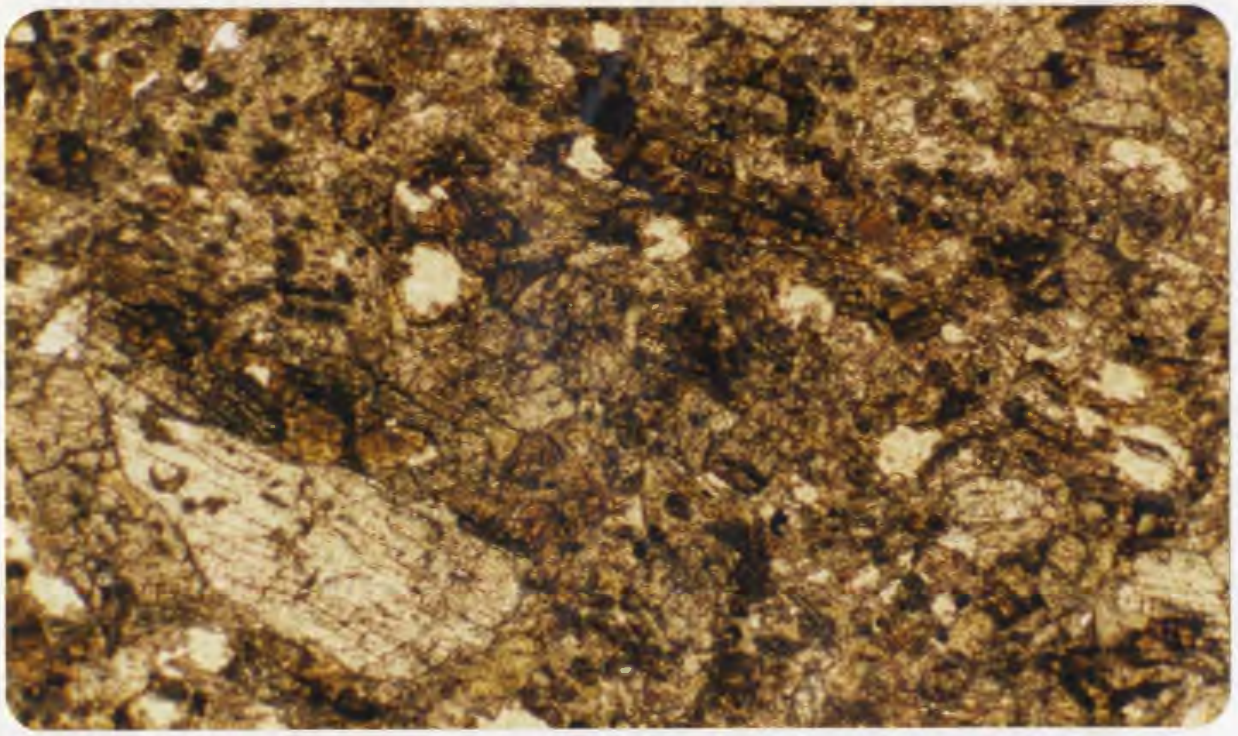

Plate 41: As above, PPL.

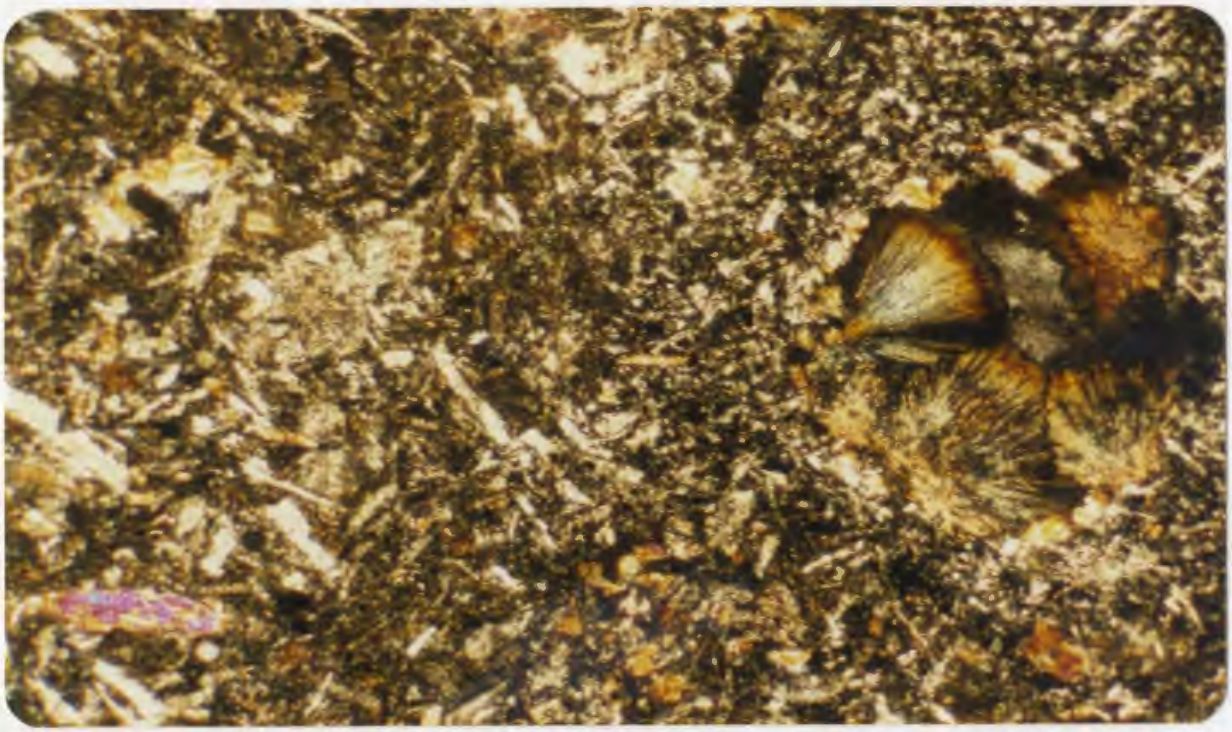

Plate 42: Aphyric basalt. Well developed zeolite mineral in amygdale. Groundmass altered to smectite. KL-122. XN. 31X.

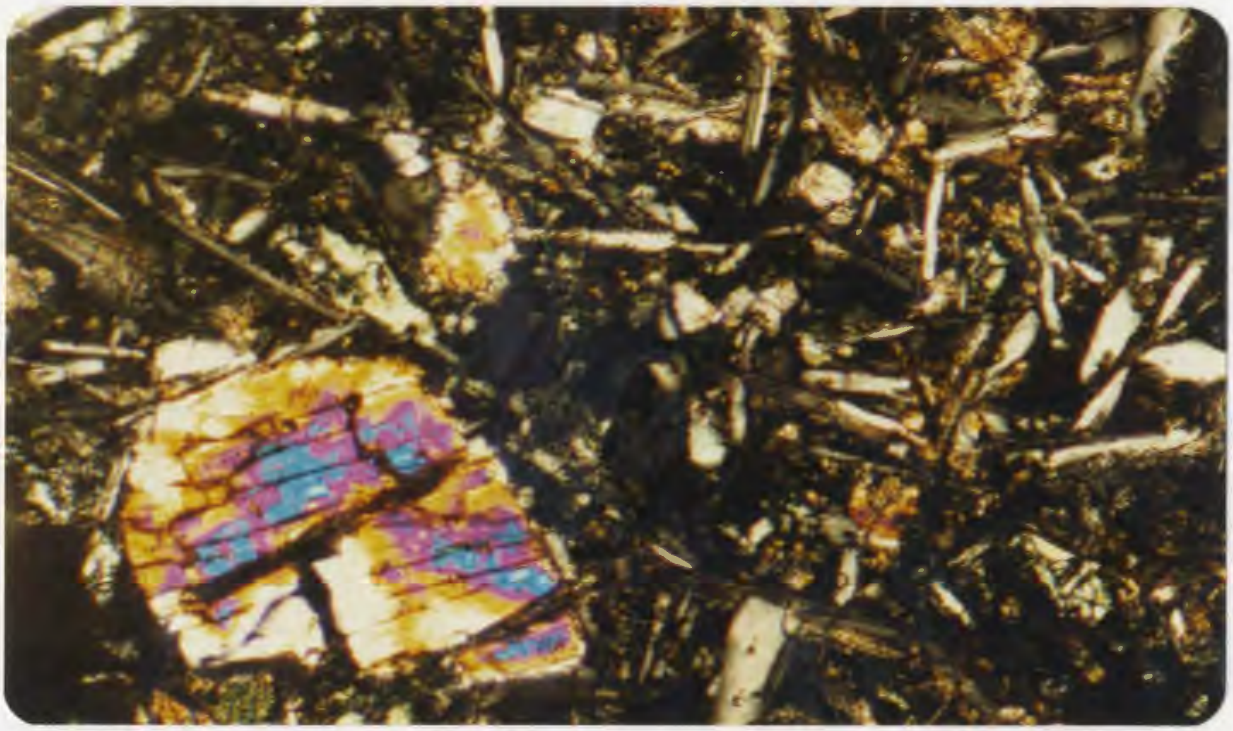

Plate 43: Aphyric basalt. Clinopyroxene microphenocryst, intersertal texture. PL-19. XN. 125X.

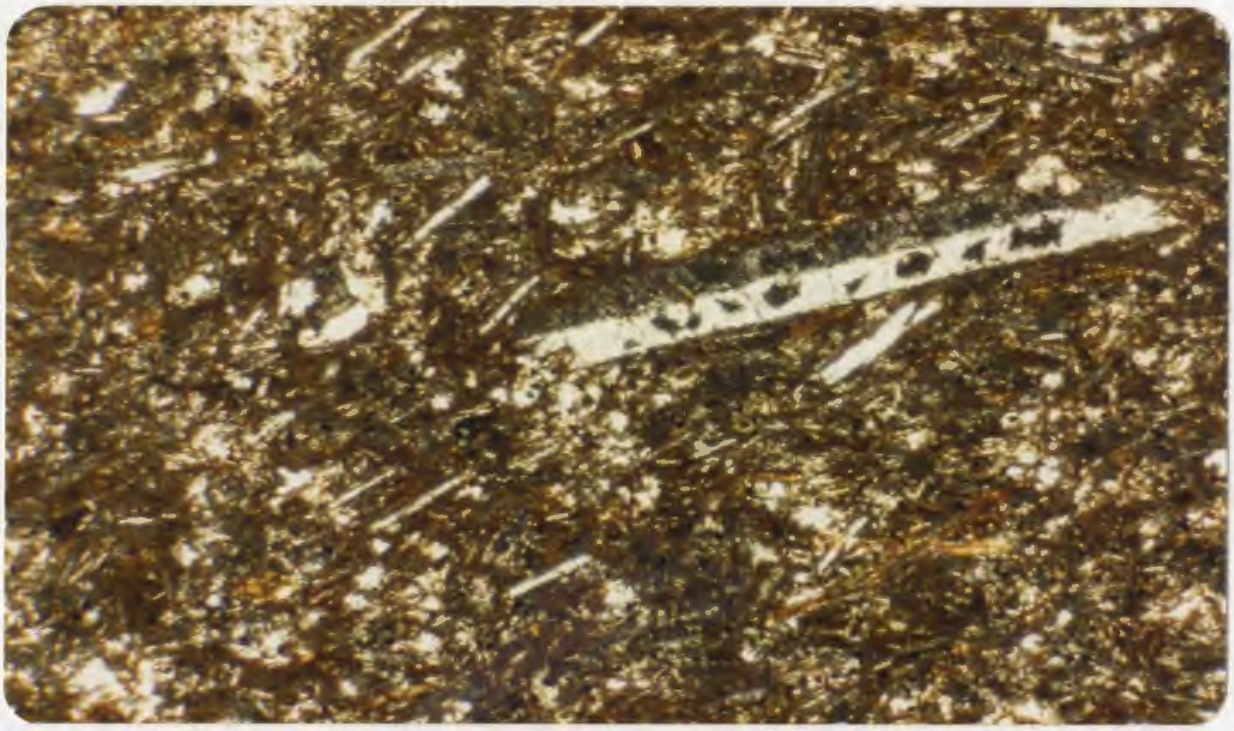

Plate 44: Aphyric basalt. Rare plagioclase phenocryst; fluxioned plagioclase laths in groundmass. KL-26. XN. 31X.

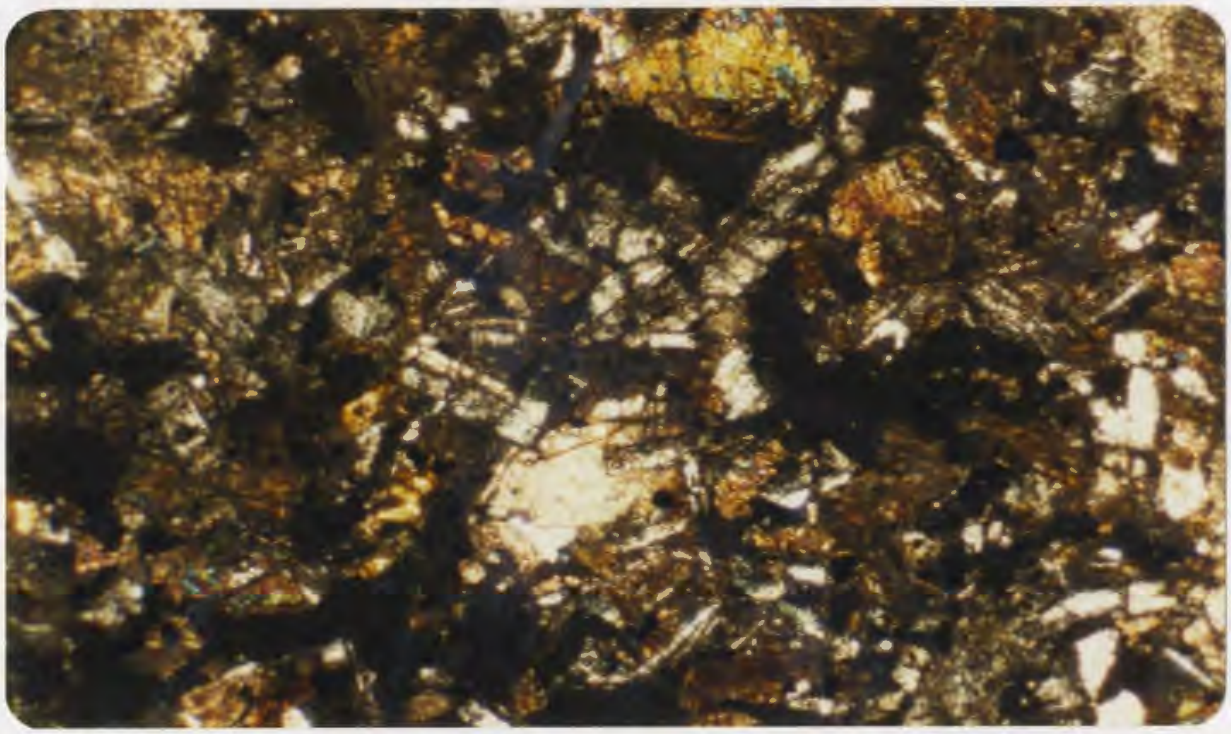

Plate 45: Microgabbro, from aphyric basalt unit. Sausseritized plagioclase; clinopyroxene replaced by iron oxide. KL-29. XN. 31X.

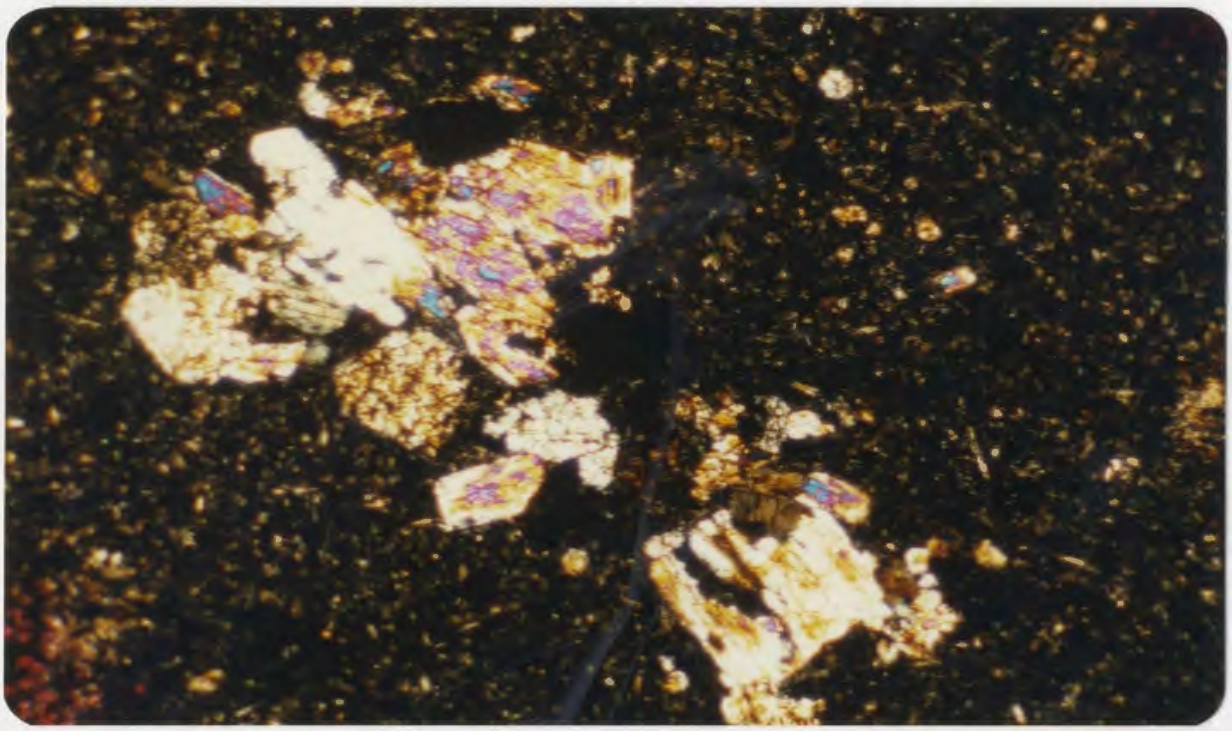

Plate 46: Fine grained basal lava. Clinopyroxene microphenocrysts; glomeroporphyritic texture.
KL-69. XN. 31X.

similar in nature to that described for finer-grained varieties; hematite pseudomorphs after clinopyroxene and smectite/calcite after plagioclase are typical.

III.2.5 Zeolite Mineralogy

The zeolite mineralogy of the whole volcanic sequence was studied in detail by Smewing (1975) and will be briefly reviewed here. Seven different species of zeolite have been identified by Smewing within the Upper Pillow Lava sequence. While gmelinite, natrolite and phillipsite are restricted to the Upper Pillow Lavas, these three, as well as analcime, chabazite, heulandite and stilbite have been identified in the uppermost Axis Sequence volcanics. Zeolite phase occurrence appears to be independant of stratigraphy; they occur generally in groups of two or three species throughout the succession, both as vesicle fillings and replacing fine-grained groundmass minerals. This diversity of zeolite mineralogy and the presence of smectite instead of the higher temperature albite as a replacement for plagioclase is conclusive evidence for widespread zeolite facies metamorphism (Smewing, 1975; Gass and Smewing, 1973).

IV. BULK ROCK GEOCHEMISTRY

IV.1 Introduction

Two hundred and fifty samples were collected from the Upper Pillow Lavas; a few were collected from the Lower Pillow Lavas near their contact with the Upper Pillow Lavas, although no attempt was made to sample the lower unit. The rock samples were examined in the laboratory for alteration and the inclusion of foreign material in veins and amygdales. One hundred and twenty of the freshest samples were selected for crushing and geochemical analyses of major and trace elements; determinations of iron oxidation state were carried out for all specimens.

C.I.P.W. normative calculations for all major element analyses were executed using the computer program of R. G. Cawthorn (unpub. document, Dept. of Geology, M.U.N.). A complete description of all analytical techniques is contained in Appendix A.

The major element analyses were examined for high contents of CaO and high Loss on Ignition values; these were taken to indicate inadvertent inclusion of calcite in the sample and the analysis was omitted from the final group of analyses used in this work. Analyses of the olivine and aphyric basalts which showed inordinately high K_2O at low TiO_2 contents were discarded as unreliable (greater than >2.55% U_2O).

An important consideration in selecting the final group of analyses for all rock types concerned was to attempt to represent uniformly the geographical distribution of the Upper Pillow Lavas. All rock specimens collected are plotted on the sample locality maps (Plates 1 -

3, back pocket); those used for geochemical analyses are thus indicated. All hydrous major element and trace element data, as well as normative mineral proportions, are presented in Appendix B.1.1. Data used in geochemical plots and calculations later in this study have been recalculated to 100% anhydrous.

IV.2 Variation Diagrams

The trace and major elements of the different rock types of the Upper Pillow Lavas have been plotted against MgO as a fractionation index (Figures IV.1 and IV.2). MgO is a more appropriate index than SiO_2 because of the tendancy toward silica metasomatism in some of the rocks, and because fractionation, as will be seen, is controlled by olivine. All analyses are recalculated to 100% anhydrous.

IV.2.1 Major Elements vs. MgO

The trends of major elements versus MgO are depicted in Figure IV.1. The plots also include olivine analyses from ultrabasic rocks to show the relationship between olivine composition and the different lava types. The field and petrographic distinction made between the different types of Upper Pillow Lava are suggested by the plots, primarily on the basis of MgO content alone. The ultrabasic rocks form a distinct group with MgO contents of 30 - 40%. Most of the major elements of the ultrabasic rocks show very small ranges against MgO; lime and silica show a wide scatter and probably indicate the effects of zeolite facies metamorphism. Alumina shows a very broad range and may reflect the varying amounts of plagioclase in the different ultrabasic rocks. The komatiites

FIGURE IV.1 Major elements vs. MgO. All analyses recalculated to 100% anhydrous.

★ olivine crystals (microprobe analyses)

■ ultrabasic rock

● komatiite

○ olivine basalt

□ aphyric basalt

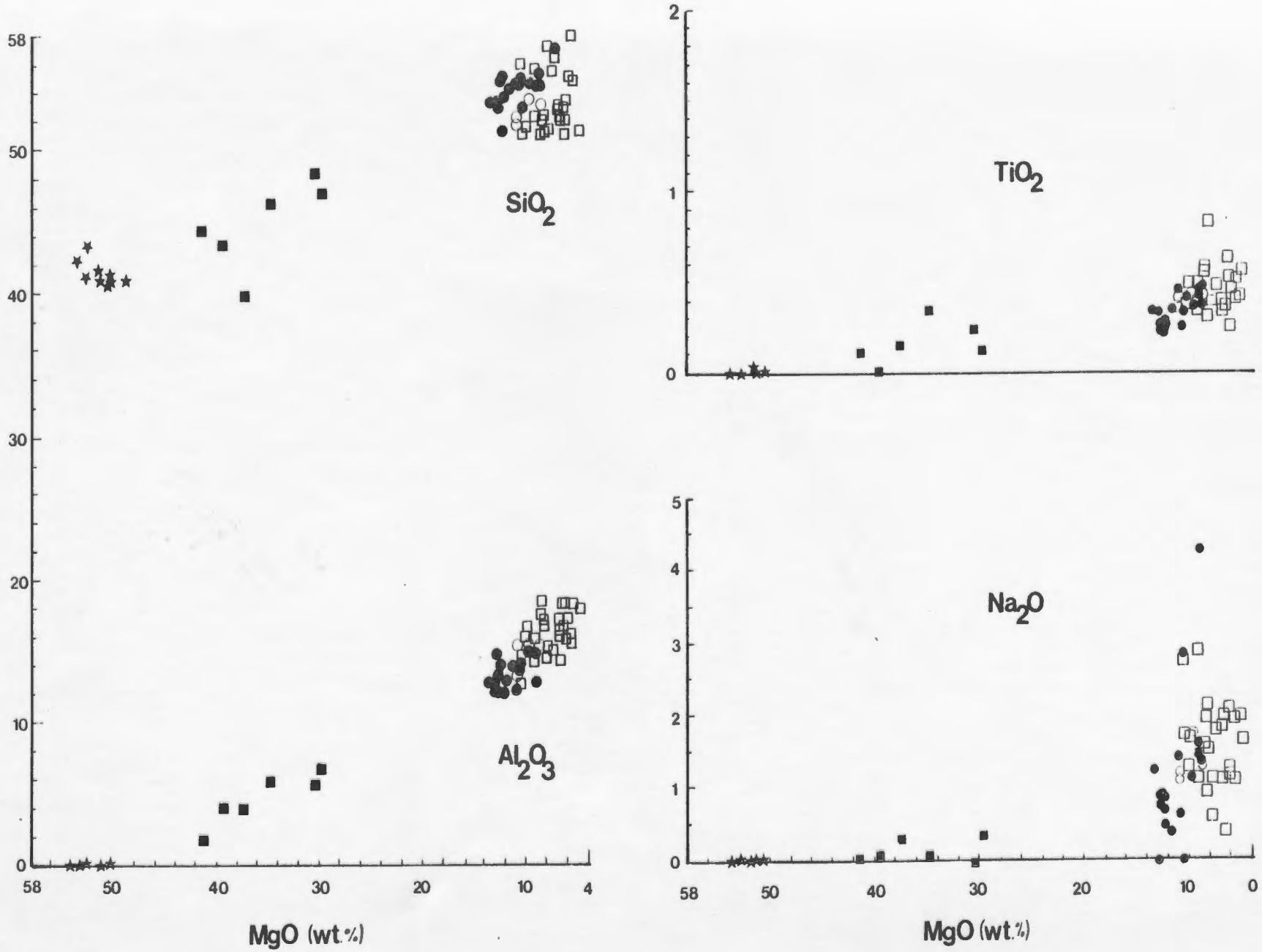
SiO2
TiO2
Al2O3
Na2O
MgO (wt.%)
MgO (wt.%)

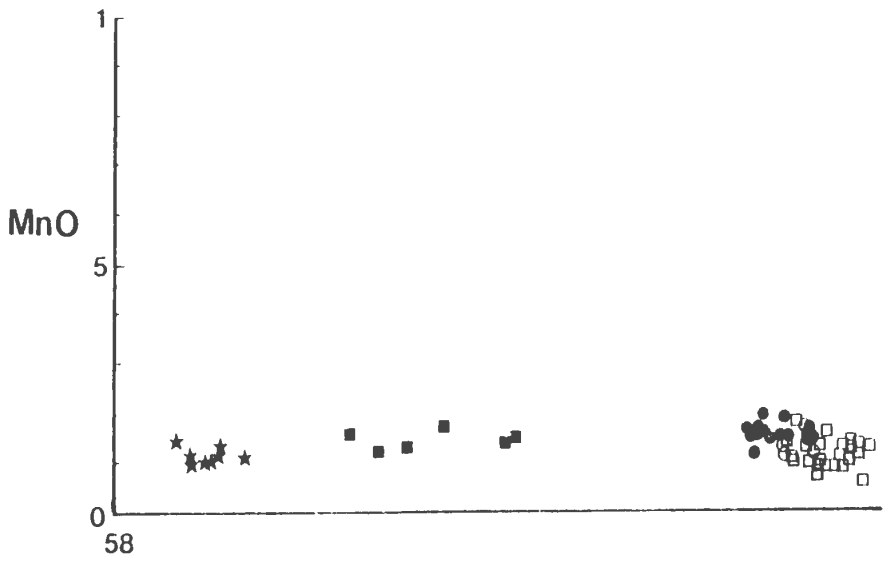
MnO
1
5
0
58

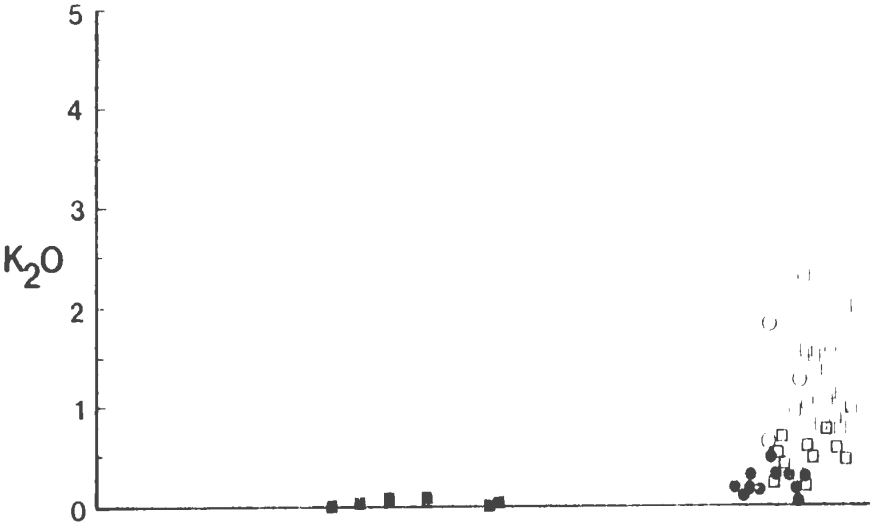
K_2O
5
4
3
2
1
0

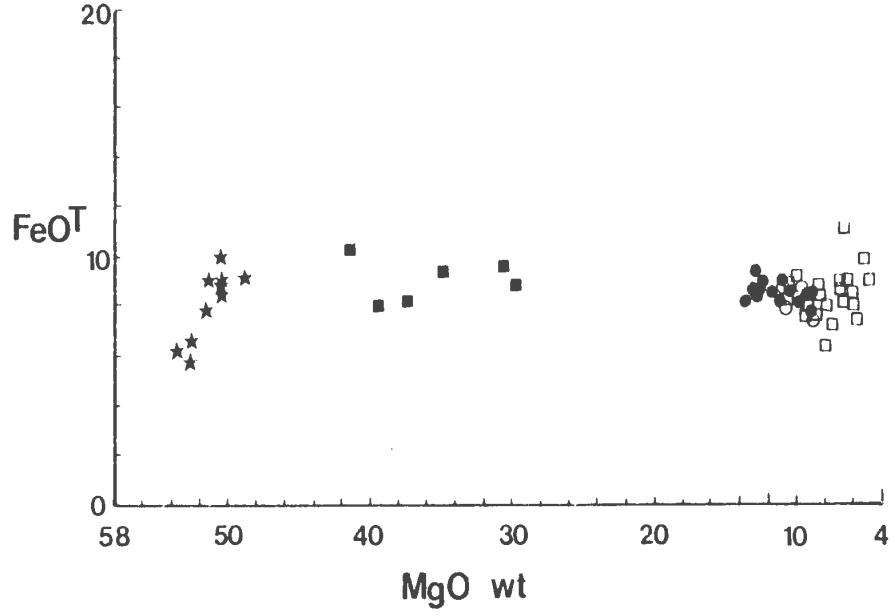
FeO^T
20
10
0
58
50
40
30
20
10
4
MgO wt

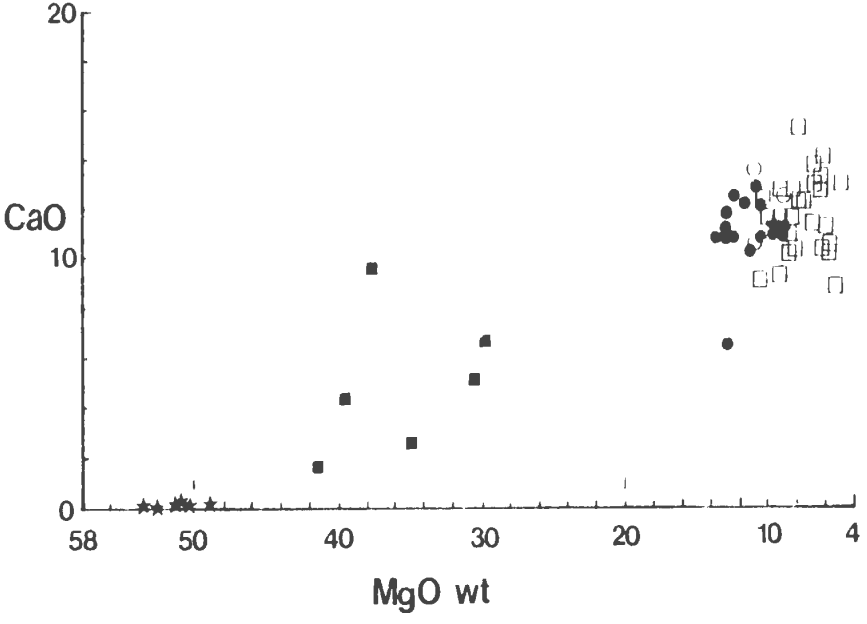
CaO
20
10
0
58
50
40
30
20
10
4
MgO wt

FIGURE IV.2 Trace elements vs. MgO. All trace element values measured in ppm. Symbols as in Figure IV.1.

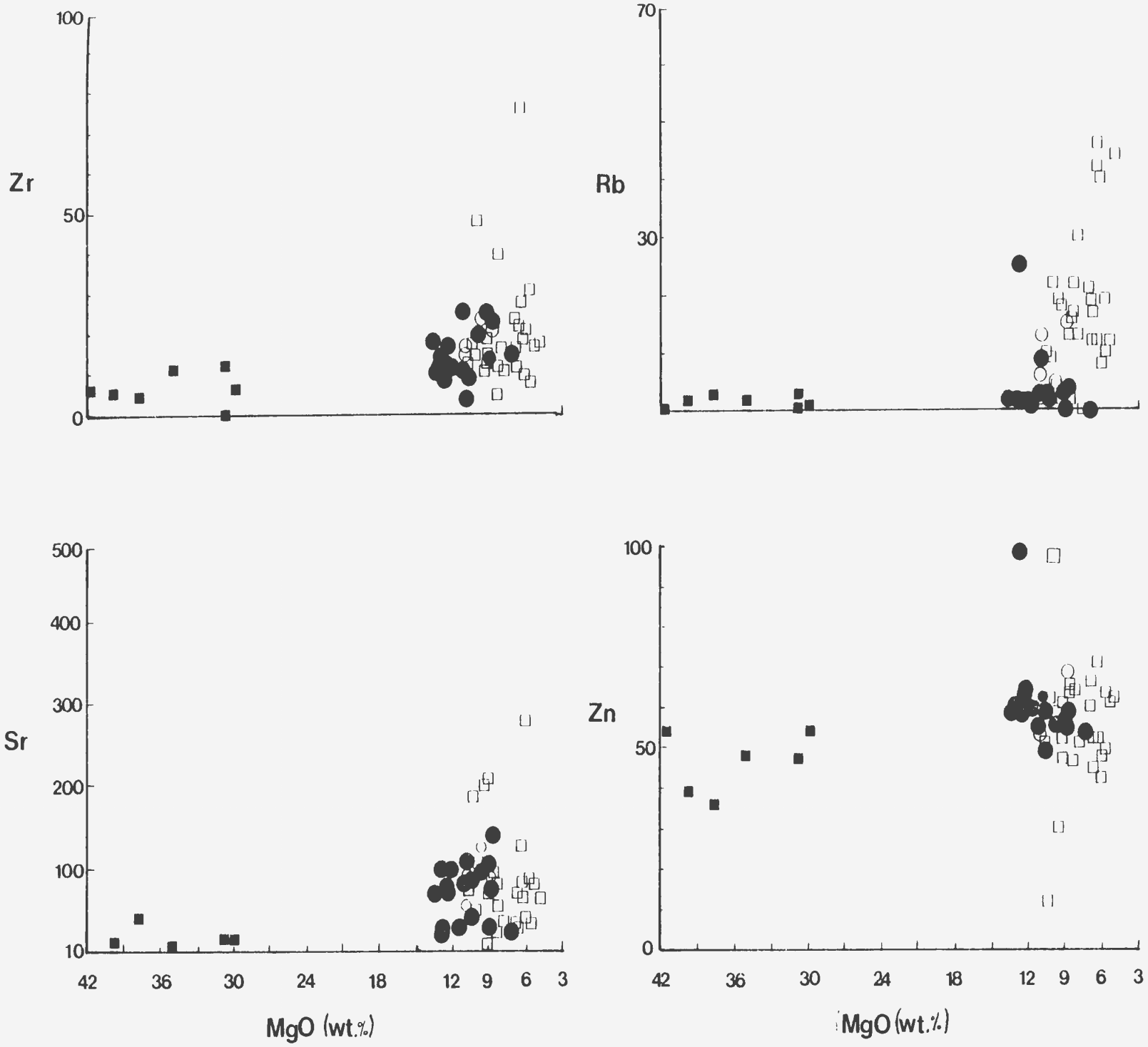
Zr
100
50
0
Rb
70
30
Sr
500
400
300
200
100
10
Zn
100
50
0
42
36
30
24
18
12
9
6
3
MgO (wt.%)
MgO (wt.%)

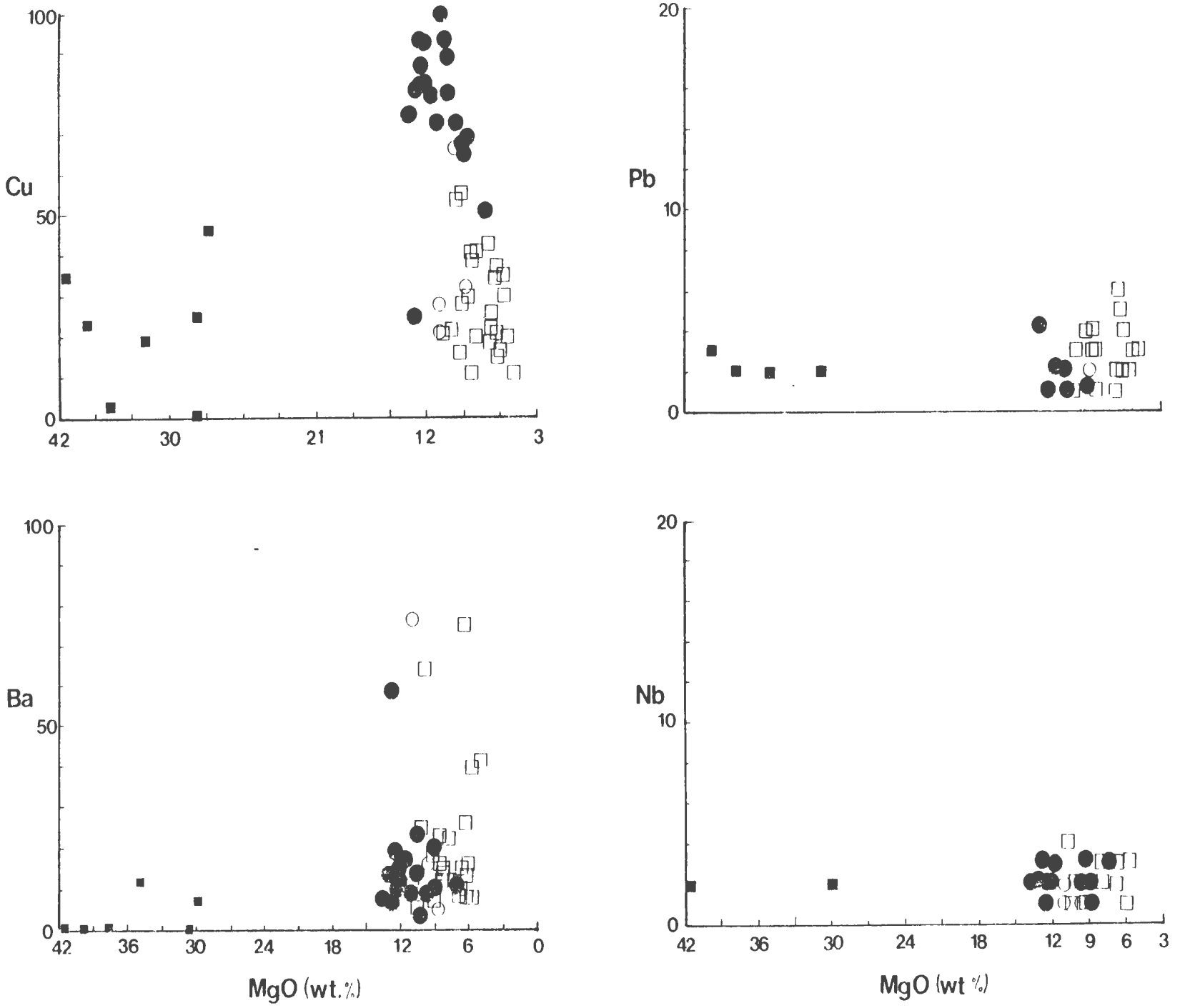
Cu
100
50
0
42
30
21
12
3
Pb
20
10
0
Ba
100
50
0
42
36
30
24
18
12
6
0
MgO (wt.%)
Nb
20
10
0
42
36
30
24
18
12
9
6
3
MgO (wt %)

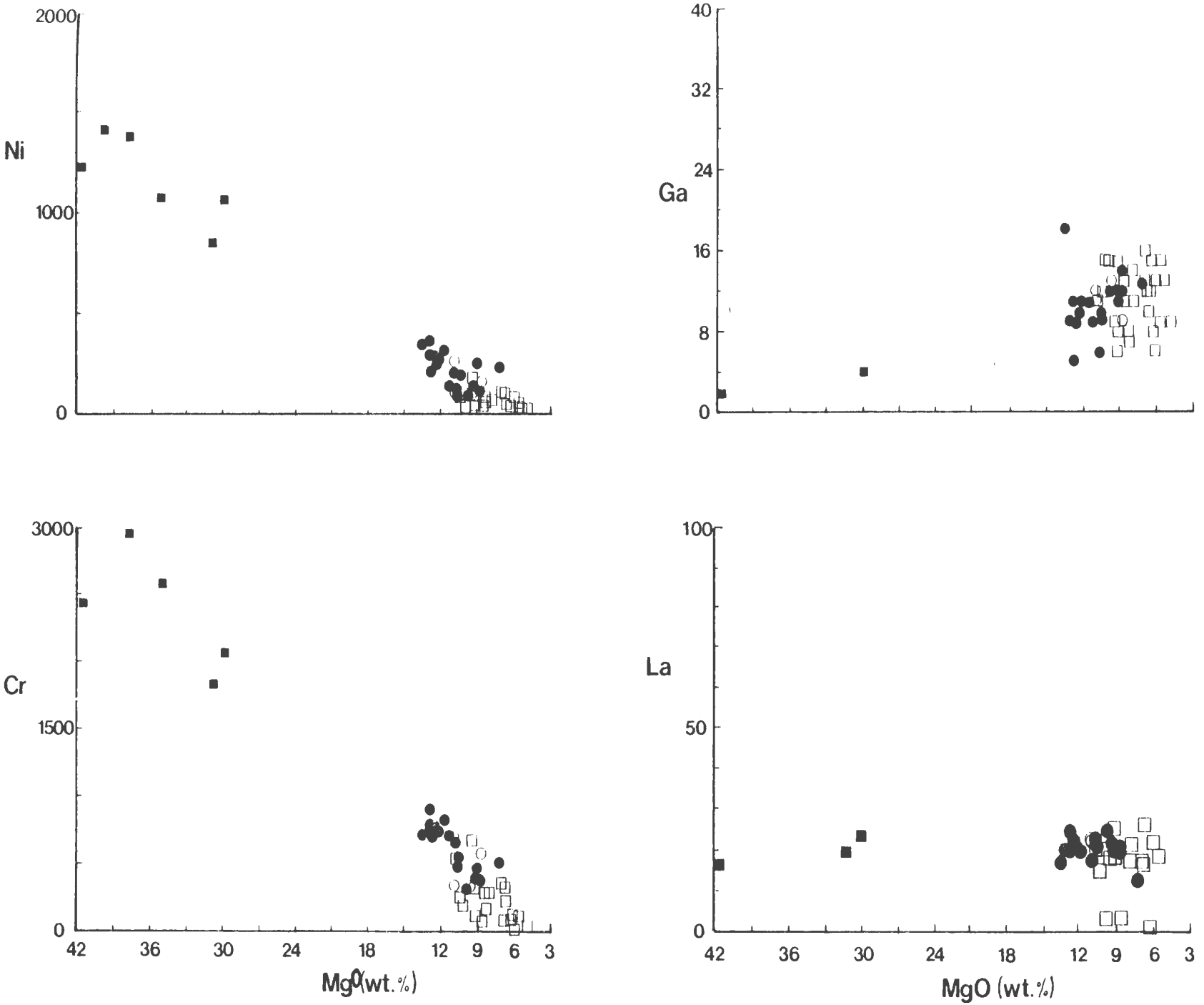
Ni
2000
1000
0
Ga
40
32
24
16
8
0
Cr
3000
1500
0
La
100
50
0
42
36
30
24
18
12
9
6
3
MgO (wt.%)

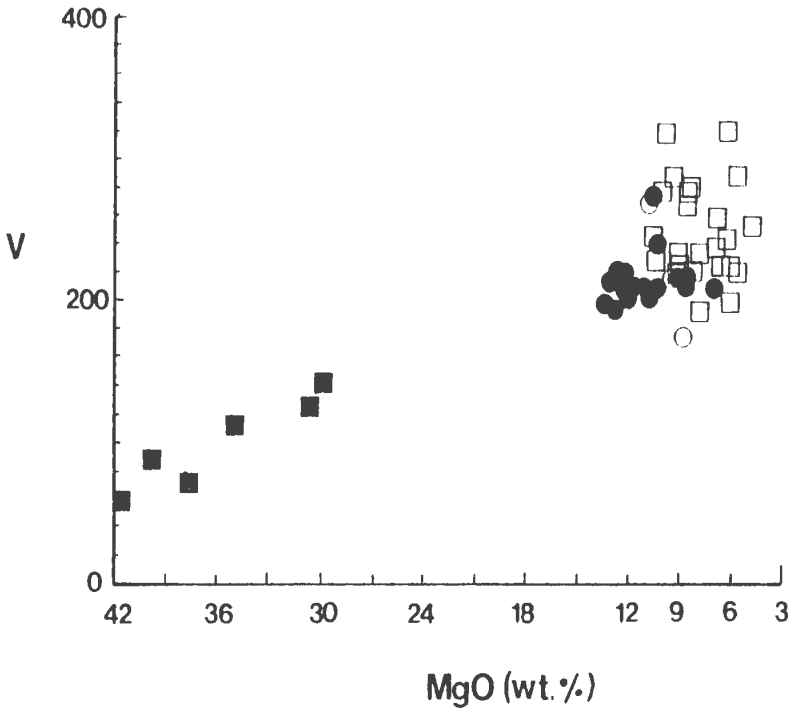
400
200
0
V
42
36
30
24
18
12
9
6
3
MgO (wt.%)

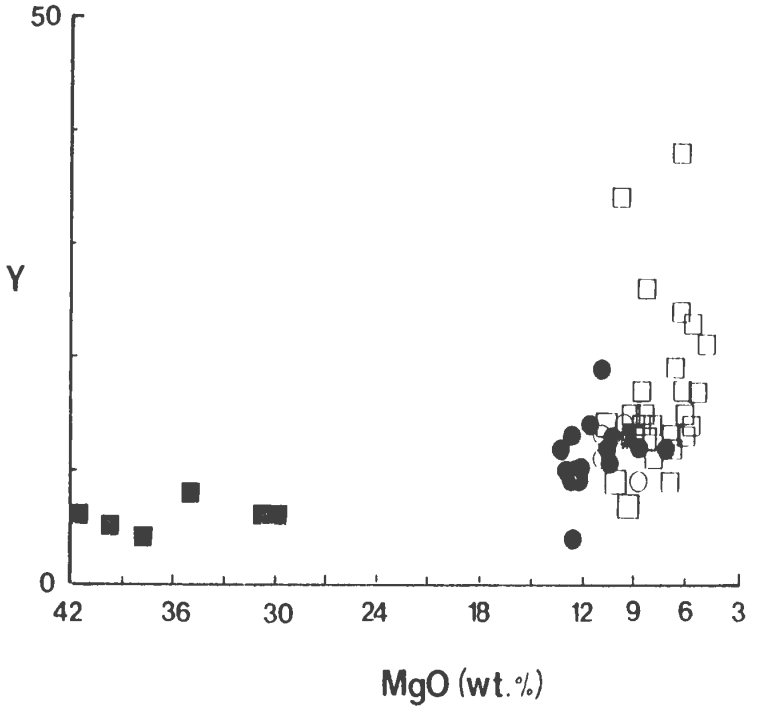
50
0
Y
42
36
30
24
18
12
9
6
3
MgO (wt.%)

also form a relatively distinct group with MgO ranging from 9.5 - 13.5%, and are characterized by very consistant values for the major oxides. Again SiO_2 and CaO show the widest absolute variation of 4% and 6% respectively. Apparently the consistent results are produced by the very fresh condition of these glassy rocks. The field of komatiites is partially overlapped by that of olivine basalts and aphyric basalts in some of the plots; these show ranges of 8% - 11% MgO and 4.5% - 11% MgO respectively. These rocks also generally show broader ranges of the other oxides as well; again SiO_2 and CaO show especially large variations. The olivine basalts and aphyric lavas are chemically, as well as petrographically, similar. The olivine-phyric basalt plots define a field inside the aphyric basalt but intermediate between the komatiites and the bulk of the aphyric lavas. K_2O values in the ultrabasic rocks were too low to measure.

The most significant feature of the major oxide vs. MgO plots is the colinear aspect of the fields defined by the different rock types. This is evident for all the plots with the possible exception of some of the fields defined by the highly weathered olivine basalts. Where the fields are broad, the points are dispersed with considerable symmetry around a line joining the fields. The dispersed nature of some plots, especially for SiO_2, Na_2O and CaO indicate possible alteration and element mobility. However, stable elements such as Al_2O_3 and TiO_2 show better cluster. The microprobe analysis of the olivine phenocrysts lie on an extension of the line connecting the fields of bulk rock analyses. This colinear aspect, as a preliminary observation, is considered to demonstrate the importance of olivine as a control phase in the genesis of the different rock types.

IV.2.2 Trace Elements vs. MgO

Fourteen different trace elements of the Upper Pillow Lavas have been plotted against MgO in Figure IV.2. Komatiites and ultrabasic rocks again plot in well-defined fields, while olivine basalts and aphyric basalts show a wide scatter, especially with regard to the more incompatible elements, e.g., Cu, 11-146 ppm., Sr, 22-289 ppm. and Rb, 2-46 ppm.; these elements are considered to be mobile during low temperature metamorphism (Pearce and Norry, 1979).

Generally the different rock types show the expected variation with MgO. The incompatible elements Zn, Ba, Y, V, Sr, Rb and Pb all increase with decreasing MgO. Ni and Cr increase with MgO content, while Cu shows an increase from ultrabasic to komatiitic rock types and a decrease from komatiites to aphyric basalts.

The very regular variation of Ni with MgO supports the major element data, i.e., that these trends can be explained by olivine fractionation. Cr against MgO shows similar behaviour and suggests incorporation of this element into crystallizing clinopyroxene or chromian spinel; this possibility is confirmed by the petrography.

IV.3 Jensen Diagram (Figure IV.3; after Jensen, 1976)

This plot uses ΣFe + Ti, Mg and Al and serves very well to characterize all the lavas concerned. The Upper Pillow Lava compositions as a whole show a continuous linear trend away from the Mg apex. The lack of a significant trend toward the ΣFe + Ti apex indicates the minor importance of clinopyroxene and plagioclase, and the predominance of olivine, as separating phases. The slight digression of some points away from both the ΣFe + Ti and Al apices may indicate small amounts of pyro-

FIGURE IV.3 Jensen Diagram (after Jensen, 1976; fields derived from Francis and Hynes, 1979). Plot uses cation proportions.

Fields:

TF:	tholeiite
MK:	mafic komatiite
PK:	peridotitic komatiite
CAF:	calc - alkaline

Solid curve represents olivine/pyroxene fractionation path; open curve represents feldspar/pyroxene fractionation path. Enclosed fields are derived from Chukotat Group (Francis and Hynes, 1979). Fields as in Figure IV.1 except:

★ Lower Pillow Lava Analyses (this work)

☆ Lower Pillow Lava Analyses (published)

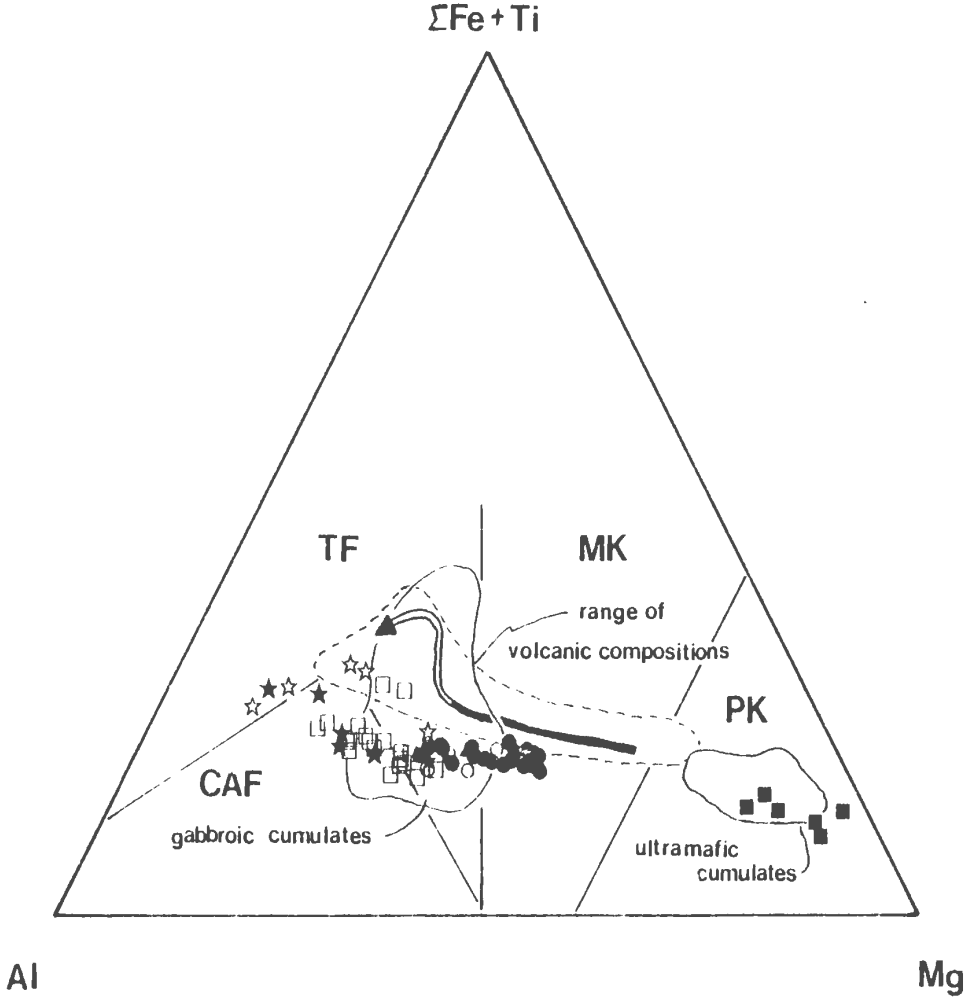
ΣFe + Ti
TF
MK
range of
volcanic compositions
PK
CAF
gabbroic cumulates
ultramafic
cumulates
Al
Mg

xene and plagioclase fractionation, albeit this effect is deemed minimal when compared to the normal tholeiitic trend as delineated by the arrow in the Jensen diagram.

Most of the komatiite samples lie in the mafic komatiite field of the diagram. The derivative olivine-phyric and aphyric basalts trend away from the komatiite field toward the field of high-Al basalt. The rocks as a whole are enriched in aluminum with respect to the komatiitic-tholeiitic trend of Francis and Hynes (1979) for the lavas of the Chukotat Group, New Quebec. The more evolved members of the Upper Pillow Lavas are comparable in composition, however, to the gabbroic cumulates of Francis and Hynes (1979) which are in fact derived from residual liquids produced by the extraction of ultramafic cumulates. Although none of these basaltic rocks are cumulates, they are analogous to the Chukotat gabbroic cumulates in their status as a derived liquid.

IV.4 TiO_2 vs. SiO_2 (Figure IV.4)

This diagram was used by Arndt et al. (1977) to chemically distinguish between tholeiites and komatiites from Munro Township, Quebec. It is considered less than ideal here, but serves to indicate the extent of metasomatism which has occurred in the highly altered olivine and aphyric basalts.

The Upper Pillow Lavas as a whole have strikingly low TiO_2 contents. Except for the ultrabasic rocks the TiO_2 values show no significant variation with SiO_2 content - in fact, the highest values are found where SiO_2 is lowest. This behaviour indicates the validity of using MgO rather than SiO_2 as a fractionation index. As TiO_2 is con-

FIGURE IV.4 TiO_2 vs. SiO_2. Tholeiitic and komatiitic fields defined by Munro Townships rocks (Arndt et al., 1977). Symbols as before.

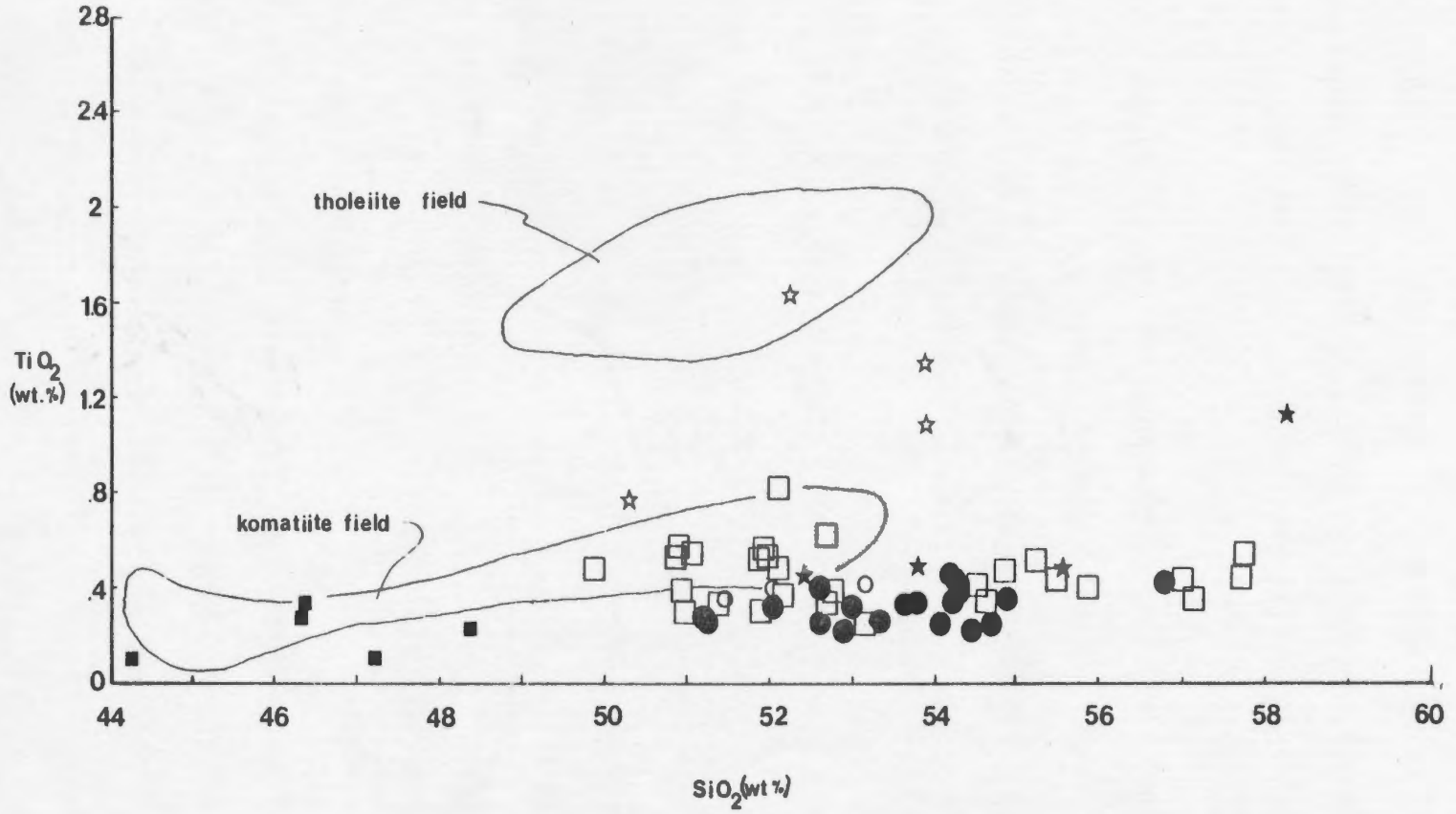
tholeiite field
komatiite field
TiO2 (wt.%)
SiO2 (wt %)
0
.4
.8
1.2
1.6
2
2.4
2.8
44
46
48
50
52
54
56
58
60

sidered to be relatively immobile during low temperature metamorphic processes, those lavas with the highest TiO_2 are likely to be the most evolved, and their lower SiO_2 contents probably represent the removal of this oxide by metasomatism; this consideration is further brought out by the large scatter of points for the olivine and aphyric basalts as compared to the komatiites.

A considerable proportion of the aphyric lavas plot inside the the komatiite field as defined for the Munro Township rocks. The remainder plot below the field with TiO_2 values for some komatiites as low as 0.2%. As a group the aphyric lavas contain significantly less SiO_2 and more TiO_2 than the komatiites.

Several analyses of the Lower Pillow Lavas from both this study and the literature (Appendices B.1.1, B.1.2) have been plotted to show the distinction between these rocks and the petrographically similar aphyric varities of the Upper Pillow Lavas. Most of the plotted Lower Pillow Lavas are notably higher in both SiO_2 and TiO_2 than their counterparts from the Upper Pillow Lavas.

IV.5 Al_2O_3 vs. $FeO^T/(FeO^T+MgO)$ (Figure IV.5)

This diagram indicates an increase in alumina content with fractionation, using $FeO^T/(FeO^T+MgO)$ as a fractionation index. The bulk of the aphyric lavas plot above the 15% Al_2O_3 mark, while all the komatiites plot below this value. The aphyric lavas also show much larger and a higher range of values for $FeO^T/(FeO^T+MgO)$. The Upper Pillow Lava rocks for the most part plot above the field of Munro komatiites (Arndt et al., 1977), the main direction of variation being along

FIGURE IV.5 Al_2O_3 vs. $FeO^T/(FeO^T+MgO)$. Fields for tholeiites, komatiites and ultramafic cumulates as defined for Munro Townships rocks (Arndt et al., 1977). Symbols as before.

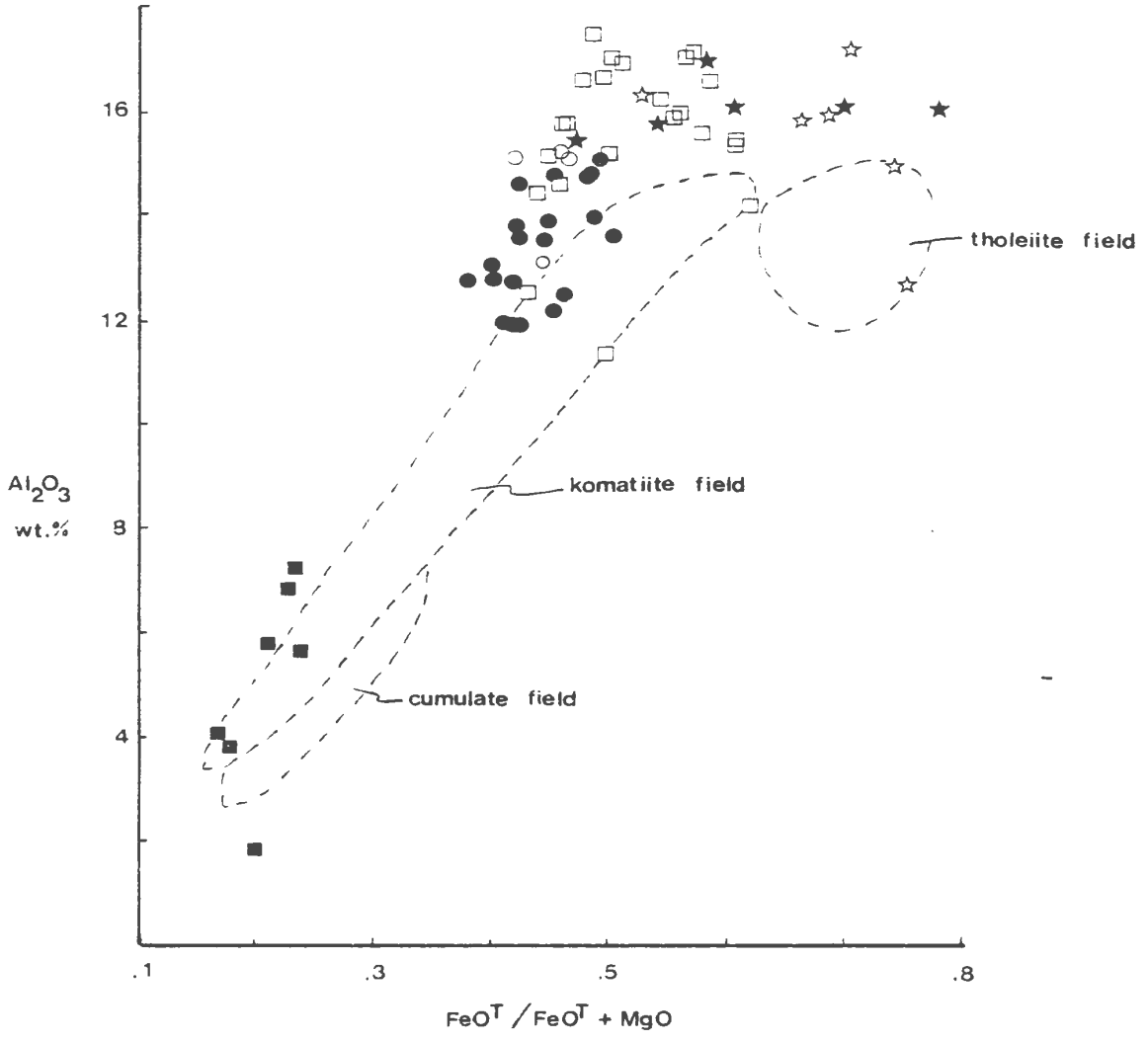
16
12
8
4
Al_2O_3
wt.%
tholeiite field
komatiite field
cumulate field
.1
.3
.5
.8
$FeO^T / FeO^T + MgO$

the Al_2O_3 axis, while a significant variation in $FeO^T/(FeO^T+MgO)$ ratios is also present. Both variations are continuous, with komatiitic and aphyric types defining the range; olivine basalts occupy an intermediate position. The ultrabasic rocks plot very closely to the cumulate komatiite field from Fred's Flow, Munro Townships.

Considered overall, the Lower Pillow Lavas have higher $FeO^T/(FeO^T+MgO)$ than the Upper Pillow Lavas, although they are similar to the more iron-rich aphyric lavas. Most of the Lower Pillow Lava plots have alumina contents similar to the Upper Pillow Lavas.

The regular increase in Al_2O_3 corroborates the earlier proposal of the importance of fractionation of nonaluminous phases in the genesis of the Upper Pillow Lavas.

IV.6 TiO_2 vs. MgO (Figure IV.6)

Again aphyric lavas, komatiites and Lower Pillow Lavas are separated on the basis of TiO_2 content, albeit the range of TiO_2 values for the aphyric lavas (0.28 - 0.74%) is much greater than that for komatiites (0.20 - 0.43%). This more regular variation of TiO_2 with MgO contrasts with the rather erratic variation of TiO_2 with SiO_2. The olivine basalts plot in the area of overlap between the komatiites and aphyric basalts. Samples from the Lower Pillow Lavas show considerably higher TiO_2/MgO ratios than those from the Upper Pillow Lavas, but are slightly less magnesian than the field of tholeiites from Theo's Flow, Munro Townships.

FIGURE IV.6 TiO_2 vs. MgO. Fields for tholeiites and komatiites defined for Munro Townships rocks (Arndt et al., 1977). Symbols as before.

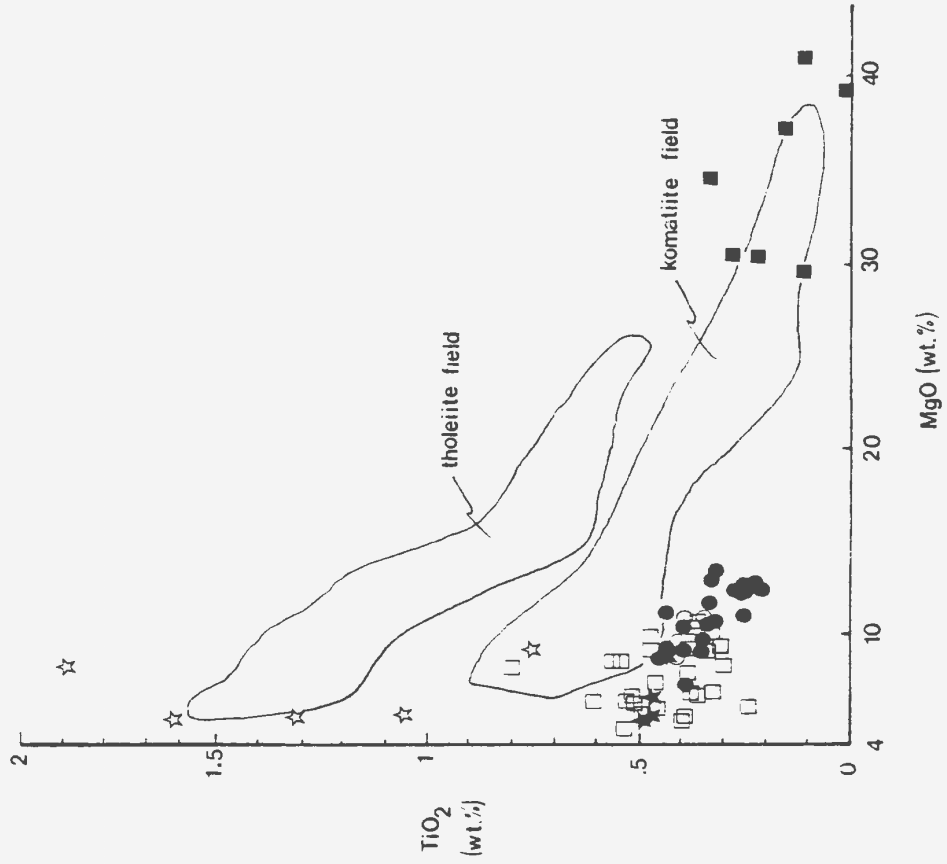
tholeiite field
komatiite field
TiO_2 (wt.%)
MgO (wt.%)
2
1.5
1
.5
0
4
10
20
30
40

IV.7 CaO/Al_2O_3 vs. MgO (Figure IV.7)

The komatiites and olivine basalts plot almost exclusively within the field of komatiites as taken from the data of Arndt et al. (1977) for Munro Townships rocks. The aphyric basalts extend from the tholeiite field across the overlap into the komatiite field. There is no great variation in CaO/Al_2O_3 ratio from MgO-rich to MgO-poor types but the average value for komatiites is higher than for aphyric basalts (0.72). Although CaO/Al_2O_3 ratios of the Upper Pillow Lavas are very similar to those of tholeiites and komatiites from Munro Townships, the actual values of both CaO and Al_2O_3 are considerably higher. Average values for these rocks are compared in Table VII.2.

IV.8 Rare Earth Elements (Figure IV.8)

Seven samples from the Upper Pillow Lavas were analysed for rare earth elements; these comprise two analyses from each of the komatiites, olivine basalts and aphyric basalts, as well as one analysis of olivine cumulate (ultrabasic rock). These data, along with five samples from the Lower Pillow Lavas as documented by Smewing and Potts (1976), have been summarized in Appendix B.1.2. and Figure IV.8. Methods and accuracy of analyses are discussed in Appendix A.2.5.

The REE patterns from the Upper Pillow Lavas form a distinct group with concentrations essentially lying between 2 and 5 times that of chondrite (Nakamura, 1974). The aphyric basalt DL-6 has concentrations similar to the least fractionated sample from the Lower Pillow Lavas, which are enriched with respect to chondritic abundances by a factor of 5

FIGURE IV.7 CaO/Al_2O_3 vs. MgO. Fields for tholeittes and komatiites as defined for Munro Township rocks (Arndt et al., 1977). Symbols as before.

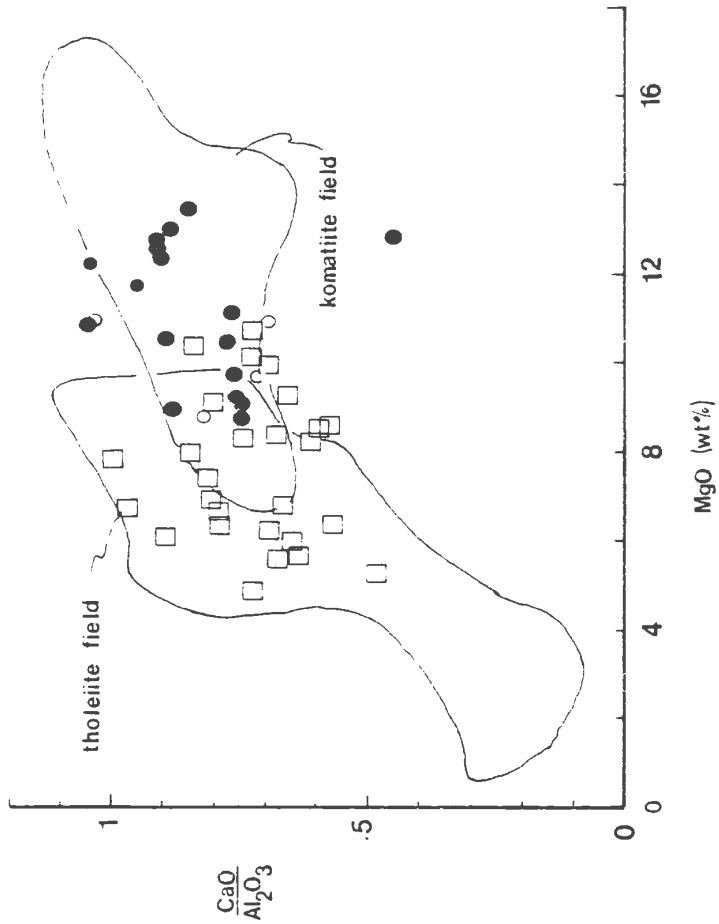
tholeiite field
komatiite field
1
.5
0
0
4
8
12
16
MgO (wt%)
CaO / Al2O3

FIGURE IV.8 Chondrite-normalized rare earth patterns for the Upper and Lower Pillow Lavas. Symbols as in Figure IV.1. Average chondrite is taken from Nakamura (1974).

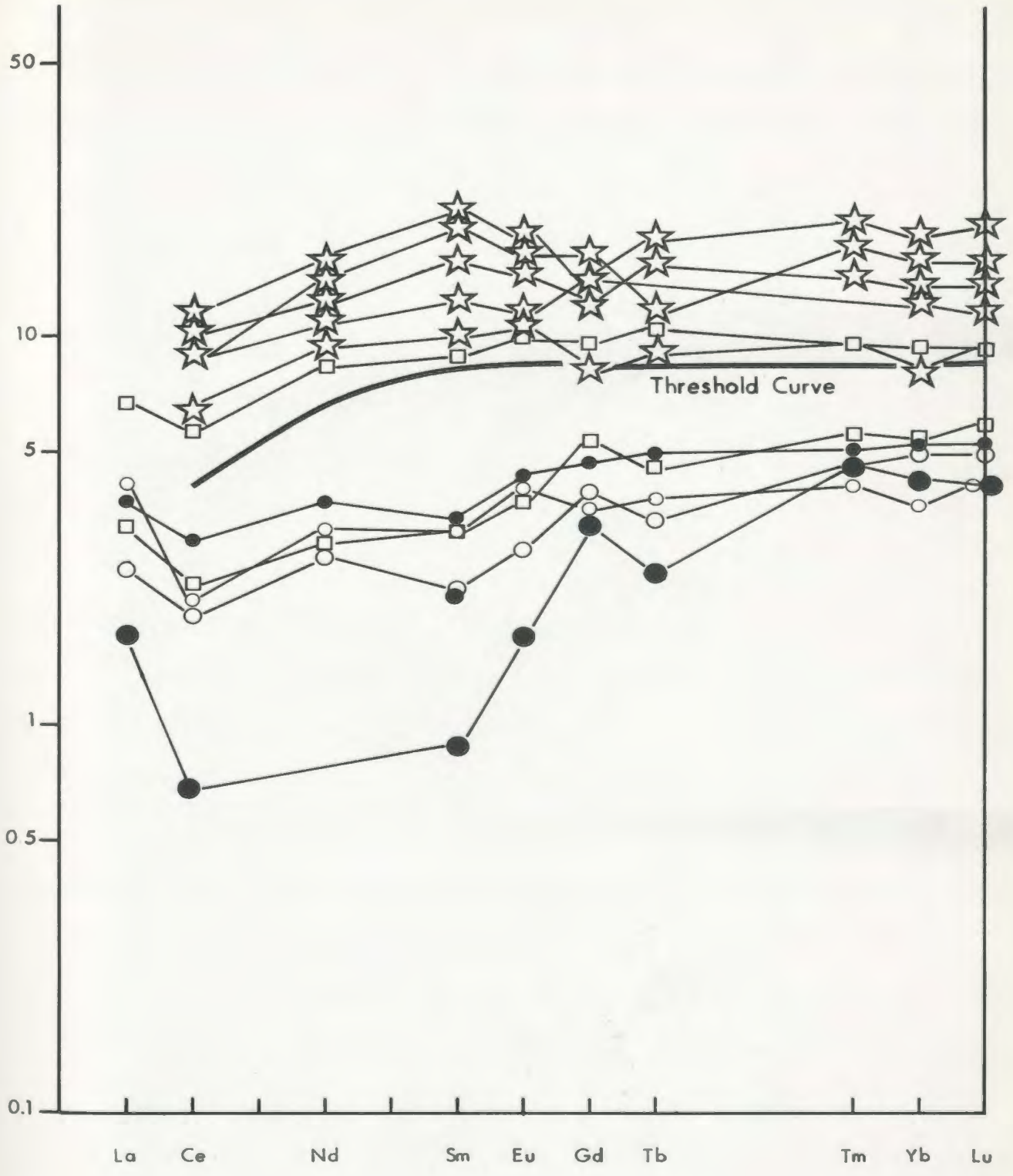
50
10
5
1
0.5
0.1
Threshold Curve
La
Ce
Nd
Sm
Eu
Gd
Tb
Tm
Yb
Lu

or more; one or two samples from the Lower Pillow Lavas have Sm and Tm concentrations nearly 20 times that of chondrite.

The two lava groups are effectively separated by a threshold level (Curve A in Figure IV.8), as proposed by Smewing and Potts (1976). Profiles below this line are typical of less fractionated olivine-phyric basalts from present day oceanic environments (Frey et al., 1974; Schilling, 1975). Above the threshold level the profiles are similar to those of olivine-free ocean floor basalts (Schilling, 1975).

The Upper Pillow Lavas, i.e., samples plotting predominantly below the threshold level, are further characterized by an increasingly positive slope from Ce to Gd, and a slight positive slope from Gd to Lu, with decreasing total rare earth concentrations. This effect is ultimately expressed in the primitive komatiitic lava KL-33; this sample shows LREE concentrations less than that of chondrites and attests to the depleted nature of the parental magma. Samples from the Upper Pillow Lavas with both higher relative concentrations of LREE and of total REE are those lavas which are elsewhere in this chapter shown to be affected by olivine fractionation (i.e., olivine and aphyric basalts). The partial profile for olivine cumulate predictably shows depletion relative to chondrite for all elements except La.

The petrogenetic implications of the foregoing rare earth data will be considered in detail in Chapter VI, in conjunction with evidence drawn from mineral chemistry, and bulk rock trace and major element geochemistry. Here it is sufficient to note that the clear distinction between the Upper and Lower Pillow Lava rare earth element profiles suggests a fundamental difference in the origin of their respective parental

magmas. Furthermore a fractionation sequence, as suggested earlier in this chapter by trace and major element variation diagrams, is also apparent from the viewpoint of rare earth element concentrations; a trend of light and total REE enrichment away from the komatiitic sample KL-33 is present.

V. MINERAL CHEMISTRY

V.1 Olivine

Detailed microprobe investigation of fresh olivines in the ultrabasic lavas and komatiites was carried out; methods are described in Appendix A.2.4. Grains from the olivine basalts were not studied because of their complete alteration to deuteric minerals. Olivine analyses are printed in Appendix B.2. Although five different grains were analysed from each particular sample, the average value only for each sample is presented, as compositional variation within samples was negligible. All olivine analyses were found to be homogeneous.

Data for olivines from three different ultrabasic rocks are listed. Specimens KL-12 and DL-45 have similar Fo contents (91.4 and 90.8) while DL-36 is richer in the forsterite molecule ($Fo_{93.1}$). Olivines from the komatiitic lavas are markedly less magnesian, ranging from $Fo_{87.6}$ - $Fo_{89.6}$. No olivine analyses from the Troodos peridotites were available. The ultrabasic olivines are comparable to those from the harzburgites of the Bay of Islands Complex (Average $Fo_{91.0}$, Malpas, (1976)) except for DL-36 which is more magnesian. They are considerably richer in Fo than olivines from cumulus rocks of the Bay of Islands Complex, i.e., dunites, critical zone rocks and gabbros which are in the order of Fo_{89}. These values are comparable to those from the present komatiitic olivines. It appears that the olivines from the present ultrabasic rocks crystallized from a magma with a much higher Mg/Fe ratio than normally erupted tholeiitic magma.

Arndt et al. (1977) provide analyses of olivine which has crystallized out of a komatiitic liquid, some grains of which are as magnesian as $Fo_{93.8}$, but averaging about $Fo_{90.4}$. It therefore seems possible that these olivines which are more magnesian than most olivines derived from a tholeiitic liquid could have crystallized from a magma with low FeO/FeO + MgO, which is one of the specific criteria for komatiitic lavas, according to Arndt et al. (1977).

Olivines from the komatiitic lava of the present study are also in the range of komatiitic olivines from Munro Township (Arndt et al., 1977) and are also comparable to cumulus olivine from the most magnesian rocks of the Bay of Islands layered series, i.e., the dunites.

V.2 Orthopyroxene

Average orthopyroxene analyses from ultrabasic rocks, komatiite and olivine basalt are listed in Appendix B.2. En content increases from 84.20 in the ultrabasic rocks to 89.46 in the olivine basalt.

According to O'Hara (1963b), in large layered complexes or ultramafic nodules where equilibrium could have been attained the value of En/Fo is approximately 1. At the other extreme, in rocks where the degree of equilibrium is considered to be somewhat less due to more rapid cooling, such as small intrusives and lavas, the ratio is considerably less than unity. The obvious discrepancy here between equilibrium ratios and those observed for the ultrabasic rocks suggests that either: 1) olivine and enstatite are in marked disequilibrium due to the rapid cooling of the lava, or 2) the larger and presumably earlier formed olivine grains precipitated out of a liquid of a different composition than the

orthopyroxene did. The size and habit of the olivine crystals makes the former premise improbable. If the olivines of the ultrabasic rock are envisaged as crystallizing in a magma chamber at the intratelluric stage, then it follows that they would sink to the bottom and form a liquid/crystal mush. The texture of the rock suggests that extrusion of this mush occurred before orthopyroxene had begun to crystallize in any great amount. The small proportion of orthopyroxene which then crystallized in the groundmass did so from a restricted batch of liquid which was depleted in Mg^{2+} by the removal of the olivine from the system.

The Mg^{2+} content of orthopyroxenes ($En_{87.9}$) in the komatiitic lavas is more comparable to that of the olivines ($Fo_{87.6}$ — $Fo_{89.6}$), although it is again slightly low. The decidedly rapid quenching of this rock can account for the observed lack of equilibrium distribution of Mg^{2+} and Fe^{2+} between the two phases. The En content of orthopyroxene for the olivine basalt is higher still and suggests conditions closer to equilibrium crystallization.

The molecular proportion of Ca^{2+} in orthopyroxene ranges from 0.065 in the ultrabasic lavas to 0.117 in the komatiitic lavas. The high value for komatiitic orthopyroxene may reflect the abundance of calcium in the magma, which may have entered the orthopyroxene lattice before clinopyroxenes began to crystallize. Atlas (1952) found that the amount of Ca^{2+} atoms accepted into enstatite in the synthetic system $MgSiO_3$ - $CaMgSi_2O_6$ reached a maximum of 0.115 at a crystallization temperature of 1100°C, but decreased to 0.30 at 700°C. This data is in accord with the quenched nature of the komatiites and the preservation of

mineral compositions achieved at high temperatures of equilibrium, such as the high Ca^{2+} content of orthopyroxenes.

The average alumina content in orthopyroxene is 3.74 wt.% in ultrabasic rocks, 1.81% in komatiites and 1.74% in olivine basalt. Al_2O_3 content in pyroxenes is dependant both upon pressure (Boyd and England, 1960) and the availability of aluminum. High-alumina orthopyroxenes from the Lizard are found with aluminous diopside and spinel (Green, 1964), but Malpas (1976) suggested that the low alumina content of spinels from dunites of the Bay of Islands Complex as compared to the lherzolites and harzburgites may reflect the low pressure crystallization of plagioclase within the former rocks.

This latter view is credible here in consideration of the Al_2O_3 content in three orthopyroxene-bearing rock types. The high values in this mineral within the ultrabasic rocks reflects the virtual absence of an aluminous phase, although amounts of plagioclase are present in DL-36 and DL-45. Small amounts of spinel occur, but this is definitively chromian (based on petrography, no probe analyses available). The komatiitic lavas on the other hand are rich in calcic pyroxene, either augite or pigeonite, which has up to 12.38% alumina (see KL-34, Appendix B.2). The glass of the groundmass of KL-34 contains up to 18% alumina, which clearly would control the amount of plagioclase precipitating had crystallization run its normal course. Ostensibly, then, orthopyroxene is but a minor host of Al_2O_3 in these lavas.

Likewise the low alumina content of orthopyroxene from the olivine basalts is attributed to the high percentage of modal plagioclase in the rock (prior to alteration).

The relationship between orthopyroxene and clinopyroxene will be discussed in the following sections. Suffice it to say at this point that, in contrast to clinopyroxene, orthopyroxene grains show no chemical zoning.

V.3 Clinopyroxene

V.3.1 Unquenched Lavas

Analyses of clinopyroxene grains from all four rock types are contained in Appendix B.2. Again, where more than one grain was analysed per section, the average of the analyses is printed. As the geochemistry of the monoclinic pyroxenes in komatiites is here fairly complex the topic will be dicussed separately from clinopyroxenes in the other three rock types.

Clinopyroxenes from the ultrabasic rocks, olivine basalts and aphyric lavas are all augite and show uniform composition from one to the other, although the former are richer in both the Wo(39.6-41.2) and En(51.0-54.0) components (Figure V.1). Generally speaking Ca^{2+} varies sympathetically with Mg^{2+} and antipathetically with Fe^{2+}, as there is an overall increase in the $MgSiO_3$ and decrease in the $FeSiO_3$ components going from ultrabasic to aphyric rocks. Cr_2O_3 was analyzed from one ultrabasic rock, KL-121, and composes 1.8% by weight as compared with 0.10-1.47% from the aphyric lavas. TiO_2 shows no significant variation. Alumina in clinopyroxenes is consistently high in both the ultrabasic rocks and olivine basalts (2.01-3.16%), as compared with smaller values and a broader range for the aphyric basalts (1.62-3.02% by wt.) There is a sufficient amount of alumina in clinopyroxenes from each

FIGURE V.1 Pyroxenes from unquenched lavas.

■ Ultrabasic rocks

● Komatiites

○ Olivine basalts

▲ Aphyric basalts

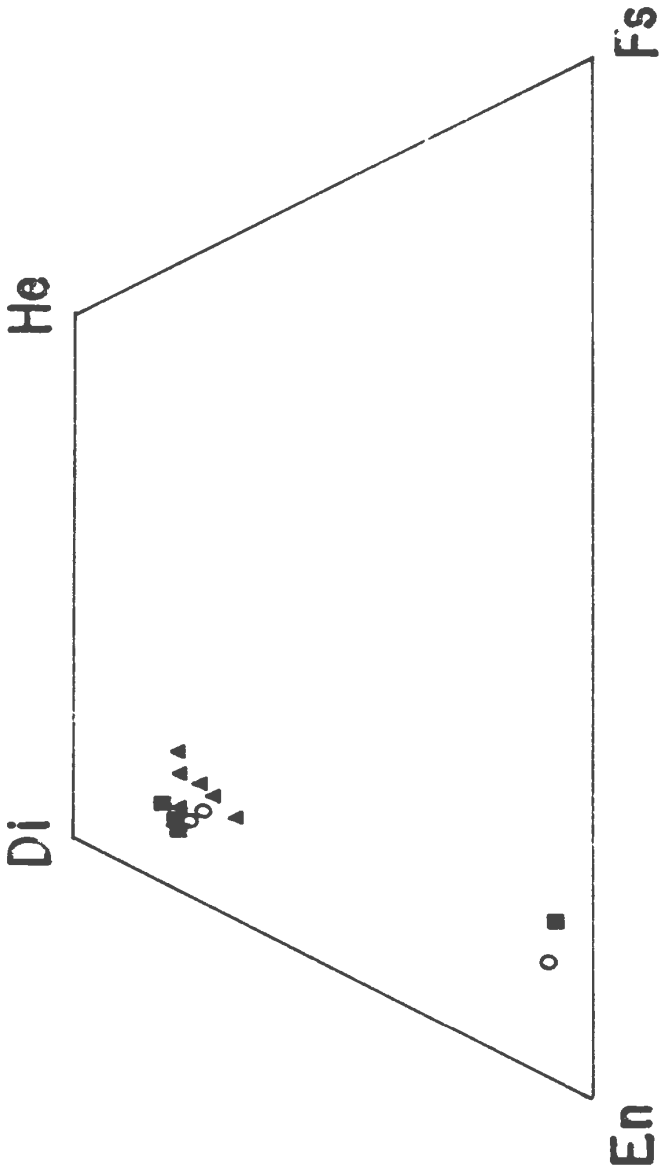
Fs
He
Di
En

of these three rock types to make up the requisite two cations (with silica) in the tetrahedral sites. MnO content ranges up to 0.17% in PL-17 (aphyric basalt) which is also the sample with the highest ferrous iron content.

Soda contents are low in all the clinopyroxenes analysed (0.03-0.25%) but are particularly low in the ultrabasic rocks and olivine basalts (0.03-0.14); K_2O, where included in the analysis, was not detected. These values are low even for basaltic rocks and in accord with the results obtained from bulk rock geochemistry, i.e., they indicate the extremely depleted nature of the magma.

V.3.2 Quenched Lavas

The zoning in the monoclinic pyroxenes which was evident from petrographical studies was investigated in some detail with the electron microprobe. A total of nine grains from the most pristine hyaloclastic samples, KL-33 and KL-34, were studied. Analyses of grains in KL-33 involved two points only, one at the core and one at the rim of the grain. In section KL-34 traverses across four grains were made, with up to seven point analyses taken per grain. These traverses in all cases confirmed the symmetrical and bilateral nature of the chemical variation. A list of the data for all points measured is supplied in Appendix B.2.

As can be observed from the table there is no unique pattern of variation within the grains. The following different cases are notable:

1. Ca^{2+}-rich (augite) cores $\longrightarrow$ rims lower in Ca^{2+} (augite or subcalcic augite)

   e.g., KL-33, Grain A, KL-34, Grains A, B and D

2. Ca^{2+}-rich (augite) cores ⟶ rims higher in Ca^{2+} (augite)
   e.g., KL-33, Grain C

3. Ca^{2+}-rich (augite) cores ⟶ rims much lower in Ca^{2+} (pigeonite)
   e.g., KL-33, Grain D

4. Ca^{2+}-poor (pigeonite) cores ⟶ Ca^{2+}-rich rims (augite)
   e.g., KL-33, Grains B and E; KL-34, Grain C

There is a strong antipathetic but very systematic variation of Mg^{2+} with Ca^{2+} (Figure V.2). The Fs component is relatively constant, except in some grains where high Ca/Mg values are attained. Al_2O_3 in augites and subcalcic augites shows normal basaltic concentrations in the grains which are not strongly zoned, and varies with Ca^{2+} content. High concentrations are found in Grains KL-34 B and D, however, where alumina weight percent ranges (core to rim) from 2.17 to 9.17%, and 5.01 to 12.37%, respectively. Al_2O_3 occurs at the expense of SiO_2 and is partitioned strongly into tetrahedral sites. In the pigeonitic zones of grains, e.g., the core of KL-33, Grain B, Al_2O_3 is typically very low (2.97% CaO, 0.50% Al_2O_3). In some analyses it is necessary to add Fe^{3+} to fill the tetrahedral sites.

TiO_2 is generally extremely low but again shows normal basaltic concentrations and varies with magnesium. MnO varies closely with FeO.

The analyses derived from the grain traverses in KL-34 (Appendix B.2, Figure V.2) show an initial Ca^{2+} enrichment trend which is followed by an enrichment in Fe^{2+} after an original $Mg \rightleftharpoons Ca$ substitution. Roeder and Emslie (1970) have demonstrated that the partitioning of Mg and Fe between mafic phases and liquids is independant of tempera-

FIGURE V.2 Pyroxenes from quenched lavas.

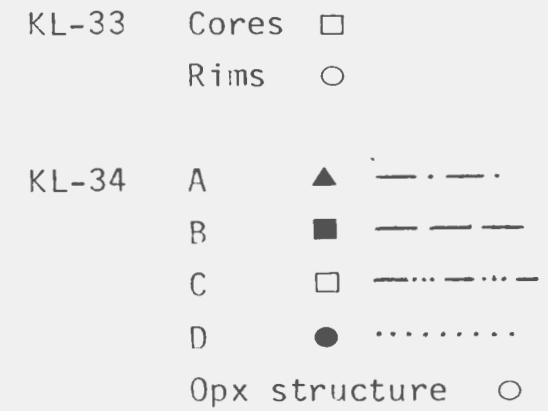

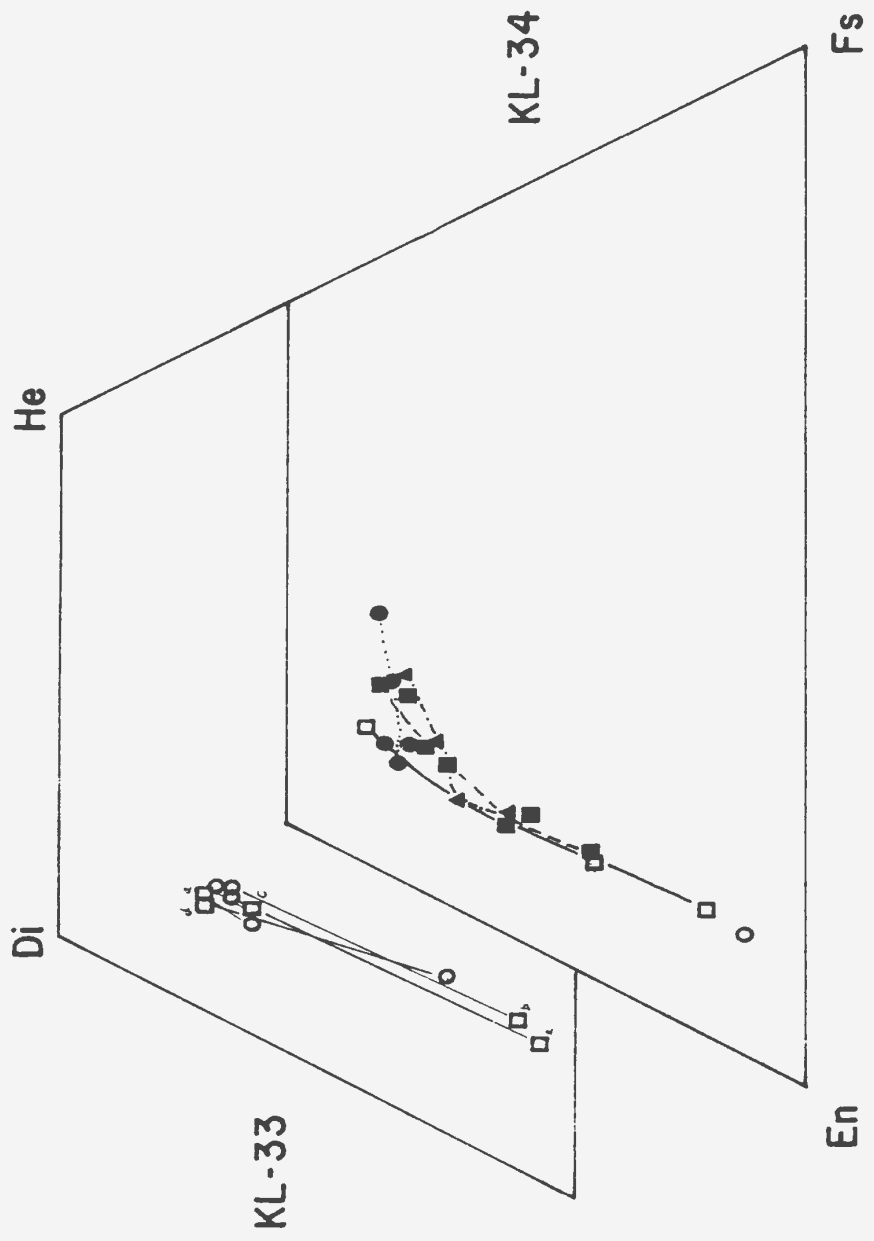
He
KL-34
Fs
Di
KL-33
En

ture. Thus the increase of Ca/Mg in the magma during this early stage of pyroxene crystallization probably reflects a depletion of Mg in the magma due to the simultaneous and continuing crystallization of olivine and/or orthopyroxene. Petrographic observations indicate that with falling temperature these two phases are superseded by clinopyroxene as the important crystalling phase. The later concentrations of iron may indicate the substitution of Fe^{2+} for Ca^{2+} in M2 sites as both elements become more concentrated in the liquid. As is seen from the diagram this iron enrichment seems to be in effect for compositions with greater than 30% of the Wo component.

The development of regular normal (and reverse) zoning in pyroxenes is predicated upon their ability under certain conditions to accept cations which are strongly partitioned into M1 (Mg^{2+}) and M2 (Ca^{2+}) sites. These conditions are best attained in slow-cooling equilibrium situations, inferred for large intrusions such as the Skaergaard. The effect of very slow cooling upon equilibrium is to allow time for the cations under consideration to migrate through the melt along a diffusion gradient to sites at crystal boundaries in which they are preferentially accepted, that is to say, the crystal continuously equilibrates with the liquid. It is obvious that rapid cooling can have a limiting effect on this mechanism, and quenched but zoned pyroxene grains may not show enrichment trends typical of equilibrium crystallization. Lofgren et al. (1974) and Donaldsen et al. (1975), based on experimental work dealing with the cooling of melts of lunar basalt composition, have shown that fast rates of cooling favour the entry of Ca, Fe, Al and Ti

into the pyroxene lattice, which in the present case supports the tenet of disequilibrium.

The core-rim pairs of KL-33 (Appendix B.2, Figure V.2) show opposing trends. Grains B, C and E exhibit Ca-poor cores with augitic rims which indicate variations similar to those described above, although CaO is very low in B and E. Grains A and D, however, show augite cores with rims lower in calcium. This may represent a concentration of Mg^{2+} ions in the vicinity of the crystal surface, which will be preferentially accepted into the pyroxene structure.

V.3.3 Discussion of the Relationship Between Coexisting Pyroxenes

Various workers have studied the compositions of pyrozenes in the $CaSiO_3$-$FeSiO_3$-$MgSiO_3$ system formed as a result of rapid cooling. Kuno (1955) related the stability of subcalcic pyroxenes to the occupation of tetrahedral sites by Fe^{3+}, which lowers the temperature of the solvus for such pyroxenes. Thus under conditions of rapid cooling the temperature of the magma may lie above the solvus temperature with the subsequent formation of subcalcic augite as a stable phase. Kuno further considered that under such conditions subcalcic augites may crystallize with an Mg/Fe ratio as high as 65/35 (as compared with 35/65 for slowly cooled basic magmas). For the present rocks this ratio is even higher (about 85/15).

Muir and Tilley (1965) observed that two pyroxene trends may be distinguished in the crystallization of tholeiitic basalts. One is the phenocrystal trend of intratelluric equilibrium crystallization leading to the formation of hedenbergitic compositions; the other is the

'quench' trend typical of the subcalcic augites of the groundmass. In a study of the Kilauean series these authors have shown that rocks containing Ca-rich pyroxene phenocrysts display a characteristic distribution on the diopside-hedenbergite side of the cotectic curve (in pyroxene quadrilateral) in contrast to those with orthopyroxene phenocrysts, which plot below the curve. The 'quench' trend of the groundmass pyroxene, however, consisting of subcalcic augites or ferroaugites, in which the principal substitution is $Ca^{2+} \rightleftharpoons Fe^{2+}$, trangresses the cotectic curve and in the more acid differentiates continues to ferropigeonitic compositions. This late iron enrichment trend is the case for some of the grains analysed in KL-33 and KL-34 (see Figure V.2).

Smith and Lindslay (1971) studied augites from a flow of the Picture Gorge basalt. Their compositions from the center of the flow show a normal plutonic Fe-enrichment trend with only a small concomitant decrease in Ca. Those of the quickly chilled base of the flow show the characteristic $Ca \rightleftharpoons Fe$ substitution, Ca_{45} to Ca_{36}, with constant Mg, of the 'quench trend', and probably represent a metastable crystal-liquid partition consequent on the rapid crystallization.

Yamakawa (1971) found similar contrasting trends in augites of the tholeiitic dolerite, Semi, Japan. He considered augite- and subcalcic augite-pigeonite pairs a disequilibrium association resulting from the undercooling of the liquid with respect to pigeonite, in accord with the 'quench trend' of Muir and Tilley (1964). Yamakawa proposed a hypothetical pseudobinary system to explain augite/pigeonite relationships in quickly cooled systems (explanation in caption, Figure V.3).

FIGURE V.3 The hypothetical pseudobinary system $(Mg,Fe)SiO_3$ - $Ca(Mg,Fe)Si_2O_6$ of Yamakawa (1971), showing crystallization of the pyroxenes in the tholeiitic dolerite of the Semi sheet, Japan. L_{1-3} and A_{1-3} represent, respectively, the equilibrium compositions of augite and liquid at temperatures T_{1-3}. P_1 represents the composition of the first pigeonite to crystallize.

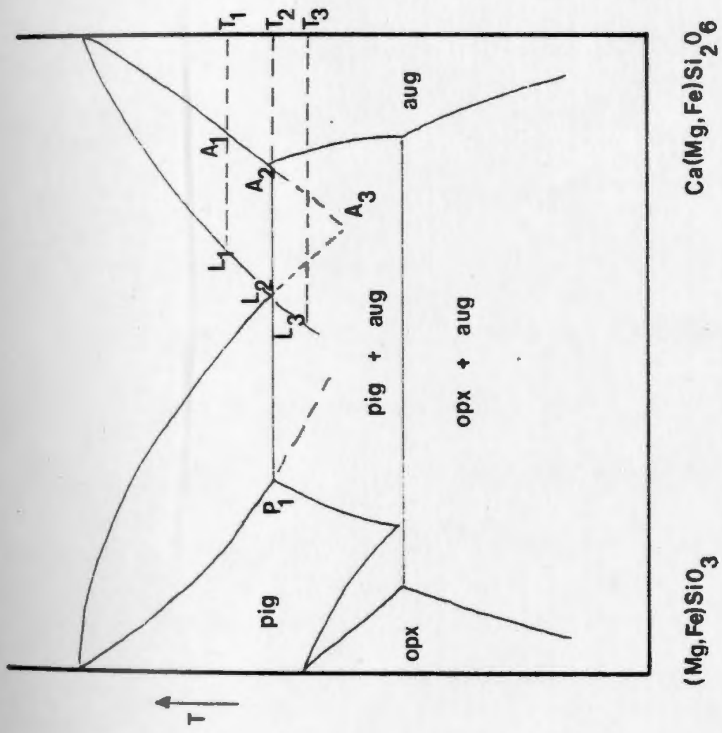
T1
T2
T3
A1
A2
A3
L1
L2
L3
P1
aug
pig + aug
opx + aug
pig
opx
T
Ca(Mg,Fe)Si2O6
(Mg,Fe)SiO3

It has long been known that under plutonic conditions a field of immiscibility exists between augite and pigeonite, but Kuno (1950, 1955) suggested that a complete range of composition between the two may occur, under certain conditions, in the rapidly crystallized clinopyroxenes of volcanic rocks. Up to the present most evidence has been optical with few actual demonstrations of pyroxenes showing gradation between augite and pigeonite. Poldevaart and Hess (1951) suggested that the amount of solid solution between diopside-hedenbergite and clinoenstatite-ferrosilite is a function more of the temperature than the speed of crystallization, the latter factor merely preserving the amount of solid solution at the crystallization temperature, but having no control over it. Deer, Howie and Zussman (1978) have upheld this view.

Ishii (1975) found a method to deduce the formation temperature of pigeonite. He discovered that during the fractionation of basic magmas the lower stability limit decreases as the Fe/Mg ratios of the pyroxenes increase. He defined a 'pigeonite eutectoid reaction line', a series of liquid compositions along which pigeonite can coexist with augite and orthopyroxene. The formation temperature of a pigeonite can be determined provided its composition lies on or close to the line and crystallization occurred at or near 1 atm. pressure (Figure V.4). The pigeonites which form the cores of KL-33 B, E and KL-34 C have an Fe/Fe+Mg value between 13.16-15.28 and would have crystallized at about 1200°C (assuming approximately 1 atm. pressure).

Nakamura and Kushiro (1970b) have studied in detail the compositional relations of augite, hypersthene and pigeonite phenocrysts in the groundmass of the andesite from Weiselberg, Germany. The phenocryst

FIGURE V.4 Pyroxene thermometry diagram, after Ishii (1975).
★ indicates quenched pyroxene in komatiite.

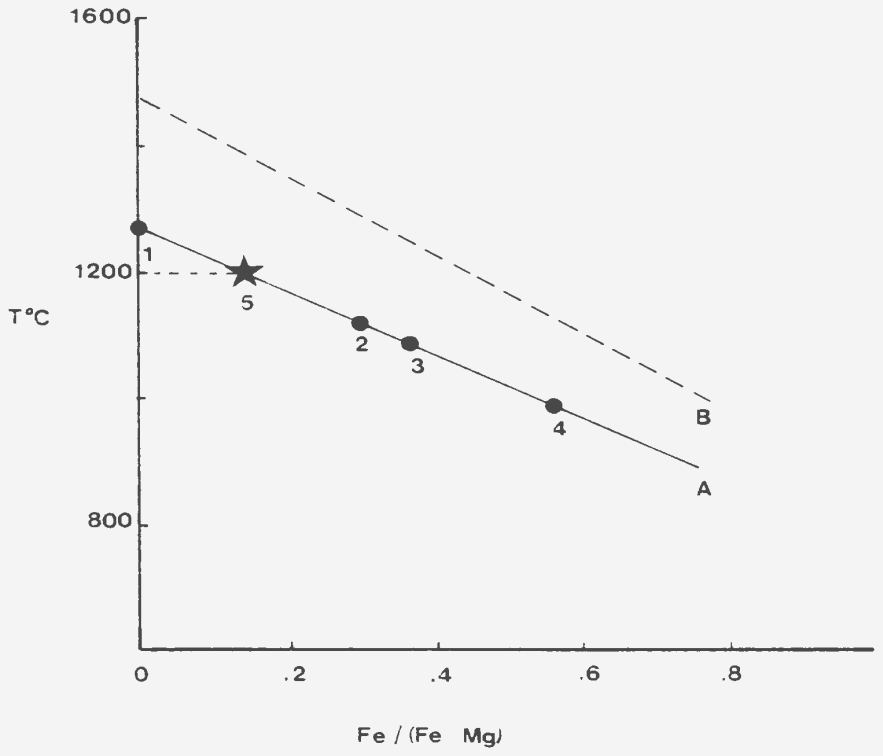
1600
1200
800
T°C
1
5
2
3
4
B
A
0
.2
.4
.6
.8
Fe / (Fe Mg)

assemblage during fractional crystallization is found to change with increasing Fe/Mg ratio from augite-hypersthene through augite-hypersthene-pigeonite to augite-pigeonite. Other authors (e.g. Isshiki, 1973) have documented an initial co-crystallization of augite and orthopyroxene until a certain Fs content was reached, when pigeonite replaced orthopyroxene as the Ca-poor phase.

The above research provides some insight into the nature of pyroxenes in fine-grained rocks, albeit there exist important differences with the present rocks. At any rate the present pyroxenes have two features in common with those discussed above. Firstly, zoning is not only a common but a ubiquitous feature indicative of continuous change in crystallization conditions, and secondly, the cores of zoned crystals are of varied compositions, ranging from calcic to calcium-poor types. Initial Ca-poor phases experience an increase in the Wo component while initial augitic compositions, which may be expected to have nucleated later and at lower temperatures, experience an increase in the Fs component. The lack of an early iron enrichment trend in Ca-poor pyroxenes appears to rule out the trend of two monoclinic pyroxenes as discussed above, with pigeonite ultimately succeeding orthopyroxene as the Ca-poor phase. Subcalcic augite (or pigeonite) is here believed to be the one important early calcic pyroxene which began to crystallize at about 1200°C and which represented at high temperatures solid solution of the $CaSiO_3$ and $MgSiO_3$ components, evidenced by the lack of a miscibility gap. Outward enrichment of Ca^{2+} in the grains occurred with Mg^{2+} depletion in the melt, perhaps partially due to the crystallization of unzoned orthopyroxene. The very high Mg/Fe ratio of the pyroxenes as compared with

those studies from basaltic analogues (e.g., Kuno, 1955) simply reflects the original high Mg content of the magma, which in fact is the factor which facilitated its rapid quenching and produced a basaltic glass under presumably normal extrusion conditions.

V.4 Plagioclase

Analyses of plagioclase were obtained only from the ultrabasic rocks and the aphyric lavas, as no free plagioclase was round in the komatiitic lavas, and the mineral within olivine basalts was invariably highly altered. The analyses are contained in Appendix B.2.

Plagioclase grains are unzoned and classified as labradorite and bytownite (An_{60}-An_{77}). There is not significant compositional variation between plagioclase from ultrabasic and less basic rocks, however, as both the highest and lowest values of An are found in the aphyric basalts. Alumina is particularly high in plagioclase from PL-24 and occupies tetrahedral positions in place of silica. The Or component is negligible in all analyses.

V.5 Classification of Basalt Based Upon Pyroxene Composition

Nisbet and Pearce (1977) have attempted, using pyroxene compositions and discriminant functions, to classify basalts as ocean floor, volcanic arc, within-plate tholeiite or within-plate alkali basalt. Statistical discrimination of clinopyroxene from known magma types indicates that any attempt to classify basalts using this method should have a 70% chance of success. It is proposed here to utilize two pertinant

diagrams, not to necessarily 'pigeonhole' the Upper Pillow Lava types but to delineate in a general way the basalts with which they have affinity.

The SiO_2(px) - TiO_2(px) and MgO/FeO(px) - TiO_2(px) plots of Nisbet and Pearce best serve the present purpose. On both plots the fields of ocean floor basalts and volcanic arc basalts are superimposed (Figures V.5 and V.6). The clinopyroxenes, like the lavas of which they are a part, are characteristically low in TiO_2. Affinities here between volcanic arc basalts and the Upper Pillow Lavas are suggested, as most samples plot in the VAB field, with lower TiO_2 content in clinopyroxenes than is characteristic for ocean floor basalts.

FIGURE V.5 Classification of basalt based upon pyroxene composition; SiO_2 vs. TiO_2. (after Nisbet and Pearce, 1977).

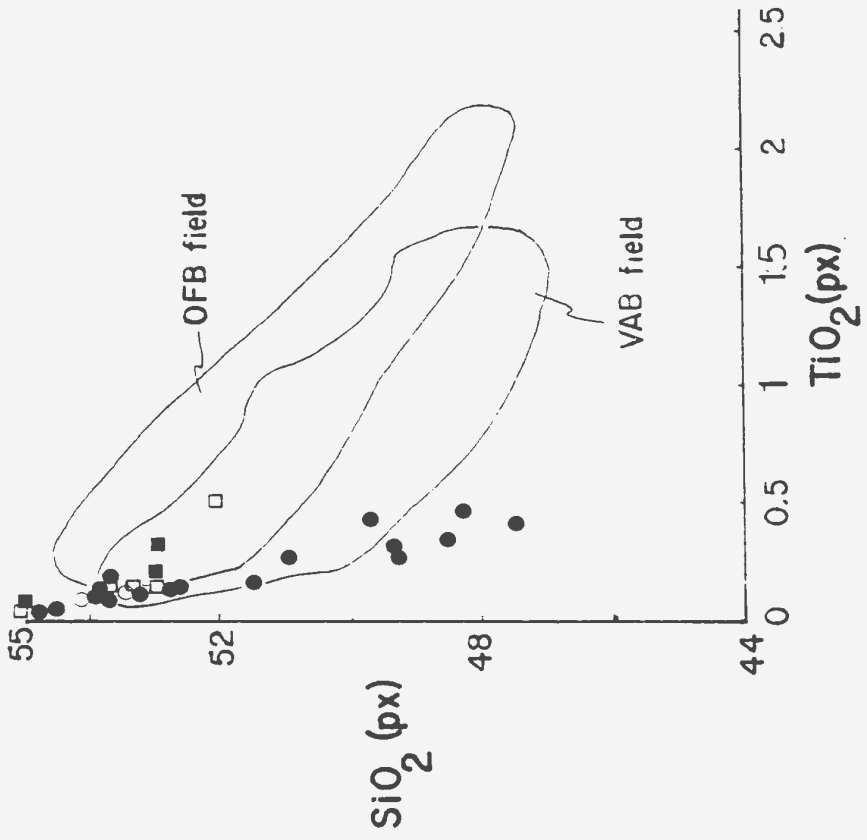
OFB field
VAB field
55
52
48
44
0
0.5
1
1.5
2
2.5
SiO_2 (px)
TiO_2(px)

FIGURE V.6 Classification of basalt based upon pyroxene composition; MgO/FeO vs. TiO_2. (after Nisbet and Pearce, 1977).

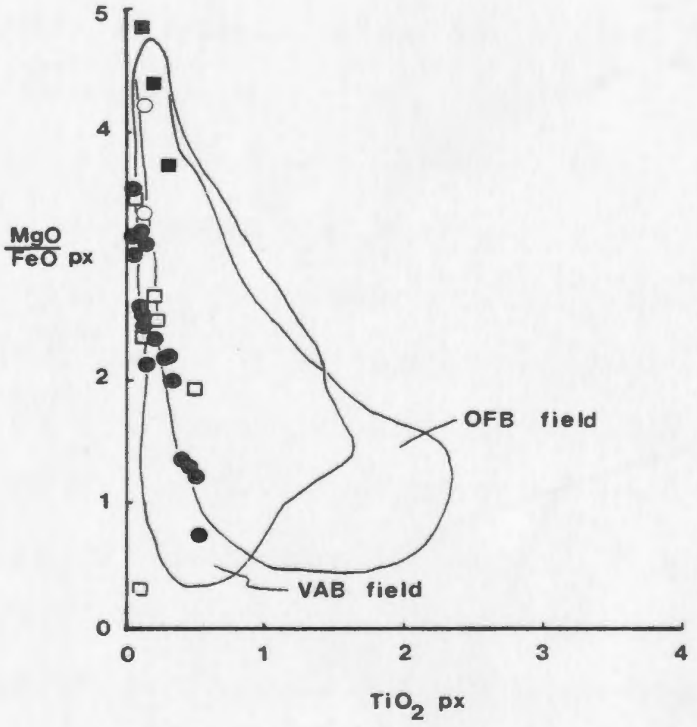
5
4
2
1
0
MgO / FeO px
OFB field
VAB field
0
1
2
3
4
TiO2 px

VI. PETROGENESIS

VI. Introduction

It is evident, from an examination of the bulk rock geochemistry of the Upper Pillow Lavas, as presented in Chapter IV, and the mineral chemistry as presented in Chapter V, that this group of rocks differs fundamentally from the majority of basaltic rock types found in the ocean basins today. The literature has dealt voluminously with rocks of common occurrence in the ocean basins, i.e., rocks broadly ascribed to mid-oceanic ridge and island arc environments of formation. Comparatively little research has been concerned with the rarer rock types often found intimately associated with those of more common occurence.

This chapter will attempt to deduce the origin of the Upper Pillow Lavas of Troodos by considering a unique parental magma which could have given rise to such a rock series. Recent research has dealt with petrogenetic problems which have a direct bearing on the present study. The following discussion reviews and draws from this work.

Duncan and Green (1980) have proposed, mainly on the basis of major element geochemistry, that extremely light rare earth-depleted magnesian quartz tholeiitic or olivine-poor tholeiitic liquids are related genetically to residual diapirs from which picritic liquids have earlier been extracted. These magmas differ fundamentally from tholeiitic picrite, which has been proposed as the primary magma for high Al_2O_3 oceanic olivine tholeiite (O'Hara, 1968) and which may be derived by about 30% partial melting of upper mantle lherzolite (Green et al., 1979). According to some workers the wide variation in ocean floor

basalts as regards chemistry and mineralogy is related to various processes of fractionation involving the phases olivine, pyroxene, plagioclase and spinel (e.g., Frey et al., 1974; Bryan et al., 1976; Bryan and Moore, 1977; Malpas, 1978), whilst other workers (e.g., Blanchard et al., 1976; Flower et al., 1977; Bender et al., 1978) maintain that this diversity necessitates a range in composition of primary magmas. This concept of different primary liquids invokes complex processes of fractional melting and crystallization, and magma mixing at the depths where primary magmas are produced, as well as upper mantle heterogeneity.

The heterogeneous nature of the upper mantle, however, is intimately tied to this premise of complex melting/crystallization. Small degrees of partial melting have the effect of concentrating highly incompatible elements in the liquid phase with a concomitant depletion of these elements in the unmelted material. The immediate effect is to produce very local zones of depletion/enrichment in regions of high geothermal gradient.

Magnesian quartz tholeiites, then, which have been derived by a second stage or advanced melting process (i.e., heterogeneous mantle) can be treated as primary liquids from which distinctive magma series may be produced by low pressure fractionation. Duncan and Green plotted the major element compositions of olivines from the ultrabasic rocks, and the bulk rock compositions of ultrabasic rock, olivine basalt and aphyric lavas of the Upper Pillow Lavas. (Figure 1 of Duncan and Green, 1980.) They suggested that the exhibited linearity could be explained by the addition or removal of olivine, and using reported chemical data (Searle and Vokes, 1969; Gass, 1958; Kay and Senechal, 1976; Simonian and Gass,

1978) determined a parental liquid composition, based on the principal that such a liquid must be in equilibrium with the most magnesian olivine observed. An olivine composition of $Fo_{91.7}$ implies a $Mg/Mg+Fe^T$ ratio of 0.77 (Roeder and Emslie, 1970); this determined parental liquid is found to be more refractory than the least fractionated basalts from ocean ridge and island arc environments.

Here the concept of olivine extraction will be tested. From the linearity expressed in the major and trace element variation diagrams, Figures IV.1 and IV.2, Chapter IV, it can be empirically stated that addition and removal of olivine accounts for the composition of all the members of the Upper Pillow Lavas. Olivine fractionation is considered in detail after it is shown that the fractionated olivines could have crystallized from a magma of the composition of the Upper Pillow Lava komatiites.

This concept will be tested in the following sections. Firstly, the feasibility of olivine-liquid equilibrium will be examined for the system, and secondly, phase equilibria studies for Upper Pillow Lava bulk rock compositions will be carried out, by projection into the normative basalt tetrahedron of Yoder and Tilley (1962) and into an analogue of the CMAS system of O'Hara (1968).

VI.2 Olivine-Liquid Equilibrium

Roeder and Emslie (1970) studied the equilibrium between olivine and basaltic liquids and determined the distribution coefficient

$$K_D = \frac{{}^{Ol}_{FeO} \; {}^{liq}_{MgO}}{{}^{liq}_{FeO} \; {}^{Ol}_{MgO}} \qquad \ldots \text{(VI.1)}$$

relating the partitioning of iron and magnesium between olivine and liquid, to be equal to 0.30 and independant of temperature. Thus the composition of olivine depends only on the ratio of magnesium to ferrous iron in the liquid from which the olivine is crystallizing; if the two are in equilibrium the FeO/MgO ratio of the crystals and liquid can be related by the constant K_D. Therefore it can be determined whether an olivine of a particular composition could have crystallized from a liquid of a particular magnesium/ferrous iron ratio.

The following calculations will compare the FeO/MgO ratio of olivines from the ultrabasic rocks to that of the komatiitic lava. The expression of the distribution coefficient above can be rearranged to read

$$\frac{{}^{Ol}_{FeO}}{{}^{Ol}_{MgO}} = \frac{K_D}{{}^{liq}_{MgO} \; {}^{liq}_{FeO}}$$

$$= \frac{K_D * {}^{liq}_{FeO}}{{}^{liq}_{MgO}} \qquad \ldots \text{(VI.2)}$$

Using this form of the equation the value of FeO/MgO for olivine can be calculated from the komatiitic FeO/MgO ratio.

If for the average komatiite,

FeO = 4.76 mole % and

MgO = 17.15 mole %, (calculated from Table VII.2)

and K_D = 0.3, as determined by Roeder and Emslie (1970), then

$$\frac{{}^{Ol}_{FeO}}{{}^{Ol}_{MgO}} = \frac{0.3 * 4.76}{17.15} = 0.0833$$

To calculate the Fo content of olivine which would cyrstallize we say that

$$Fo + Fa = 100$$

and therefore

$${}^{Ol}_{MgO} + {}^{Ol}_{FeO} = 100 \qquad \ldots (VI.3)$$

$${}^{Ol}_{MgO} = 100 - {}^{Ol}_{FeO} \qquad \ldots (VI.4)$$

But $${}^{Ol}_{FeO} = 0.0833 * {}^{Ol}_{MgO} \qquad \ldots (VI.5)$$

and substituting VI.5 into VI.4 we have

$${}^{Ol}_{MgO} = 100 - (0.0833 * {}^{Ol}_{MgO}) \qquad \ldots (VI.6)$$

$${}^{Ol}_{MgO} + (0.0833 * {}^{Ol}_{MgO}) = 100 \qquad \ldots (VI.7)$$

$$1.0833 \left({}^{Ol}_{MgO}\right) = 100$$

and $${}^{Ol}_{MgO} = 100/1.0833 = 92.31 \qquad \ldots (VI.8)$$

The calculated olivine composition is $Fo_{92.31}$ or expressed in significant figures, $Fo_{92.3}$. This can be directly compared with the average olivine composition from the ultrabasic lavas, $Fo_{91.6}$ (see Appendix B.2). This mathematical derivation is depicted graphically

in Figure VI.1, after Roeder and Emslie (1970, Figure 7). The komatiitic ratio FeO/MgO defines a line which lies close to Fo_{90} - Fa_{10} on the graph.

The excellent correlation between measured and calculated values indicates that the olivine crystals within the ultrabasic lavas could have separated by equilibrium crystallization from the liquid now represented by the komatiites.

VI.3 Basalt Tetrahedron (Figure VI.2)

All the compositions of the Upper Pillow Lavas have been projected into the normative basalt tetrahedron of Yoder and Tilley (1962). Projections are made from the four apices onto the opposite side of the tetrahedron; the dry cotectics of the synthetic system Fo-Di-An-Qz and natural system Ol-Cpx-Plag-Qtz at 1 atm. pressure are shown. The positioning of the natural cotectics are affected by the presence of Na and Fe in the natural systems which tend to expand the primary phase volumes of the mafic minerals against that of plagioclase. The natural cotectics are derived from Tilley et al. (1963; 1964; 1965; 1967) and Clarke (1970).

For comparison several analyses from the Lower Pillow Lavas as determined by the author, as well as four published analyses have been included in these plots (Appendices B.1.1, B.1.3).

In the projection from olivine the spread of the ultrabasic rocks is a result of their proximity to the olivine apex. The natural system cotectic appears to be more favourable as it corroborates the petrographic data - after olivine, clinopyroxene would be the next phase

FIGURE VI.1 Graphical representation of olivine/liquid equilibrium calculations. represents MgO/FeO ratio (mole%) of komatiites. Heavy dashed line indicates calculated equilibrium olivine composition. (Diagram from Roeder and Emslie, 1970, Fig. 7.)

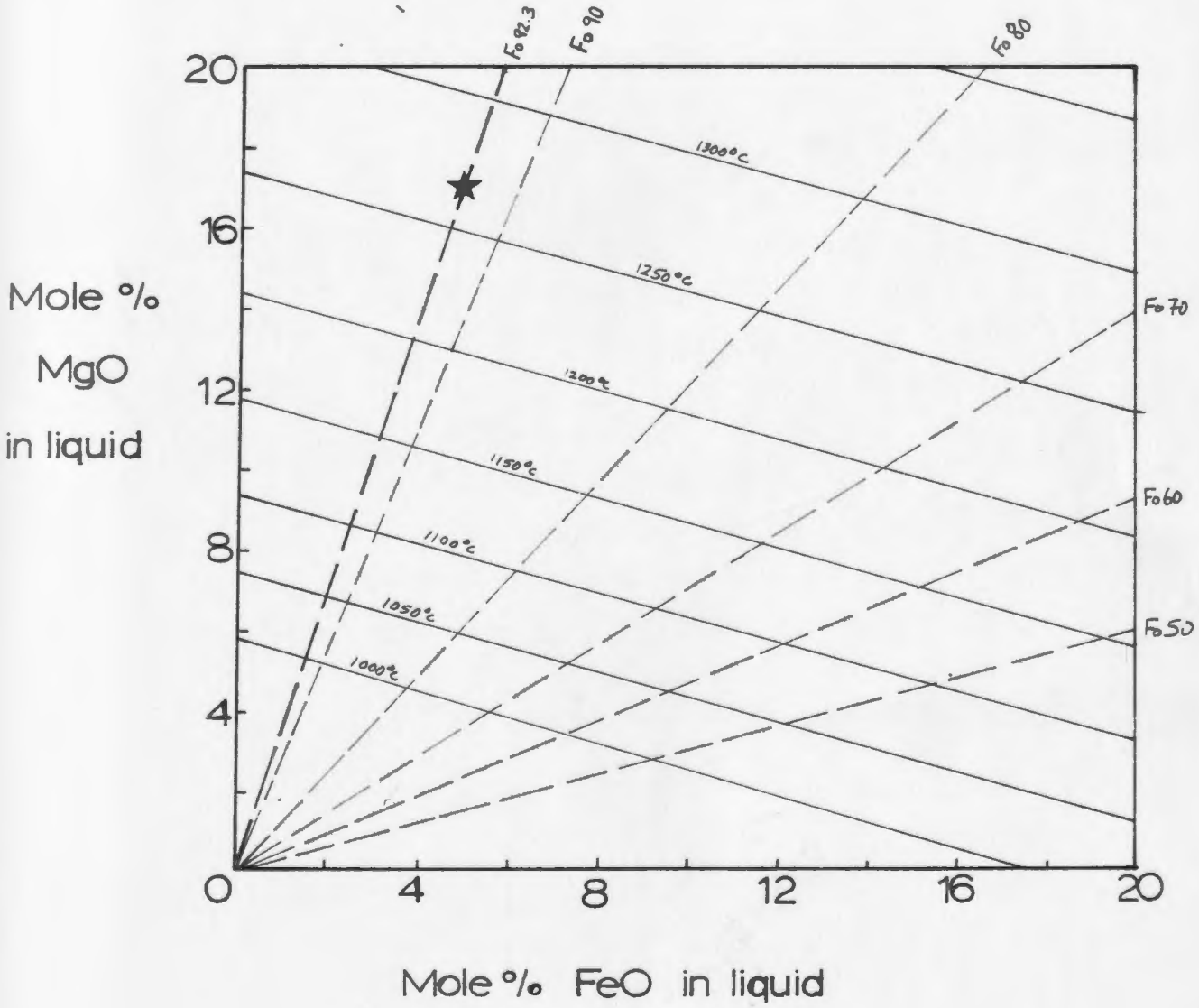
Fo 92.3
Fo 90
Fo 80
1300°C
1250°C
1200°C
1150°C
1100°C
1050°C
1000°C
Fo 70
Fo 60
Fo 50
20
16
12
8
4
0
4
8
12
16
20
Mole % MgO in liquid
Mole % FeO in liquid

FIGURE VI.2 Basalt tetrahedron projections (after Yoder and Tilley, 1962).

A. Projection from olivine
B. Projection from plagioclase
C. Projection from diopside
D. Projection from quartz

Symbols:

■ Ultrabasic rock
● Komatiites
○ Olivine basalt
□ Aphyric basalt
★ Lower Pillow Lava (this study)
☆ Lower Pillow Lava (published)

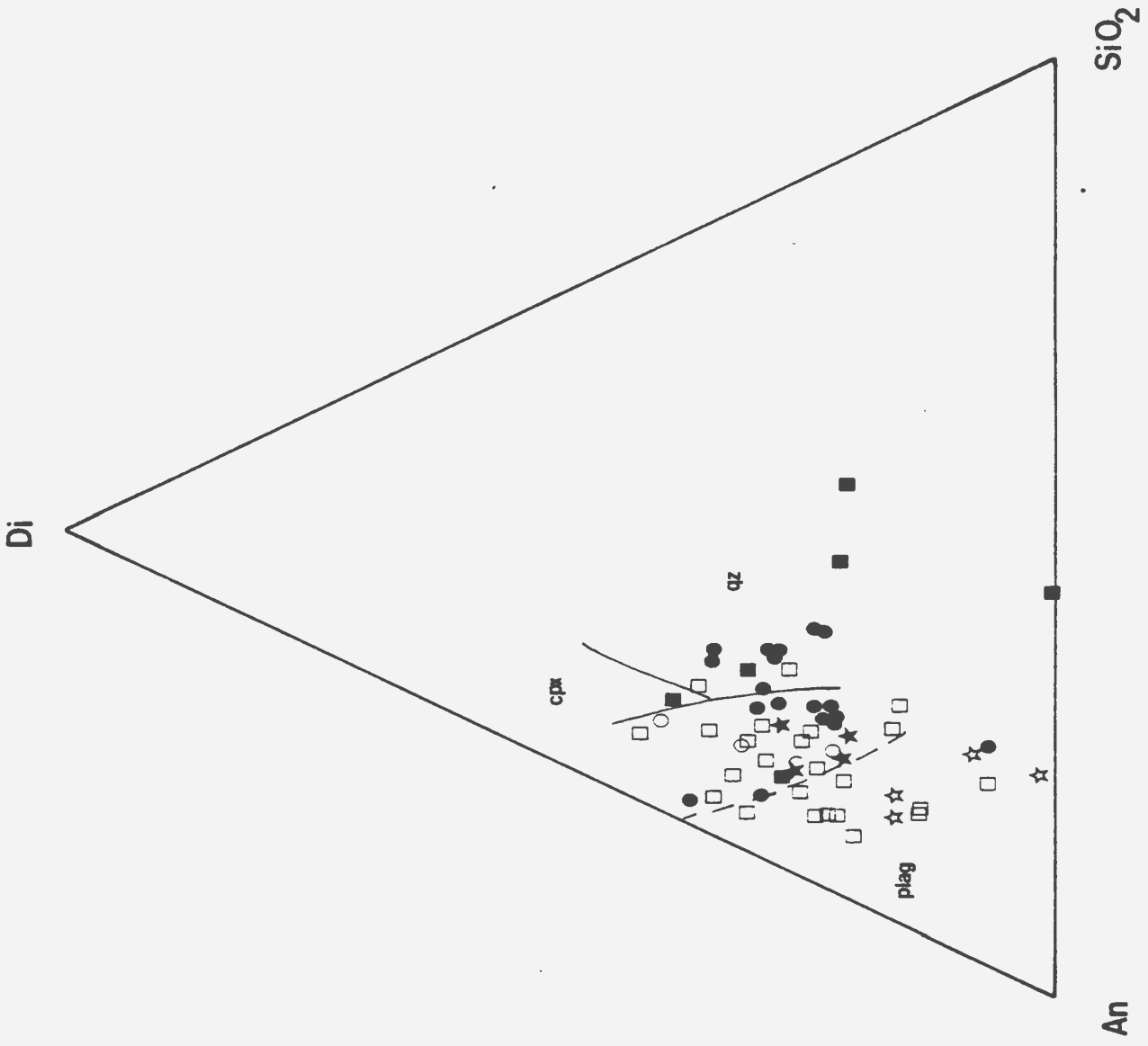
Di
SiO_2
An
qz
cpx
plag

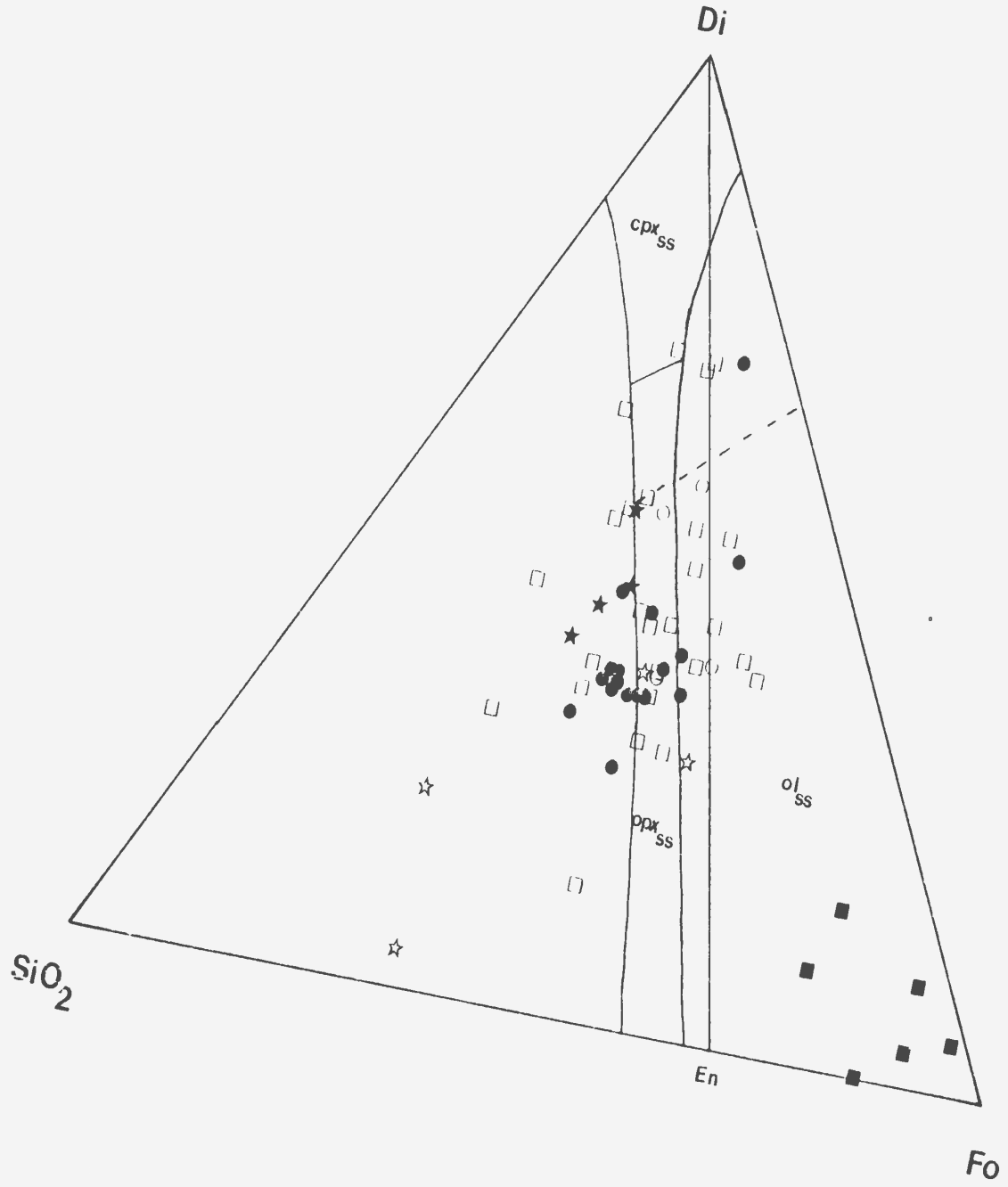
Di
cpx ss
ol ss
opx ss
SiO2
En
Fo

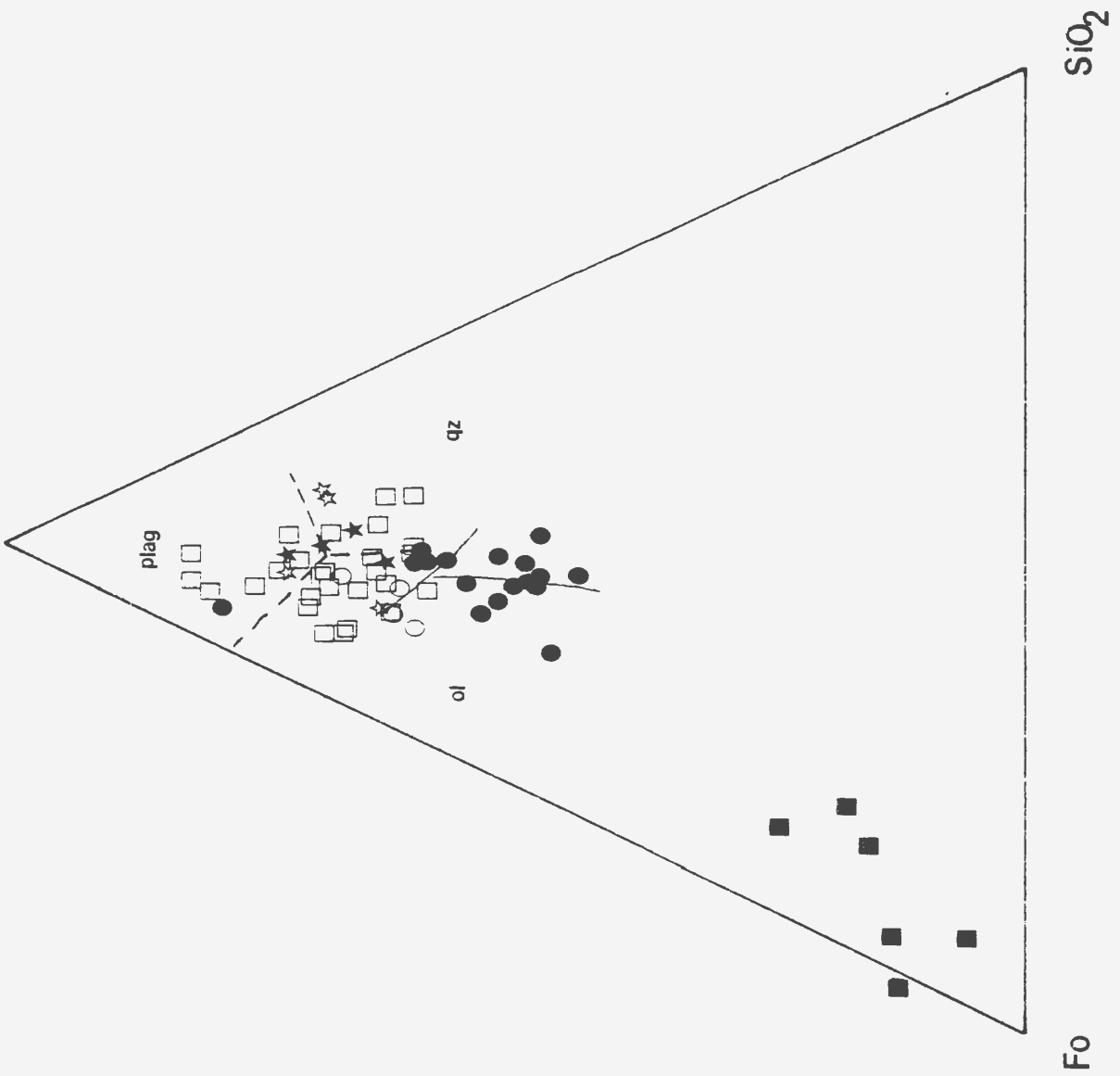
An
plag
qz
ol
SiO_2
Fo

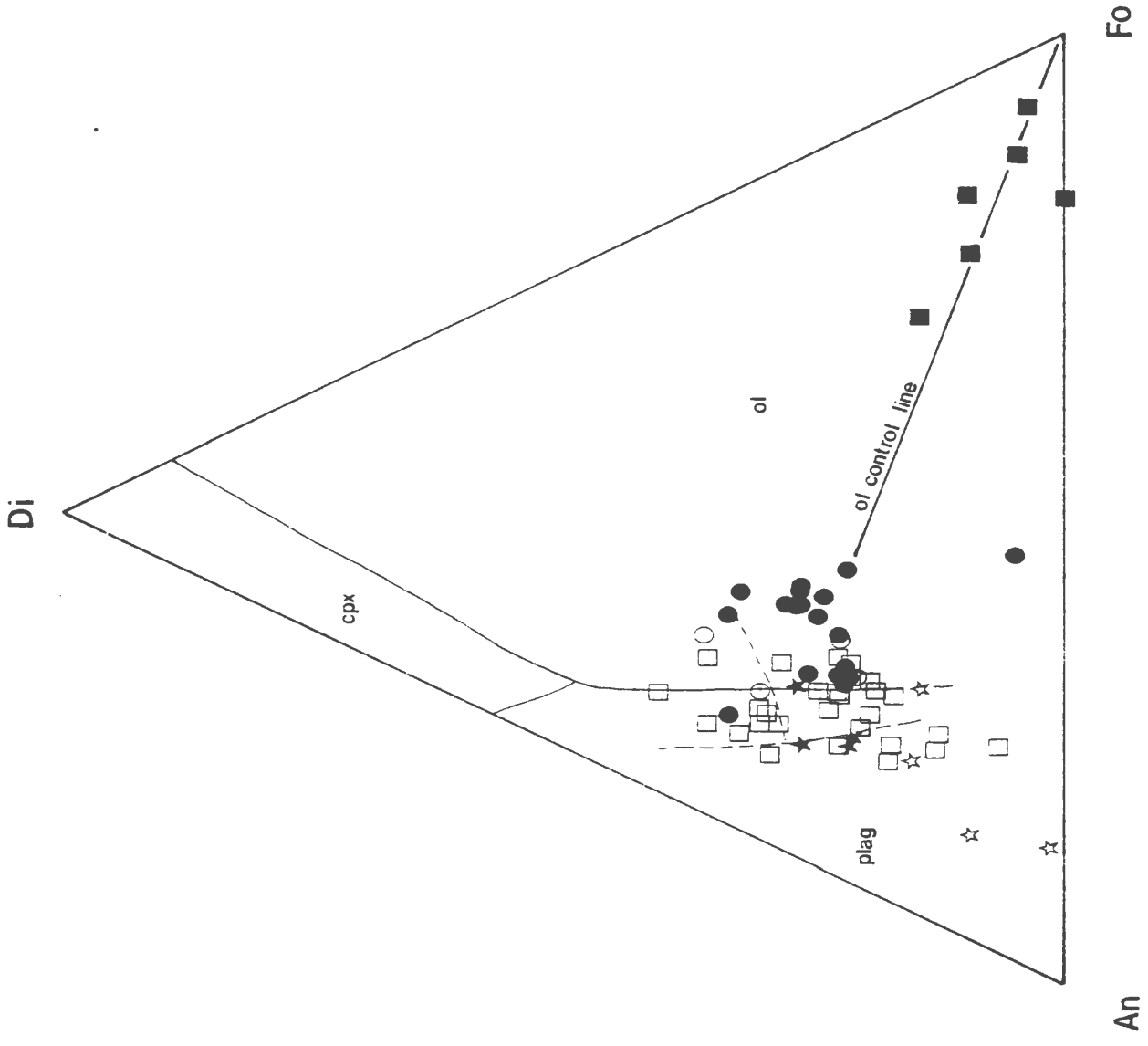
Di
Fo
An
cpx
ol
ol control line
plag

to crystallize in the komatiites and olivine basalts. In the olivine-free rocks, i.e., the aphyric basalts, initial crystallization of plagioclase or augite will be followed by cotectic crystallization of the two phases. The published Lower Pillow Lava analyses contain a higher normative proportion of An; here plagioclase would be the initial crystallizing phase.

The disposition of normative analyses toward the Fo apex of the ultrabasic rocks is evident in the projection from anorthite. The position of most komatiites on the silica side of the Di-En join reflects the oversaturated character of the magma, and suggests that the early-crystallizing olivine was removed quickly from the system and did not react with the silica-rich liquid to form orthopyroxene. The wide scatter of olivine and aphyric basalts and Lower Pillow Lavas indicates the irregularity of silica content and/or the proximity of these points to the An apex.

Projected from the diopside apex the komatiite lavas fall decisively into the field of normative Fo but close to the natural system Ol-Qz reaction curve, attesting to their Mg-rich but silica-oversaturated nature. Olivine basalts plot in the Fo field but closer to the ternary eutectic, while aphyric basalts are spread around it. There is a general trend in the lavas away from a composition located close to olivine on the Fo-SiO_2 join, suggesting olivine $\pm$ orthopyroxene control. Lower Pillow Lava projections resemble those for oceanic tholeiite basalts as plotted elsewhere (e.g., Malpas, 1976).

The initial control of olivine is evident in the projection from silica. Most of the komatiite and olivine basalt plots lie on the

diopside side of the control line, and using the natural system cotectic clinopyroxene would be the next phase to crystallize, while for compositions below the control line plagioclase would have crystallized in equilibrium with olivine, if quenching had not occurred.

VI.4 CMAS System (Figure VI.3)

O'Hara (1968) developed a scheme based on experimental studies of natural basalts that allows ten of the major and minor oxides of basic rocks to be expressed in terms of the four components R_2O_3-XO-YO-ZO_2. This differs from the analogous synthetic system Al_2O_3-CaO-MgO-SiO_2 (A-C-M-S, O'Hara, 1968, Fig. 4) principally by its calculation of all FeO, MnO and MgO as one component, YO. Jamieson (1970) demonstrated the ability of the pseudo-quaternary R_2O_3-XO-YO-ZO_2 data projections scheme to reproduce the phase relations during the early crystallization of Hawaiian tholeiitic lavas at low pressure. By restricting the use of this projection scheme to the illustration of the early crystallization features of tholeiitic magma, Jamieson considered that the resultant small departures from the quaternary analogy were acceptable.

Two projections are best suited to represent phase relations in tholeiitic rocks - a projection to, or from, the Fo composition point into the plane R_2O_3-YO·ZO_2-XO·ZO_2 (O'Hara, 1968, Fig. 4), and a projection to, or from, the Cpx composition point into the plane ZO_2-YO-XO·R_2O_3 (O'Hara, 1968, Fig. 6). Also projected are the solid lines which represent the loci of liquid compositions in isobaric pseudo-univariant equilibria in the pseudo-quaternary system

FIGURE VI.3 Projections within the natural system R_2O_3-XO-YO-ZO_2 (O'Hara, 1968; Jamieson, 1970), with reference to analogous synthetic system A-C-M-S (O'Hara, 1968, Figure 4).

A. Projection from olivine
B. Projection from diopside

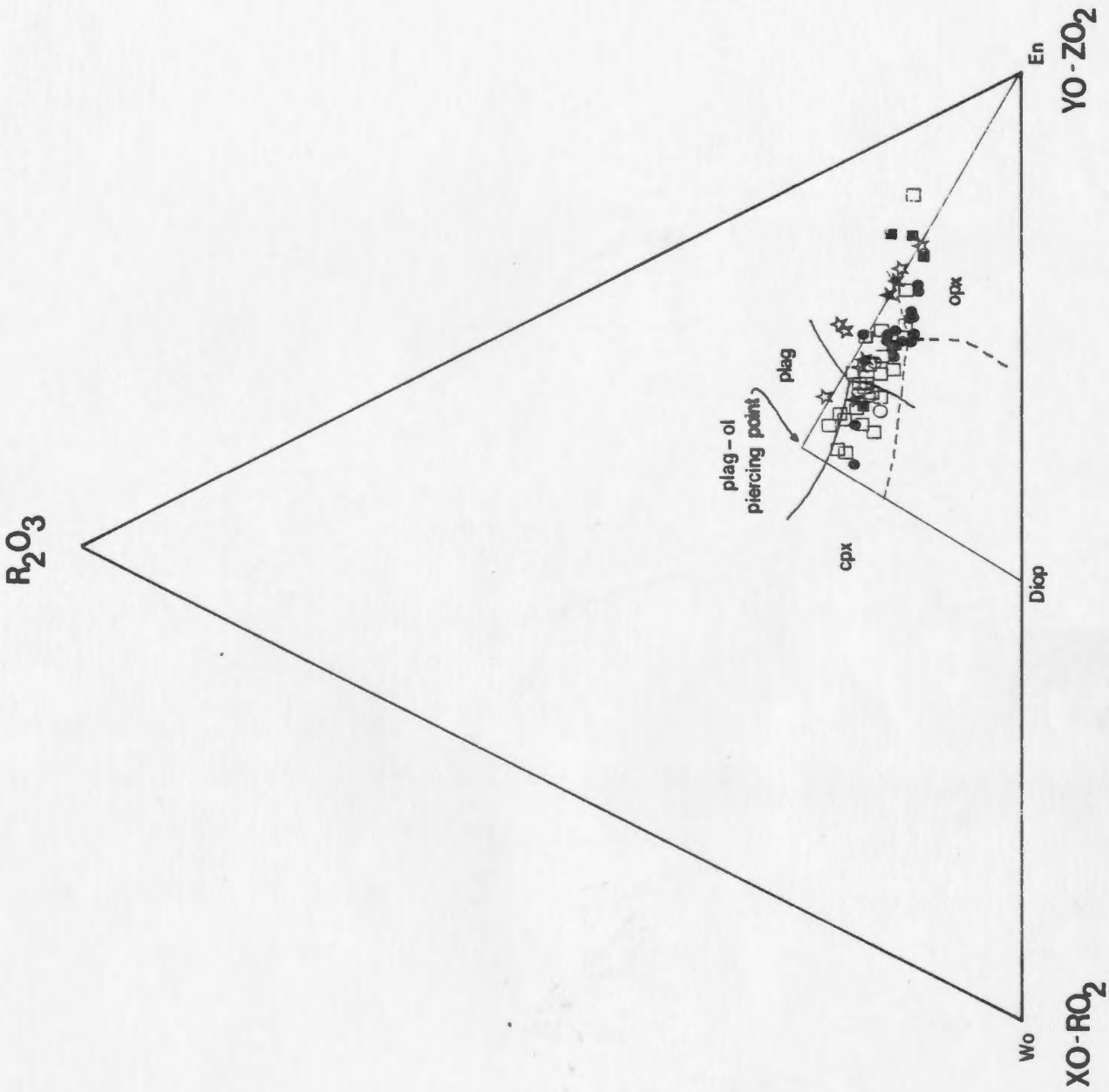
R_2O_3
$YO-ZO_2$
$XO-RO_2$
En
Wo
Diop
opx
cpx
plag
plag - ol
piercing point

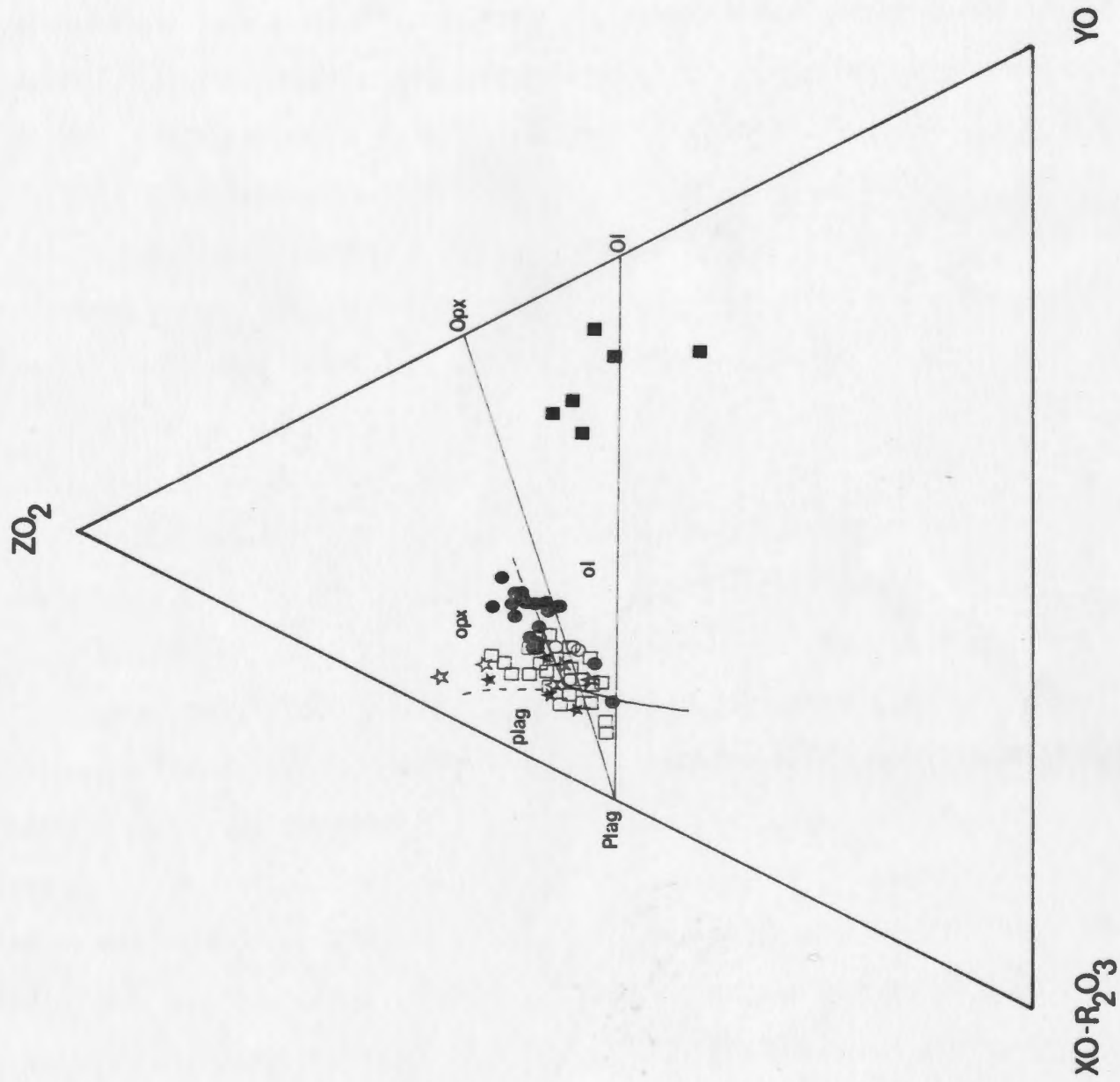
ZO2
YO
XO-R2O3
Opx
Ol
Plag
opx
ol
plag

R_2O_3-XO-YO·ZO_2, and broken lines, which represent the loci of liquid compositions in some of the isobaric univariant equilibria bounding the olivine primary phase volume in the synthetic system Al_2O_3-CaO-MgO-SiO_2.

The olivine projection traces the liquid line of descent for olivine-bearing rocks. The ultrabasic rocks show some scatter due to this particular projection but they mostly plot in the high-temperature part of the orthopyroxene field. As regards the komatiites, co-precipitation of olivine and orthopyroxene is joined down temperature clinopyroxene precipitation, at which stage the magma was quenched, before the liquid composition reached the plagioclase-clinopyroxene pseudo-univariant line. Olivine basalts exhibit initial olivine and clinopyroxene crystallization which is followed down temperature by olivine-clinopyroxene-plagioclase co-precipitation.

The diopside projection is necessary to show the position of the analyses points with respect to the olivine composition point. The position of komatiite lavas shows that either orthopyroxene or olivine may have been the liquidus phase in the magma which gave rise to this rock type; at any rate a small drop in temperature would have initiated co-precipitation of both phases. Care must be taken in interpreting this projection, however, as clinopyroxene is not an early crystallizing phase and the points may be distorted toward the orthopyroxene field. Olivine basalts plot with olivine on the liquidus, with subsequent co-precipitation of clinopyroxene and plagioclase, as is the case for the olivine projection. The plots for the aphyric basalts indicate that the magmas represented by these rocks could have had olivine or orthopyroxene on the liquidus, although many of these points may be artificially displaced toward the YO-RO_2 join by greater contents of FeO and MnO in the natural

system. Further uncertainty is introduced by the poor definition of the pseudo-univariant line denoting plagioclase-orthopyroxene cotectic crystallization for this part of the system.

In general equilibrium phase relations deduced from this projection scheme are supportive of the petrographical data. The position of the ultrabasic rocks near the olivine composition point indicates enrichment in this mineral. The komatiitic lavas could have been derived by the removal of material equivalent in composition to the Upper Pillow Lava ultrabasic rocks (i.e., olivine crystals + trapped liquid) from a parental magma which plots somewhere between them. Further removal of olivine $\pm$ orthopyroxene could produce the olivine and aphyric basalts.

VI.5 Estimates of Melting and Fractionation

To further employ this petrogenetic model calculations will be carried out in an effort to estimate (1) the amount of partial melting required to produce a magma which can be regarded as parental to the Upper Pillow Lava series, and (2) the phases and amount of fractionation involved in deriving the different lava types. To make these estimates two methods were used; one utilizes trace elements and known mineral/liquid distribution coefficients, while the other is a major element mass balance calculation.

VI.5.1 Trace Element Modelling

VI.5.1.1. General

The concept of trace element modelling is based on the assumption that when a mineral is in chemical equilibrium with a liquid, ele-

ments are partitioned between the two phases according to their chemical activity in each. For trace elements whose concentrations are low in both phases (i.e., <10,000 ppm or 1%) the following relationship can be defined:

$$\frac{\text{conc. element in mineral}}{\text{conc. element in liquid}} = K_D$$

where K_D is the distribution or partition coefficient for the given crystal/liquid equilibrium. Since K_D is a constant its value is generally derived from synthetic crystallization experiments or from phenocryst - matrix relations in glassy rocks. Estimates of its value vary widely, however, as many probably are based on glassy rocks where equilibrium was not attained.

The concentration of any element in a liquid produced by melting a source rock must take into consideration the proportions of minerals comprising that source. Thus a bulk distribution coefficient (D) is calculated from the weight proportions (w) of each mineral in the source:

$$D = \sum_{n=i}^{n} w_i K_{Di} \qquad \ldots \text{(VI.9)}$$

Whereas elements with $D < 1$ are termed incompatible, i.e., they will be concentrated in the liquid during melting and crystallization, and elements with $D > 1$ are compatible, that is, they are retained in a solid residuum or are extracted in a crystallizing phase, it can be seen that this is entirely dependent upon the phase assemblage present. Thus in any discussion of mantle compositions (olivine + pyroxene + aluminous phase) imcompatible elements are roughly synonomous with the large ion lithophile (LIL) trace elements (e.g., K, Rb, Sr, Ba, Zr, Th and light rare earths). These are the elements whose ionic radii are too large or

whose valencies are too high to allow them to substitute readily for major elements in crystal lattices.

Various workers have developed models which predict the changes in trace element concentrations during processes of partial melting and fractionation (e.g., Arth, 1976; Wood and Fraser, 1976). The different models and their theoretical bases are discussed in detail by these authors, and the reader is referred to them for further information; to suit the exigencies of this paper only simplified versions of these models will be considered. A good review of the best known models is contained in Chapter 14 of Cox et al., (1979), from which much of the present discussion is drawn.

VI.5.1.2 Partial (Batch) Melting

Trace elements will here be used to model the amount of partial melting required to produce a derived liquid from a given source composition. The simplest model for the partial melting of a complex mineral assemblage is one in which the liquid remains at the site of melting and is in chemical equilibrium with the solid residuum until mechanical conditions allow it to escape as a single 'batch' of primary magma. Under these circumstances the concentration of an element in the liquid, C_l, is related to the original source material by the equation:

$$\frac{C_l}{C_o} = \frac{1}{F + D - FD} \qquad \ldots \text{(VI.10)}$$

where F is the weight proportion of melt formed and D is the bulk distribution coefficient for the residual solids at the moment when the melt is removed from the system.

It has already been discussed above in Section VI.1 how Duncan and Green (1980) have proposed the derivation of upper lava series in some ophiolites by second-stage partial melting of a mantle diapir. This concept of two-stage development of ophiolite lavas will here be examined using published trace element data and new data collected in this study from the Upper Pillow Lavas. For this purpose two different sets of calculations will be carried out; one will estimate the amount of 'batch' melting required to produce the Lower Pillow Lavas from a 'fertile' source in the upper mantle (i.e., spinel lherzolite), while a second set of calculations will estimate the amount of 'batch' melting required to produce the liquid parental to the Upper Pillow Lavas from a harzburgitic composition which has been depleted in incompatible elements by the first-stage melting process.

VI.5.1.2.1 First-Stage Melting

Ideally the ultramafic rocks involved in the first-stage melting calculation would be from the Troodos Massif, but no trace element data are available from these rocks. Consequently average trace element contents as documented by Goles (1967) are used. These concentrations are here considered to represent that of 'fertile' upper mantle, i.e., a source region which could give rise by fairly extensive amounts of partial melting to picritic liquids parental to oceanic tholeiites.

For this particular calculation the elements rubidium and strontium will be used. The average value determined by the author for Rb is much higher than normal for tholeiitic rocks, perhaps due to metasomatism and the small number of samples collected from the Lower Pillow

Lavas in this study. A more representative value for Rb to be used in these calculations is taken from Peterman et al. (1970). Both values are included in Table VI.1.

Calculations using potassium gave high estimates of partial melting when compared with those of rubidium and strontium, and were omitted upon the consideration that K may have been highly affected by metasomatic processes.

Mineral/liquid partition coefficients are taken from Arth (1976) except for the coefficient for spinel which is taken from Cox et al. (1979, pp. 334). These values are listed in Table VI.2. An average upper mantle lherzolite composition of 60% olivine/25% orthoproxene/10% clinopyroxene/5% spinel will be taken, as suggested by Cox et al. (1979, pp. 336).

Rubidium

Bulk Distribution Coefficient (D_{Rb}) =

(wt. fraction olivine * $K_{D liq}^{ol}(Rb)$) +

(wt. fraction orthopyroxene * $K_{D liq}^{opx}(Rb)$) +

(wt. fraction clinopyroxene * $K_{D liq}^{cpx}(Rb)$) +

(wt. fraction spinel * $K_{D liq}^{sp}(Rb)$) . . . (VI.11)

= (0.6 * 0.0098) + (0.25 * 0.022) + (0.10 * 0.015)

+ (0.05 * 0.01)

= 0.0134

If Equation VI.2 is solved for F we have

$$F = \frac{\frac{C_o}{C_l} - D_{Rb}}{1 - D_{Rb}},$$

Table VI.1 Average Trace Element Concentrations Used in Calculations

ppm	'Fertile' Upper Mantle	LPL's		Dep. Harz.		Upper Pillow Lavas		
		A	B	A	B	Komat.	Ol. bas.	Aph. bas.
K	200	8827	3651	-	110	1909	7740	7305
Rb	1	19	4.1	0.1	0	4	9.5	27.4
Sr	20	104	124	0.4	32	104	100	91.2
Ba	0.4	35	-	-	64	14.6	27	24.6
Zr	35	28	57	1.5	4	15.8	19.2	21.1
Cu	30	51	-	14	10	76.7	36.7	31.7
Ni	1500	45	-	2290	2262	217	159	62.3
Ti	300	6480	6720	270	240	1977	2336	2576
V	40	304	-	39	38	209	215	266
Pb	0.05	3.69	-	3.5	-	0.5	0.5	2.5
Cr	2400	72	90	2150	2840	617	479	155
Zn	-	61	-	50	36	61	60	64.9
Nb	-	2.57	3	1	0	1.7	1	2
La	-	7.4	-	-	-	20.1	19.7	15.6
Y	-	21.5	26	1.5	2	11.7	11.7	17.1
Ce	-	2.5	11.7	-	-	3.5	3	4.6
Ga	-	12.3	-	1.25	1	10.8	11.2	11.5

Sources:

'Fertile' Upper Mantle: Goles (1967), Table 11.1.

Lower Pillow Lavas, A: this work; B: Pearce (1979), Table 1, Locality 18.

Depleted Harzburgite, A: Suen (1979), average of 2 harzburgites, Table II.3;
B: Talkington, Ray (pers. comm., 1980).

Upper Pillow Lavas: This work; Komatiites, avg. of 18; Olivine basalts, avg. of 4; Aphyric basalts, avg. of 26.

Table VI.2 Partition Coefficients

	Olivine	Orthopyroxene	Diopside	Spinel
Potassium	0.0068	0.014	0.011	0.01
Rubidium	0.0098	0.022	0.015	0.01
Strontium	0.014	0.017	0.12	0.01
Titanium	0.02	-	-	-
Zirconium	0.01	-	-	-
Yttrium	0.01	-	-	-

Values for K, Rb, Sr from Arth (1976), except for spinel, which is from Cox et al. (1979).

Values for Ti, Zr, Y from Pearce and Norry (1979).

where C_o is the concentration in the original source material (peridotite), and C_l is the concentration produced in the liquid by melting, i.e., the liquid parental to the Lower Pillow Lavas. Given, from Table VI.1, that C_o = 1 ppm and C_l = 4.1 ppm, then

$$F = \frac{\frac{1 \text{ ppm}}{4.1 \text{ ppm}} = 0.0134}{1 \text{ ppm} - 0.0134} = 0.2336,$$ which means a melt fraction of approximately 23%.

Strontium

$$D_{Sr} = (0.6 * 0.014) + (0.25 * 0.017) + (0.1 * 0.12) + (0.05 * 0.01)$$

$$= 0.0251$$

If C_o = 29 and C_l = 87.2 (Table VI.1), then

$$F = \frac{20/87.2 - 0.0251}{1 - 0.0251} = 0.2096,$$ or approximately 21% melt.

The calculated values for rubidium and strontium are in general agreement and provide a rough estimate of the amount of melting required to produce the Lower Pillow Lavas from an average upper mantle composition. The values given by the Rb and Sr calculations are not far removed from other estimates of partial melting in the upper mantle to produce tholeiitic liquids (e.g., Gas, 1968; Kay et al., 1970).

VI.5.1.2.2 Second-Stage Melting

The source material, C_o, for this part of the calculation is depleted harzburgite; trace element concentrations are taken from two sources, from harzburgites of the Bay of Islands Complex (Talkington, pers. comm., 1980), and from harzburgites of the Ronda Ultramafic Complex, Spain, as studied by Suen (1978). The purpose here was to obtain

data considered representative of upper mantle depleted harzburgite since no trace element data are available from the Troodos Complex. The good general agreement from these two separate localities suggests that melting and depletion processes are consistent on a broad scale in the upper mantle, and that mantle rocks from widely separated localities which are alike in petrologic character can be attributed to a similar genetic process, i.e., similar histories of melting and depletion.

It is the hypothesis of the present model that the komatiitic lavas represent or lie very close to the primitive liquid which gave rise to the Upper Pillow Lavas, and the average trace element contents of the komatiites will be substituted for C_l in the calculations.

As a test of the validity of the two-stage melting concept to explain trace element concentrations in Troodos pillow lavas, concentrations in the residue of the first melting event can be calculated and compared to that of the depleted harzburgites. Thus the idea of depleted harzburgites as the source material for the upper lavas of ophiolites forms an integral part of the present model.

The concentration in the residue after an episode of 'batch' melting is given by

$$C_R = C_l * D, \qquad \ldots \text{(VI.12)}$$

where C_R is the concentration of the element in the residue, and C_l is the concentration of the element in the liquid. Thus, for rubidium, where C_l = 4.1 ppm and D = 0.0134,

$$C_R = 4.1 \text{ ppm} * 0.0134$$
$$= 0.05 \text{ ppm}$$

And for strontium, where C_l = 87.2 ppm and D = 0.0251

C_R = 87.2 ppm * 0.0251

= 2.18 ppm

These values are compared with those of the actual depleted harzburgite in Table VI.3, and are found to be in general agreement.

For the following calculations modal proportions of minerals composing harzburgite were obtained from Talkington (pers. comm., 1980): olivine, 0.694/orthopyroxene, 0.302/clinopyroxene, 0.003.

Potassium

D_K = (0.694 * 0.0068) + (0.302 * 0.014) + (0.003 * 0.011)

= 0.0089

If C_o = 110 ppm and C_1 = 1909 ppm (Table VI.1), then

$$F = \frac{110 \text{ ppm}/ 1909 \text{ ppm} - 0.0089}{1 - 0.0089} = 0.492$$

or 4.9% melt.

Rubidium

D_{Rb} = (0.694 * 0.0098) + (0.302 * 0.022) + (0.003 * 0.015)

= 0.0134

If C_o = -.1 ppm and C_1 = 5.4 ppm (Table VI.1), then

$$F = \frac{0.1 \text{ ppm}/ 4.0 \text{ ppm} - 0.0134}{1 - 0.0134} = 0.0117,$$

or 1.2% melt.

Strontium

D_{Sr} = (0.694 * 0.014) + (0.302 * 0.017) + (0.003 * 0.12)

= 0.0152

Two values are listed in Table VI.1 for the concentration of Sr in the harzburgite. If a value of C_o = 32 ppm is used, the fraction of melt is calculated to be $\sim$26%, which disagrees markedly with the value

Table VI.3 Comparison of Calculated and Observed Residual Trace Element Concentrations

	C_R	Depleted Harzburgite
Rb	0.05 ppm	0.1 ppm
Sr	2.18 ppm	0.4 - 32 ppm

given by rubidium. If a value of C_o = 0.4 ppm is used, the solution is negative and meaningless. However, if the calculated residual value from the first stage melting event is used (Table VI.3), and C_1 = 117 ppm, then

$$F = \frac{2.18 \text{ ppm}/ 104 \text{ ppm} - 0.0152}{1 - 0.0152} = 0.0059, \text{ or } \quad 0.6\% \text{ melt.}$$

While this approach is somewhat artificial it is useful, in conjunction with the other estimates of partial melting, in predicting an appropriate concentration in the source, of which the composition can only roughly be approximated by comparison to known abundances; i.e., in this case the Sr value of 32 ppm may be too high.

It can be seen from the foregoing calculations that the Upper Pillow Lavas could have been produced by very small degrees of partial melting of mantle material which had been already depleted in incompatible elements by earlier melting. Whether there was a distinct early or first-stage event succeeded by a late-stage event, as envisaged by Duncan and Green (1980), or whether there was one continuous evolutionary event of which the komatiites represent the final liquid derivative, similar to the model proposed for the Burin Group, southeastern Newfoundland, by Strong and Dostal (1980), cannot be determined.

VI.5.1.3 Fractional Crystallization

Preliminary examination of the major element data suggests that the komatiites, olivine basalts and aphyric lavas of the Upper Pillow Lavas form a series which can be petrogenetically related by the frac-

tionation of olivine from a parental magma equivalent in composition to the komatiites. Here trace elements will be used to provide an estimate of the amounts of olivine that may have been involved in this process.

In a crystallization model C_o is redefined as the initial concentration of an element in the primary magma. The simplest case to consider is a closed system in which a body of magma is isolated in a magma chamber and undergoes continuous crystal fractionation. The liquid is a uniform reservoir and the olivine crystals are removed very soon after they are formed, giving them no time to equilibrate with the changing magma composition. The relationship between the original and fractionated liquid is expressed as

$$\frac{C_1}{C_o} = F^{(D-1)}, \qquad \ldots \text{(VI.13)}$$

where F is now the proportion of the original liquid remaining. Since we are concerned with the fraction of melt remaining we solve for F:

$$\sqrt[(D-1)]{\frac{C_1}{C_o}} = \sqrt[(D-1)]{F^{(D-1)}} = F \qquad \ldots \text{(VI.14)}$$

and since D will always be less than 1 for incompatible elements we can restate this as

$$F = \sqrt[(1-D)]{\frac{C_o}{C_1}} \qquad \ldots \text{(VI.15)}$$

From the above expression it can be seen that for elements with a very small bulk distribution coefficient, D (i.e., the incompatible elements),

$$F \cong \frac{C_o}{C_1}$$

Thus with the sole extraction of olivine the lithophile elements can be treated as incompatible elements, and can be included in the calculations.

Elements with a high field strength (charge/radius ratio), Ti, Zr, Y and Nb are not likely to be transported in aqueous fluids (Pearce and Norry, 1979). Since their values show a regular variation from komatiite to aphyric lava (except Nb) they will provide a more reliable estimate of fractionation. Because of its very low concentrations which are below the accepted detection limit for the method used, Nb will be excluded from the calculations. The inclusion of olivine only in the model is designed to facilitate comparison with a major element extraction program utilized later in this chapter. In reality, the extraction of clinopyroxene or titanomagnetite in minor amounts will affect concentrations in residual liquids but because olivine is by far the most important fractionating phase, other minor constituents will be omitted from the calculations.

Partition coefficients for Ti, Zr and Y are taken from Pearce and Norry (1979) and are included in Table VI.2.

Titanium

$$D_{Ti}(Ol) = 0.02$$

$$F = \frac{(1 - D)}{\sqrt{\frac{C_o}{C_l}}},$$

Where C_o = 1977 ppm and C_l = 2576 ppm (Table VI.1),

$$F = \frac{(1 - 0.02)}{\sqrt{\frac{1977 \text{ ppm}}{2576 \text{ ppm}}}} = .7633$$

or ~76% melt remaining, or ~24% olivine fractionation.

Zirconium

$$D_{Zr}(01) = 0.01$$

Where C_o = 15.8 ppm and C_l = 21.1 ppm (Table VI.1),

$$F = (1 - 0.01)\sqrt{\frac{15.8 \text{ ppm}}{21.1 \text{ ppm}}} = 0.7466$$

or ~75% melt remaining, or ~25% fractionation of olivine.

Yttrium

$$D_{Y}(01) = 0.01$$

Where C_o = 11.6 ppm and C_l = 17.1 ppm (Table VI.1),

$$F = (1 - 0.01)\sqrt{\frac{11.6 \text{ ppm}}{17.1 \text{ ppm}}} = 0.6757$$

or ~68% melt remaining, or ~32% fractionation of olivine.

These values are generally in agreement and together with the olivine extraction data presented later in this chapter define a range in the amount of olivine crystallization required to derive the Upper Pillow Lava series from a parental magma.

VI.5.2 Major Element Extraction Program

Cawthorn (unpub.) developed a major element extraction program based on mass balance calculations which was designed to solve the equation:

evolved magma = parental magma - crystalline phases

This program will indicate what proportions of crystalline phases must be removed to produce a particular liquid composition from another more primitive composition. The entire program and printout are reproduced in Appendix C.

If the average olivine composition of the ultrabasic lavas and the average composition of the aphyric lavas are input as the complementary crystal and liquid compositions (respectively), it is computed that 8.8% removal of olivine from a body of magma corresponding to the komatiitic lavas in composition would produce 91.2% of a derivative liquid equivalent in composition to the aphyric lavas.

The program also repeats the calculation using proportional weightings rather than absolute values of major element concentrations. This is designed to minimize the effect of unknown element concentrations for any of the inputted analyses, which if unknown have to be entered as zero. The zero values for three elements in the olivine analyses which are of significant value in the derived liquid composition (TiO_2, Fe_2O_3, K_2O) may considerably affect the initial absolute values calculation; this effect is minimized by the second, weighted calculation which delegates more significance to elements included in both analyses. The result of 19.4% olivine removal is therefore more reliable, and furthermore, is not far removed from the range of estimates of fractionation based on trace element modelling.

VI.6 Interpretation of Rare Earth Data

A number of qualitative statements can be made based on observations of the rare earth element data, as presented in Chapter IV, which lend support to the present petrogenetic interpretation of both the Upper and Lower Pillow Lava units. The clear distinction between rare earth element profiles of these two groups is regarded as further evidence of a two-stage partial melting event as is propounded with reference to major

and trace element data. The Lower Pillow Lavas, representing the initial melt fraction, show higher relative and absolute concentrations of the incompatible LREE's, while the Upper Pillow Lavas represent a second melt fraction depleted in total REE's, as well as in light relative to intermediate and heavy REE's.

Several authors (e.g., Frey et al., 1974; Schilling, 1974; 1975) have empirically stated that profiles below and above a particular threshold level represent olivine-bearing and olivine-free basalts, respectively, from the oceanic environment. This distinction is generally held to be true for the Upper and Lower Pillow Lavas, although certain aspects of their REE disposition point to a more fundamental difference in their character. For instance olivine-bearing and olivine-free samples plot below the threshold level, although one olivine-free sample from the Upper Pillow Lavas plots above this line. A distinction based on the presence or absence of olivine in actuality invokes the fractionation of olivine as the unique process which separates lavas below and above the threshold level. It is suggested here that more fundamental difference exists in this case between the two lava groups, that two parental magmas are represented, and that the Upper Pillow Lava parental magma differentiated to produce unique series of rocks of which the recognizable members plot below the threshold level.

This interpretation would be meaningless in the absence of other studies; however, in conjunction with the foregoing presentation, further evidence is provided for the binary aspect of Upper and Lower Pillow Lava petrogenesis.

VII. ON THE NATURE AND SIGNIFICANCE OF KOMATIITES

VII.1 Introduction

One type of mafic lava from the Upper Pillow Lavas has been heretofore referred to as komatiite, based primarily on petrographic evidence. There has been some minor disagreement in the literature, however, on how to chemically define this class of rocks, and the komatiites documented in this work may adhere totally to some definitions while standing in disagreement with others. To discuss the validity of interpreting quenched mafic lavas from the Upper Pillow Lavas as komatiites, this chapter will review the present literature on komatiites, and subsequently compare and contrast pertinent aspects of documented and Upper Pillow Lava komatiites.

VII.2 Classification and Character of Komatiites

Viljoen and Viljoen (1969a) introduced the term 'komatiite' to describe mafic and ultramafic lavas of the Barberton Mountain Land in South Africa, which they distinguished from more familiar ultramfic rocks by certain textural features. The rocks showed quench textures indicative of extrusive origin as mobile lavas, as well as high SiO_2, high Fe/Mg, low total alkalies, and in particular, high CaO/Al_2O_3. A more quantitative approach was taken by Brooks and Hart (1974) who suggested that komatiites were non-cumulate rocks with $MgO > 9\%$, $K_2O < 0.5\%$, $TiO_2 < 0.9\%$ and $CaO/Al_2O_3 > 1$.

Many ultramafic lavas documented by a variety of workers throughout the world, e.g., Australia (Williams, 1973), India (Viswana-

than, 1974) and Rhodesia (Bickle et al., 1975) resemble the Barberton lavas closely, but consistently lack a high CaO/Al_2O_3 ratio.

In a comprehensive study of komatiites of Munro Township, northeastern Ontario, Arndt et al., (1977) found their average CaO/Al_2O_3 ratio to be 0.84, with over half the analysed ultramafic lavas having ratios < 1. Hence the Brooks and Hart (1974) definition applied to only a limited number of ultramafic lavas from Munro and elsewhere, and Arndt et al. (1977) proposed a new definition of komatiite that included a wider range of ultramafic volcanic and hypabyssal rocks. On the basis of field, petrologic and chemical studies these authors recognized three types of komatiite: peridotitic (Mg > 20%), pyroxenitic (MgO, 12 - 20%), and basaltic (MgO < 12%). For a description of these the reader is referred to Table VII.1 (after Arndt et al., 1977). The average chemical analyses of the rocks is contained in Table VII.2.

The basaltic komatiites will here be scrutinized more closely in the context of their close similarity to a group of rocks from the Upper Pillow Lavas. The Munro basaltic komatiites are defined as having MgO < 12%, but further subdivision into MgO-rich and -poor types is possible. At Munro textures in the more mafic basaltic komatiite varieties (MgO > 10%) are similar to those in olivine-poor pyroxenitic komatiites. At the tops of the flows spinifex texture, defined by parallel clinopyroxene grains, grades downward to microspinifex texture, where needles of clinopyroxene are randomly orientated. Olivine is not present as bladed grains in the groundmass of the basaltic komatiites as is the case with pyroxenitic komatiites, but only as rare skeletal equant phenocrysts, and the clinopyroxene needles are smaller than those in the pyroxenitic koma-

TABLE VII.1 Classification of Komatiites in Munro Township

(After Arndt et al., 1977)

	Petrologic Character	MgO *
Peridotitic komatiite	All types are composed of olivine grains and minor chrome spinel in a matrix of fine-grained clinopyroxene and devitrified glass. In cumulates olivine grains are closely packed, solid, roughly equant and compose 60 to 80% of the rock; in spinifex texture olivine forms large skeletal platy grains (35 to 60%); and in spinifex-free non-cumulate rock, olivine may be equant or skeletal (45 to 70%).	MgO > 20%
Pyroxenitic komatiite	Equant solid or platy skeletal grains of olivine (0 to 35%) in fine-grained matrix of clinopyroxene and devitrified glass; or skeletal subcalcic clinopyroxene needles in devitrified glass groundmass; or closely-packed equant grains of pyroxene and olivine. No plagioclase.	MgO between 12 and 20%
Basaltic komatiite	No olivine in the groundmass; plagioclase instead. Clinopyroxene and plagioclase form spinifex texture, 'graphic' intergrowths, or normal subophitic texture.	MgO < 12%

* Anhydrous values

Table VII.2 Comparison of Representative Komatiite Analyses

	1	2	3	4	5	6	7	8
SiO_2	44.90	46.00	50.20	51.60	50.85	53.37	52.83	53.72
TiO_2	0.19	0.32	0.61	0.65	0.68	0.86	0.16	0.33
Al_2O_3	5.30	7.40	11.50	13.30	10.27	9.95	9.49	13.36
Cr_2O_3	0.26	0.39	-	-	-	-	-	-
Fe_2O_3	10.40	11.50	11.11	11.70	10.90	12.04	10.71	2.98
FeO								5.57
MnO	0.18	0.22	0.19	0.19	0.18	0.22	0.17	0.15
MgO	33.60	26.50	14.30	10.00	15.07	10.22	14.21	11.25
NiO	0.02	0.01	-	-	-	-	-	-
CaO	5.00	7.40	9.60	10.40	11.10	10.11	10.22	11.14
Na_2O	0.35	0.45	2.34	2.16	0.83	2.68	2.00	1.16
K_2O	0.08	0.10	0.05	0.11	0.08	0.46	0.12	0.23
P_2O_5	-	-	-	-	-	0.06	0.07	0.10
Recalculated to 100% anhydrous								
CaO/Al_2O_3:	0.94	1.00	0.83	0.78	1.08	1.02	1.08	0.83

Sources:

1 - Average comp. of perid. komat. with MgO 30%. Arndt et al. (1977).
2 - Average comp. of perid. komat. with MgO 30%. "
3 - Average comp. of pyroxenitic komatiite. "
4 - Average comp. of basaltic komatiite. "
5 - Sample 60641, from ol-phyric flow, Chukotat Gp. Francis and Hynes (1979).
6 - Average of 3 basaltic komat. of Barberton type. Viljoen and Viljoen (1969).
7 - Average of 9 basaltic komat., Rambler, Nfld. Gale (1973).
8 - Average of 18 basaltic komat., Upper Pillow Lavas, Cyprus. This work.

Ba	33	14.6
Nb	3	1.7
Zr	14	15.8
Sr	136	104
Rb	3	4
Zn	70	61
Cu	14	76.7
Ni	330	217
Y	3	11.7
La	2	20.1
Cr	1300	617

tiites (avg. length 0.5 - 1 mm). The matrix to these needles is entirely devitrified glass or an intergrowth of prismatic grains of clinopyroxene and plagioclase.

The less mafic varieties (MgO < 10%) are characterized by textures and modal compositions resembling those of non-komatiitic basaltic rocks; they comprise prismatic, subhedral grains of clinopyroxene and plagioclase, and minor amounts of amphibole, quartz and iron oxides. Rare olivine or clinopyroxene phenocrysts are replaced by serpentine or chlorite. Clinopyroxene and plagioclase may display a 'graphic' texture similar to that found between quartz and orthoclase in granitic rocks.

Francis and Hynes (1974) studied komatiites and tholeiites from the Proterozoic Chukotat Group of New Quebec, where a series of layered sills and flows consists of a lower ultramafic member with an overlying gabbroic complex, and are bounded by margins of quench-textured, pyroxene-rich melanogabbro. Features such as cyclic layering of pyroxenite and peridotite, successive appearance in the sequence of olivine, clinopyroxene and plagioclase, and polarized compositional variation indicate that the ultramafic member and lower gabbro are crystal cumulates. The uppermost gabbros, then, appear to represent liquids derived by removal of these cumulates.

Most of these mafic volcanics are olivine-phyric, consisting of equant to elongate skeletal olivine mincrophenocrysts (0.5 mm), with skeletal needles of augite in a groundmass of dendritic to spherulitic actinolite and epidote. The chemistry of the group is represented in Table VII.2. The ultrabasic rocks subscribe to Brooks and Hart's (1974) definition of komatiite: MgO ranges from 11 - 17%, CaO/Al_2O_3 > 1,

and TiO_2 and K_2O make up less than 0.9% and 0.5% of the rock, respectively. Peridotitic komatiite is not found in the Chukotat Group.

The significance of these bodies draws from the fact that their primary liquids were at least as basic as pyroxenitic komatiites (14% MgO), while the residual liquids, represented by the uppermost gabbro, are Fe-Ti-rich tholeiites. The liquid line of descent inferred from the chemistry and the spectrum of the volcanic composition of the whole Chukotat Group led Francis and Hynes to suggest that the komatiites and tholeiites may constitute a single magmatic suite whose chemical diversity is a function of low pressure crystal fractionation.

Gale (1973) described pillow lavas from the Rambler area, Burlington Peninsula, Newfoundland and defined an association of basaltic komatiite and ocean floor tholeiite of pre-lower Ordovician age within the Appalachian orogenic belt. These basic lavas have been metamorphosed in the quartz-albite epidote-almandine subfacies of the greenschist facies, but Gale considered the metamorphism to be isochemical and the low Al_2O_3-high MgO content of some of the lavas to be representative of their primary chemistry.

By analogy with major and trace element values quoted in the literature for ocean-floor basalts, Gale considered Rambler high-Al_2O_3 basaltic pillow lavas to be tholeiitic ocean floor basalts which probably represented a part of a pre-lower Ordovician ophiolite sequence (Gale, Ph.D. thesis, Durham University). The majority of the Rambler lavas, however, can be distinguished from ocean floor tholeiites by their low Al_2O_3 and high MgO contents; on the basis of their correspondence with basaltic komatiites as described by Viljoen and Viljoen (1969) Gale

documented the Rambler lavas as belonging to the komatiite class of rocks.

Representative major and trace element contents of the Rambler lavas are listed in Table VII.2. The basaltic komatiites have extremely low contents of the incompatible elements Nb, Rb, La, Zr and Y and are enriched in Cr and Ni.

In his proposition of a genetic model Gale essentially adhered to those of earlier writers (Green, 1972; Brooks and Hart, 1957) but believed that komatiite genesis can be explained in terms of modern concepts of magma generation and without recourse to special Precambrian conditions such as meteorite impact (Green, 1972) and high geothermal gradients (Brooks and Hart, 1957). The association of amygdaloidal basaltic komatiite pillow lavas with chert and rocks that are chemically analogous to ocean floor basalt suggest that they were probably erupted onto the floor of an ancient ocean, but that they represent more primitive magmas than the ocean floor basalts which overlie them.

According to Gale, then, basaltic komatiites may be interpreted as fragments of oceanic crust which could have formed by a melting event in the mantle more extensive than that popularly invoked to produce ocean floor basalts. Differentiation between peridotitic and basaltic komatiites may have transpired by diapiric upwelling and consequent low pressure ($\sim$5 kb) olivine fractionation.

Cawthorn and Strong (1974) suggested a continuum of CaO/Al_2O_3 ratios between tholeiites and komatiites, and considered komatiites and primitive oceanic tholeiites (Clarke, 1970) to be extensive partial melts of the mantle, leaving a harzburgite residue essentially devoid of CaO

and Al_2O_3. These rock types however, are found to have CaO/Al_2O_3 ratios higher than the ranges for suggested mantle compositions, and these authors suggested that they were derived from a parental composition with a higher proportion of clinopyroxene to garnet than the inferred parental material for normal oceanic tholeiites, this proportion increasing with decreasing depth. Thus the higher komatiitic CaO/Al_2O_3 values are effectively due to a bulk composition enriched in CaO relative to Al_2O_3. This implies that the variety of CaO/Al_2O_3 ratios found in komatiites may be due to extensive melting at varying, but generally shallow depths.

Cawthorn and Strong further suggested that because the chemical characteristics of komatiites are not unique the group is not a distinctive isolated new class of basic and ultrabasic magma, but a more extreme composition in a spectrum of rocks with chemical characteristics imposed by shallow depth and a high degree of partial melting.

The tectonic environment wherein komatiites may be expected to form has been treated by some of the above researchers, particularly Brooks and Hart (1974). Most early work on komatiites, e.g., Viljoen and Viljoen (1969) dealt with Archean and Proterozoic terrains, and it was implied that komatiites were more or less restricted to environments of this period of earth history, and thus may represent primitive crust. With the identification of basaltic komatiites of post-Precambrian age, however, more modern tectonic environments were proposed, e.g., sea floor (Glikson, 1971; Gale, 1973) or island arc (Brooks and Hart, 1972) environments.

Peridotitic komatiites are restricted totally to Precambrian and Paleozoic terrains and therefore cannot be readily discussed in terms of modern tectonic environments. Most of the basaltic komatiites identified by Brooks and Hart (1974) come from island arcs but their scarcity in any environment makes such a correlation tenuous. The fact that komatiites are usually accompanied by low-K tholeiites has led some authors to suggest an ocean floor analogue (McCall, 1973; Gale, 1973); low-K tholeiites of very similar chemistry, however, are found from nearly every tectonic environment (Jamieson and Clark, 1970). Although low-K tholeiites from these different tectonic enviroments are separable in the Phanerozoic by other chemical criteria possibly related to previous 'depletion' events in the mantle (Tatsumoto et al., 1965; Gast, 1968; Kay et al., 1970), such events may not have transpired in the Archean and there may have been no chemical differences between low-K tholeiites from different Archean tectonic environments. Thus a stringent komatiite - low-K tholeiite association appears untenable.

Brooks and Hart (1974) concluded that field relations more so than chemistry will be diagnostic of tectonic environment, and that "careful reconstruction of structure, stratigraphic sequence and petrology will undoubtedly be essential to understanding the tectonic environment represented by Archean komatiites and low-K tholeiites". Upon examination of field relations they noted that komatiites of the Archean seem to occur consistently in series containing intermediate to felsic members, which ostensibly precludes formation at a mid-ocean spreading ridge. This scarcity of ocean floor felsic rocks, in contrast to the relative abundance of intermediate-felsic types from ophiolite suites led

Miyashiro (1973) to question whether ophiolite sequences are oceanic crust alone, and to propose instead that they may be part of arc sequences. Brooks and Hart (1974) also considered this line of reasoning as good evidence for an island arc origin.

VII.3 Evaluation of the Komatiite Analogue

Graphical comparison of Upper Pillow Lava and documented komatiites is contained in Figures IV.3 - IV.7 of Chapter IV. Table VII.2 allows comparison of komatiites from the Upper Pillow Lavas and those from the literature discussed above. While there are differences between the analyses for basaltic komatiites in the literature, they for the most part conform to the parameters of Brooks and Hart (1974), i.e., SiO_2, 46-53%, $CaO/Al_2O_3 > 1$, $TiO_2 < 0.9\%$, $MgO > 9\%$, and $K_2O < 0.5\%$. The komatiites from the Upper Pillow Lavas show a good general conformity with analyses from the literature but with several reservations. The average SiO_2 content of the Upper Pillow Lava komatiites (54.24%) is higher than any of the others and lies significantly above the defined maximum value of 53%. This feature is here considered to be in accord with the genesis of these rocks as put forth in this work. The concept of high-MgO liquids which are oversaturated with respect to SiO_2 can account for the high silica contents of the present komatiites. It is also notable that the average content of three basaltic komatiites from the Barberton Mountain Land (6, Table VII.2) is slightly higher than 53% and within one percent of the Upper Pillow Lava value.

Al_2O_3 content of the Upper Pillow Lava komatiites is significantly higher than that from most localities, but is slightly lower

than the value for Munro basaltic komatiites (4, Table VII.2, Arndt et al., 1977). CaO contents of all the komatiites in Table VII.2 are consistent; it is notably the change in Al_2O_3 content which effects a change in CaO/Al_2O_3 ratio between the komatiites. The komatiites from the Chukotat Group (5), the Barberton Mountain Land (6) and Rambler (7) have very similar ratios, ranging from 1.02 - 1.08. The more aluminous averages from Munro Township and the Upper Pillow Lavas show ratios of 0.78 and 0.84, respectively. Cawthorn and Strong (1974) compared the CaO/Al_2O_3 ratios of tholeiites and komatiites from a wide variety of localities and found that while oceanic tholeiites characteristically have CaO/Al_2O_3 ratios less than 1, many komatiites as well have ratios considerably less than 1 (e.g., average of eight Archean komatiites from Labrador, 0.71; average of 34 komatiites from Canadian Shield, 0.82). As has already been mentioned, these authors suggested a continuum of CaO/Al_2O_3 ratios between oceanic tholeiites and komatiites. This range may represent the derivation of komatiitic liquids at different depths in the upper mantle, those with higher values of this ratio having formed at shallower levels in the region where tholeiitic liquids may be expected to form, i.e., where the clinopyroxene/garnet ratio is greater.

Cawthorn and Strong (1974) also pointed out that other basaltic rock types such as ankaramite characteristically have CaO/Al_2O_2 ratios greater than 1. Komatiites, however, are depleted in TiO_2, K_2O and incompatible elements relative to ankaramites and it is evident that other parameters such as these must be used in conjunction with CaO/Al_2O_3 ratios in any geochemical classification of komatiites.

The TiO_2 content of Upper Pillow Lava komatiites (0.35%) is lower than all others with the exception of those from Rambler (0.16%). Trace elements along with major elements from these two localities are compared in Table VII.2. Contents of the incompatible trace elements are very similar between the two rock types, with the Rambler komatiites being slightly more depleted in Zr, Rb and La and enriched in Cr and Ni.

There are many occurrences of extrusive or hypabyssal high-MgO basalts, of which the ultrabasic rocks of this study are a prime example, which owe their high-MgO contents to a cumulus enrichment in olivine. Any discussion of komatiite must therefore stress its existence as a liquid composition; in this matter a close examination of textures must accompany a discussion of geochemical affinity. The various textures attributed to komatiites in the literature, and by which they were originally identified, i.e., spinifex-textured grains in a glassy matrix, are prima facie evidence for the existence of the rock as a liquid, and especially as a high-MgO liquid. It is in fact the chemical nature of the liquid which facilitates its rapid quenching, as very basic magmas have a higher solidus temperature than those less enriched in MgO. Extrusion of magma, which in normal basaltic compositions would produce a fine-grained but essentially holocrystalline rock, may, where a high-MgO magma is concerned, lead to supercooling of the liquid with minimal crystal nucleation and growth. Thus it follows that rocks of basaltic komatiite composition, as defined by Arndt et al. (1977), i.e., rocks intermediate in composition between basalts and pyroxenitic komatiites, may show a small degree of crystal growth before the quenching of the groundmass to glass. This is considered the mode of origin for the komatiites

of the Upper Pillow Lavas. The hyalopilitic rocks in particular show evidence of intratelluric growth of olivine and post-extrusive growth of pyroxene, whose forms are attributed to quenching.

The common occurrence of the komatiites in the field as pillow lavas provides final conclusive evidence for their existence as liquids; on these principles the high-MgO basalts in the Upper Pillow Lavas are interpreted as komatiites.

VII.4 Consideration of a Komatiitic Series

Some writers have regarded the komatiite class of rocks as being representative of a distinct magma series, akin to the tholeiitic and alkali basalt series. Arndt et al. (1977) in particular were advocates of this line of thought, and considered the komatiitic rocks of Munro Township to be part of a unique and definitive magma series, comprising peridotitic, pyroxenitic and basaltic members which are related to one another by differing degrees of olivine, and to a lesser extent clinopyroxene and plagioclase, fractionation. Others, however, have taken a different view; Cawthorn and Strong (1974), because of the continuum of CaO/Al_2O_3 ratios, suggested that "komatiite is not a distinctive isolated new class of basic and ultrabasic magma, but a more extreme composition in a spectrum of rocks with chemical characteristics imposed by shallow depth and a high degree of partial melting". Francis and Hynes suggested that the tholeiitic and komatiitic lavas of the Chukotat volcanic sequence were co-magmatic, the former derived from the latter via low-pressure fractionation of olivine, clinopyroxene and plagioclase. This mechanism is represented in the Jensen plot, Figure IV.3, Chapter

IV, where an Fe + Ti-enrichment trend is indicated. All the Upper Pillow Lava plots, however, form a linear trend away from the ultrabasic rock composition points, with no deflection toward either the ≤Fe + Ti or Al apex, and thus showing no conformity with a tholeiitic trend. The tendency of all rock types within the Upper Pillow Lavas to show low TiO_2 contents suggests that these rocks were derived from a starting composition which also had low concentrations of TiO_2. The lack of transition from low- to high- TiO_2 types further suggests that the Upper Pillow Lavas are an autonomous group of rocks which conform to the definition of a komatiite magma series.

VIII. SUMMARY AND CONCLUSIONS

VIII.1 Synthesis

This work has involved the study of field relationships, petrography and geochemistry of the different magma types of the Upper Pillow Lavas, Troodos Complex. Here the salient aspects will be summarized and discussed, with the purpose in mind of providing a succinct but fairly comprehensive petrogenetic model.

The Upper Pillow Lavas have been accepted in all previous work as a unit distinct in character from the Lower Pillow Lavas, the difference being brought out by complementary compositional and metamorphic criteria. The present work has reinforced such a distinction. The classification of rock types put forth by Smewing (1975) has been only slightly modified.

The Upper Pillow Lavas are here divided into four types: ultrabasic rocks, basaltic komatiites, olivine basalts and aphyric basalts. Major element computer extraction calculations and trace element modelling have shown that: 1) the magma parental to the Upper Pillow Lava series could have been produced by very small amounts of partial melting ($\sim$5%) of a source peridotite already highly depleted in lithophile elements, i.e., those elements which would be strongly partitioned into the liquid during an initial melting event; and 2) the less primitive rocks of the Upper Pillow Lavas, olivine and aphyric basalts, could have been derived by the fractionation of 24-32% olivine from this parental magma. Statement (2) assumes that the basaltic komatiites effectively represent the parental magma as derived from a depleted source, although realis-

tically the komatiites may be slighly removed from this composition by olivine fractionation.

This concept of olivine extraction was tested in a number of ways. The composition of olivine which would crystallize from a liquid similar in composition to the basaltic komatiites ($Fo_{92.3}$) was calculated and is comparable to the actual measured olivines ($Fo_{91.6}$), indicating that the two could have been in equilibrium.

The proposed petrogenetic sequence was corroborated by projections into both the basalt tetrahedron and CMAS system. Phase relations so predicted by the normative mineralogy and bulk rock chemistry agree with petrographic data that early-crystallizing olivine was followed down-temperature by orthopyroxene and clinopyroxene in the komatiites; quenching of the groundmass glass occurred before plagioclase became a liquidus phase. Furthermore, the position of aphyric basalts away from the olivine/orthopyroxene primary phase fields attests to their status as a derived liquid.

VIII.2 Magma Chamber Considerations

The actual physical development of the lava types and their extrusion must be discussed. It is suggested that the parental magma (~basaltic komatiite) accumulated in small magma chambers at a shallow crustal level. The early high temperature precipitation of olivine led to the accumulation of this mineral at the bottom of the chambers, with a portion of liquid being trapped between the crystals. The crystal/liquid mush formed in this manner is represented by the volumetrically small ultrabasic rocks. The aphyric basalts thus represent magma in the upper

parts of the chamber from which the olivine fraction has been removed. The gamut of compositions may thus represent the particular level in a magma chamber at which the magma batch attained its character. Olivine basalts, then, may represent a level intermediate between the olivine-rich and olivine-poor parts of the chamber. Extrusion of primitive magma soon after its accumulation in a chamber with minimal fractionation gave rise to the basaltic komatiites.

The close association of the different rock types in the field, i.e., the common random interlaying of the different types also lends support to their association in and extrusion from the same magma chamber or a number of small, consanguineous, closely-spaced chambers. The relative abundance of the aphyric basalts again is in agreement with this model, as the derived aphyric liquid will be most preponderant in the magma chamber. Ultrabasic rocks occur at the top of the pillow lava sequence, suggesting their extrusion as a crystal/liquid mush upon advanced tapping of the magma chamber, subsequent to the extrusion of the aphyric lavas.

The textures developed in the primitive liquid, i.e., the basaltic komatiite, are supportive of the above scheme. As pointed out in the petrography section, olivine crystals were nucleated and experienced much of their growth in the intratelluric stage, while orthopyroxene may have undergone some post-extrusive growth. Clinopyroxene is restricted to the eruptive stage.

As a complement to the above genetic interpretation of the Upper Pillow Lavas, the Lower Pillow Lavas are postulated to be (indirectly) related in their genesis to the former rocks. The extraction of the

Lower Pillow Lava parental magma from a 'fertile' upper mantle source peridotite (i.e., spinel lherzolite) could have left as a residue a harzburgite composition, which upon further or renewed melting gave up a small depleted melt fraction; this migrated upward to a magma chamber and became the magma parental to the Upper Pillow Lavas. The trace element data used for both depleted and undepleted mantle compositions are taken from sources thought to approximate the compositions of the source rocks.

The Lower Pillow Lavas parental magma is roughly calculated as representing 21-23% partial melting of an upper mantle lherzolite; this figure is in the range of other estimates for production of tholeiite magmas from an undepleted upper mantle source (e.g., Malpas, 1978).

VIII.3 The Possible Tectonic Environment of the Upper Pillow Lavas

The past few years has seen much debate on the matter of tectonic setting of the Troodos Ophiolite Complex. Prior to 1970 workers, preoccupied with a concept of ophiolites as relict portions of oceanic crust formed at mid-ocean ridges, had almost unquestioningly accepted a similar origin for Troodos. Miyashiro (1973) opened a series of heated exchanges with his proposition that the Troodos ophiolites were more likely to have formed in an island arc situated between the African and Eurasian plates in the early Mesozoic. This debate has already been reviewed in Chapter II and will not be repeated here. Various aspects, however, will be involved in the present consideration of the tectonic environment in which the Upper Pillow Lavas may have originated, as there must be intimate genetic ties between the upper and lower lava units.

Recently authors have moved away from the tenet that ophiolites are formed exclusively at mid-ocean spreading centres, and many have agreed that a back-arc or marginal basin environment is more realistic when the combined aspects of petrology, geochemistry and stratigraphy are considered (e.g., Upadhyay et al., 1971; Dewey and Bird, 1971; Kidd, 1977). This seems a logical progression of thought, as basalts from back-arc basins may be expected to show characteristics of both spreading centres and subduction zones.

The idea that the Troodos Complex formed at a spreading centre is more or less universally accepted. Of the writers who have advocated a back-arc basin origin, Sun and Nesbitt (1978) have probably provided the most comprehensive discussion. They took into account the following factors in their suggestion of a genetic model: 1) the Troodos Ophiolite Complex was formed at a spreading centre, as seen from the strong development of dyke swarms; 2) it is associated with the remelting of a depleted residual mantle that had high Al_2O_2/TiO_2 and CaO/TiO_2 ratios; and 3) subducted oceanic crust was responsible for the water which effectively promoted melting by lowering the solidus. Whereas Smewing et al. (1975) had proposed a continuous generation process involving progressive depletion of incompatible elements and remelting of refractory peridotite in the same thermal regime to produce the highly depleted Upper Pillow Lavas, Sun and Nesbitt (1978) considered this unlikely because substantially more heat would be necessary to produce further remelting of a refractory source. These authors suggested that the most probable environment was a spreading centre near a subduction zone. This situa-

tion could be achieved either within an interarc basin or within a young or incipient island arc.

Whereas the above authors have dealt mainly with the genesis of the low-Ti Troodos Ophiolite Complex as a whole, and have not differentiated genetically between the slightly depleted Lower Pillow Lavas and the highly depleted Upper Pillow Lavas, Pearce (1975) used basalt geochemistry to investigate past tectonic environments on Cyprus and suggested a two-stage petrogenetic model. In the first stage melting of mantle above a subduction zone occurs under water-saturated conditions, a possible result of upward diapiric movement of mantle caused by stresses related to the subduction process. This leads to back-arc spreading and production of the Lower Pillow Lavas as new oceanic crust. In the second stage, the spreading axis moves away from the site of subduction. Accumulation of water generated from the dehydration of subducted oceanic lithosphere causes melting of mantle material under water-saturated conditions and the eruption of the Upper Pillow Lavas as an island arc seamount.

Laboratory work has supported the concept of hydrous melting. Green (1976) has shown that at 10 kb. pressure ($\sim$30 km depth), at 1100°C and 1200°C under water-saturated conditions, pyrolite will yield liquid fractions of 28 $\pm$ 1% and 35 $\pm$ 15%, respectively. The liquid composition will be magnesian quartz tholeiite; higher degrees of melting will result in greater dissolution of olivine and/or orthopyroxene and more primitive liquids.

Green (1976) went on to suggest that if the source peridotite in island arc regions is depleted from pyrolite by the earlier loss of a

basaltic melt fraction (i.e., magma which could be parental to the Lower Pillow Lavas), then the K_2O, TiO_2 and Na_2O contents (and related traces) will be strongly depleted, whereas SiO_2, MgO, FeO, Al_2O_3 and CaO would have undergone less relative change.

Further water-saturated melting of this source material will produce a lower proportion of liquid than is present in pyrolite at a particular near-solidus temperature because of the earlier removal of the low-melting fraction. This liquid will have 'pyrolite' concentrations of most major elements but will be depleted in Na_2O, K_2O, TiO_2 and light rare earth elements.

Consideration of trace element concentrations in the Upper Pillow Lavas and possible source material argue for the concept of two-stage melting. The postulate of hydrous melting of a subducted slab fits well into the present interpretation, as it not only provides a means of melting highly refractory source material but also serves to incorporate the Upper Pillow Lavas into the above-discussed genetic scheme envisaged for the Lower Pillow Lavas.

VIII.4 Conclusions

1. The Lower Pillow Lavas represent 21 - 23% partial melting of a lherzolitic source rock in the upper mantle.

2. The Upper Pillow Lava parental magma was produced by very small amounts ($\sim$5%) of partial melting of a depleted source peridotite

(harzburgite), from which a portion of melt parental to the Lower Pillow Lavas had already been removed.

3. The olivine and aphyric basalts, i.e., the less primitive members of the Upper Pillow Lavas, were derived by the fractional crystallization of 24 -32% olivine from the parental magma, represented by the komatiites. The ultrabasic rocks represent the accumulation of this fractionated olivine.

4. The magma parental to the Upper Pillow Lavas accumulated in small magma chambers at a shallow level in the oceanic crust, where differentiation and subsequent extrusion unto the ocean floor produced the different compositional and textural types.

5. The Upper and Lower Pillow Lavas were formed in a back-arc basin environment. A two-stage event, linked to a two-stage genetic model, is envisaged. In the first stage the Lower Pillow Lavas, derived from a primary melting event, were erupted at a back-arc basin spreading centre above a subduction zone. The spreading axis subsequently moved away from the subduction zone, and, in the second stage, accumulation of water from the dehydrating subducted oceanic lithosphere resulted in renewed melting; this melt migrated to high level magma chambers and was eventually extruded as the Upper Pillow Lavas. This model in no way implies a significant break in time between eruption of the two lava suites, and, in fact, a continuum seems more likely.

R E F E R E N C E S

Abbey, S., 1968: Analysis of rocks and minerals by atomic absorption spectroscopy. Pt. 2, Determination of Tot. Fe, Mg, Ca, Na and K. Geol. Surv. Can., Pap. 68-20: 21 p.

Arndt, N.T., Naldrett, A.J. and Pyke, D.R., 1977: Komatiitic and Iron-rich Tholeiitic Lavas of Munro Township, Northeast Ontario, Jour. Petrol., v. 18, Part 2: 319-369

Arth, J.G., 1976: Behaviour of Trace Elements During Magmatic Processes - a summary of theoretical models and their applications. Jour. Res. U.S. Geol. Surv., v.4, 1: 41-47

Atlas, L. 1952: The polymorphism of $MgSiO_3$ and solid state equilibria in the system $MgSiO_3$-$CaMgSi_2O_6$. Jour. Geol., 60: 125

Bagnall, P.S., 1960: The Geology and Mineral Resources of the Pano Lefkara - Larnaca Area. Geol. Surv. Dept., Cyprus, Memoir No. 5

Bear, L.M., 1960: The Geology and Mineral Resources of the Akaki - Lythrodondha Area. Geol. Surv. Dept., Cyprus, Memoir No. 3

Bear, L.M., 1963a: The geological map of Cyprus (1:250,000). Geol. Surv. Dept. Cyprus.

Bear, L.M., 1963b: The Mineral Resources and Mining Industry of Cyprus. Rep. Cyprus Geol. Surv. Dept., Bull. No. 1

Beccaluva, L., Ohnenstetter, D. and Ohnenstetter, M., 1979: Geochemical discrimination between ocean-floor and island arc tholeiites - application to some ophiolites. Chem. Geol.

Bellamy, C.V. and Jukes-Browne, A.J., 1905: The Geology of Cyprus, London.

Bender, J.F., Hodges, F.N. and Bence, A.E., 1978: Petrogenesis of basalts from the Project FAMOUS area: Experimental study from 0 to 10 kbars. Earth. Planet. Sci. Lett., 41: 277-302

Bergeat, A., 1892: Zur Geologie der massigen Gesteine der Insel Cypern. Tschemaks Min. Petr. Mitt. xii: 263

Bickle, M.S., Martin, A. and Nisbet, E.G., 1975: Basaltic and peridotitic komatiites and stromatolites above a basal unconformity in the Belingwe greenstone belt, Rhodesia. Earth. Planet. Sci. Lett., 27: 155-162

Bishopp, D.W., 1952: The Troodos Massif, Cyprus. Nature,169: 489

Blanchard, D.P., Rhodes, J.M., Jacobs, J.W. and Gibson, E.K., 1976: The chemistry and petrology of basalts from Leg 37 of the Deep Sea Drilling Project. J. Geophys. Res., 81: 4285-4306

Bottinga, Y., Kudo, A.M. and Werle, D.F., 1966: Some Observations on Oscillatory Zoning and Crystallization of Magmatic Plagioclase, Amer. Mineral., v. 51: 792-806

Boyd, F.R. and England, J.L., 1960: The quartz-coesite transition. J. Geophys. Res., 65: 749-756

Brooks, C. and Hart, S., 1972: An extrusive basaltic komatiite from a Canadian Archean metavolcanic belt. Can. Jour. Earth Sci., 9: 1250

Brooks, C. and Hart, S., 1974: On the significance of komatiite. Geology, 2: 107-110

Brown, G.M., 1957: Pyroxenes from the early and middle stages of fractionation of the Skaergaard intrusion, east Greenland. Mineral. Mag., 31: 511-543

Bryan, W.B. and Moore, J.G., 1977: Compositional variations of young basalts in the Mid-Atlantic Ridge rift valley near latitude 36°49'N. Geol. Soc. America Bull. 88: 556-570

Bryan, W.B., Thompson, G., Frey, F.A. and Dickey, J.S., 1976: Inferred geologic settings and differentiation in basalts from the Deep Sea Drilling Project. J. Geophy. Res., 81: 4285-4304

Carr, J.G. and Bear, L.M., 1960: The Geology and Mineral Resources of the Peristerona - Lagoudhera Area. Geol. Surv. Dept., Cyprus, Mem. No. 2

Cawthorn, R.G. and Strong, D.F., 1974: The Petrogenesis of Komatiites and Related Rocks as Evidence for a Layered Upper Mantle. Earth Planet. Sci. Lett., 21, 4: 369-375

Clarke, D.B., 1970: Tertiary basalts of Baffin Bay: Possible primary magma from the mantle. Contrib. Mineral. Petrol., 25: 203

Coleman, R.G., 1977: Ophiolites: Ancient Oceanic Lithosphere? Minerals, Rocks and Organic Materials Series, No. 12, Springer-Verlag, Berlin, Heidelberg, New York

Cox, K.G., Bell, J.D. and Pankhurst, R.J., 1979: The Interpretation of Igneous Rocks. Allen and Unwin Ltd., London. 450p.

Cullis, C.G. and Edge, A.B., 1922: Report on the cupiferous deposits of Cyprus. London (Crown agents for overseas governments and administrations).

Deer, W.A., Howie, R.A. and Zussman, J., 1978: Rock-Forming Minerals. v. 2A, Single Chain Silicates. Longman Gp. Ltd., London, 2nd Ed.

Dewey, J.F. and Bird, J.M., 1971: Origin and emplacement of the ophiolite suite: Appalachian ophiolites in Newfoundland. Jour. Geophys. Res., 76: 3179-3206

Donaldsen, C.H., Usselman, T.M., Williams, R.J. and Lofgren, G.E., 1975: Experimental modelling of the cooling history of Appollo 12 olivine basalts. Proc. 6th Lunar Sci. Conf: 843-869

Dowty, E., Keil, K. and Prinz, M., 1974: Lunar pyroxene-phyric basalts: crystallization under supercooled conditions. J. Petrol., 15: 419-453

Duncan, R.A. and Green, D.H., 1980. Roll of multistage melting in the formation of oceanic crust. Geology, 8: 22-26

Evans, B.W. and Moore, J.G., 1968: Mineralogy as a function of depth in the prehistoric Makaopulu tholeiitic lava lake, Hawaii. Contrib. Mineral. Petrol., 17: 85-115

Ewart, A., 1976: A petrological study of the younger Tongan andesites and dacites, and the olivine tholeiites of Niva Fo'ou Island, Southwest Pacific. Contrib. Mineral. Petrol., 58: 1-22

Ewart, A. and Bryan, W.B., 1973: The petrology and geochemistry of the Tongan Islands. In P.J. Coleman (ed), The Western Pacific, Univ. of Western Australia Press.

Faure, G. and Powell, J.L., 1972: Strontium Isotope Geology. Springer, New York

Finkh, L., 1898: Beitr. Kennt. Gabbro in Serpentingest v. Nord. Syrien. Zeitschr. duet. geol. Gesell. Bd. 1.

Flanagan, F.J., 1973: 1972 values for international geochemical reference samples. Geochim. Cosmochim. Acta, 37: 1189-1200

Flower, M.F.J., Robinson, P.T., Schmincke, H.V. and Ohnmacht, W., 1977: Petrology and geochemistry of igneous rocks, DSDP leg 37. Contrib. Mineral. Petrol., 64: 167-196

Francis, D.M. and Hynes, A.J., 1979: Komatiite-derived tholeiites in the Proterozoic of New Quebec. Earth Planet. Sci. Lett., 44: 473- 481

Frey, F.A., Bryan, W.B. and Thompson, G, 1974: Atlantic ocean floor: Geochemistry and petrology of basalts from Legs 2 and 3 of the Deep Sea Drilling Project. Jour. Geophys. Res., 79: 5507-5527

Gale, G.H., 1973: Paleozoic basaltic komatiite and ocean floor-type basalts from northeastern Newfoundland. Earth. Planet. Sci. Lett., 18: 22-28

Gale, G.H., 19 : An investigation of some sulphide deposits of the Rambler Area, Nfld., Ph.D. thesis, Univ. of Durham

Gass, I.G., 1958: Ultrabasic pillow lavas from Cyprus. Geological Magazine, 95: 241-251

Gass, I.G., 1960: The Geology and Mineral Resources of the Dhali Area. Geol. Surv. Dept., Cyprus, Mem. No. 4

Gass, I.G., 1968: Is the Troodos Massif of Cyprus a fragment of Mesozoic ocean floor? Nature, 220: 39-42

Gass, I.G. and Masson-Smith, D., 1963: The geology and gravity anomalies of the Troodos massif, Cyprus. Phil. Trans. Roy. Soc. London Ser. A255: 417-467

Gass, I.G. and Smewing, J.D., 1973: Intrusion, extrusion and metamorphism at a constructive margin: evidence from the Troodos Massif, Cyprus. Nature, 242: 26-29

Gass, I.G., Neary, C.R., Plant, J., Robertson, A.H.F., Simonian, K.O., Smewing, J.D., Spooner, E.T.C. and Wilson, R.A.M., 1975: Comments on "The Troodos Ophiolite Complex was probably formed in an island arc", by A. Miyashiro and subsequent correspondence by A. Hynes and A. Miyashiro. Earth. Planet. Sci. Lett., 25: 236-238

Gast, P.W., 1968: Trace element fractionation and the origin of tholeiitic and alkaline magma types. Geochim. Cosmochim, Acta, v. 32: 1057

Gaudry, A., 1862: Geologie de l'ile de Chypre. Mem. Geol. Soc. France, ser. 2, VII: 149

Glikson, A.Y., 1971: Primitive Archaean element distribution patterns: Chemical evidence and geotectonic significance. Earth Planet. Sci. Lett., 15: p. 263

Goles, G.C., 1967: Trace Elements in Ultramafic and Related Rocks. Wyllie, P.J. (ed.) New York: Wiley: 222-238

Green, D.H., 1972: Archean greenstone belts may include terrestrial equivalents of Lunar Maria, Earth Planet. Sci. Lett., 15: 263

Green, D.H., 1974: The Petrogenesis of the High-temperature Peridotite Intrusion in the Lizard Area, Cornwall. J. Petrol., 5: 134-188

Green, D.H., 1976: Experimental testing of "equilibrium" partial melting of peridotite under water-saturated high pressure conditions: Canadian Mineralogist, 14: 255-268

Green, D.H., Hibberson, W.O. and Jaques, A.L., 1979: Petrogenesis of mid-ocean ridge basalts, in McElhinny, M.W., (ed.), The Earth: Its origin, structure and evolution. London, Academic Press: 265-290

Greenbaum, D., 1972: Magmatic processes at Ocean Ridges: evidence from the Troodos Massif (Cyprus). Nature, 238 (10): 19-21

Henson, F.R.S., Browne, R.V. and McGurty, J., 1949: A Synopsis of the Stratigraphy and Geological History of Cyprus. Quart. Journal Geol. Soc. Lond. V. LV: 1-41

Hynes, A., 1975: Comment on "The Troodos ophiolite complex was probably formed in an island arc", by A. Miyashiro., Earth and Planet. Sci. Lett., 25: 213-216

Ishii, T., 1975: The relations between temperature and composition of pigeonite in some lavas and their application to geothermometry. Mineral Jour. Japan, 8: 48-57

Isshiki, N., 1963: Petrography of Hachijo-jima volcanic group, Seven Izv Islands, Japan. J. Fac. Sci. Univ. Tokyo, Sec. 2, 15: 91-134

Jamieson, B.G., 1970: Phase relations in some tholeiitic lavas illustrated by the system R_2O_3-XO-YO-ZO_2. Mineral Mag., 37; No. 289

Jamieson, B.G. and Clarke, D.B., 1970: Potassium and associated elements in tholeiitic basalts. Jour. Petrol., 11: 183-204

Jensen, L.S., 1976: A new cation plot for classifying subalkalic volcanic rocks. Ont. Dept. Mines Misc. Paper 66.

Juteau, T., 1970: Petrogenese des ophiolites des nappes d'Antalya (Taurus lycien oriental, Turquie). Leur liason avec une phase d'expansion oceanique active au Trias superieur. Sci. Terr, Nancy, 3: 265-288

Kay, R.W. and Senechal, R.G., 1976: The rare earth geochemistry of the Troodos ophiolite complex. Jour. Geophys. Res., 81: 964-970

Kay, R., Hubbard, N.J. and Gast, P.W., 1970: Chemical characteristics and origin of oceanic ridge volcanic rocks. J. Geophys. Res., 75: 1585

Kidd, R.G.W., 1976: Unpub. Ph.D. Thesis, University of E. Anglia, U.K.

Kidd, R.G.W. and Cann, J.R., 1974: Chilling statistics indicate an ocean-floor spreading origin for the Troodos complex, Cyprus. Earth Planet. Sci. Lett., 24: 151-155

Kober, L., 1915: Geoligische Forschungen in Vorderasien Teil A. Das Taurusgebirge B. Zur Tektonik des Libanon. Deukschr. K. Akad. Wiss. Wien. Math-Nat Kl. 91, . 379.

Kuno, H., 1950: Petrology of Hakene volcano and the adjacent areas, Japan. Bull. Geol. Soc. Amer., 61: 947-1019

Kuno, H., 1955: Ion substitution in the diopside ferropigeonite series of clinopyroxenes. Amer. Mineral., 40: 70-93

Langmhyr, F.J. and Paus, P.E., 1968: The analysis of inorganic siliceous materials by atomic absorption spectrophotometry and the HF acid decomposition technique. Part 1. The analysis of silicate rocks. Anal. Chim. Acta, 43: 397-408

Lapierre, H. and Rocci, G., 1975: Alkaline volcanism in southwestern Cyprus in relation to the opening of the Tethysian domain during Triassic times. Tectonophysics, 30: 299-313

Lapierre, H. and Parrot, J.F., 1972: Identite geologique des regions de Paphos (Chypre) et du Baer-Bassit (Syrie). C.R. Acad. Sci. Paris, 274: 1999-2002

Lofgren, G., Donaldsen, C.H., Williams, R.J., Mullins, O. and Usselman, T.M., 1974: Experimentally-reproduced textures and mineral chemistry of Apollo 15 quartz normative basalts. Proc. 5th Lunar Conf., suppl. 5. Geochim. Cosmochim. Acta, 1: 549-567

Mace, C., 1939: Gravity measurements on Cyprus. R.A.S. Geophysical Supplement.

Magaritz, M. and Taylor, H.P. Jr., 1974: Oxygen and hydrogen isotope studies of serpentinization in the Troodos ophiolite complex, Cyprus. Earth Planet Sci. Lett., 23: 8-14

Malpas, J.G., 1976: The Petrology and Petrogenesis of the Bay of Islands Ophiolite Suite, Western Newfoundland. (2 parts). Unpub. Ph.D. Thesis, M.U.N., 433 pp.

Malpas, J., 1978: Magma generation in the Upper Mantle, field evidence from ophiolite suites, and application to the generation of oceanic lithosphere. Phil. Trans. Royal Soc. London, Series A, 288: 527-546

McCall, G.J.H., 1973: Geochemical characteristics of some Archean greenstone suites of the Yilgarn Structural province, Australia. Chem. Geol., v. 11: 243-269

Menzies, M. and Allen, C., 1974: Plagioclase Lherzolite - Residual Mantle Relationships within Two Eastern Mediterranean Ophiolites. Contr. Mineral and Petrol., 45: 197-213

Mesorian, H., Juteau, T., Lapierre, H., Nicolas, A., Parrot, J.-F., Rocci, G. and Rolli, M., 1974: Les assemblages ophiolitiques mesogeens. Bull. Soc. Geol. Fr. (7), XV(5-6): 478-493

Miyashiro, A., 1973: The Troodos Ophiolitic Complex was probably formed in an island arc. Earth Planet. Sci. Lett., 19: 218-224

Miyashiro, A., 1975: Origin of the Troodos and other ophiolites: a reply to Hynes. Earth Planet. Sci. Lett., 25: 217-222

Moore, T.A., 1960: The Geology and Mineral Resources of the Astromeritis-Kormakiti Area. Geol. Surv. Dept., Cyprus, Mem. No. 6

Moores, E.M., 1975: Discussion of "Origin of Troodos and other ophiolites: a reply to Hynes", by Akiho Miyashiro, Earth Planet. Sci. Lett., 25: 223-226

Moores, E.M. and Vine, F.J., 1971: Troodos Massif, Cyprus and other ophiolites as oceanic crust: evaluation and implications. Roy. Soc. London Phil. Trans. A, 268: 443-466

Muir, I.D. and Tilley, C.E., 1964: Iron enrichment and pyroxene fractionation in tholeiites. Geol. Jour., 4: 143-156

Nakamura, Y. and Kushiro, I., 1970b: Equilibrium relations of hypersthene, pigeonite and augite in crystallizing magmas; microprobe study of a pigeonite andesite from Weiselberg, Germany. Amer. Min., 55: 1999-2015

Nicholls, I.A., 1971: Petrology of Santorin volcano, Cyclades, Greece. J. Petrol., 12: 67-119

Nisbet, E.G. and Pearce, J.A., 1977: Clinopyroxene Compositions in Mafic Lavas from Different Tectonic Settings. Contr. Mineral. Petrol., 63: 149-160

O'Hara, M.J., 1963b: The join diopside-pyrope at 30 kb. Carnegie Inst. Wash. Yearbook, 62: 116-118

O'Hara, M.J., 1968: Are ocean floor basalts primary magmas? Nature, 220: 683-686

Pantazis, Th.M., 1967: The Geology and Mineral Resources of the Pharmakas - Kalavasos Area. Geol. Surv. Dept., Cyprus. Mem. No. 8

Pearce, J.A., 1975: Basalt geochemistry used to investigate past tectonic environments on Cyprus. Tectonophysics, 25: 41-67

Pearce, J.A. and Norry, M.J., 1979: Petrogenetic Implications of Ti, Zr, Y and Nb Variations in Volcanic Rocks: Contrib. Mineral. Petrol., 69: 33-47

Peterman, Z.E., Coleman, R.G. and Hildreth, R.A., 1971: Sr^{87}/Sr^{86} in mafic rocks of the Troodos Massif, Cyprus. U.S. Geol. Surv. Prof. Paper, 7500: D157-D161

Peterman, Z.E., Hedge, C.E. and Tourtelot, H.A., 1970: Isotopic composition of strontium in sea water throughout Phanerozoic time. Geochim. Cosmochim Acta, 34: 105-120

Poldevaart, A. and Hess, H.H., 1951: Pyroxenes in the crystallization of basaltic magmas. Jour. Geol., 59: 472-489

Roeder, P.L. and Emslie, R.F., 1970: Olivine-Liquid Equilibrium. Contrib. Mineral. Petrol., 29: 275-289

Schilling, J.G., 1975: Rare-earth variations across 'normal segments' of the Reykjanes Ridge 60-53°N, Mid-Atlantic Ridge 29°S, and East Pacific Rise, 2-19°S and evidence on the composition of the underlying low-velocity layer. J. Geophys. Res. 80: 1459-1473

Searle, D.L. and Vokes, F.M., 1969: Layered ultrabasic rocks from Cyprus. Geol. Mag., 106: 513-530

Shapiro, L. and Brannock, W.W., 1962: Rapid analysis of silicate, carbonate and phosphate rocks. U.S.G.S., Bull. 1144A: A31

Simonian, K.O. and Gass, I.G., 1978: Arakapas fault belt, Cyprus: A fossil transform fault. Geol. Soc. Am. Bull., 89: 1220-1230

Smewing, J.D., 1975: Metamorphism of the Troodos Massif, Cyprus. Unpub. Ph.D. Thesis, Open Univ., England, 267 pp.

Smewing, J.D. and Potts, P.J., 1976: Rare Earth Abundances in Basalts and Metabasalts from the Troodos Massif, Cyprus. Contrib. Mineral. Petrol., 57: 245-258

Smith, A.G., 1971: Alpine deformation and the oceanic areas of the Tethys, Mediterranean and Atlantic. Geol. Soc. Am. Bull., 82: 2039-2070

Smith, D. and Lindsley, D.H., 1971: Stable and metastable augite crystallization trends in a single basalt flow. Amer. Mineral., 56: 225-233

Smith, P.J., 1975: Disagreement over Troodos. Nature, 255: 192-194

Spooner, E.T.C., Beckinsale, R.D., Fyfe, W.S., and Smewing J.D., 1974: O^{18} enriched ophiolite metabasic rocks from E. Liguria (Italy), Pindos (Greece) and Troodos (Cyprus). Contrib. Mineral. and Petrol., 47: 41-62

Strong, D.F. and Dostal, J., 1980: Dynamic Melting of Proterozoic Upper Mantle: Evidence from Rare Earth Elements in Oceanic Crust of Eastern Newfoundland. Contr. Mineral. Petrol., 72: 165-173

Sven, C-Y.J., 1978: Geochemistry of peridotites and associated mafic rocks, Ronda ultramafic complex, Spain. Unpub. D.Sc. thesis, Mass. Inst. Tech., Cambridge, Mass. 283 p.

Swarbrick, R.E., 1980: The Mamonia Complex of S.W. Cyprus: a Mesozoic continental margin and its relationship to the Troodos Complex. in Panayiotou, A: Proc. Int. Ophio. Symp. Cyprus, Geol. Surv. Dept. Cyprus, pp. 86-92

Sun, S-S. and Nesbitt, R.W., 1978: Geochemical regularities and genetic significance of ophiolite basalts. Geology, 6: 689-693

Talkington, R.W., 1981: The Geology, Petrology and Petrogenesis of the White Hills Peridotite, St. Anthony Complex, N.W. Nfld. Unpub. Ph.D. Thesis, M.U.N., 432 pp.

Tatsumoto, M., Hedge, C.E. and Engel, A.E.J., 1965: Potassium, rubidium, strontium, thorium, uranium and the ratio of strontium-87 to strontium-86 in oceanic tholeiitic basalt. Science, 150: p. 886

Tilley, C.E., Yoder, H.S. and Schairer, J.F., 1963: Melting relations of basalts. Carn. Inst. Wash. Yearbook 62: 77-84

Tilley, C.E., Yoder, H.S. and Schairer, J.F., 1964: New relations on melting of basalts. Carn. Inst. Wash. Yearbook 63: 92-97

Tilley, C.E., Yoder, H.S. and Schairer, J.F., 1965: Melting relations of volcanic tholeiite and alkali rock series. Carn. Inst. Wash. Yearbook 64: 69-82

Tilley, C.E., Yoder, H.S. and Schairer, J.F., 1967: Melting relations of volcanic rock series. Carn. Inst. Wash. Yearbook 65: 260-269

Unger, F. and Kotschy, T., 1865: Die Insel Cypern: ihrer physichen und organischen Natur etc. Vienna.

Upadhyay, H.D., Dewey, J.F. and Neale, E.R.W., 1971: The Bett's Cove Ophiolite Complex, Newfoundland: Appalachian oceanic crust and mantle. Geol. Assoc. Can. Proc.: 24, 27-34

Viljoen, M.J. and Viljoen, R.P., 1969a: The geology and geochemistry of the lower ultramafic unit of the Onverwacht Group and a proposed new class of igneous rock. Upper Mantle Project. Spec. Publ. Geol. Soc. S. Afr. 2: 221-244

Viljoen, M.J. and Viljoen, R.P., 1969b: Evidence for the composition of the primitive mantle and its products of partial melting from a study of the rocks of the Barberton Mountain Land. Geol. Soc. South Africa Spec. Pub. 2: p. 275

Virgo, D. and Ross, M., 1973: Pyroxenes from Mull Andesites. Carnegie Inst. Wash. Ann. Rept. Dir. Geophys. Lab., 1972-1973: 535-540

Vine, F.J., Poster, C.K. and Gass, I.G., 1973: Aeromagnetic survey of the Troodos igneous massif, Cyprus. Nature Physical Science, 24: 34-48

Viswanathan, S., 1974: Basaltic komatiite occurrences in the Kolar gold field of India. Geol. Mag. III: 353-354

Williams, D.A.C., 1972: Archean ultramafic, mafic and associated rocks, Mt. Monger, Western Australia. J. Geol. Soc. Aust. 19: 163-188

Wilson, A.D., 1955: A new method for the determination of ferrous iron in rocks and minerals. Geol. Surv. Gt. Brit. Bull., 9: 56-58

Wilson, R.A.M., 1959: The Geology of the Xeros-Troodos Area, with an Account of the Mineral Resources (by F.T.Ingham). Geol. Surv. Dept., Cyprus, Mem. No. 1.

Wood, B.J. and Fraser, D.G., 1976: Elementary Thermodynamics for Geologists. London, Oxford Univ. Press.

Yamakawa, M., 1971: Two different crystallization trends of pyroxene in a tholeiitic dolerite, Semi, northern Japan. Contrib. Mineral. Petrol, 33: 232-238

Yoder, H.S. and Tilley, C.E., 1962: Origin of basaltic magmas: an experimental study of natural and synthetic rock systems. Jour. Petrol., 3: 342-532

Zdarsky, A., 1910: Eruptivgesteine des Troodos - Gerbirges auf der Insel Cypern und seine Abestlagersträtten. Zeitschr. prakt. Geol. Jahrg. xviii: 340-346. Berlin.

APPENDIX A Discussion of Analytical and Determinative Methods

A.1 Sampling Procedure

Samples were collected from the Upper Pillow Lavas with the intention of representing uniformly the different rock types. The Upper Pillow Lavas, being generally very fine grained and invaded by calcite along joints and minute cracks, often presented a problem as regards fresh samples. These were sought assiduously, and in areas of considerable outcrop, as in the northern foothills of the Troodos Mountains, it was almost always possible to find fresh samples with a little persistance. In areas of more discontinuous outcrop, however, as in the southern foothills, good samples were more restricted to dried-up stream beds. Where fracturing made it impossible to collect a single bulk sample a collection of clean chip samples was made, with care taken to avoid calcitic or zeolitic vein material. Samples were bagged, labelled and boxed for shipment from the field area.

A.2 Analytical Methods

A.2.1 Preparation of Powders for Bulk-Rock Geochemical Study

In the laboratory all bulk samples were divided into two portions. Thin sections as well as powders were made from each sample, not solely for petrographic study, but to assist in the selection of samples for geochemical analysis. Samples which were seen under the microscope to be highly altered were not pulverized. Those chosen for analysis were broken into 2 to 3 inch chips with a ten pound sledge hammer. The chips were subsequently placed in a tungsten carbide swing mill for one minute and pulverized to about -100 mesh. The tungsten carbide bowl and rings were thoroughly cleansed with hot water and an abrasive silica cleanser

after each sample. The powders were stored in glass bottles and labelled.

A.2.2 Major and Minor Element Analyses

Major and minor element concentrations were determined by G. Andrews on a Perken Elmer Model 404 atomic absorption spectrophotometer. Samples were prepared by the author according to the method of Langmhyr and Paus (1968):

(1) 0.1000 g of rock powder was placed in a Nalgene polycarbonate digestion bottle.

(2) 5 ml of concentrated HF was added to the digestion bottle to facilitate dissolution of the powder. The bottle was then placed on a steam bath for one half hour.

(3) After cooling undissolved flourides were complexed by adding 50 ml of saturated H_3BO_4 solution followed by 145 mil of distilled H_2O. The solution was then homogenized and stored in a clean polyethylene bottle.

G. Andrews prepared standards following the method of Abbey (1968) and determined percentage phosphorus using a colourimetric method modified after Shapiro and Brannock (1962).

The author made ferrous iron determinations by a variation of the titrimetric method of Wilson (1965). Loss on ignition was determined by heating a portion of sample in a crucible for two hours at 1050°C, cooling in a dessicator, and weighing to determine the percent loss of volatiles.

To determine analytical precision a sample was run in each batch of analyses; results are included in Table A.2.2a. Accuracy of major element analyses was determined by comparison with the standard basalt (U.S.G.S.) BCR-1 (Table A.2.2b).

A.2.3 Trace Element Analyses

Trace element concentrations were determined under the supervision of D. Press using a Phillips 1450 fully automated X-ray fluorescence spectrometer. U.S.G.S. rock powders were used as standards for calibrations. Hardened discs for analyses were prepared in the following manner:

(1) About 10 g of rock powder was combined in a clean glass jar with 1.1 g of Union Carbide Phenolic Resin binder and shaken for 10 minutes.

(2) The mixture was then pressed into a disc in a Herzog hydraulic press for 1 minute at a pressure of 30 tons per square inch.

(3) The disc was baked at 200°C for 10 minutes and cooled.

(4) The disc was labelled and stored in a dessicator until analysis.

Precision and accuracy data for trace element analyses are given in Tables A.2.3a and A.2.3b.

A.2.4 Electron Microprobe Analyses

Thin sections for microprobe analysis were prepared by the author. Sections were polished using an aluminum oxide abrasive powder and coated with carbon in a Varian VE-10 vacuum evaporator.

Analyses of all minerals employed a fully automated JEOL JXA - 50A electron probe microanalyser with KRISEL Control through a PDP-11 computer. A beam current of about 0.3 microamps and an acceleration potential of 15 kV were used. A spot size of about 1 to 2 microns, a count rate of 30,000 and a default time of 30 were the parameters for all mineral phases.

A.2.5 Rare Earth Element Analyses

Analyses for rare earth elements were carried out by neutron activation (INAA) under the supervision of Dr. J. Pearce of the Open University, England. The elements La and Sm were determined by a short count (800 sec.) method with data measured relative to the Open University standard AC(OURS) using calibration VIII. All other elements were determined by long count and were measured relative to the standard U.S.G.S. BHVO-1. Statistical errors of 10% and 20% were measured for various elements and are recorded in the table of rare earth analyses, Appendix B.1.2.

TABLE A.2.2a

Precision of Major Element Analyses

Element	No. of Determinations	$\bar{X}$ (wt. %)	SD (standard dev.)	C (coef. variation)
SiO_2	10	45.97	0.73	1.59
TiO_2	10	0.48	0.01	2.08
Al_2O_3	10	22.01	0.18	0.82
Fe_2O_3	10	4.12	0.10	2.43
MnO	10	0.07	0.01	14.29
MgO	10	9.70	0.01	0.10
CaO	10	13.21	0.05	0.38
Na_2O	10	1.55	0.02	1.29
K_2O	10	0.11	0.04	36.36
P_2O_5	10	0.02	0.01	50.00
L.O.I.	10	3.48	0.15	4.31

TABLE A.2.2b

Accuracy of Major Element Analyses

Element	Proposed Value (Abbey, 1968)	$\bar{X}$ (wt. %)	SD	No. of Determinations
SiO_2	54.36	55.38	0.26	6
TiO_2	2.24	2.31	0.19	6
Al_2O_3	13.56	13.52	0.25	6
Fe_2O_3	13.40	13.01	0.27	6
CaO	6.94	6.82	0.06	6
MnO	0.19	0.17	0.01	6
MgO	3.46	3.52	0.06	6
Na_2O	3.26	3.26	0.04	6
K_2O	1.67	1.70	0.04	6

TABLE A.2.3a
Precision of Trace Element Analyses

Element	$\bar{X}$ (ppm)	SD	C
Zr	201	8	4.0
Sr	193	5	2.6
Rb	8	2	25
Zn	90	8	8.9
Cu	110	7	6.4
Ba	73	8	11.0
Nb	46	2	4.3
Pb	6	1	17
Ni	38	7	18.4
La	73	5	6.8
Cr	109	9	8.3
V	69	3	4.3
Y	20	0.3	1.5
Ce	112	4	3.6
Ga	19	1	5.3

TABLE A.2.3b

Accuracy of Trace Element Analyses

Element	Proposed Value (Flanagan, 1973)	$\bar{X}$ (ppm)	SD	No. of Determinations
Zr	190	193	9	10
Sr	330	345	12	10
Rb	46.6	49	4	10
Zn	120	110	10	10
Cu	18.4	20	4	10
Ba	675	682	12	10
Nb	13.5	14	2	10
Pb	17.6	13	1	10
Ni	15.8	17	4	10
La	26	37	4	10
Cr	17.6	22	7	10
V	399	379	23	10
Y	37.1	42	4	10
Ce	53.9	72	6	10
Ga	20	21	2	10

APPENDIX B: Analytical Tables

APPENDIX B.1 Bulk Rock Analyses

APPENDIX B.1.1 Major and Trace Element Analyses

ULTRABASIC ROCKS

	KL-17	KL-95	KL-121	DL-36	DL-37	DL-38	DL-45
SiO_2	43.90	38.80	45.07	39.30	36.40	42.80	41.50
TiO_2	0.10	0.09	0.21	0.00	0.14	0.26	0.30
Al_2O_3	6.37	1.59	5.26	3.67	3.48	6.67	5.22
Fe_2O_3	1.56	5.60	1.07	2.71	3.22	3.19	3.09
FeO	6.53	3.60	7.74	4.57	4.44	5.53	5.40
MnO	0.14	0.14	0.13	0.11	0.12	0.15	0.15
MgO	27.80	36.00	28.61	35.90	34.35	28.45	31.33
CaO	6.16	1.53	4.82	4.00	8.77	5.00	2.41
Na_2O	0.32	0.05	0.00	0.08	0.28	0.37	0.10
K_2O	0.06	0.00	0.05	0.04	0.08	0.04	0.08
P_2O_5	0.00	0.00	0.09	0.00	0.00	0.00	0.00
L.O.I.	5.84	10.84	7.51	9.05	8.61	7.25	10.74
TOTAL	98.78	98.19	100.57	99.43	99.89	99.71	100.32
ppm							
Zr	7	7	7	6	5	13	12
Sr	26	3	5	23	51	26	18
Rb	1	0	0	2	3	3	2
Zn	54	54	54	39	36	47	48
Cu	46	35	35	23	3	25	19
Ba	7	0	3	0	0	-	12
Nb	2	2	2	0	0	-	-
Pb	0	0	0	3	2	2	2
Ni	1064	1226	1136	1407	1378	848	1072
La	23	16	20	-	-	-	-
Cr	2054	2438	2497	3025	2951	1829	2584
V	141	59	136	87	71	124	110
Y	6	6	6	5	4	10	8
Ce	-	-	-	2	4	-	2
Ga	4	2	5	0	0	-	0
wt. %							
Qz	0.00	0.00	0.00	0.00	0.00	0.00	0.00
Or	0.38	0.00	0.32	0.26	0.00	0.26	0.53
Ab	2.90	0.49	0.00	0.75	0.00	3.38	0.94
An	16.90	4.73	15.19	10.51	9.23	17.73	13.31
Ne	0.00	0.00	0.01	0.00	1.48	0.00	0.00
Le	0.00	0.00	0.00	0.00	0.43	0.00	0.00
Wo	6.63	1.67	4.08	4.74	2.14	3.78	0.00
Di Ens	5.19	1.32	3.16	3.85	1.73	2.95	0.00
Fs	0.71	0.16	0.47	0.33	0.16	0.42	0.00
En Ens	23.82	20.59	35.70	9.36	0.00	23.40	33.80
Fs	3.25	2.46	5.75	0.81	0.00	3.33	4.12
Ol Fo	31.68	56.94	24.06	59.78	67.96	35.15	37.17
Fa	4.76	7.50	3.94	5.70	6.93	5.51	5.00
Mg	3.11	3.34	3.10	3.20	3.35	3.13	3.23
Ilm	0.20	0.20	0.43	0.00	0.31	0.53	0.63
Chr	0.47	0.60	0.57	0.72	0.73	0.43	0.62
Ap	0.00	0.00	0.22	0.00	0.00	0.00	0.00
Cor	0.00	0.00	0.00	0.00	0.00	0.00	0.65

Fe_2O_3 recalculated as 2.00% for normative analyses

-: not determined

KOMATIITES

%	KL-12	KL-13	KL-15	KL-18	KL-24	KL-33	KL-34	KL-36	KL-38	KL-55	KL-71	KL-77
SiO_2	51.60	50.04	50.50	51.21	50.20	50.20	50.30	49.20	49.20	46.40	40.40	50.00
TiO_2	0.43	0.43	0.38	0.32	0.33	0.20	0.23	0.24	0.23	0.25	0.24	0.32
Al_2O_3	14.05	13.90	13.70	12.71	13.70	11.00	11.00	11.00	11.10	12.50	12.00	11.87
Fe_2O_3	7.80	2.41	2.42	1.58	3.48	2.29	2.09	2.00	2.76	2.39	1.87	1.98
FeO	0.72	5.39	5.40	6.17	4.10	5.76	5.94	6.15	5.35	5.75	5.83	5.86
MnO	0.13	0.13	0.15	0.13	0.16	0.14	0.14	0.18	0.16	0.14	0.15	0.13
MgO	8.68	8.11	8.55	9.93	9.04	11.65	11.39	11.30	9.91	11.26	11.78	10.94
CaO	10.49	10.37	10.37	11.31	10.42	9.95	9.95	11.41	11.56	11.25	10.88	11.25
Na_2O	1.53	1.27	1.33	0.00	1.05	0.84	0.79	0.63	0.57	0.44	0.69	0.38
K_2O	0.18	0.28	0.23	0.21	0.28	0.17	0.16	0.17	0.19	0.29	0.12	0.14
P_2O_5	0.14	0.10	-	0.12	-	-	-	-	-	-	-	0.11
H_2O^+	4.85	8.03	8.26	6.22	7.34	7.90	7.65	8.41	10.09	8.08	6.31	6.76
TOTAL	100.60	100.46	101.62	99.91	100.10	100.10	99.64	100.69	101.12	98.75	98.27	99.74
ppm												
Zr	23	23	25	10	20	10	11	12	11	17	12	12
Sr	83	83	117	56	109	87	79	109	118	506	37	41
Rb	4	4	3	3	4	3	2	2	3	2	2	1
Zn	57	58	57	59	56	60	62	64	62	61	59	60
Cu	67	68	65	89	72	87	92	92	99	82	81	79
Ba	14	13	19	3	8	18	14	12	11	9	6	16
Nb	2	1	3	2	2	2	1	2	1	1	3	3
Pb	-	-	-	-	-	-	-	1	-	-	-	-
Ni	128	121	87	126	95	228	262	265	199	271	281	314
La	19	19	20	22	24	24	22	20	17	22	19	19
Cr	376	374	322	529	313	720	724	740	665	768	757	812
V	210	216	214	239	216	219	208	204	203	219	215	210
Y	14	12	13	12	13	9	10	10	11	9	13	14
Ce	-	-	-	-	-	-	-	-	-	-	-	-
Ga	11	14	12	9	12	9	10	11	11	10	11	11
wt. %												
Qz	7.73	8.60	8.05	13.18	8.46	7.44	8.31	6.20	8.69	3.16	4.84	9.19
Or	1.12	1.79	1.46	1.32	1.79	1.09	1.03	1.09	1.23	1.89	0.77	0.89
Ab	13.59	11.63	12.10	0.00	9.59	7.70	7.26	5.77	5.30	4.10	6.34	3.45
An	32.49	33.98	33.03	36.31	34.36	27.90	28.23	28.88	29.84	34.45	31.81	32.51
Ne	0.00	0.00	0.00	0.00	0.00	0.00	0.00	0.00	0.00	0.00	0.00	0.00
Cor	0.00	0.00	0.00	0.00	0.00	0.00	0.00	0.00	0.00	0.00	0.00	0.00
Di Wo	8.87	8.79	9.31	9.48	8.96	10.70	10.01	13.59	13.86	11.36	11.20	11.14
Di Ens	5.86	5.78	6.17	6.47	6.09	7.45	7.35	9.31	9.32	7.84	7.91	7.75
Di Fs	2.37	2.38	2.48	2.26	2.17	2.37	2.38	3.14	3.49	2.60	2.32	2.47
En Ens	16.84	16.07	16.72	19.89	18.20	23.99	23.45	21.14	17.78	23.05	23.95	21.51
En Fs	6.80	6.62	6.71	6.94	6.49	7.64	7.59	7.12	6.67	7.64	7.03	6.85
Ol Fo	0.00	0.00	0.00	0.00	0.00	0.00	0.00	0.00	0.00	0.00	0.00	0.00
Ol Fa	0.00	0.00	0.00	0.00	0.00	0.00	0.00	0.00	0.00	0.00	0.00	0.00
Mg	3.04	3.14	3.12	3.09	3.13	3.14	3.15	3.14	3.18	3.19	3.15	3.11
Ilm	0.86	0.88	0.78	0.65	0.68	0.41	0.47	0.49	0.48	0.52	0.49	0.65
Chr	0.86	0.09	0.07	0.12	0.07	0.17	0.17	0.17	0.16	0.18	0.18	0.19
Ap	0.34	0.25	0.00	0.30	0.00	0.00	0.00	0.00	0.00	0.00	0.00	0.27

Fe_2O_3 recalculated as 2.0% for normative analyses

-: not determined

KOMATIITES, cont'd.

%	KL-78	KL-86	KL-108	KL-110	DL-41	PL-31
SiO_2	51.32	48.80	48.49	49.81	51.10	46.70
TiO_2	0.32	0.30	0.37	0.33	0.42	0.20
Al_2O_3	12.24	11.70	12.80	11.33	12.80	12.90
Fe_2O_3	1.66	1.62	2.79	4.57	2.79	2.93
FeO	6.52	5.85	5.04	2.62	4.91	5.38
MnO	0.14	0.15	0.13	0.12	0.14	0.10
MgO	12.48	12.44	9.66	8.18	10.53	11.33
CaO	10.70	9.88	9.22	9.96	9.75	5.78
Na_2O	0.00	1.12	2.60	3.87	1.35	0.79
K_2O	0.12	0.18	0.31	0.05	0.47	2.28*
P_2O_5	0.12	-	0.12	0.15	-	-
L.O.I.	4.84	6.32	8.30	7.59	5.42	11.68
TOTAL	100.46	98.36	100.53	98.58	99.68	100.07

ppm						
Zr	11	18	16	14	26	14
Sr	33	77	97	41	93	108
Rb	2	2	2	0	9	25
Zn	60	58	59	55	54	98
Cu	81	75	80	65	72	25
Ba	13	7	23	10	9	58
Nb	2	2	2	2	0	0
Pb	-	-	-	1	2	4
Ni	363	347	197	260	143	221
La	19	16	20	20	-	-
Cr	891	702	516	466	695	731
V	215	198	211	168	209	196
Y	10	12	13	12	19	4
Ce	-	-	-	-	6	1
Ga	9	18	10	12	9	5

wt. %							
	Qz	9.98	3.31	0.00	0.00	6.00	0.64
	Or	0.74	1.15	1.99	0.33	2.951	15.24
	Ab	0.00	10.28	23.85	36.06	12.12	7.56
	An	34.50	28.60	24.22	14.75	29.14	28.18
	Ne	0.00	0.00	0.00	0.00	0.00	0.00
	Cor	0.00	0.00	0.00	0.00	0.00	0.00
	Wo	8.40	10.27	11.83	16.12	9.26	1.79
Di	Ens	5.91	7.39	8.06	11.04	6.48	1.23
	Fs	1.78	1.95	2.84	3.80	2.01	0.42
En	Ens	26.54	26.21	14.11	6.61	21.33	30.68
	Fs	8.00	6.90	4.97	2.28	6.63	10.36
Ol	Fo	0.00	0.00	0.00	0.00	0.00	0.00
	Fa	0.00	0100	0.00	0.00	0.00	0.00
	Mg	3.03	3.15	3.14	3.19	3.08	3.28
	Ilm	0.63	0.62	0.76	0.69	0.85	0.43
	Sp	0.20	0.16	0.12	0.11	0.16	0.18
	Ap	0.29	0.00	0.30	0.38	0.00	0.00

Fe_2O_3 recalculated as 2.00% for normative analyses

-: not analysed * not included in average

APHYRIC BASALTS

%	KL-22	KL-23	KL-32	KL-44	KL-46	KL-62	KL-66	KL-67	KL-68	KL-69	KL-73	KL-119
SiO_2	55.2	55.15	47.90	47.70	46.00	49.90	49.71	46.60	51.32	50.73	45.90	52.38
TiO_2	0.38	0.48	0.31	0.30	0.35	0.36	0.35	0.43	0.36	0.43	0.34	0.34
Al_2O_3	14.00	15.27	14.70	14.40	13.70	16.10	13.48	14.13	13.04	15.86	13.20	11.79
Fe_2O_3	2.51	3.55	5.23	5.73	4.11	4.83	5.43	3.63	3.75	4.57	4.82	2.70
FeO	3.60	3.72	3.23	2.49	3.23	3.89	2.70	4.03	3.34	3.13	3.14	5.06
MnO	0.09	0.12	0.09	0.10	0.14	0.10	0.12	0.13	0.12	0.13	0.10	0.13
MgO	7.74	5.46	9.49	6.31	7.12	6.48	6.47	8.22	8.63	5.57	9.41	10.11
CaO	11.89	9.72	10.72	11.64	13.69	10.75	13.05	11.36	8.58	10.34	11.13	8.51
Na_2O	1.09	1.85	1.20	1.01	0.55	1.73	0.40	1.01	2.67	1.17	1.55	2.57
K_2O	0.48	0.44	0.64	1.23	1.35	0.73	1.06	0.30	0.89	0.72	0.47	0.23
P_2O_5	-	-	-	-	-	-	0.14	0.14	0.10	0.11	-	0.10
L.O.I.	2.98	4.84	7.74	8.82	8.06	3.91	7.01	10.26	7.13	5.33	9.47	4.86
TOTAL	99.96	100.75	101.25	99.73	98.30	98.78	99.92	100.24	99.93	98.09	99.53	98.78
ppm												
Zr	17	31	15	-	11	17	12	19	13	21	18	13
Sr	41	97	60	-	47	44	38	218	22	289	199	85
Rb	13	19	9	-	30	19	12	4	18	8	10	2
Zr	48	49	62	-	51	66	45	61	52	47	12	51
Cu	20	35	20	-	41	18	26	28	16	16	20	21
Ba	12	39	25	-	22	8	15	7	18	16	10	5
Nb	3	3	2	-	2	2	3	1	2	1	1	4
Pb	-	0	1	-	-	1	1	-	-	-	-	-
Ni	66	47	95	-	73	65	102	99	89	78	87	202
La	17	18	20	-	21	16	26	18	25	22	15	20
Cr	285	107	188	-	176	72	325	317	322	113	250	533
V	233	219	276	-	191	236	224	233	219	223	228	245
Y	14	14	9	-	11	13	12	13	15	13	12	14
Ce	-	-	-	-	-	-	-	-	-	-	-	-
Ga	-	15	15	-	11	16	12	15	8	13	12	11
wt. %												
Qz	13.46	14.97	1.65	4.97	2.54	4.32	2.99	5.48	4.32	11.45	0.00	4.64
Or	2.93	2.72	4.06	8.02	8.86	4.56	5.58	1.98	4.56	4.60	3.08	1.45
Ab	9.51	16.37	10.89	9.43	5.17	15.48	24.38	9.55	15.48	10.70	14.56	23.15
An	32.89	33.54	35.23	34.35	34.34	35.95	22.63	37.03	35.95	38.79	30.71	21.24
Ne	0.00	0.00	0.00	0.00	0.00	0.00	0.00	0.00	0.00	0.00	0.00	0.00
Cor	0.00	0.00	0.00	0.00	0.00	0.00	0.00	0.00	0.00	0.00	0.00	0.00
Di Wo	0.00	6.65	9.13	12.36	17.16	8.54	9.44	10.45	8.54	6.67	12.79	9.62
Di Ens	8.34	4.16	6.00	7.51	11.25	5.06	6.55	7.13	5.06	4.03	8.58	6.63
Di Fs	2.30	2.09	2.38	4.17	4.71	3.05	2.12	2.50	3.05	2.28	3.25	2.21
En Ens	11.53	10.06	19.27	9.83	8.44	12.00	16.64	15.75	12.00	10.96	14.83	20.17
En Fs	3.17	5.06	7.53	5.45	3.53	7.24	5.38	5.53	7.94	6.20	5.62	6.73
Ol Fo	0.00	0.00	0.00	0.00	0.00	0.00	0.00	0.00	0.00	0.00	1.82	0.00
Ol Fa	0.00	0.00	0.00	0.00	0.00	0.00	0.00	0.00	0.00	0.00	0.76	0.00
Mg	2.99	3.03	3.11	3.20	3.22	3.07	3.13	3.24	3.07	3.13	3.22	3.09
Ilm	0.74	0.95	0.63	0.63	0.74	0.72	0.74	0.91	0.72	0.88	0.72	0.69
Chr	0.00	0.02	0.04	0.08	0.04	0.02	0.07	0.08	0.02	0.03	0.06	0.12
Ap	0.00	0.36	0.00	0.00	0.00	0.00	0.25	0.36	0.00	0.28	0.00	0.25

Fe_2O_3 recalculated as 2.0% for normative analyses

-: not determined

APHYRIC BASALTS, cont'd.

%	DL-13	DL-20	DL-28	DL-54	DL-55	DL-62A	DL-84	DL-87	PL-6	PL-7
SiO_2	45.90	49.50	48.50	47.80	45.50	47.20	49.70	48.50	48.70	49.30
TiO_2	0.44	0.51	0.49	0.51	0.51	0.74	0.31	0.50	0.52	0.58
Al_2O_3	15.30	15.80	15.20	16.80	15.60	15.10	13.80	17.30	17.00	17.00
Fe_2O_3	4.06	5.18	5.26	5.53	7.63	6.86	5.85	5.65	5.75	6.48
FeO	4.57	3.73	2.59	1.79	0.29	1.43	1.40	2.75	3.14	2.37
MnO	0.17	0.13	0.08	0.06	0.12	0.09	0.09	0.10	0.12	0.08
MgO	9.18	6.09	6.27	7.91	7.74	7.48	8.36	6.00	4.67	6.00
CaO	10.65	12.53	12.06	10.00	9.03	9.27	10.53	12.00	12.36	9.70
Na_2O	1.56	1.23	1.85	1.81	1.43	1.93	1.20	1.70	1.57	1.97
K_2O	0.40	0.87	1.50	0.19	2.05	1.40	0.16	0.82	1.89	0.55
P_2O_5	-	-	-	-	-	-	-	-	-	-
L.O.I.	6.98	4.38	6.79	8.09	9.38	9.13	8.75	5.14	4.38	5.60
TOTAL	99.21	99.95	100.59	100.49	99.28	100.13	100.15	100.46	100.10	99.63
ppm										
Zr	48	76	22	23	23	40	15	19	18	28
Sr	117	138	80	93	105	92	80	75	75	92
Rb	22	42	17	2	13	22	2	46	44	12
Zn	97	102	52	63	65	64	47	52	62	71
Cu	22	34	22	146	30	11	55	21	11	37
Ba	64	75	10	16	23	15	15	13	41	26
Nb	-	-	-	-	-	-	-	-	-	-
Pb	3	6	2	3	4	1	4	2	3	5
Ni	39	25	46	32	38	44	43	38	28	36
La	3	1	-	-	3	-	-	0	-	-
Cr	1	-	225	71	63	158	114	86	36	9
V	318	643	230	277	266	226	224	243	251	318
Y	34	38	19	14	17	26	13	17	21	24
Ce	7	3	2	3	10	7	2	5	5	1
Ga	15	15	10	11	13	7	6	8	9	12
wt.%										
Qz	0.00	4.67	0.00	3.21	0.00	0.18	9.21	1.41	0.45	4.71
Or	2.57	5.40	9.48	1.22	13.56	9.13	1.04	5.08	11.71	3.47
Ab	14.34	10.93	16.74	16.64	13.54	18.03	11.16	15.09	13.93	17.81
An	36.47	36.76	30.79	40.36	33.68	31.36	34.94	38.97	35.40	38.38
Ne	0.00	0.00	0.00	0.00	0.00	0.00	0.00	0.00	0.00	0.00
Cor	0.00	0.00	0.00	0.00	0.00	0.00	0.00	0.00	0.00	0.00
Di Wo	8.76	11.92	13.89	5.66	6.89	8.12	9.39	9.81	12.08	5.46
Di Ens	5.72	6.90	8.70	3.89	4.59	5.44	6.50	5.73	6.40	3.20
Di Fs	2.43	4.48	4.34	1.32	1.79	2.07	2.13	3.62	5.31	1.99
En Ens	15.04	9.02	7.91	17.51	11.75	15.12	16.38	9.95	5.80	12.76
En Fs	6.04	5.86	3.95	5.97	4.60	5.76	5.38	6.29	4.82	7.93
Ol Fo	2.86	0.00	0.06	0.00	3.67	0.00	0.00	0.00	0.00	0.00
Ol Fa	1.34	0.00	0.03	0.00	1.58	0.00	0.00	0.00	0.00	0.00
Mg	3.15	3.04	3.16	3.15	3.25	3.20	3.19	3.04	3.04	3.10
Ilm	0.91	1.02	1.00	1.05	1.08	1.55	0.65	1.00	1.04	1.18
Chr	0.00	0.00	0.05	0.02	0.02	0.04	0.03	0.02	0.01	0.00
Ap	0.00	0.00	0.00	0.00	0.00	0.00	0.00	0.00	0.00	0.00

Fe_2O_3 recalculated as 2.0% for normative analyses

-: not determined

APHYRIC BASALTS, cont'd.

%	PL-17	PL-18	PL-19	PL-20	PL-22
SiO_2	47.70	47.30	49.70	54.60	50.80
TiO_2	0.28	0.28	0.23	0.38	0.38
Al_2O_3	15.60	15.80	14.60	14.60	16.90
Fe_2O_3	6.16	4.44	4.88	5.48	8.19
FeO	2.33	3.59	3.29	3.12	1.58
MnO	0.08	0.12	0.12	0.10	0.06
MgO	7.73	7.73	5.73	5.33	4.93
CaO	10.63	11.75	13.13	9.94	8.21
Na_2O	0.86	1.40	1.09	1.05	1.85
K_2O	0.95	0.57	0.98	0.43	0.91
P_2O_5	-	-	-	-	-
L.O.I.	6.19	5.29	4.79	4.71	6.29
TOTAL	98.51	98.27	98.54	99.74	100.10
ppm					
Zr	5	12	10	8	17
Sr	33	65	52	43	91
Rb	16	17	40	10	12
Zn	47	46	42	63	61
Cu	40	39	15	30	20
Ba	14	12	8	8	122
Nb	-	-	-	0	-
Pb	1	3	9	2	3
Ni	82	62	51	29	24
La	-	-	-	-	-
Cr	279	166	114	2	3
V	281	220	199	287	402
Y	13	15	15	23	17
Ce	7	3	3	4	-
Ga	8	8	6	9	13
wt.%					
Qz	4.60	1.41	6.41	17.60	8.40
Or	6.11	3.63	6.20	2.68	5.77
Ab	7.91	12.77	9.87	9.38	16.80
An	39.05	37.89	34.29	35.76	37.69
Ne	0.00	0.00	0.00	0.00	0.00
Cor	0.00	0.00	0.00	0.00	0.00
Di Wo	7.65	10.43	14.79	6.82	2.54
Di Ens	4.86	6.71	8.64	3.83	1.31
Di Fs	2.31	3.03	5.44	2.71	1.16
En Ens	16.08	14.05	6.62	10.18	11.87
En Fs	7.64	6.35	4.16	7.20	10.57
Ol Fo	0.00	0.00	0.00	0.00	0.00
Ol Fa	0.00	0.00	0.00	0.00	0.00
Mg	3.15	3.13	3.10	3.06	3.11
Ilm	0.58	0.57	0.97	0.76	0.77
Chr	0.07	0.04	1.03	0.00	0.00
Ap	0.00	0.00	0.00	0.00	0.00

OLIVINE BASALTS

%	KL-9	KL-39	DL-80	KL-16
SiO_2	46.80	48.20	47.50	48.60
TiO_2	0.32	0.37	0.38	0.38
Al_2O_3	11.90	14.00	13.70	13.80
Fe_2O_3	4.97	5.16	5.29	2.71
FeO	3.25	2.48	1.76	5.18
MnO	0.12	0.10	0.11	0.16
MgO	10.00	10.09	7.91	8.89
CaO	12.26	9.72	11.24	9.89
Na_2O	0.99	1.10	1.17	1.58
K_2O	0.59	1.69	1.15	0.30
P_2O_5	-	0.00	-	-
L.O.I.	9.02	8.94	8.28	9.00
TOTAL	100.22	101.85	98.49	100.49
ppm				
Zr	15	17	21	24
Sr	66	102	98	136
Rb	6	13	15	4
Zn	53	60	68	58
Cu	28	21	32	66
Ba	11	76	5	16
Nb	2	1	-	1
Pb	-	-	2	-
Ni	269	107	158	103
La	22	22	-	15
Cr	691	336	564	326
V	205	267	173	214
Y	11	13	9	14
Ce	-	-	6	-
Ga	11	12	9	13
wt.%				
Qz	1.15	0.30	3.65	4.44
Or	3.83	10.78	7.55	1.94
Ab	9.20	10.05	11.00	14.62
An	28.88	30.52	31.94	32.45
Ne	0.00	0.00	0.00	0.00
Cor	0.00	0.00	0.00	0.00
Di Wo	15.86	9.01	12.56	8.87
Di Ens	10.80	6.32	8.67	5.91
Di Fs	3.82	1.92	2.87	2.31
En Ens	16.57	20.10	13.22	18.29
En Fs	5.87	6.33	4.38	7.14
Ol Fo	0.00	0.00	0.00	0.00
Ol Fa	0.00	0.00	0.00	0.00
Mg	3.19	3.13	3.22	3.17
Ilm	0.67	0.76	0.80	0.79
Chr	0.16	0.08	0.13	0.08
Ap	0.00	0.00	0.00	0.00

Fe_2O_3 recalulated as 2.0% for normative analyses

-: not determined

LOWER PILLOW LAVAS

%	KL-20	KL-21	KL-76	KL-98	DL-18	DL-19
SiO_2	52.88	50.20	49.05	53.82	58.80	55.30
TiO_2	0.47	0.45	0.42	0.46	0.91	1.03
Al_2O_3	15.11	15.80	14.46	15.27	15.60	15.30
Fe_2O_3	3.90	5.27	4.35	3.89	5.77	7.18
FeO	3.35	2.38	3.36	3.80	3.20	2.40
MnO	0.13	0.13	0.12	0.12	0.11	0.11
MgO	4.96	5.25	8.40	6.39	2.45	3.91
CaO	9.01	10.60	12.25	10.20	8.04	7.58
Na_2O	1.68	1.48	0.88	2.47	2.13	2.14
K_2O	2.23	2.09	0.36	0.54	0.58	0.58
P_2O_5	0.10	0.00	0.14	0.12	0.00	0.00
L.O.I.	6.81	6.04	6.02	3.22	3.23	5.15
TOTAL	100.63	99.69	99.81	100.31	100.82	100.68
ppm						
Zr	25	23	17	26	38	41
Sr	97	96	47	80	102	101
Rb	51	20	4	14	12	12
Zn	38	43	67	66	79	80
Cu	20	20	18	54	22	20
Ba	41	42	14	23	30	39
Nb	2	1	3	3	0	0
Pb	0	0	3	1	2	4
Ni	35	39	89	75	21	13
La	22	21	17	17	2	1
Cr	95	109	205	213	-	-
V	226	214	232	226	371	436
Y	11	13	14	30	34	31
Ce	-	-	-	-	3	1
Ga	14	14	14	15	17	10
wt. %						
Qz	8.61	4.71	6.48	7.47	21.59	16.46
Or	13.99	13.23	2.27	3.29	3.53	3.61
Ab	15.09	13.42	7.56	21.56	18.54	19.06
An	28.77	32.46	36.80	29.90	32.19	32.03
Ne	0.00	0.00	0.00	0.00	0.00	0.00
Cor	0.00	0.00	0.00	0.00	0.00	0.00
Wo	7.53	9.99	11.35	8.99	3.71	3.17
Di Ens	4.34	5.49	7.62	5.64	1.50	1.55
En Fs	2.85	3.48	2.88	2.79	2.29	1.56
En Ens	8.77	8.02	14.73	10.77	4.78	8.70
En Fs	5.75	4.66	5.56	5.33	7.16	8.75
Ol Fo	0.00	0.00	0.00	0.00	0.00	0.00
Ol Fa	0.00	0.00	0.00	0.00	0.00	0.00
Mg	3.08	3.11	3.10	2.99	2.98	3.05
Ilm	0.95	0.92	0.85	0.90	1.78	2.06
Chr	0.02	0.03	0.05	0.05	0.00	0.00
Ap	0.25	0.00	0.35	0.24	0.00	0.00

Fe_2O_3 recalculated as 2.00% for normative analyses

-: not determined

APPENDIX B.1.2 Normalised Rare Earth Data for Upper and Lower Pillow Lavas

	Chond	KL-12	KL-33	KL-9	DL-80	DL-6	KL-22	01 Cum	LPL-3	LPL-4	LPL-5	LPL-6	LPL-7
La	0.330	3.80	1.73	2.50	4.20	6.80	3.21	1.84	n.d.	n.d.	n.d.	n.d.	n.d.
Ce	0.865	3.03	((0.69))	1.96	2.08	5.89	2.31	n.d.	5.89	9.11	10.07	9.63	11.49
Nd	0.630	(3.80)	n.d.	((2.70))	3.17	8.25	(2.86)	n.d.	9.48	11.27	13.17	14.23	15.70
Sm	0.203	3.35	0.88	2.26	3.05	9.11	2.95	<0.49	9.80	12.95	16.65	19.26	19.46
Eu	0.077	4.29	1.69	2.85	4.02	10.00	3.77	0.39	10.65	11.17	15.58	17.14	18.31
Gd	0.276	4.71	(3.26)	3.98	3.62	9.78	(5.43)	n.d.	8.33	14.20	13.70	16.16	14.28
Tb	0.052	4.80	2.50	3.46	3.85	10.38	4.61	((0.58))	9.42	n.d.	15.96	11.54	17.88
Tm	0.034	5.00	(4.70)	(4.70)	4.12	9.70	5.59	n.d.	9.70	n.d.	14.70	18.53	20.00
Yb	0.220	5.32	4.27	5.00	3.72	9.41	5.36	0.41	8.59	12.82	13.86	17.27	18.64
Lu	0.034	5.29	(4.12)	(5.00)	4.12	9.41	5.88	0.59	9.41	12.35	14.12	15.88	20.00
Ce/Sm		0.89	0.78	0.87	0.68	0.65	0.83	n.d.	0.60	0.70	0.60	0.50	0.59

Raw data are normalized to average chondritic abundances of Nakamura (1974).

Data in single brackets have statistical errors >10%; those in double brackets have statistical errors >20%.

n.d.: not determined.

APPENDIX B.1.3 Published Analyses from Lower Pillow Lavas

%	1	2	3	4	5	6	7
SiO_2	53.20	53.89	49.84	69.50	53.40	51.26	62.39
TiO_2	1.12	1.08	0.76	1.30	1.33	1.60	1.35
Al_2O_3	-	15.83	16.17	12.70	15.75	16.83	14.80
Fe_2O_3	-	-	7.48	-	8.33	8.39	-
FeO	-	11.22*	2.86	5.50*	3.63	4.36	8.28*
MnO	-	0.17	0.12	0.10	0.16	0.16	0.17
MgO	5.00	5.71	9.23	1.80	5.49	5.33	2.88
CaO	-	8.81	9.67	4.80	7.77	7.39	5.47
Na_2O	-	2.70	2.53	4.00	2.76	2.55	3.43
K_2O	-	0.59	0.29	0.20	0.33	0.06	0.18
P_2O_5	0.90	-	0.11	-	0.13	0.16	0.15
H_2O	-	-	1.29	-	1.36	2.06	1.05
TOTAL	-	100.00**	100.25	100.00**	100.00	100.44	100.15
ppm							
Zr	57	-	43	76	70	90	99
Sr	124	-	-	-	-	-	-
Nb	3	-	-	-	-	-	-
Cr	90	-	379	-	-	-	-
Y	26	-	20	-	29	41	38
Ce	11.7	-	5.1	7.88	8.71	8.33	9.94

Sources:

1 - Pearce (preprint, 1979), Table 1, Locality 18.
2 - Moores and Vine (1971), Table 1, Average of 17.
3 to 7 - Smewing and Potts (1976), Table 2.

* Total iron as FeO
** Recal. to 100% anhydrous

APPENDIX B.2 Average Mineral Analyses of Upper Pillow Lavas

( ) indicates number of samples included in average

OLIVINE

	Ultrabasic Rocks			Komatiites				
	KL-121(4)	DL-36(4)	DL-45(3)	KL-18(5)	KL-33(3)	KL-34(3)	KL-77(2)	DL-23(1)
SiO_2	40.67	41.66	40.84	40.15	40.77	40.62	39.13	40.64
Al_2O_3	0.07	0.04	0.02	0.22	0.02	0.05	0.08	0.19
TiO_2	0.01	0.00	0.01	0.00	0.01	0.00	0.00	0.02
Cr_2O_3	-	-	0.03	0.05	0.05	0.04	0.02	-
FeO	8.48	6.90	9.20	10.46	10.03	10.80	9.88	12.12
MnO	0.12	0.11	0.12	0.12	0.11	0.13	0.14	0.16
MgO	50.40	52.63	50.57	47.43	48.51	48.41	50.29	47.88
CaO	0.21	0.17	0.19	0.22	0.18	0.21	0.22	0.23
Na_2O	0.00	0.01	0.04	-	-	-	-	-
K_2O	0.01	0.00	0.00	-	-	-	-	-
NiO	-	-	0.25	0.21	0.32	0.23	0.32	-
SiO_2	41.090	41.408	40.977	40.671	40.780	40.650	40.857	40.420
FeO	8.588	6.888	9.186	10.822	10.240	10.933	9.828	12.163
MgO	50.322	51.704	49.836	48.507	84.980	48.417	49.315	47.417
Fo	91.3	93.0	90.6	88.9	89.5	88.8	89.9	87.4
Si	0.992	0.993	0.989	1.000	1.003	0.997	0.966	0.994
Ti	0.000	0.000	0.000	0.000	0.000	0.000	0.000	0.000
Al	0.002	0.001	0.001	0.006	0.001	0.001	0.002	0.005
Cr	0.000	0.000	0.001	0.001	0.001	0.001	0.000	0.000
Fe_2	0.173	0.138	0.186	0.218	0.206	0.222	0.204	0.248
Mn	0.002	0.002	0.002	0.003	0.002	0.003	0.003	0.003
Mg	1.832	1.869	1.825	1.762	1.778	1.772	1.851	1.746
Ca	0.005	0.004	0.005	0.006	0.005	0.006	0.006	0.006
Na	0.000	0.000	0.002	0.000	0.000	0.000	0.000	0.000
K	0.000	0.000	0.000	0.000	0.000	0.000	0.000	0.000
Ni	0.000	0.000	0.004	0.004	0.005	0.004	0.005	0.000

ORTHOPYROXENE

	Ultrabasic Rock KL-12(3)	Komatiite KL-34(1)	Olivine Basalt KL-104(1)
SiO_2	54.47	56.70	55.11
Al_2O_3	3.74	1.81	1.76
TiO_2	0.09	0.04	0.02
Cr_2O_3	-	0.00	0.00
FeO	11.26	7.64	6.74
MnO	0.20	0.18	0.14
MgO	28.60	31.04	31.99
CaO	1.75	3.17	2.29
Na_2O	0.02	-	0.01
K_2O	0.01	-	-
NiO	-	0.00	0.00
Ca	3.47	6.04	4.39
Mg	78.81	82.32	85.31
Fe	17.72	11.64	10.30
En	81.5	87.6	89.2
Si	1.931	1.968	1.949
Al^4	0.069	0.032	0.051
Al	0.086	0.042	0.022
Ti	0.002	0.001	0.001
Fe^3	0.000	0.000	0.029
Fe^2	0.331	0.222	0.171
Mg	1.497	1.606	1.686
Mn	0.006	0.005	0.004
Ni	0.000	0.000	0.000
Ca	0.066	0.118	0.087
Na	0.001	0.000	0.001
K	0.000	0.000	0.000

CLINOPYROXENE

	Ultrabasic Rocks			Olivine Basalts	
	KL-121(5)	DL-36(5)	DL-45(3)	PL-34(4)	KL-104(2)
SiO_2	54.95	53.00	52.91	53.52	54.06
Al_2O_3	2.01	2.26	3.16	2.56	2.13
TiO_2	0.07	0.19	0.31	0.12	0.08
Cr_2O_3	1.05	-	-	-	-
FeO	3.97	4.30	4.83	5.65	4.58
MnO	0.11	0.13	0.12	0.16	0.12
MgO	19.30	19.00	18.04	19.05	19.43
CaO	19.70	19.84	20.31	18.52	19.57
Na_2O	0.07	0.13	0.14	0.10	0.03
K_2O	0.00	-	-	0.00	0.00
NiO	0.02	0.00	0.00	-	-
Ca	93.61	39.40	41.23	37.37	38.93
Mg	53.98	53.14	50.93	53.47	53.77
Fe	6.41	6.96	7.84	9.15	7.30
Si	1.961	1.939	1.925	1.947	1.955
Al^4	0.039	0.061	0.075	0.053	0.045
Al^6	0.045	0.036	0.061	0.057	0.046
Ti	0.002	0.005	0.008	0.003	0.002
Cr	0.030	0.000	0.000	0.000	0.000
Fe^3	0.000	0.024	0.007	0.000	0.000
Fe^2	0.118	0.108	0.140	0.172	0.139
Mg	1.026	1.036	0.978	1.033	1.047
Mn	0.003	0.004	0.004	0.005	0.004
Ni	0.000	0.000	0.000	0.000	0.000
Ca	0.753	0.778	0.792	0.722	0.758
Na	0.005	0.009	0.010	0.007	0.002
K	0.000	0.000	0.000	0.000	0.000

CLINOPYROXENE, cont'd.

Komatiites - KL-33

	Grain A		Grain B		Grain C		Grain D		Grain E	
	Core	Rim	Core	Rim	Core	Rim	Core	Rim	Core	Rim
SiO_2	53.22	54.73	56.66	52.78	53.24	53.19	52.77	55.61	55.52	53.82
Al_2O_3	3.22	1.47	.0.50	3.41	3.00	2.49	3.21	2.78	1.11	3.24
TiO_2	0.13	0.04	0.03	0.19	0.13	0.13	0.15	0.10	0.04	0.15
Cr_2O_3	0.55	0.57	0.28	0.27	0.41	0.13	0.23	0.66	0.59	0.34
FeO	7.20	6.83	9.78	8.15	7.84	7.93	7.28	9.63	9.18	7.75
MnO	0.13	0.14	0.18	0.19	0.17	0.16	0.14	00.20	0.18	0.16
MgO	18.51	21.13	30.92	18.94	19.56	19.19	19.43	26.08	32.55	19.51
CaO	17.22	18.84	2.97	16.50	15.68	17.62	18.43	6.37	1.86	16.73
Na_2O	0.10	0.07	0.09	0.10	0.10	0.08	0.10	0.03	0.02	0.10
K_2O	-	-	-	-	-	-	-	-	-	-
NiO	0.01	0.00	0.00	0.00	0.05	0.00	0.00	0.08	0.03	0.05
Ca	35.37	35.10	5.53	24.22	31.89	34.80	35.96	12.66	3.42	33.43
Mg	52.88	54.76	80.01	60.76	55.34	52.72	52.73	72.09	83.16	54.23
Fe	11.75	10.14	14.47	15.02	12.77	12.48	11.30	15.25	13.42	12.34
Si	1.932	1.910	1.966	2.001	1.933	1.921	1.885	1.951	1.919	1.925
Al^4	0.068	0.061	0.021	0.000	0.067	0.079	0.115	0.049	0.045	0.075
Al^6	0.070	0.000	0.000	0.014	0.062	0.027	0.021	0.066	0.000	0.062
Ti	0.004	0.001	0.001	0.007	0.004	0.004	0.004	0.003	0.001	0.004
Cr	0.017	0.016	0.008	0.008	0.012	0.004	0.006	0.018	0.016	0.010
Fe^3	0.000	0.105	0.044	0.000	0.000	0.046	0.086	0.000	0.099	0.000
Fe^2	0.219	0.094	0.240	0.259	0.239	0.194	0.131	0.283	0.167	0.232
Mg	1.001	1.089	1.599	1.073	1.059	1.033	1.035	1.364	1.677	1.040
Mn	0.004	0.004	0.005	0.006	0.005	0.005	0.004	0.006	0.005	0.005
Ni	0.000	0.000	0.000	0.000	0.001	0.000	0.000	0.002	0.000	0.001
Ca	0.670	0.705	0.110	0.428	0.610	0.682	0.706	0.239	0.069	0.641
Na	0.007	0.005	0.006	0.007	0.007	0.006	0.007	0.002	0.001	0.007
K	0.000	0.000	0.000	0.000	0.000	0.000	0.000	0.000	0.000	0.000

CLINOPYROXENE, cont'd.

	Komatiites - KL-34		Zoned Grain Traverses				
	Grain A						
	Point 1	2	3	4	5	6	7
SiO_2	48.29	50.98	53.60	53.93	52.61	49.34	47.52
Al_2O_3	9.17	5.25	3.33	2.74	3.77	6.56	7.65
TiO_2	0.48	0.27	0.08	0.11	0.16	0.33	0.43
Cr_2O_3	0.05	0.13	0.23	0.32	0.28	0.12	0.04
FeO	10.08	8.24	6.55	7.68	7.93	8.45	10.52
MnO	0.17	0.16	0.17	0.20	0.14	0.20	0.19
MgO	13.11	17.96	21.41	24.39	21.46	16.72	14.36
CaO	18.38	16.76	14.33	10.53	13.11	17.49	17.76
Na_2O	-	-	-	-	-	-	-
K_2O	-	-	-	-	-	-	-
NiO	0.03	0.02	0.04	0.05	0.08	0.03	0.00
Ca	41.20	34.70	29.03	20.81	26.61	36.82	38.53
Mg	40.87	51.72	60.34	67.03	60.60	48.96	43.33
Fe	17.94	13.58	10.63	12.16	12.79	14.22	18.14
Si	1.795	1.867	1.934	1.930	1.910	1.822	1.788
Al^4	0.205	0.133	0.066	0.070	0.090	0.178	0.212
Al^6	0.197	0.093	0.076	0.047	0.072	0.108	0.128
Ti	0.013	0.007	0.002	0.003	0.004	0.009	0.012
Cr	0.001	0.004	0.007	0.009	0.008	0.004	0.001
Fe^3	0.000	0.021	0.000	0.008	0.000	0.048	0.058
Fe^2	0.313	0.231	0.197	0.222	0.241	0.213	0.273
Mg	0.726	0.980	1.150	1.302	1.161	0.924	0.805
Mn	0.005	0.005	0.005	0.006	0.004	0.006	0.006
Ni	0.000	0.000	0.000	0.001	0.002	0.000	0.000
Ca	0.732	0.659	0.553	0.404	0.510	0.692	0.716
Na	0.000	0.000	0.000	0.000	0.000	0.000	0.000
K	0.000	0.000	0.000	0.000	0.000	0.000	0.000

CLINOPYROXENE, cont'd.

	Komatiites - KL-34			Zoned Grain Traverses	
	Grain B				
	Point 1	2	3	4	5
SiO_2	45.16	50.86	51.32	50.72	47.26
Al_2O_3	12.37	6.33	5.01	4.51	8.12
TiO_2	0.51	0.25	0.12	0.17	0.52
Cr_2O_3	0.00	0.03	0.09	0.04	0.06
FeO	13.40	7.22	6.90	8.54	11.08
MnO	0.16	0.19	0.19	0.13	0.21
MgO	10.46	15.60	17.28	18.24	13.70
CaO	17.68	18.90	19.27	16.81	18.36
Na_2O	0.00	0.00	0.00	0.00	0.00
K_2O	0.00	0.00	00.00	0.00	0.00
NiO	0.05	0.01	0.05	0.00	0.03
Ca	41.29	40.75	39.46	34.34	39.72
Mg	33.98	46.78	49.21	51.83	41.22
Fe	24.72	12.47	11.33	13.83	19.07
Si	1.704	1.872	1.870	1.861	1.770
Al^4	0.296	0.128	0.130	0.139	0.230
Al^6	0.254	0.146	0.087	0.069	0.128
Ti	0.014	0.007	0.003	0.005	0.015
Cr	0.000	0.001	0.003	0 001	0.002
Fe^3	0.013	0.000	0.034	0.059	0.071
Fe^2	0.410	0.222	0.176	0.203	0.176
Mg	0.588	0.856	0.938	0.998	0.765
Mn	0.005	0.006	0.006	0.004	0.007
Ni	0.001	0.000	0.001	0.000	0.000
Ca	0.716	0.745	0.752	0.661	0.737
Na	0.000	0.000	0.000	0.000	0.000
K	0.000	0.000	0.000	0.000	0.000

CLINOPYROXENE, cont'd.

	Komatiites KL-34		Zoned Grain Traverses				
	Grain C				Grain D		
	Point 1	2	3	4	1	2	3
SiO_2	49.73	51.48	53.64	49.27	48.52	55.30	54.54
Al_2O_3	8.53	3.04	3.94	6.24	6.35	1.46	1.38
TiO_2	0.45	0.16	0.20	0.28	0.35	0.05	0.04
Cr_2O_3	0.02	0.41	0.25	0.09	0.07	0.61	0.58
FeO	11.59	6.92	6.63	9.18	7.50	7.75	7.20
MnO	0.21	0.19	0.20	0.20	0.16	0.18	0.20
MgO	13.71	21.39	19.78	16.82	14.57	29.14	24.21
CaO	17.87	14.28	16.61	17.13	19.45	5.11	10.67
Na_2O	0.00	0.00	0.00	0.00	0.00	0.00	0.00
K_2O	0.00	0.00	0.00	0.00	0.00	0.00	0.00
NiO	0.04	0.04	0.03	0.02	0.03	0.08	0.06
Ca	38.72	28.80	33.59	35.80	42.56	9.86	21.29
Mg	41.32	60.00	55.63	48.89	44.35	78.20	67.18
Fe	19.96	11.20	10.78	15.31	13.04	11.95	11.53
Si	1.812	1.895	1.918	1.822	1.843	1.957	1.972
Al^4	0.188	0.105	0.082	0.178	0.157	0.043	0.028
Al^6	0.178	0.027	0.084	0.094	0.128	0.018	0.030
Ti	0.012	0.004	0.005	0.008	0.010	0.001	0.001
Cr	0.001	0.002	0.007	0.003	0.002	0.017	0.017
Fe^3	0.000	0.056	0.000	0.066	0.007	0.005	0.000
Fe^2	0.353	0.157	0.1981	0.218	0.238	0.224	0.218
Mg	0.744	1.174	1.054	0.932	0.825	1.536	1.304
Mn	0.006	0.006	0.006	0.006	0.005	0.005	0.006
Ni	0.000	0.001	0.000	0.000	0.000	0.002	0.001
Ca	0.698	0.563	0.636	0.683	0.792	0.194	0.413
Na	0.000	0.000	0.000	0.000	0.000	0.000	0.000
K	0.000	0.000	0.000	0.000	0.000	0.000	0.000

CLINOPYROXENE, cont'd.

	Aphyric Basalts					
	KL-23(4)	KL-69(2)	PL-17(1)	PL-19(2)	PL-24(2)	DL-21(3)
SiO_2	52.95	54.97	55.63	53.70	53.47	52.07
Al_2O_3	2.10	1.62	1.63	3.02	1.89	2.78
TiO_2	0.14	0.05	0.09	0.16	0.12	0.50
Cr_2O_3	0.27	0.47	0.39	0.28	0.26	0.10
FeO	6.89	5.61	6.27	7.11	7.24	8.49
MnO	0.14	0.06	0.16	0.17	0.14	0.16
MgO	18.68	19.61	20.22	17.78	17.21	16.52
CaO	17.88	18.01	17.15	18.23	19.38	19.49
Na_2O	0.13	0.09	0.08	0.12	0.15	0.25
K_2O	-	-	-	-	-	-
NiO	0.06	0.10	0.05	0.00	0.02	0.03
Ca	36.23	36.23	34.10	37.48	39.49	39.60
Mg	52.65	54.87	55.92	50.84	48.77	48.68
Fe	11.12	8.90	9.98	11.68	11.74	13.72
Si	1.945	1.976	1.978	1.946	1.962	1.911
Al^4	0.055	0.024	0.022	0.054	0.038	0.089
Al^6	0.036	0.044	0.047	0.075	0.044	0.030
Ti	0.004	0.004	0.002	0.004	0.003	0.014
Cr	0.008	0.013	0.011	0.008	0.008	0.003
Fe^3	0.012	0.000	0.000	0.000	0.000	0.047
Fe^2	0.199	0.169	0.187	0.216	0.222	0.214
Mg	1.023	1.050	1.072	0.960	0.941	0.904
Mn	0.004	0.002	0.005	0.005	0.004	0.005
Ni	0.000	0.002	0.001	0.000	0.000	0.000
Ca	0.704	0.694	0.654	0.708	0.762	0.766
Na	0.009	0.006	0.006	0.008	0.011	0.018
K	0.000	0.000	0.000	0.000	0.000	0.000

PLAGIOCLASE

	Ultrabasic Rocks		Aphyric Basalts		
	DL-36(2)	DL-45(2)	KL-23(1)	PL-24(1)	DL-21(4)
SiO_2	53.53	50.97	50.45	44.03	53.66
Al_2O_3	29.11	30.98	29.70	39.21	27.20
TiO_2	0.03	0.03	0.04	0.03	0.05
FeO	0.72	0.54	0.80	0.90	0.80
MnO	0.01	0.00	0.02	0.00	0.00
MgO	0.33	0.26	0.46	0.16	0.13
CaO	13.81	14.29	15.00	12.05	12.24
Na_2O	3.54	3.15	2.65	2.48	4.65
K_2O	0.04	0.03	0.05	0.07	0.02
An	68.15	71.36	75.55	72.50	59.19
Ab	31.61	28.46	24.15	27.00	40.69
Or	0.24	0.18	0.30	0.50	0.12
Si	9.626	9.267	9.303	8.106	9.818
Al	6.172	6.641	6.458	8.512	5.976
Ti	0.004	0.004	0.006	0.004	0.007
Fe^2	0.108	0.082	0.123	0.139	0.122
Mn	0.002	0.000	0.003	0.000	0.000
Mg	0.088	0.070	0.126	0.044	0.035
Ca	2.661	2.784	2.964	2.378	2.400
Na	1.234	1.111	0.948	0.885	1.650
K	0.009	0.007	0.012	0.016	0.005

APPENDIX C Reproduction of Major Element Extraction Program

```
                MAIN

C       PROGRAM F
C       LEAST SQUARES SOLUTION TO PETROLOGICAL MIXING PROBLEMS
        INTEGER TITLE (13,80)
        DIMENSION WT(12,20),W(12,20), Y(12,13), A(11,12)
        DIMENSION ANS(12),BULK (20),SOL(20),DIFF(20)
        DIMENSION AVE (20)
        DIMENSION ANZ (12)
     5  READ 1,J
     1  FORMAT (T2)
        IF(J,EQ,0) GO TO 11
        ZZ=0.
        JJ=J-1
        PRINT 50
    50  FORMAT ('1',' EXTRACT CALCULATION.  A LEAST SQUARE ERROR SOLUTION T
       1O PETROLOGIC MIXING PROBLEMS')
        READ 70, (TITLE(13,I),I=1,80)
    70  FORMAT (80A1)
        PRINT 71,(TITLE(13,I),I=1,80)
    71  FORMAT ('0','THIS PROBLEM IS - ',80A1)
        DO 4 I=1.20
        DO 4 K=1.12
        W(K,I)=0.001
     4  WT(K,I)=0.001
        DO 10 K=1.JJ
        READ 2,(TITLE(K,I),I=1,80)
     2  FORMAT (80A1)
        READ 3,(WT(K,I),I=1,13)
     3  FORMAT(13F6,2)
        READ 73,(WT(K,I),T=14,20)
    73  FORMAT (7F6,2)
    10  CONTINUE
        READ 2,(TITLE(12,I),I=1,80)
        READ 3,(WT(12,I),I=1,13)
        READ 73,(WT(12,I),I=14,20)
   107  DO 30 K=1,JJ
        PRINT 21,K,(TITLE(K,I),I=1,80)
    21  FORMAT(' ','COMPOSITION',I4,' IS   ',80A1)
    30  CONTINUE
        PRINT 16,(TITLE(12,T),I=1,80)
    16  FORMAT (' ','BULK COMPOSITION IS   ',80A1)
        PRINT 22,JJ
    22  FORMAT (' ','THIS CALCULATION GIVES PROPORTIONS OF ANALYSES 1 TO'.
       1I2,' WHICH COMBINE TO FORM BULK COMPOSITION')
        PRINT 27
    27  FORMAT ('0', 'ANALYSIS INPUT')
        PRINT 23
    23  FORMAT (' ',/,T8, 'SIO2  TIO2  AL2O3  CR2O3  FE2O3  FEO  MNO  MGO
       1CAO   NA2O  K2O    P2O5  CO2   NI     RB     SR     ZR   X    Y
```

```
              MAIN

   1Z')
    PRINT 25,(K,(WT(K,I),T=1,20),K=1,JJ)
 25 FORMAT (' ', I4,20E6.2)
    PRINT 24,(WT(12,I),I=1,20)
 24 FORMAT (' ','BULK',20E6,2)
    DO 12 K=1,12
    DO 12 I=1,20
 12 W(K,I)=WT(K,T)
    Z=0.
102 DO 6 I=1,20
    DO 6 K=1,12
    IF(W(K,T),LT,0,001) GO TO 7
    GO TO 6
  7 DO 8 K=1,12
  8 W(K,I)=0.
  6 CONTINUE
    DO 9 K=1,13
    DO 9 I=1,12
  9 Y(I,K)=0.
    DO 13 K=1,11
    DO 13 M=1,11
    DO 13 I=1,20
 13 Y(K,M)=Y(K,M)+W(M,I)*W(K,I)
    DO 14 L=1,11
    DO 14 I=1,20
 14 Y(L,12)=Y(L,12)+W(12,I)*W(L,I)
    II=12
    NR=11
    N=J-1
    DO 15 K=1,12
    DO 15 L=1,11
 15 A(L,K)=Y(L,K)
    CALL GUASS (A,N,II,NR,ISOLN)
    IF(ISOLN,FQ,Q) PRINT 61
    IF(ISOLN,FQ,L) PRINT 62
    IF(ISOLN,FQ,2) PRINT 63
 61 FORMAT (' ','SOLUTION - NO SOLUTION EXISTS')
 62 FORMAT (' ','SOLUTION - THERE IS A UNIQUE SOLUTION')
 63 FORMAT (' ','SOLUTION - AN INFINITE NUMBER OF SOLUTIONS EXISTS')
    X=0.
    DO 31 I=1,N
 31 X=X+A(T,TT)
    X=X/100.
    IF(X.EQ.0.) PRINT 17
 17 FORMAT ('0',' NO NEW ANSWER, CALCULATION TERMINATING')
    IF(X.EQ.0.) GO TO 5
    DO 40 T=1,N
 40 ANS (I)=A(T,TT)/X
```

```
              MAIN

     X=0.
     DO 33 I=1,13
33   X=X+WT(12,I)
     X=X/100.
     DO 34 I=1.20
     SOL(I)=0.
34   BULK(I)=WT(12,I)/X
     DO 35 I=1.20
     DO 35 K=1,N
35   SOL(I)=ANS(K)*WT(K,I)+SOL(I)
     X=0.
     DO 36 I=1,13
36   X=X+SOL(I)
     X=X/100.
     IF(X.EQ.0.) PRINT 17
     IF(X.EQ.0) GO TO 5
     DO 37 T=1,20
37   SOL(I)=SOL(I)/X
     DO 38 I=1,20
38   DIFF(I)=0.
     DO 39 I=1,20.
39 DIFF(I)=BULK(I)-SOL(I)
     SSM=0.
     SST=0.
     DO 42 T=1,13
42   SSM=SSM+DIFF(I)*DIFF(I)
     DO 43 T=14,20
43   SST=SST+DIFF(I)*DIFF(I)
     PRINT 44.N
44   FORMAT ('0'),'PROPORTION OF FIRST',I2,' ANALYSES, COMBINING TO FORM
    1 THE BULK COMPOSITION ARE',/,' ******************************
    1*')
     IF(Z,EQ,1,) GO TO 99
     DO 98 I=1,N
98   ANZ(I)=ANS(I)
99   PRINT 45,(T,ANS(I),I=1,N)
45   FORMAT (' ','*****',T10,' ANALYSIS',T3,F8,2,' % *****')
     PRINT 46.J,(BULK(I),I=1,20)
46   FORMAT (' ','************************************',',' ROW 1 TS AN
    1ANALYSIS',T2,' NORMALISED TO 100%,/,' ROW 2 IS CALCULATED SOLUTION
    1FROM ABOVE PROPORTIONS',/,'  SIO2  TIO2   AL2O3  CR2O3  FE2O3  FEO
    1MNO    MGO   CAO   NA2O   K2O   P2O5  CO2  NI     RB     SR     ZR
    1X      YU      Z',/,T2,2OF6,2)
     PRINT 47,(SOL(I),T=1.20)
47   FORMAT (' ',2OF6,2)
     PRINT 48,SSM,SST
48   FORMAT ('0','SUM SQUARES OF ERRORS ON MAJOR ELEMENTS ',F8.3./.'SU
    1M SQUARES OF ERRORS ON TRACE ELEMENTS',F8.3)
```

```
      PRINT 60,(DIFF(I),I=1,20)
 60   FORMAT (' ','DIFFERENCES ARE './. 20F6,3)
      DO 26 I=1,20
      BULK(I)=0.
      DO 26 K=2,N
 26   BULK(I)=BULK(I)+WT(K,I)*ANS(K)
      SUM=0.
      DO 32 I=1,13
 32   SUM=SUM+BULK(I)
      SUM=SUM/100.
      IF(SUM,EQ.0.) PRINT 17
      IF(SUM,EQ.0.) GO TO 5
      DO 28 I=1,20
 28   BULK(I)=BULK(I)/SUM
      PRINT 29,N.(BULK(I),T=1,20)
 29   FORMAT ('0'),'BULK COMPOSITION OF EXTRACTED MATERIAL.    I.F. COMBINED
     1COMPOSITION OF ANALYSES 2 to ',T2,/,20F6,2)
      IF(ZZ.EQ.1.) GO TO 104
      IF(Z.EQ.1.) GO TO 104
      Z=1.
      DO 100 T=1,20
      DO 100 K=1,12
100   W(K,T)=WT(K,I)
      DO 111 T=1,20
      IF(W(12,I).NE.0.) GO TO 101
      W(12,I)=1E10
      DO 109 K=1,11
 109  W(K,T)=Q.
 101  DO 111 K=1,12
 111  W(K,T)=W(K,I)/W(12,I)
      PRINT 103
 103  FORMAT ('1',' CALCULATION REPEATED USING PROPORTIONAL WEIGHTINGS R
     1ATHER THAN ABSOLUTE VALUES')
      GO TO 102.
 104  IF(ZZ.FQ.L.) GO TO 110
      ZZ=ZZ+1.
      ALTER=0.
      DO 105 T=1,N
      IF(ANZ(I).GE.0.) GO TO 105
      ALTER=ALTER+1.
      DO 106 K=1,20
106   WI(T,K)=0.
105   CONTINUE
      IF(ALTER,EQ.0.) GO TO 5
      GO TO 117
110   ZZ=ZZ+1.
      DO 115 T=1,N
      ALTER=0.
```

```
      IF(ANS(I).GE.O.) GO TO 115
      ALTER=ALTER+1.
      DO 116 K=1,20
116   WT(I,K)=O.
115   CONTINUE
      IF(ALTER.EQ.O.) GO TO 5
117   PRINT 108
108   FORMAT ('1',' RECALCULATION REPEATED IGNORING MINERALS WITH
     1NEGATIVE PROPORTIONS')
      GO TO 107
 11   STOP
      END
```

```
                MAIN

      SURROUNDING GAUSS (A.N.II,NR,ISOLN)
C     ** GAUSS-JORDAN ELIMINATION METHOD **
C     ** AX=H
C     ** A=(N*N)
C     ** X=(N*N)
C     ** AUGMENTED MATRIX (A:B) = (N)*(N+M) = A
C     ** TI = N + M
C     ** NR IS THE ROW DIMENSION OF A IN THE MAIN PROGRAM **
C     ** ISOLM = O. MEANS THAT NO SOLUTION EXISTS **
C              = 1. MEANS THAT A UNIQUE SOLUTION EXISTS **
C              = 2. MEANS THAT AN INFINITE NUMBER OF SOLUTIONS EXIST **
      DIMENSION A(NR.II)
      DIMENSION TND(1OO)
      NV=O
      DO 1 I=1,N
    1 IND(T)=1
      MN=N+1
      ISOLN=1
      DO 5O K=1,N
      B=A(K,K)
      IF (ARS(B). GE.O.OOO1) GO TO 17
      DO 15 L=K,N
      IE (ABS(A(L,K)).LT.O.OOO1) GO TO 15
      DO 13 LN=K,II
      T=A(1,LI)
      A(L,LL)=A(K,LL)
      A(K,LL)=T
   13 CONTINUE
      B=A(K,K)
      GOTO 17
   15 CONTINUE
C     ** CHECK ROW FOR NON-ZERO ELEMENT **
      DO 12O I=K,N
      IF (ABS(A(K,I)). LT. O.OOO1) GO TO 12O
      DO 11O J=1,II
      T=A(J,1)
      A(J,T)A(J,K)
      A(J,K)=T
  11O CONTINUE
C     ** MODIFY INDICES OF VARIABLES ARRAY **
      IT=IND(T)
      IND(I)=TND(K)
      IND(K)=IT
      B=A(K,K)
      NV=1
      GO TO 17
  12O CONTINUE
C     ** INCONSISTENCY OR INFINITE NUMBER OF SOLUTIONS? **
```

```
          GAUSS

      ISOLN=2
      DO 130 T=K.N
      IF (ABS(A(I.II)).GE.0.0001) ISOLN=0
  130 CONTINUE
      GO TO 990
   17 CONTINUE
      K1=K
      DO 20 J=K1,II
      A(K,J)=A(K,J)/B
      A(K,J)=ROUND(A(K,J),5)
   20 CONTINUE
      DO 40 T=1.N
      IF (I.EQ.K) GO TO 40
      B=A(I,K)
      DO 30 J=K1,II
      A(T,J)=A(1,J)-R*A(*K.J)
      A(I,J)=ROUND(A(I,J),5)
   30 CONTINUE
   40 CONTINUE
   50 CONTINUE
  990 CONTINUE
      IF (NV.FQ.0) GO TO 1000
      DO 70 1=1,N
      IF (IND(T).EQ.I) GO TO 70
      DO 60 J=NN,II
      T=A(I,J)
      A(IND(I),J)=T
   60 CONTINUE
      IT=IND(I)
      IND(I)=IND(IT)
      IND(IT)=IT
   70 CONTINUE
 1000 CONTINUE
      RETURN
      END
```

EXTRACT CALCULATION. A LEAST SQUARE ERROR SOLUTION TO PETROLOGIC MIXING PROBLEMS

THIS PROBLEM IS - FRACTIONAL CRYSTALLIZATION MODEL. CAWTHORN
COMPOSITION 1 IS OLIVINES
COMPOSITION 2 IS DERIVED LIQUID (APHYRIC)
BULK COMPOSITION IS PARENTAL LIQUID (KOMATIITES)
THIS CALCULATION GIVES PROPORTIONS OF ANALYSES 1 TO 2 WHICH COMBINE TO FORM BULK COMPOSITION

ANALYSIS INPUT

	SIO2	TIO2	AL203	CR203	FE203	FEO	MNO	MGO	CAO	NA20	K20	P205	CO2	NI	RB	SR	ZR	X	Y	Z
1	41.06	0.0	0.04	0.0	0.0	8.19	0.12	51.20	0.19	0.01	0.0	0.0	0.0	0.0	0.0	0.0	0.0	0.0	0.0	0.0
2	52.82	0.43	16.13	0.0	5.47	3.16	0.12	7.64	11.65	1.56	0.88	0.0	0.0	0.0	0.0	0.0	0.0	0.0	0.0	0.0
BULK	53.72	0.33	13.36	0.0	2.98	5.57	0.15	11.25	11.14	1.16	0.23	0.0	0.0	0.0	0.0	0.0	0.0	0.0	0.0	0.0

SOLUTION - THERE IS A UNIQUE SOLUTION

PROPORTION OF FIRST 2 ANALYSES. COMBINING TO FORM THE BULK COMPOSITION ARE
****
***** ANALYSIS 1 9.50% *****
***** ANALYSIS 2 90.50% *****
****
ROW 1 IS ANALYSIS 3 NORMALISED TO 100%
ROW 2 IS CALCULATED SOLUTION FROM ABOVE PROPORTIONS

SIO2	TIO2	AL203	CR203	FE203	FEO	MNO	MGO	CAO	NA20	K20	P205	CO2	NI	RB	SR	ZR	X	Y	Z
53.78	0.33	13.37	0.0	2.98	5.58	0.15	11.26	11.15	1.16	0.23	0.0	0.0	0.0	0.0	0.0	0.0	0.0	0.0	0.0
51.73	0.39	14.61	0.0	4.95	3.64	0.12	11.78	10.57	1.41	0.80	0.0	0.0	0.0	0.0	0.0	0.0	0.0	0.0	0.0

SUM SQUARES OF ERRORS ON MAJOR ELEMENTS 14.361
SUM SQUARES OF ERRORS ON TRACE ELEMENTS 0.0
DIFFERENCES ARE
2.051-0.059-1.234 0.0 -1.969 1.936 0.030-0.522 0.586-0.252-0.567 0.0 0.0 0.0 0.0 0.0 0.0 0.0 0.0 0.0

BULK COMPOSITION OF EXTRACTED MATERIAL. I.E. COMBINED COMPOSITION OF ANALYSES 2 TO 2
52.89 0.43 16.15 0.0 5.48 3.16 0.12 7.65 11.67 1.56 0.88 0.0 0.0 0.0 0.0 0.0 0.0 0.0 0.0 0.0

CALCULATION REPEATED USING PROPORTIONAL WEIGHTINGS RATHER THAN ABSOLUTE VALUES
SOLUTION - THERE IS A UNIQUE SOLUTION

PROPORTION OF FIRST 2 ANALYSES. COMBINING TO FORM THE BULK COMPOSITION ARE
****
***** ANALYSIS 1 30.98% *****
***** ANALYSIS 2 69.02% *****
****
ROW 1 IS ANALYSIS 3 NORMALISED TO 100%
ROW 2 IS CALCULATED SOLUTION FROM ABOVE PROPORTIONS

	SIO2	TIO2	AL2O3	CR2O3	FE2O3	FEO	MNO	MGO	CAO	NA2O	K2O	P2O5	CO2	NI	RB	SR	ZR	X	Y	Z
	53.78	0.33	13.37	0.0	2.98	5.58	0.15	11.26	11.15	1.16	0.23	0.0	0.0	0.0	0.0	0.0	0.0	0.0	0.0	0.0
	49.10	0.30	11.13	0.0	3.77	4.71	0.12	21.10	8.09	1.08	0.61	0.0	0.0	0.0	0.0	0.0	0.0	0.0	0.0	0.0

SUM SQUARES OF ERRORS ON MAJOR ELEMENTS 134.641
SUM SQUARES OF ERRORS ON TRACE ELEMENTS 0.0
DIFFERENCES ARE

4.678	0.034	2.246	0.0	-0.786	0.865	0.030	-9.839	3.065	0.083	-0.376	0.0	0.0	0.0	0.0	0.0	0.0	0.0	0.0	0.0

BULK COMPOSITION OF EXTRACTED MATERIAL. I.E. COMBINED COMPOSITION OF ANALYSES 2 TO 2

52.89	0.43	16.15	0.0	5.48	3.16	0.12	7.65	11.67	1.56	0.88	0.0	0.0	0.0	0.0	0.0	0.0	0.0	0.0	0.0